Timing in the cerebellum during motor learning: from neuron to athlete to patient

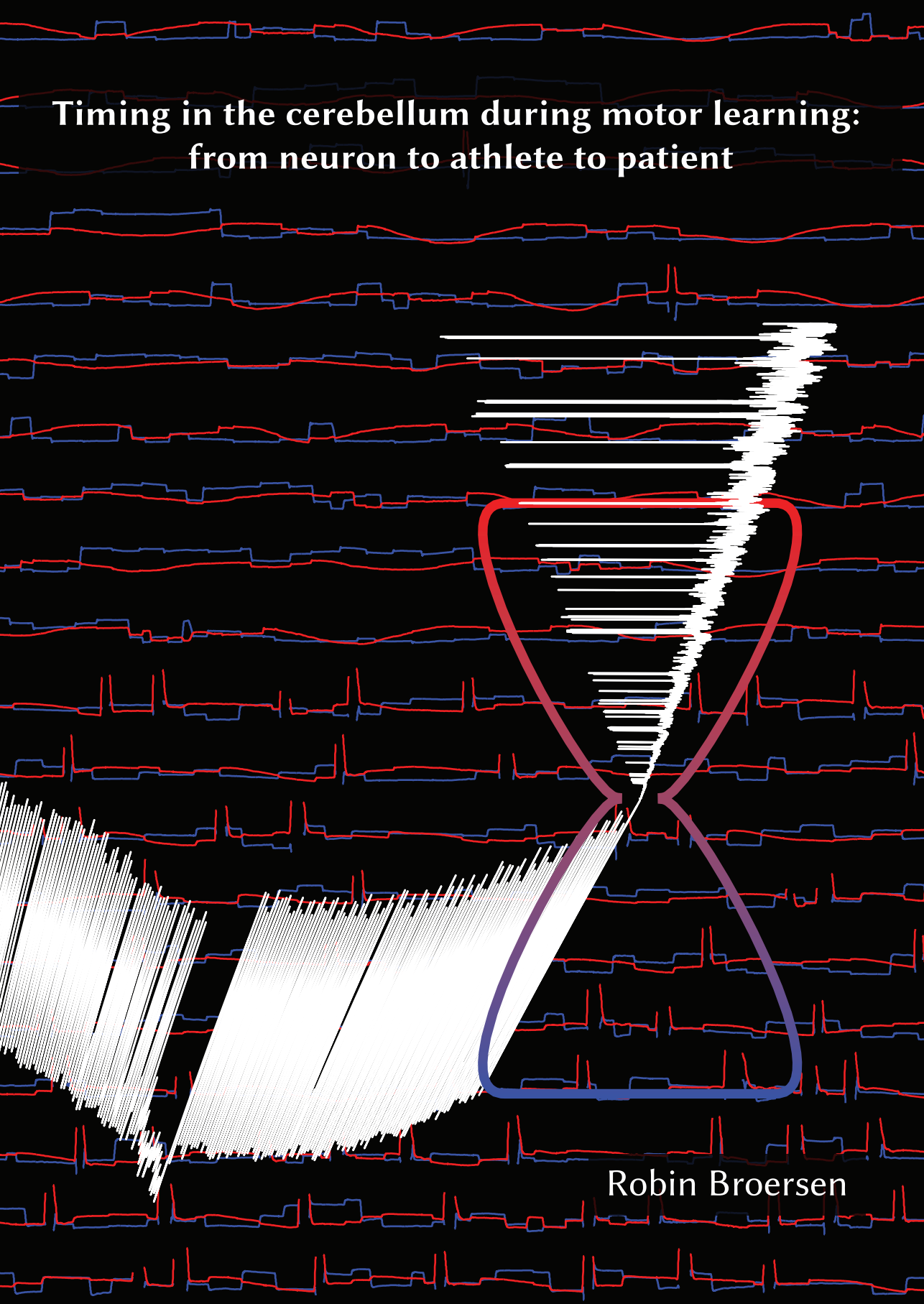

Robin Broersen

Timing in the cerebellum during motor learning: from neuron to athlete to patient

Robin Broersen

The research described in this thesis was carried out under the supervision of Prof.dr. C.I. De Zeeuw at the Department of Neuroscience of the Erasmus MC in Rotterdam, the Netherlands. The experiments presented in this thesis were carried out at the Netherlands Institute for Neuroscience (NIN-KNAW) in Amsterdam and the Erasmus MC in Rotterdam. Research was conducted with the financial support from the Netherlands Organization for Scientific Research (NWO), the European Research Counsil (ERC) and the Boehringer Ingelheim Fonds.

Cover design: R. Broersen

Cover represents an artistic expression of the relationship between neuronal input-output computations in the cerebellar nuclei and eye movements during spinocerebellar ataxia type 6 (SCA6), to some degree inspired by the cover of the Pink Floyd album 'The Dark Side of the Moon' (1973). Healthy eye movements (top-half of page) in the y-axis (red) and x-axis (blue) during the weight-discrimination task (Chapter 5) versus SCA6 eye movements (bottom-half). Altered cerebellar nuclei output caused by SCA6, changes the eye movements (*e.g.* note increased blinks as trace interruptions), which in turn changes the visual-based neuronal input to the cerebellum, which in turn changes the cerebellar output.

Printed by: ProefschriftMaken || www.proefschriftmaken.nl

ISBN: 978-94-6380-416-5

The publication of this thesis was financially supported by the ADCA Vereniging Nederland.

Timing in the cerebellum during motor learning: from neuron to athlete to patient

Timing in het cerebellum tijdens motorisch leren: van neuron tot atleet tot patiënt

Proefschrift

ter verkrijging van de graad van doctor aan de
Erasmus Universiteit Rotterdam
op gezag van de Rector Magnificus

Prof.dr. R. Engels

en volgens het besluit van het College voor Promoties.

De openbare verdediging zal plaatsvinden op
woensdag 2 oktober 2019 om 09:30 uur

door

Robin Broersen
geboren op 8 september 1989
te Ridderkerk, Nederland

Erasmus University Rotterdam

Promotiecommissie:

Promotor:	Prof.dr. C.I. De Zeeuw
Overige leden:	Prof.dr. M.A. Frens Prof.dr. J. Verhaagen Prof.dr. G.J. Stuart
Copromotor:	Dr. C.B. Canto

For my parents, my brothers and my wife

Table of contents

List of abbreviations

The following table explains the most important abbreviations used in this thesis.

Abbreviation	*Explanation*
ActionOBS	action observation task (experimental condition)
AIC	Akaike's information criterion
ANOVA	analysis of variance
AR(1)	first-order autoregressive model
AUC	area under the curve
AUCCR	area under the curve of the correct ratio
BG	basal ganglia
BOLD	blood oxygenation level-dependent
cEPSP	compound excitatory postsynaptic potentials
CF	climbing fiber
CFC	climbing fiber collateral
ch'ase	chondroitinase
cIPSP	compound inhibitory postsynaptic potentials
cond	conditioned (mice)
CR	conditioned response
CS	conditioned stimulus
CS-cEPSP	cEPSP following the CS
CS-cIPSP	cIPSP following the CS
CSPG	chondroitin sulfate proteoglycan
CTR / Ctrl	control
CtrlOBS	action observation task (control condition)
CV	coefficient of variation
DAO	dorsal accessory olive
DCN	deep cerebellar nuclei
DLH	dorsolateral hump
EBC	eyeblink conditioning
EO	eyelid opening
FEC	fraction eyelid closure
fMRI	functional magnetic resonance imaging
GABA	γ-aminobutyric acid
GAG	glycosaminoglycan
GC	granule cell
GFP	green fluorescent protein
GLM	generalized linear model
GLMM	generalized linear mixed model
GSD	gaze-to-stimulus distance
HAS	hyaluronan synthase
IntA	anterior interposed nucleus
IO	inferior olive
IpN	interposed nucleus
ISI	interspike interval

ITI	intertrial interval
Lat	lateral nucleus
LED	light-emitting diode
LTD	long-term depression
LTP	long-term potentiation
LV	lentivirus
MD	mean difference
MDMT	magnetic distance measurement technique
MF	mossy fiber
MLI	molecular layer interneuron
MWU test	Mann-Whitney U test
NM	no movement
NO	nucleo-olivary
PBS	phosphate-buffered saline
PC	Purkinje cell
PCA	principal component analysis
PCx	'x'-th principal component (PC1, PC2…)
PF	parallel fiber
PFA	paraformaldehyde
PGK	phosphoglycerate kinase
PN	pontine nuclei
PNN	perineuronal net
PO	principal olive
pseudo	pseudo-conditioned (mice)
PSTH	peristimulus time histogram
RM	repeated-measures
ROI	region of interest
RTT	reaction time task
SARA	Scale of the Assessment and Rating of Ataxia
SCA6	spinocerebellar ataxia type 6
SD	standard deviation
SEM	standard error of the mean
Sema3A	Semaphorin-3A
SS	simple spike
TEPR	task-evoked pupillary response
TPT	trajectory prediction task
UR	unconditioned response
US	unconditioned stimulus
US-cEPSP	cEPSP following the US
US-cIPSP	cIPSP following the US
VBM	voxel-based morphometry
VGAT	vesicular GABA transporter
VGLUT	vesicular glutamate transporter
V_m	membrane potential
VN	vestibular nuclei
WD	weight discrimination
WFA	*Wisteria floribunda* agglutinin

Chapter 1

General introduction

Parts of this chapter have been adopted from:

Robin Broersen, Beerend H.J. Winkelman, Özgecan Özyıldırım and Chris I. De Zeeuw (2016). Physiology of Olivo-Cerebellar Loops. In: Gruol D., Koibuchi N., Manto M., Molinari M., Schmahmann J., Shen Y. (eds.)

Essentials of Cerebellum and Cerebellar Disorders. Springer, p 323-327.

At the center of all our experiences, thoughts and actions lies our brain. This organ, the most complex we have, continuously registers information from our sensory organs and allows us to perceive and act upon changes in our environment. In order to do this appropriately, we need to be able to comprehend information from the fourth dimension, time. As a result of our brain's ability to process time-related information, we are able to predict *where* (spatial information) something will be at a certain *time* (temporal information), a process also known as 'spatio-temporal prediction'. We do this constantly, for example when we are walking outside and we have to cross a street, while from our right side we see a car approaching. At that moment we make a judgement of whether it is safe to cross the street, based on our prediction of where the car will be at a certain time. Failure to do so may have serious consequences. Our ability to perceive time is therefore crucial for our survival.

A part of the brain that is important for time processing is the cerebellum (Ivry and Keele 1989; Ivry 1996; Ivry et al. 2002; Spencer and Ivry 2013). The cerebellum has been shown to become active during activities that require temporal processing (Rao et al. 1997; Jänke et al. 2000; Pollok et al. 2008; Bareš et al. 2011). Furthermore, patients with cerebellar damage or disorders have been shown to be impaired at various tasks that require timing (Ivry et al. 1988; Ivry and Keele 1989; Casini and Ivry 1999; Jahanshahi et al. 2006; Bareš et al. 2007; Bueti et al. 2008; Bareš et al. 2010; Grube et al. 2010; Matsuda et al. 2015). Other functions that rely on the cerebellum are motor coordination, motor adaptation, fine-tuning of movements and some forms of associative learning (Krakauer and Shadmehr 2006; Manto et al. 2012; Lang et al. 2017). More recent research has also connected the cerebellum to cognitive processes and emotion (Timmann and Daum 2007; Schmahmann 2010; Baumann et al. 2015; Adamaszek et al. 2016). Even today, contemporary research still uncovers novel functions ascribed to the cerebellum.

A central question throughout this doctoral thesis is how the cerebellum processes time-related information and how disruptions to this process affect behavior. The experiments that are presented in this thesis involve a wide selection of techniques that stretch over multiple levels of neuroscientific research: from measuring miniscule electrical currents in individual neurons to studying human behavior in health and disease. To enable a better understanding of the results presented in this thesis, we will first summarize and review the anatomical and physiological principles of the cerebellum and its connected structures. We will then discuss the circuit physiology underlying cerebellar associative learning, where making a precisely timed movement is essential. Finally, we will describe how cerebellar dysfunction affects different forms of human behavior that involve timing.

1.1 The cerebellum

1.1.1 Macrostructure and function of the cerebellum

The cerebellum ('little brain' in Latin) is a highly foliated structure that covers the brainstem. In humans, this structure is located ventrocaudally to the occipital lobe of the cerebral cortex, and in rodents it is located directly caudal to the occipital lobe. The cerebellum is connected with the brainstem through the superior, middle and inferior cerebellar peduncles (Fig 1A). Although the cerebellum is small in size compared to the cerebral cortex (~10% of total brain volume), it contains roughly 80% of the total number of neurons in the brain (Pakkenberg and Gundersen 1988; Andersen et al. 1992). On a macroscopic level the cerebellum consists of two separated parts: the cerebellar cortex and deep cerebellar nuclei (DCN) (Fig. 1B).

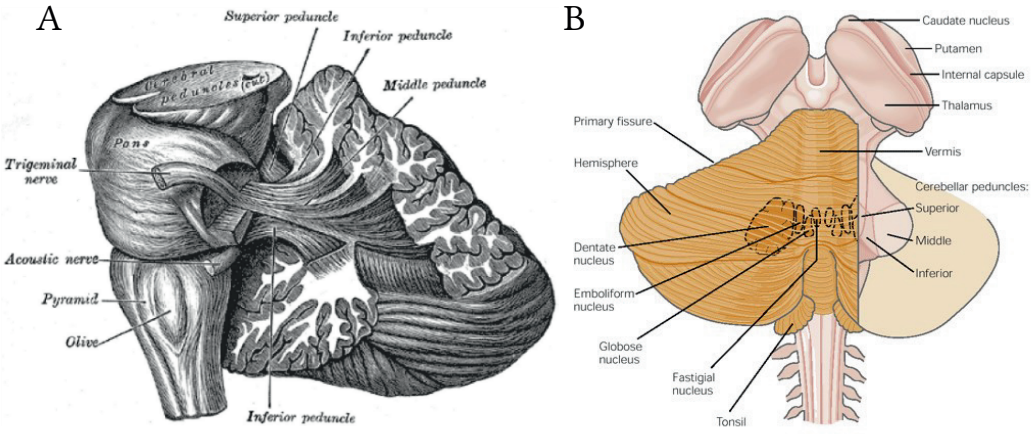

Fig 1. Gross anatomy of the human cerebellum. (A) Drawing of the lateral view of the human cerebellum (sagittal cut) and its position relative to the brainstem nuclei. From: *Gray's anatomy of the human brain* (1918), from van Baarsen and Grotenhuis (2014), with permission. (B) Schematic drawing of dorsal view of the cerebellum and brainstem up till the dorsal striatum, indicating major anatomical regions as well as the location of the deep cerebellar nuclei. From: Kandel et al. (2000), original from: Nieuwenhuys et al. (1988), with permission.

Anatomically, the cerebellar cortex can be subdivided into a central vermis ('worm' in Latin, after his shape) and two cerebellar hemispheres. On both sides of the vermis a shallow groove in the surface, the so-called the paramedian sulcus, demarcates the transition between the vermis and the hemispheres (Voogd and Glickstein 1998; Voogd and Marani 2016). The surface of the cerebellar cortex contains fissures that run in the transverse direction and separate the different lobes and lobules both in the vermis and the hemispheres (Fig 1B) (Voogd and Marani 2016). In the vermis ten lobules have been distinguished and these have been named using Roman letters I-X (Larsell 1952; Voogd and

Glickstein 1998), whereas in the hemispheres the lobular identification and nomenclature are dependent on the species.

Functionally, the cerebellar cortex can be subdivided into three main areas based on functional and phylogenetic criteria: the vestibulocerebellum, the spinocerebellum, and the cerebrocerebellum. The vestibulocerebellum has developed earliest in evolution and represents the floccolonodular lobe, which is predominantly involved in balance, and control and regulation of eye movements (Ito 1982; De Zeeuw et al. 1995). The spinocerebellum consists of the vermis and the intermediate part of the cerebellar hemispheres. This area receives somatosensory inputs from the spinal cord via the spinocerebellar tract and is involved in body muscle control, contributing to the control of balance, gaze and locomotion (Kandel et al. 2000). Developed most recent in evolution is the cerebrocerebellum, representing the lateral cerebellar hemispheres which receive inputs from the cerebral cortex. This area of the cerebellum has been associated with motor planning, motor rehearsal and other cognitive functions (Baumann et al. 2015; Adamaszek et al. 2016). Particularly the cerebrocerebellum is larger and more developed in humans and monkeys compared to animals lower in the evolutionary tree (Barton and Venditti 2014).

Neuronal projections from the cerebellar cortex connect to neurons in the DCN and vestibular nuclei (VN). These areas are located deep in the cerebellar structure and form the only source of cerebellar output to other (downstream) brain areas (Chan-Palay 1977; Teune et al. 2000). The DCN consist of different parts, from lateral to medial one can distinguish the dentate (lateral nucleus), emboliform and globose (interposed nuclei), and the fastigial (medial nucleus) (Fig 1B). Each nucleus receives afferent projections from specific areas of the cerebellar cortex that express different molecular markers (Sugihara and Shinoda 2007; Sugihara 2011). Output neurons in the cerebrocerebellum project predominantly to the lateral nuclei, neurons in the spinocerebellum project to the interposed and fastigial nuclei, and neurons in the vestibulocerebellum innervate the VN (Kandel et al. 2000).

1.1.2 Microstructure of the cerebellar cortex

The cerebellar cortex consists of different neuronal elements that together facilitate a general information processing pathway across multiple cerebellar regions, but also form local feedback and feedforward loops. In the cerebellar cortex, different layers can be identified based on their cytoarchitecture, where each layer consists of specific populations of neuronal cell-types. From the pia to deeper layers one can distinguish the molecular layer, the Purkinje cell layer and the granular layer (Fig 2). We will discuss each layer in order of neuronal information flow within the cerebellar cortex.

The main input layer in the cerebellar cortex is the *granular layer*. This layer consists primarily of a large number of granule cells (GCs), the most abundant cell-type in the brain. These are small glutamatergic neurons that have 3 to 4 short dendrites. Another cell-type

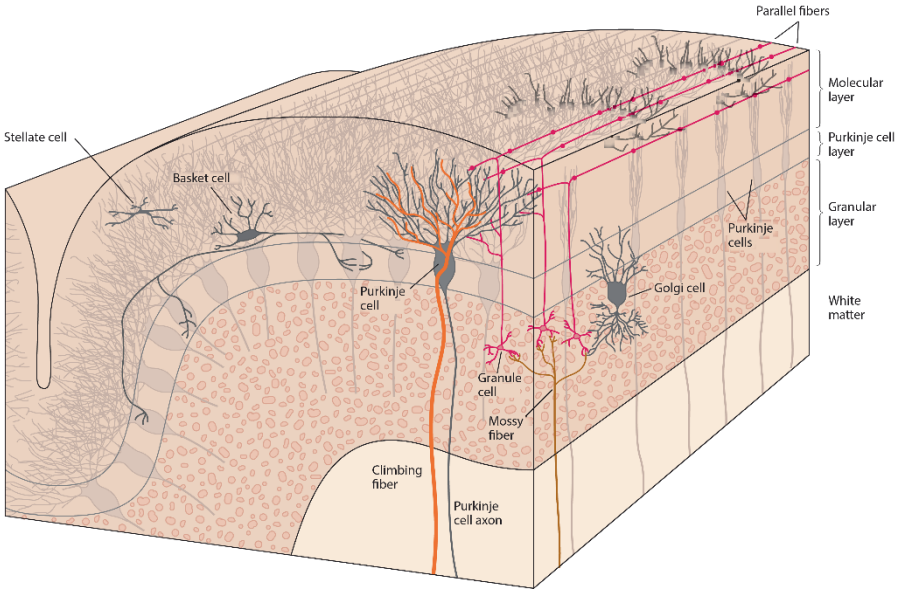

Fig 2. Cytoarchitecture of layers of the cerebellar cortex. Vertical section of a single cerebellar folium, indicating the position of the main neuronal cell-types across the three layers of the cerebellar cortex. Modified from: Kandel et al. (2013), with permission.

in the granular layer is the Golgi cell, a class of inhibitory neurons that can use γ-aminobutyric acid (GABA), glycine or a both as neurotransmitter (Cesana et al. 2013). Golgi cells provide feed-backward inhibition to GCs and their dendrites are located in the molecular layer. A third cell-type in the granular layer is an excitatory interneuron called the unipolar brush cell, which is located preferentially in the floccular and nodular regions (van Dorp and De Zeeuw 2014, 2015). Information from the granular layer is transmitted to the *molecular layer* via long 'T'-shaped' axons of GCs, called parallel fibers (PFs). PFs travel into the molecular layer, bifurcate and form axonal bundles traveling in the coronal plane, parallel to the lobular orientation. The molecular layer also contains a vast amount of Purkinje cell (PC) dendrites, which form a 'fan'-like structure oriented in the sagittal plane. PFs and PC dendritic arbors thus have a relative perpendicular orientation and because of this relative orientation, PFs can connect many PCs. Each PC can have approximately 100,000 *en passant* synaptic connections with many PFs. PFs can therefore have a widespread glutamate-based excitatory effect on PCs. The molecular layer contains several types of inhibitory interneurons, *i.e.* basket and stellate cells, which are collectively called molecular layer interneurons (MLIs). They use GABA as primary neurotransmitter to provide feed-forward inhibition to PCs, while receiving excitatory input from PFs. The inhibition from MLIs has been shown to be essential for motor learning, because removing $GABA_A$ receptor-mediated inhibition on PCs compromises learning performance (Wulff et al. 2009).

Neuronal information that is conveyed to PC dendrites in the molecular layer reaches the large somata (~40 µm diameter) of PCs, which are located in the *Purkinje cell layer*. This layer is essentially a mesh of neighboring PC somata and it has the thickness of one PC soma (Fig 2). PCs are the principal cell-type in the cerebellar cortex and they use GABA as neurotransmitter. Another type of cell that is located adjacent to PC somata is the Bergmann glia cell, a type of glia cell with processes extending radially through the molecular layer to reach the pia (De Blas 1984). In addition, bordering the Purkinje cell - and the granular layer are Lugaro cells, which are innervated by PCs and have an inhibitory effect on MLIs (Lainé and Axelrad 1998). PCs are the sole output neurons of the cerebellar cortex. The main axon projects to the DCN (De Zeeuw et al. 1994; Wylie et al. 1994) with collaterals to PCs (Witter et al. 2016) and GCs (Guo et al. 2016).

1.1.3 Microstructure of the cerebellar nuclei

The DCN are separated from the granular layer by a thick layer of white matter that contains bundles of myelinated axonal projections to and from the cerebellar cortex. DCN neurons receive a vast variety of axonal projections and by far the most prominent type of inputs are the axons from PCs, where ~860 PCs may connect to a single DCN neuron (Chan-Palay 1977; Palkovits et al. 1977; De Zeeuw and Berrebi 1995). The DCN consist of a diversity of neuronal cell-types with large differences in soma size (ranging from 8 to >40 µm), that can use glutamate, GABA or glycine as neurotransmitter (Chan-Palay 1977; McCrea et al. 1978; Aizenman et al. 2003; Uusisaari et al. 2007; Uusisaari and Knöpfel 2011, 2012; Husson et al. 2014). The large majority of DCN neurons (>95%) are projection neurons, highlighting the role of the DCN as final processing station providing the cerebellar output to downstream areas. A considerable proportion (~86.5%) of the medium and large sized neurons (soma >20 µm) project to the red nucleus and thalamus and ~73.2% of small neurons (soma <20 µm) project to the inferior olive (IO) (McCrea et al. 1978). The former medium and large projection neurons are glutamatergic, whereas the latter small neurons are GABAergic and inhibit neurons in the IO (Uusisaari et al. 2007; Uusisaari and Knöpfel 2011, 2012). Glutamatergic DCN projection neurons may form collaterals projecting to the granular layer, where they have an excitatory effect on Golgi cells and GCs (Tolbert et al. 1976; Gould and Graybiel 1976; Houck and Person 2015; Gao et al. 2016). GABA-glycinergic DCN neurons may also project to the granular and molecular layer, where they inhibit Golgi cells (Ankri et al. 2015).

1.1.4 Physiology of cerebellar nuclei neurons

DCN neurons are spontaneously active and their firing frequencies lie between 35 and 50 Hz *in vivo* (Thach 1968; LeDoux et al. 1998; Rowland and Jaeger 2005), although frequencies between 0 and 176.6 Hz have been measured in anesthetized mice (Canto et al. 2016).

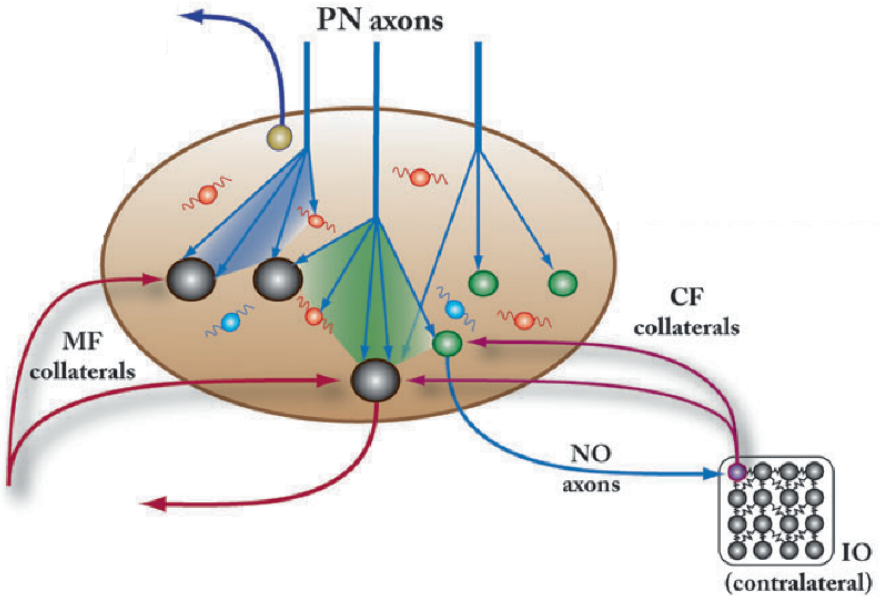

Fig 3. Overview of the cerebellar nuclei. The DCN consists of different neuronal cell-types including glutamatergic projection neurons (black cells), GABAergic projection neurons (green cells), GABA/glycinergic local neurons (blue cells), non-GABAergic neurons (orange cells) and nucleo-cortical neurons (yellow cell). Purkinje neuron axons ('PN axons') provide the main type of inhibitory input which, together with excitatory input from mossy fiber (MF) and climbing fiber (CF) collaterals, converge in the DCN. MF axons originate in several different precerebellar areas, whereas CF axons originate in the contralateral IO. Excitatory DCN output is provided by glutamatergic projection neurons and to a lesser extent by a population of nucleo-cortical projecting neurons (dark blue arrow). Part of the GABAergic neurons give rise to nucleo-olivary (NO) axons inhibiting IO neuron, thereby forming a local feedback circuit. Modified from: Uusisaari and De Schutter (2011), with permission.

In vitro recordings of neurons demonstrated that glutamic acid decarboxylase (GAD)-negative neurons (including large glutamatergic neurons) show higher spike frequencies compared to GAD-positive neurons (14.8 versus 9.9 Hz) (Uusisaari et al. 2007). As a result of both their unique connectivity as well as their intrinsic properties, DCN neurons show interesting physiological features (Jahnsen 1986; Canto et al. 2016; Yarden-Rabinowitz and Yarom 2017). DCN neurons receive a vast amount of PC inputs and since PCs are intrinsically active (Cerminara and Rawson 2004), each DCN neuron receives strong continuous inhibition from many PCs simultaneously (Bengtsson et al. 2011). Synchronous activity among PCs can lead to powerful inhibition of DCN neurons (Telgkamp and Raman 2002; Pedroarena and Schwartz 2003; Witter et al. 2013). In contrast, synchronized pauses in PC activity may lead to time-locked spiking in DCN neurons. PCs therefore tightly control spiking in DCN neurons (Gauck and Jaeger 2000, 2003; Person and Raman 2011). After cessation of strong synchronized PC inhibition, many DCN neurons show transient increases in spike frequency - so-called rebound activity (Aizenman and Linden 1999;

Alviña et al. 2008; Hoebeek et al. 2010; Witter et al. 2013). The ionic channels that facilitate this phenomenon are several types of calcium channels of which the T-type calcium channel is the most predominant (Aizenman and Linden 1999; Molineux et al. 2008; Hoebeek et al. 2010). The exact contribution of rebound potentiation however remains undecided (Reato et al. 2016). In **Chapter 2** we will describe the intra- and extracellular correlates of DCN neuronal physiology and associative behavior dependent on the cerebellum.

1.2 Olivo-cerebellar system

1.2.1 Input pathways

Neuronal information enters the cerebellum via two main pathways: the mossy fibers (MFs) and climbing fibers (CFs) (Fig 3). MFs originate from a myriad of pre-cerebellar areas, such as the pontine nuclei in the brainstem (Leergaard and Bjaarlie 2007). MF axons terminate in 'claw'-like structures (or mossy fiber boutons) that together with dendrites from GCs and axons from Golgi cells form glomeruli in the granular layer (Fig 2) (Hámori and Somogyi 1983; Jakab and Hámori 1988). One MF contacts many GCs, but one GC is usually contacted by four MF rosettes (Jörntell and Ekerot 2006). MFs can be active at very high instantaneous firing frequencies, with measurements showing over 700 Hz burst firing to occur *in vivo* (Rancz et al. 2007; Delvendahl and Hallermann 2016). Different types of MFs can be identified based on the expression of the molecular markers vesicular glutamate transporters (VGLUT) 1 and 2, which are organized in parasagittal stripes in the cerebellar cortex (Voogd et al. 2003; Hioki et al. 2003; Gebre et al. 2012).

Another cerebellar input pathway is formed by the CFs, which are long axonal projections from neurons in the IO, a brain area located in the ventral part of the brainstem (Fig 1A). CFs terminate in the molecular layer, where they wrap around the PC dendritic arbors - basically they 'climb up' to the PC and form many synaptic contacts using glutamate for excitatory neuronal transmission (Sugihara et al. 1999; Shinoda et al. 2000). CFs not only provide excitatory input to PCs, they also influence activity of MLIs through the process of glutamate spillover (Szapiro and Barbour 2007; Coddington et al. 2013). Although PCs receive input from different CFs during development (Crépel et al. 1976), in the adult cerebellum one PC receives input from only one CF and deviations from this process may result in motor deficits (Watanabe and Kano 2011; Kano et al. 2018). Both MFs and CFs have collaterals that directly innervate DCN neurons (Kitai et al. 1977; Andersson and Oscarsson 1978; Dietrichs et al. 1983; Brodal et al. 1986; Dietrichs and Walberg 1987; van der Want et al. 1989; De Zeeuw et al. 1997; Gauck and Jaeger 2003; Pugh and Raman 2006), where synapses are primarily formed at the dendrites (Chan-Palay 1977). Although the importance for MF collateral input to DCN physiology is indisputable (Gauck and Jaeger 2003; Pugh and Raman 2006, 2008, 2009), the role and significance of CF collaterals is still

debated (Pickford and Apps 2017). Several studies have observed much smaller excitatory currents from CF collaterals in adult compared to juvenile animals (Lu et al. 2016; Najac and Raman 2017), although other studies show that at least a part of DCN neurons receive considerable excitation that can lead to spike modulation (Audinat et al. 1992; Blenkinsop and Lang 2011). One possible hypothesis that has been put forward is that CF collateral input is particularly important during development for circuit formation (White and Sillitoe 2017) .

1.2.2 Olivo-cerebellar circuit physiology

Neuronal information that has entered the cerebellum generally travels along an anatomical loop between three brain regions, called the olivo-cerebellar circuit. This loop consists of the DCN, IO and cerebellar cortex (Fig 4). Within this circuit neurons are organized in spatial modules. Specific zones of PCs in the cerebellar cortex send inhibitory projections to defined clusters of target neurons in the DCN, while receiving CF input from specifically that part of the IO that receives inhibitory NO projections from the same neurons in the DCN (Ruigrok 2011). Neuronal signals thus flow between these regions in a closed-loop circuit, called a cerebellar module (Fig 4). A module can comprise multiple microzones, which are defined as clusters of neighboring PCs that are coherently active during particular physiological operations (Oscarsson 1979; De Zeeuw et al. 2011).

An important mechanism in the olivo-cerebellar circuit is synchronization of activity, particularly among PCs in the same cerebellar module. PCs have two types of action potentials: the simple spike (SS) and complex spike. SSs are intrinsically generated in PCs with average frequencies between 50-90 Hz (Zhou et al. 2014), whereas complex spikes are the result of CF activity and are much slower (on average 1-2 Hz) (Thach 1967, 1968). In the IO, neuronal discharges generate small bursts of axonal spikes that in PCs evoke a complex spike. In contrast to regular action potentials, a complex spike is a high-frequency burst where the main spike is followed by multiple spikelets (Davie et al. 2008). Synchrony in complex spike activity among PCs can occur following strong transient stimuli inducing conjunctive afferent input to the IO, such as an air puff in the eye. Since IO neurons are electrotonically connected via gap-junctions (Llinás et al. 1974), IO neurons can become active simultaneously, evoking synchronized complex spikes in PCs (Mathy et al. 2009; Bazzigaluppi et al. 2012). The level of gap-junction coupling between IO neurons is regulated by inhibitory NO fibers. When the activity of IO-projecting DCN neurons is lowered by artificially raising SS activity in PCs, an elevated complex spike synchrony can be observed (Marshall and Lang 2009), whereas reducing SS activity results in less complex spike synchrony and a lower complex spike frequency. IO-projecting DCN neurons thus control the level of coupling/decoupling of IO neurons (Fig 4).

Furthermore, altering the activity of one of the circuit components directly affects the other components. For example, activity in the IO also influences SS activity of PCs. By abolishing spontaneous CS activity through IO inactivation or lesioning a steady rise in SS frequency is caused (Cerminara and Rawson 2004). CFs thus exert both transient excitation (evoking complex spikes) and tonic inhibition (suppressing SSs) on PCs, the latter of which is likely to be caused by simultaneous activation of MLIs. Diminishing the activity in the IO also diminishes the activity in the DCN, which is caused by an increased SS frequency of PCs (Benedetti et al. 1983). In line with the modular organization of the cerebellar system, these changes are restricted to the affected cortical region.

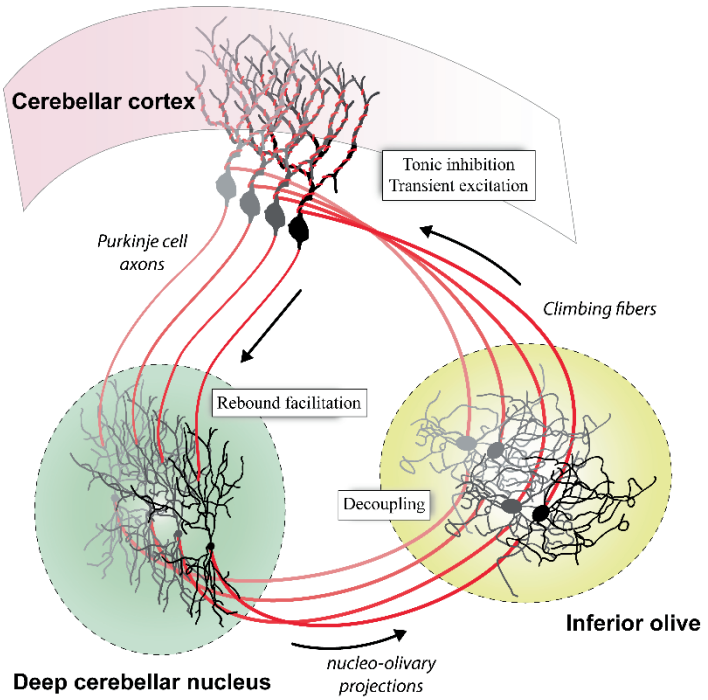

Fig 4. Simplified anatomy of the olivo-cerebellar circuit. Neuronal information travels in modular organization along the three-component loop. Axons from PCs in the cerebellar cortex inhibit DCN neurons and facilitate rebound activity after cessation of a strong inhibition. Inhibitory projections from nuclei neurons cause decoupling and restrict synchronous activity in the inferior olive. The effects of activity in the inferior olive are both tonic inhibition, as well as excitation causing complex spike activity in PCs. From: Broersen et al. (2016), with permission.

1.2.4 Plasticity in the cerebellum

Connections between neurons in the olivo-cerebellar circuit and afferent inputs are subject to changes in strength, *i.e.* they undergo different forms of plasticity. Research in the past

decades has focused on the cellular mechanisms of cerebellar learning. One of the most well-known theoretical frameworks is based on the work of David Marr and James Albus, who posited that motor learning in the cerebellar cortex involves synaptic plasticity between PFs and PCs, under the control of CFs (Marr 1969; Albus 1971). Masao Ito further developed this idea and this led to the Marr-Albus-Ito theory, which states that cerebellar learning depends on long-term depression (LTD) between PFs and PCs, a process that occurs under the supervision of CFs that transmit an error or 'teaching signal' (Ito 1984). During LTD, the activation of a synapse has a reduced effect on the postsynaptic target (connection becomes weaker), whereas during long-term potentiation (LTP) a synapse has an increased effect (connection becomes stronger). An error signal may arise when something unexpected or unanticipated happens, such as the occurrence of a corneal air puff or the execution of a limb movement that does not meet the expected or anticipated model of the movement.

Many studies have elaborated this classical model of cerebellar learning, by showing that plasticity occurs at various other locations within the circuit (Gao et al. 2012). Some studies have even challenged the classical view described above (Schonewille et al. 2011; Galliano and De Zeeuw 2014). In the DCN, a prominent location where both LTP and LTD has been shown to occur is between MFs and DCN neurons (Racine et al. 1986; Zhang and Linden 2006; Pugh and Raman 2006, 2008, 2009; Zheng and Raman 2010). Not only synaptic plasticity, but also structural plasticity takes place in the DCN. MF outgrowth and sprouting, as well as upregulation of excitatory terminals and changes in the ultrastructural morphology of MF synapses have been demonstrated during learning (Kleim et al. 2002; Weeks et al. 2007; Boele et al. 2013). Finally, learning-related changes in intrinsic excitability have been shown in PCs and DCN neurons (Schreurs et al. 1998; Hirono et al. 2018). Plasticity can be regulated at the cellular level by the presence of perineuronal nets (van 't Spijker and Kwok 2017), which we will discuss more in depth in the next section.

1.3 Perineuronal nets

1.3.1 Structure and function

A specialized extracellular matrix called the perineuronal net (PNN) enwraps different types of neurons in the central nervous system (CNS). This matrix wraps around the soma, proximal dendrites and axon initial segment of neurons, and its structure shows 'holes' where synaptic contacts are made on the neuronal surface (Fig 5A). The main components of PNNs are hyaluronan (HA), chondroitin sulfate proteoglycans (CSPGs), tenascin-R (Tn-R), and link proteins, which through specific interactions form dense 'net'-like aggregates on the surface of the soma, and in some neurons also the proximal dendrites (Celio et al. 1998; Kwok et al. 2011) (Fig 5B). HA is linear polymer of *N*-acetylglucosamine and glucuronic acid (GlcA) disaccharide units (Meyer et al. 1951) and is synthetized by different isoforms of the hyaluronan synthase (HAS) family, which are also responsible for

anchoring the PNN to the neuronal membrane (Kwok et al. 2010). Particularly, PNN-containing neurons in the cerebellum express HAS-2 and HAS-3 isoforms (Carulli et al. 2006). Anchored HA polymers form a backbone structure to which other components such as lecticans can bind. Lecticans are members of the CSPG family and consist of four forms: aggrecan, versican and neurocan and brevican. Which form is expressed depends on the cell-type (reviewed in Iozzo 1998; Kwok et al. 2011). The interaction between lecticans and HA is stabilized through local binding of link proteins. Link proteins are important for PNN stability, and knocking out the cartilage link protein Crtl1 (Hapln1) or the link protein Bral2 in the adult mouse has been shown to result in strongly attenuated PNNs throughout the brain (Carulli et al. 2010; Bekku et al. 2012). Further strengthening of PNNs is given by Tn-R, a glycoprotein that can bind up to three lecticans. Knock-out mice for Tn-R show a weak and diffuse distribution of CSPGs, suggesting that Tn-R is important for PNN structure (Weber et al. 1999). PNNs are formed late in postnatal development and play a crucial role in the maturation of synapses and closure of critical periods by limiting synaptic/structural plasticity (Wang and Fawcett 2012). PNNs restrict plasticity through different mechanisms, *e.g.* by blocking lateral diffusion of receptors and by providing a substrate for binding of chemorepulsive proteins (van 't Spijker and Kwok 2017).

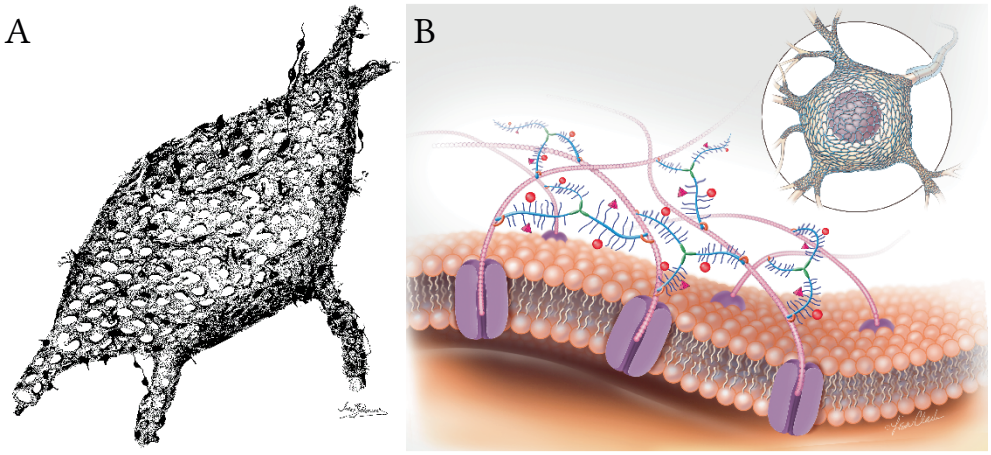

Fig. 5. Structure of the perineuronal net. (A) Detailed schematic drawing of a perineuronal net surrounding a large neuron in the cerebellar fastigial nucleus. Note the holes throughout the net, representing potential sites for synaptic boutons to connect. (B) Schematic drawing of the PNN in relation to the neuronal membrane. The core CSPGs are indicated in blue, with a number of sugar chains in dark purple. Membrane-anchored HAS enzymes (purple structures in the membrane) synthesize HA chains (pink balls) to which CSPGs are bound. This binding is strengthened by link proteins (orange). Tenascin-R (green) further stabilizes the PNN by binding to the CS-GAG-chains of CSPGs. Sema3A and Otx2 (pink pyramid and red ball, respectively) are bound to the sugar chains of CSPGs. (A) Modified from: Lafarga et al. 1984, with permission. (B) From: Carulli (2018), ©2018, Lisa A. Clark, www.clark-illustration.com, reuse with permission.

In the cerebellum PNNs are found around DCN neurons (Lafarga et al. 1984) in particular around the large glutamatergic (Kv3.1b-positive) neurons (Carulli et al. 2006). In the cerebellar cortex only Golgi cells show fully developed PNNs, whereas other abundant neuronal types such as GCs, PCs and MLIs show only a thin 'semiorganized matrix' (Carulli et al. 2006). Many studies use *Wisteria floribunda* agglutinin (WFA) staining to histochemically detect PNNs. WFA binds to CSPG-glycosaminoglycan (GAG) chains and other glycoproteins (Härtig et al. 1992).

1.3.2 Perineuronal nets and plasticity during behavior in the intact brain

To study the role of PNNs in behavior, many studies have used targeted digestion of PNNs with chondroitinase (ch'ase), an enzyme that breaks down the PNN component chondroitin sulfate. PNN digestion in the visual cortex has been shown to enable ocular dominance plasticity in adult animals after their critical period. Ocular dominance plasticity normally only occurs in juvenile animals (Pizzorusso et al. 2002; Carulli et al. 2010). Digestion of PNNs in the anterior interpositus nucleus (IntA) of the DCN has been shown to facilitate learning during eyeblink conditioning and to increase PC-mediated GABAergic transmission (Hirono et al. 2018). PNNs in the auditory cortex have also been shown to restrict plasticity and PNN removal restored juvenile plasticity (Happel et al. 2014). Together, these findings indicate that removal of PNNs may result in increased plasticity and enhanced learning. However, PNN digestion does not always lead to enhanced plasticity. Removal of PNNs in the auditory cortex reduces auditory fear conditioning (Banerjee et al. 2017) and removal of PNNs in the medial prefrontal cortex leads to impaired acquisition and reconsolidation of cocaine-induced conditioned place preference memory (Slaker et al. 2015). Moreover, it has been shown that PNNs in the amygdala are essential for fear memory retention in adult rodents (Gogolla et al. 2009; Xue et al. 2014).

Environmental changes can also alter the morphology of PNNs. In the cerebellum, PNNs enwrapping DCN neurons have been shown to undergo morphological changes in adult mice that were placed in an enriched environment (Foscarin et al. 2011), effects that were accompanied by changes in both excitatory and inhibitory terminals. This demonstrates that some forms of memory are restricted by PNNs, whereas others depend on intact PNNs and their dynamic regulation. Exactly which molecules residing in the PNN are responsible for those effects remains to be elucidated. In **Chapter 3** we will further describe the interplay between PNNs and associative learning, showing that PNNs in the DCN may exert a tight control over plasticity. The behavioral paradigm that we used for **Chapter 2 and 3** is Pavlovian eyeblink conditioning (EBC), the focus of our next section.

1.4 Cerebellar-dependent behavior

A number of behavioral paradigms are available to study mechanisms underlying cerebellar learning in rodents. The most often used are the accelerating rotarod (Shiotsuki et al. 2010), compensatory eye movements: the optokinetic reflex (OKR) and vestibuloocular reflex (VOR) (Alphen et al. 2002), the Erasmus ladder (Cupido 2009) and EBC, the latter of which we will focus on next.

1.4.1 Pavlovian eyeblink conditioning

1.4.1.1 Basic principles

A paradigm that has been used extensively to investigate mechanisms of cerebellar motor learning is delayed EBC. It relies on the same principle underlying the well-known 'salivating dog' experiments performed by the Russian physiologist Ivan Pavlov (1849-1936). During his experiments a neutral conditioned stimulus (CS; sound of a bell) was paired with an unconditioned stimulus (US; presentation of food), which caused a reflexive behavior or unconditioned response (UR; salivation). After repeated pairing of the sound of the bell (CS) and food (US), the dog showed salivation after the bell alone, in anticipation of the food. This salivation reaction is called a conditioned response (CR) and represents the behavioral result of this form of classical conditioning. In EBC, the CS is usually a light or tone. The US is usually an air puff directed at the eye. The UR is an eyelid closure (or eyeblink) caused by the US. The resulting behavior after paired presentation of CS and US is an anticipatory eyelid closure following the CS (CR), effectively closing the eye before the air puff arrives at the cornea (Ivarsson and Svensson 2000). It is a relatively straightforward paradigm and an excellent tool to study associative-learning mechanisms.

1.4.1.2 Involved cerebellar circuitry

Many studies contributed to mapping out the brain circuits involved in this paradigm. Studies in the 70s by Oakley and Russell first showed that the cerebral cortex is not important for acquisition of CRs (Oakley and Russell 1972, 1975, 1976), which hinted researchers towards the cerebellar circuit. Subsequent lesion studies showed that the medial parts of the rostral dorsal accessory olive (DAO) and principal olive (PO) of the IO are essential (Yeo et al. 1986; Zbarska et al. 2007), as well as the pontine nuclei (Bao et al. 2000) and the middle cerebellar peduncle (Solomon et al. 1986; Lewis et al. 1987). In the cerebellum, a functional dichotomy was shown between the cerebellar cortex and DCN, where inactivation of the IntA resulted in clear loss of performance in conditioned animals (Clark et al. 1984; Lavond et al. 1985; Bracha et al. 1994; Bao et al. 2000; Freeman and Rabinak 2004; Ohyama et al. 2006; Mojtahedian et al. 2007) and prevented CR acquisition (Yeo et al. 1985; Lavond and Steinmetz 1989; Sears and Steinmetz 1990; Freeman et al. 2005).

Lesions to the cerebellar cortex lobule HVI in conditioned animals did not fully abolish CRs, but strongly affected their profile and timing (McCormick and Thompson 1984; Perrett et al. 1993; Garcia et al. 1999, but see also: McCormick et al. 1981, 1982). During acquisition, inactivation of lobule HVI prevented the learning of conditioned behavior completely (Yeo and Hardiman 1992; Garcia et al. 1999; Attwell et al. 2001, but see also: Lavond and Steinmetz 1989; Lavond 2002). Electrophysiological studies further implicated the cerebellum (McCormick et al. 1981, 1982), where activity of cerebellar cortex and interposed nuclei neurons is related to learned behavior (McCormick and Thompson 1984; Berthier and Moore 1986, 1990; Hesslow 1994; Mostofi et al. 2010; Heiney et al. 2014; Ten Brinke et al. 2015; Ten Brinke et al. 2017). Modern non-invasive tools such as 7T fMRI have further allowed us to observe simultaneous activity in cerebellar lobule HVI and IntA during EBC in humans (Thürling et al. 2015).

Our current understanding of the cerebellar circuit involved in EBC is shown in Fig 6. Its modular connections follow a closed-loop format as discussed earlier. In this circuit, CS information enters the cerebellum via MF projections from parts of the pontine nuclei, depending on the sensory modality (Leergaard and Bjaarlie 2007). US information is relayed to the cerebellum via the CF pathway, signaling both expected and unexpected errors and evoking complex spikes in PCs (Ohmae and Medina 2015; Ten Brinke et al. 2015). Eyeblink-related PCs involved in this closed loop circuit are largely Zebrin-II-negative and show high firing rates (Zhou et al. 2014).

1.4.1.3 Cerebellar plasticity during EBC

Multiple forms of plasticity take place during EBC in both the cerebellar cortex and nuclei (Freeman and Steinmetz 2011; Gao et al. 2012). It has been hypothesized that a memory trace is first formed in the cerebellar cortex and then transsynaptically shifts towards the DCN for long-term memory consolidation (Shutoh et al. 2006). In the cerebellar cortex, one of the hallmark features of conditioning is that PCs develop a marked decrease in SS activity coinciding with the emergence of CRs (Berthier and Moore 1986; Jirenhed et al. 2007; Ten Brinke et al. 2015). By developing a suppression of SS activity, PCs disinhibit neurons in the DCN, which in turn may result in rebound activity in these cells. Rebound activity may be facilitated by excitatory inputs from MF and/or CF collaterals (De Zeeuw et al. 2011). One mechanism that has been proposed to cause SS suppression is activation of mGluR7 receptors at the PF-PC synapse (Johansson et al. 2015, 2016). PC inhibition through activation of MLIs may also be involved and these mechanisms could work in concert (Boele et al. 2018). US-evoked complex spike activity is widely seen in PCs and is important for plasticity, because prolonging the complex spike pause enhances conditioning, possibly by facilitating PF-PC LTD (Maiz et al. 2012). More recently complex spike activity following the CS alone (CS-evoked complex spike) has been shown to occur in conditioned animals (Ohmae and Medina 2015; Ten Brinke et al. 2015).

During conditioning, changes in dendritic membrane excitability have been shown in PCs (Schreurs et al. 1998), as well as IntA neurons (Wang et al. 2018). These changes may contribute to task-related spike activity changes at the level of the DCN (Gould and Steinmetz 1996). Moreover, excitatory terminals in the DCN are upregulated during conditioning where MF terminals undergo sprouting and outgrowth (Kleim et al. 2002; Boele et al. 2013). Not only the number of terminals but also increases in synapse length have been shown (Weeks et al. 2007).

Conditioning is reversible, when the CS and US are randomly paired, the CRs as well as the PC SS response are concurrently extinguished. The NO projection plays an important role in extinction of the CRs. Blocking the inhibitory input to the IO prevents extinction of the CRs (Medina et al. 2002) and stimulation of these projections during pairing of the CS and US leads to altered IO transmission, resulting in gradual extinction of the CR (Bengtsson et al. 2007). However, relearning after extinction (or reacquisition) occurs with an increased rate compared to the initial acquisition rate. It is thought that previously formed connections (or 'savings') may facilitate quicker relearning after extinction (Medina et al. 2001).

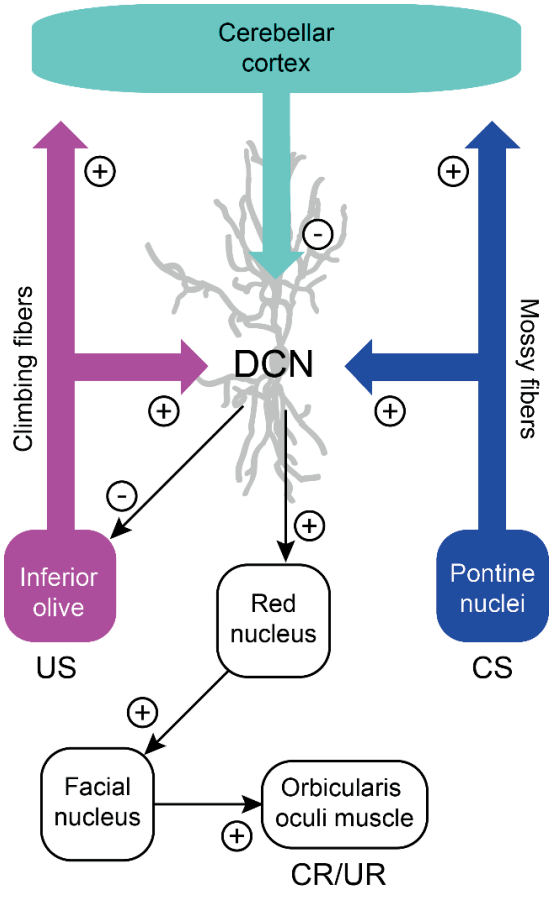

Fig. 6. Schematic diagram of the cerebellar circuit underlying EBC. CS information enters the cerebellar network through mossy fiber connections originating in the pontine nuclei, projecting directly to the EBC-involved regions of the DCN and the cerebellar cortex. US information is conveyed by climbing fibers from the inferior olive in the brainstem, via projections to the cerebellar cortex as well as the DCN. GABAergic DCN output neurons inhibit neurons in the inferior olive and excitatory projection neurons in the DCN provide the cerebellar output to downstream motor nuclei, eventually causing the CR and possibly contributing to the UR. + and - symbols indicate excitatory and inhibitory projections, respectively. Modified from: Canto, Broersen & De Zeeuw, (2018), with permission.

1.4.2 Human psychophysiology

In this thesis, whereas common behavioral paradigms were used for the rodent experimental work, the psychophysical experiments with human subjects were specifically tailored to test behavior associated with timing mechanisms in the cerebellum. We will first briefly review evidence for the role of the cerebellum in time processing.

1.4.2.1 Timing and the cerebellum

It is widely accepted that the cerebellum contributes to time processing particularly in the sub-second range, whereas supra-second timing seems to rely on a broader network including the cerebellum, frontal areas and basal ganglia (Ivry and Keele 1989; Ivry 1996; Mangels et al. 1998; Ivry et al. 2002; Dreher and Grafman 2002; Jahanshahi et al. 2006; Lee et al. 2007; Koch et al. 2007; Fierro et al. 2007; Bueti et al. 2008; Meck et al. 2008; Aso et al. 2010; Spencer and Ivry 2013). Timing in experimental tasks can be explicit, where an overt estimation of time is required, or implicit, where a time estimation is used to reach the goal of a non-temporal task (Coull and Nobre 2008). The work in this thesis focused primarily on implicit timing in the millisecond-range.

Evidence has pointed towards cerebellar involvement in both types of timing. Neuroimaging studies have reported cerebellar activation during explicit (Rao et al. 1997; Jänke et al. 2000; Pollok et al. 2008), as well as implicit timing tasks (Bueti et al. 2008; Bareš et al. 2011), where cerebellar activation may coincide with activation in the cerebral cortex (Aso et al. 2010; Onuki et al. 2015). Implicit timing also plays a prominent role in EBC, where the cerebellum is essential for the timed execution of a movement, as discussed previously. Cerebellar patient and lesion studies have further demonstrated the importance of the cerebellum in temporal processing using a variety of task conditions, where cerebellar damage results in diminished performance (Ivry et al. 1988; Ivry and Keele 1989; Casini and Ivry 1999; Bareš et al. 2007; Bareš et al. 2010; Grube et al. 2010; Matsuda et al. 2015). In addition to the explicit versus implicit timing dissociation, a further taxonomy of timing can be made based on the continuity of events, highlighting a cerebellar contribution particularly to event timing (isolated temporal intervals), rather than continuous timing (Ivry et al. 2002; Zelaznik et al. 2002; Spencer et al. 2003, 2005, 2007; Breska and Ivry 2016; Bareš et al. 2018).

The cerebellar anatomy has been proposed to be appropriate for time processing, a hypothesis that has been put forward some time ago (Braitenberg 1961, 1967). This is most prominent at the level of GCs, where temporally precise information evokes high-frequency spike bursts in normally silent GCs, facilitating reliable and fast information transduction with a high signal-to-noise ratio (Chadderton et al. 2004; Rancz et al. 2007). Together with particular properties of other cerebellar circuit components that depend on the temporally precise activation of afferents, such as rebound spiking of DCN neurons, this makes the cerebellum optimally suited for carrying out temporally precise computations (De Zeeuw et al. 2011). A recognized theoretical model of how the cerebellum can contribute to timing and motor execution involves the use of internal models. In the 'forward model' the neural representation of a prediction of the motor system in a future state is based on present external sensory input and the motor command. An 'inverse model' is the neural representation of the transformation of the desired state into motor commands to reach that state (Miall and Wolpert 1996; Wolpert et al. 1998). Cerebellar damage or disorders may compromise the ability of the cerebellum to apply these models.

1.4.2.2 Cerebellar dysfunction in spinocerebellar ataxia type 6

Other indications for temporal processing in the cerebellum are evident when studying the nature of the symptoms occurring during the progression of cerebellar ataxias. In **Chapter 5 and 6** of this thesis, studies were carried out with patients diagnosed with spinocerebellar ataxia type 6 (SCA6). SCA6 is a late-onset autosomal dominant genetic disorder with an estimated prevalence of less than 1 in 100,000. Geographically it is most prevalent in Germany, Japan, Korea and Australia (Geschwind et al. 1997; Soong et al. 2001; Stoyas and La Spada 2018). The average age of onset is variable and lies between 45-52 years, but may range from 19 to 71 years (Geschwind et al. 1997; Schöls et al. 1998). Patients experience a range of slowly progressing symptoms including truncal, gait and appendicular ataxia, dysarthria, imbalance, upper limb incoordination and tremor. Most patients also experience impaired eye movements, such as diplopia, dysmetric saccades, impaired smooth pursuit and downbeat nystagmus (Gomez et al. 1997; Geschwind et al. 1997; Schöls et al. 1998; Yabe et al. 2003; Solodkin and Gomez 2011; Bunn et al. 2015; Falcon et al. 2015). Some of these eye movement impairments may already be present in the presymptomatic SCA6 phase (Christova et al. 2008). Contrasting findings have been published regarding the effect of SCA on cognitive functions (Globas et al. 2003; Suenaga et al. 2008).

The disease is caused by a CAG repeat expansion at the 3' end of the CACNA1A4 locus on chromosome 19p13, which encodes the α1A ($Ca_v2.1$) subunit of the neuronal P/Q-type voltage-gated calcium channel (Gomez et al. 1997; Zhuchenko et al. 1997; Jodice et al. 1997; Solodkin and Gomez 2011; Stoyas and La Spada 2018). Normal alleles carry between 4 and 18 CAG repeats, but in SCA6 this number is between 19 and 33 (Zhuchenko et al. 1997; Matsuyama 1997; Soong et al. 2001). The age of onset is inversely correlated with the number of CAG repeats (Matsuyama 1997; Geschwind et al. 1997). SCA6 is considered to a

pure cerebellar disorder, caused by a predominant loss of PCs through the occurrence of cytoplasmic aggregations of α1A channel proteins (Ishikawa et al. 1999; Koeppen 2005). To clinically assess the severity of symptoms during progression of SCA6, one can use the Scale of the Assessment and Rating of Ataxia (SARA) (Schmitz-Hübsch et al. 2006; Saute et al. 2012). Subjects are scored on 8 items (gait, stance, sitting, speech disturbance, finger chase, nose-finger test, fast alternating hand movements and heel-shin slide) which serve as an adequate metric for the neurological manifestations of SCA6 (Weyer et al. 2007).

1.5 Scope of this thesis

There is consensus on the involvement of the cerebellum in forms of motor learning and timing processes. Its exact contribution to temporal processing during different behaviors, such as precisely timed execution of conditioned eyelid movements, spatio-temporal trajectory prediction and perceiving hand/arm actions, remains to be elucidated. Furthermore, the cerebellar neuronal mechanisms that underlie these behaviors still have to be disclosed. Both are important issues that have motivated the work described in this thesis.

Chapter 2 provides a detailed study on the intra- and extracellular electrophysiological characteristics of DCN neurons during delayed EBC, a paradigm where precise timing is imperative. The DCN provide the sole output of the cerebellum and this area is a particularly important hub for controlling eyelid behavior. Using a combination of whole-cell recordings in awake behaving animals, input-specific optogenetic modulation of neuronal activity and histology, we ask the following questions: (i) what is the contribution of afferent inputs to task-related activity in the DCN, (ii) what learning-related changes occur in these afferents, and (iii) how do they contribute to conditioned behavior? This study provides for the first time insight in membrane potential fluctuations occurring in DCN neurons during EBC.

In **Chapter 3** we describe how PNNs in the DCN, known regulators of plasticity, are involved in motor learning during EBC. We first investigated whether PNNs are adaptive during learning, *i.e.* do they show learning-associated changes in morphology? We then proceeded by enzymatically decreasing these PNNs while examining the resulting effect on learning and long-term memory retention. Since PNNs are an important for structural plasticity and a potential imbalance between inhibitory and excitatory inputs could lead to physiological changes, we asked whether enzymatically decreasing PNNs influences the temporal characteristics of DCN physiology. This study emphasizes the role of extracellular matrix macromolecules in motor learning and consolidation, as well as the physiology of DCN neurons.

With **Chapter 4** the step is made from rodent work to human psychophysical experiments. Elite athletes have optimized neuronal circuits for excellent performance in demanding

situations such as sport at the national level. The aim of this study is to investigate (i) the cerebellar activation correlates of spatio-temporal trajectory prediction, (ii) how a trained cerebellar network in athletes contributes to superior feedback control, and (iii) whether athletes exhibit changed eye movements and cognitive load dynamics. The results indicate that the cerebellum, as part of a larger neuronal network, becomes active in tasks that require optimal feedback control and time processing, where athletes may employ cost-efficient cognitive mechanisms to achieve optimal performance.

In contrast to athletes, cerebellar patients have an impaired ability to interpret temporal information. In **Chapter 5** a study is presented investigates the role of the cerebellum in interpreting kinematic information from actions made by others. The following main questions are posed: is the cerebellum recruited during the observation of meaningful hand/arm actions and does cerebellar dysfunction associated with SCA6 influence the ability to judge the weight of an object being lifted based on movement kinematics? Evidence is presented that answers these questions, which points towards a cerebellar involvement in perceiving action kinematics. This study sets the stage for the study described in the next chapter.

Having established that the cerebellum is recruited during perceiving kinematic information, in **Chapter 6** we further describe the effects of SCA6 on spatio-temporal trajectory prediction. Using a task requiring the latter process as a basis for making well-timed finger movements, we asked how cerebellar dysfunction influences this process and how learning of temporal intervals is affected. In line with contemporary views, cerebellar patients do show impairments on temporal processing and learning in this task.

In **Chapter 7** we discuss the findings described in this thesis in relation to the literature and current views on cerebellar function.

1.6 References

Adamaszek M, D'Agata F, Ferrucci R, et al (2016) Consensus Paper: Cerebellum and Emotion. The Cerebellum. doi: 10.1007/s12311-016-0815-8

Aizenman CD, Huang EJ, Linden DJ (2003) Morphological Correlates of Intrinsic Electrical Excitability in Neurons of the Deep Cerebellar Nuclei. J Neurophysiol 89:1738–1747. doi: 10.1152/jn.01043.2002

Aizenman CD, Linden DJ (1999) Regulation of the rebound depolarization and spontaneous firing patterns of deep nuclear neurons in slices of rat cerebellum. J Neurophysiol 82:1697–1709

Albus JS (1971) A theory of cerebellar function. Math Biosci 10:25–61

Alphen AM, Schepers T, Luo C, Zeeuw CI (2002) Motor Performance and Motor Learning in Lurcher Mice. Ann N Y Acad Sci 978:413–424. doi: 10.1111/j.1749-6632.2002.tb07584.x

Alviña K, Walter JT, Kohn A, et al (2008) Questioning the role of rebound firing in the cerebellum. Nat Neurosci 11:1256–1258. doi: 10.1038/nn.2195

Andersson G, Oscarsson O (1978) Projections to lateral vestibular nucleus from cerebellar climbing fiber zones. Exp Brain Res 32:. doi: 10.1007/BF00239552

Ankri L, Husson Z, Pietrajtis K, et al (2015) A novel inhibitory nucleo-cortical circuit controls cerebellar Golgi cell activity. eLife 4:. doi: 10.7554/eLife.06262

Aso K, Hanakawa T, Aso T, Fukuyama H (2010) Cerebro-cerebellar interactions underlying temporal information processing. J Cogn Neurosci 22:2913–2925

Attwell PJE, Rahman S, Yeo CH (2001) Acquisition of Eyeblink Conditioning Is Critically Dependent on Normal Function in Cerebellar Cortical Lobule HVI. J Neurosci 21:5715–5722. doi: 10.1523/JNEUROSCI.21-15-05715.2001

Audinat E, Gähwiler BH, Knöpfel T (1992) Excitatory synaptic potentials in neurons of the deep nuclei in olivo-cerebellar slice cultures. Neuroscience 49:903–911. doi: 10.1016/0306-4522(92)90366-A

Banerjee SB, Gutzeit VA, Baman J, et al (2017) Perineuronal Nets in the Adult Sensory Cortex Are Necessary for Fear Learning. Neuron 95:1–11. doi: 10.1016/j.neuron.2017.06.007

Bao S, Chen L, Thompson RF (2000) Learning- and cerebellum-dependent neuronal activity in the lateral pontine nucleus. Behav Neurosci 114:254–261. doi: 10.1037//0735-7044.114.2.254

Bareš M, Apps R, Avanzino L, et al (2018) Consensus paper: Decoding the Contributions of the Cerebellum as a Time Machine. From Neurons to Clinical Applications. The Cerebellum 18:266-286. doi: 10.1007/s12311-018-0979-5

Bareš M, Lungu O, Liu T, et al (2007) Impaired predictive motor timing in patients with cerebellar disorders. Exp Brain Res 180:355–365

Bareš M, Lungu OV, Husárová I, Gescheidt T (2010) Predictive Motor Timing Performance Dissociates Between Early Diseases of the Cerebellum and Parkinson's Disease. The Cerebellum 9:124–135. doi: 10.1007/s12311-009-0133-5

Bareš M, Lungu O V, Liu T, et al (2011) The neural substrate of predictive motor timing in spinocerebellar ataxia. The Cerebellum 10:233–244

Barton RA, Venditti C (2014) Rapid Evolution of the Cerebellum in Humans and Other Great Apes. Curr Biol 24:2440–2444. doi: 10.1016/j.cub.2014.08.056

Baumann O, Borra RJ, Bower JM, et al (2015) Consensus Paper: The Role of the Cerebellum in Perceptual Processes. The Cerebellum 14:197–220. doi: 10.1007/s12311-014-0627-7

Bazzigaluppi P, De Gruijl JR, van der Giessen RS, et al (2012) Olivary subthreshold oscillations and burst activity revisited. Front Neural Circuits 6:1-13. doi: 10.3389/fncir.2012.00091

Bekku Y, Saito M, Moser M, et al (2012) Bral2 is indispensable for the proper localization of brevican and the structural integrity of the perineuronal net in the brainstem and cerebellum. J Comp Neurol 520:1721–1736. doi: 10.1002/cne.23009

Benedetti F, Montarolo PG, Strata P, Tempia F (1983) Inferior olive inactivation decreases the excitability of the intracerebellar and lateral vestibular nuclei in the rat. J Physiol 340:195–208

Bengtsson F, Ekerot C-F, Jörntell H (2011) In Vivo Analysis of Inhibitory Synaptic Inputs and Rebounds in Deep Cerebellar Nuclear Neurons. PLoS ONE 6:e18822. doi: 10.1371/journal.pone.0018822

Bengtsson F, Jirenhed D-A, Svensson P, Hesslow G (2007) Extinction of conditioned blink responses by cerebello-olivary pathway stimulation. Neuroreport 18:1479–1482

Berthier NE, Moore JW (1986) Cerebellar Purkinje cell activity related to the classically conditioned nictitating membrane response. Exp Brain Res 63:341–350

Berthier NE, Moore JW (1990) Activity of deep cerebellar nuclear cells during classical conditioning of nictitating membrane extension in rabbits. Exp Brain Res 83:44–54

Blenkinsop TA, Lang EJ (2011) Synaptic Action of the Olivocerebellar System on Cerebellar Nuclear Spike Activity. J Neurosci 31:14708–14720. doi: 10.1523/JNEUROSCI.3323-11.2011

Boele H-J, Koekkoek SKE, De Zeeuw CI, Ruigrok TJH (2013) Axonal Sprouting and Formation of Terminals in the Adult Cerebellum during Associative Motor Learning. J Neurosci 33:17897–17907. doi: 10.1523/JNEUROSCI.0511-13.2013

Boele H-J, Peter S, Brinke MMT, et al (2018) Impact of parallel fiber to Purkinje cell long-term depression is unmasked in absence of inhibitory input. Sci Adv 9. doi: 10.1126/sciadv.aas9426

Bracha V, Webster ML, Winters NK, et al (1994) Effects of muscimol inactivation of the cerebellar interposed-dentate nuclear complex on the performance of the nictitating membrane response in the rabbit. Exp Brain Res 100:453–468

Braitenberg V (1961) Functional Interpretation of Cerebellar Histology. Nature 190:539–540

Braitenberg V (1967) Is the Cerebellar Cortex a Biological Clock in the Millisecond Range? In: Progress in Brain Research. Elsevier, pp 334–346

Breska A, Ivry RB (2016) Taxonomies of timing: where does the cerebellum fit in? Curr Opin Behav Sci 8:282–288. doi: 10.1016/j.cobeha.2016.02.034

Brodal P, Dietrichs E, Walberg F (1986) Do pontocerebellar mossy fibres give off collaterals to the cerebellar nuclei? An experimental study in the cat with implantation of crystalline HRP-WGA. Neurosci Res 4:12–24

Broersen R, Winkelman BHJ, Ozyildirim O, De Zeeuw CI (2016) Physiology of Olivo-Cerebellar Loops. In: Essentials of cerebellum and cerebellar disorders. Gruol D., Koibuchi N., Manto M., Molinari M., Schmahmann J., Shen Y. (eds.). Springer, Cham

Bueti D, Walsh V, Frith C, Rees G (2008) Different brain circuits underlie motor and perceptual representations of temporal intervals. J Cogn Neurosci 20:204–214

Bunn LM, Marsden JF, Voyce DC, et al (2015) Sensorimotor processing for balance in spinocerebellar ataxia type 6: SENSORIMOTOR PROCESSING IN SCA6. Mov Disord 30:1259–1266. doi: 10.1002/mds.26227

Canto CB, Broersen R, De Zeeuw CI (2018) Intrinsic excitement in cerebellar nuclei neurons during learning. PNAS 115:9824–9826

Canto CB, Witter L, De Zeeuw CI (2016) Whole-Cell Properties of Cerebellar Nuclei Neurons In Vivo. PloS One 11:e0165887

Carulli D (2018) Perineuronal Nets: A Mechanism to Control Brain Plasticity. Sci. Mag.

Carulli D, Pizzorusso T, Kwok JCF, et al (2010) Animals lacking link protein have attenuated perineuronal nets and persistent plasticity. Brain 133:2331–2347. doi: 10.1093/brain/awq145

Carulli D, Rhodes KE, Brown DJ, et al (2006) Composition of perineuronal nets in the adult rat cerebellum and the cellular origin of their components. J Comp Neurol 494:559–577. doi: 10.1002/cne.20822

Casini L, Ivry RB (1999) Effects of divided attention on temporal processing in patients with lesions of the cerebellum or frontal lobe. Neuropsychology 13:10

Celio MR, Spreafico R, De Biasi S, Vitellaro-Zuccarello L (1998) Perineuronal nets: past and present. Trends Neurosci 21:510–515. doi: 10.1016/S0166-2236(98)01298-3

Cerminara NL, Rawson JA (2004) Evidence that Climbing Fibers Control an Intrinsic Spike Generator in Cerebellar Purkinje Cells. J Neurosci 24:4510–4517. doi: 10.1523/JNEUROSCI.4530-03.2004

Cesana E, Pietrajtis K, Bidoret C, et al (2013) Granule Cell Ascending Axon Excitatory Synapses onto Golgi Cells Implement a Potent Feedback Circuit in the Cerebellar Granular Layer. J Neurosci 33:12430–12446. doi: 10.1523/JNEUROSCI.4897-11.2013

Chadderton P, Margrie TW, Hausser M (2004) Integration of quanta in cerebellar granule cells during sensory processing. Nature 428:856–860. doi: 10.1038/nature02467

Chan-Palay V (1977) Cerebellar dentate nucleus. Organization, cytologyand transmitters. Springer Berl 126:275–280

Christova P, Anderson JH, Gomez CM (2008) Impaired eye movements in presymptomatic spinocerebellar ataxia type 6. Arch Neurol 65:530–536

Clark GA, McCormick DA, Lavond DG, Thompson RF (1984) Effects of lesions of cerebellar nuclei on conditioned behavior and hippocampal neuronal responses. Brain Res 291:125–136

Coddington LT, Rudolph S, Vande Lune P, et al (2013) Spillover-Mediated Feedforward Inhibition Functionally Segregates Interneuron Activity. Neuron 78:1050–1062. doi: 10.1016/j.neuron.2013.04.019

Coull JT, Nobre AC (2008) Dissociating explicit timing from temporal expectation with fMRI. Curr Opin Neurobiol 18:137–144. doi: 10.1016/j.conb.2008.07.011

Crépel F, Mariani J, Delhaye-Bouchaud N (1976) Evidence for a multiple innervation of purkinje cells by climbing fibers in the immature rat cerebellum. J Neurobiol 7:567–578. doi: 10.1002/neu.480070609

Cupido A (2009) Detecting Cerebellar Phenotypes with the Erasmus Ladder. Erasmus University Rotterdam

Davie JT, Clark BA, Hausser M (2008) The Origin of the Complex Spike in Cerebellar Purkinje Cells. J Neurosci 28:7599–7609. doi: 10.1523/JNEUROSCI.0559-08.2008

De Blas AL (1984) Monoclonal antibodies to specific astroglial and neuronal antigens reveal the cytoarchitecture of the Bergmann glia fibers in the cerebellum. J Neurosci 4:465–273

De Zeeuw CI, Berrebi AS (1995) Postsynaptic Targets of Purkinje Cell Terminals in the Cerebellar and Vestibular Nuclei of the Rat. Eur J Neurosci 7:2322–2333. doi: 10.1111/j.1460-9568.1995.tb00653.x

De Zeeuw CI, Hoebeek FE, Bosman LWJ, et al (2011) Spatiotemporal firing patterns in the cerebellum. Nat Rev Neurosci 12:327–344. doi: 10.1038/nrn3011

De Zeeuw CI, Van Alphen AM, Hawkins RK, Ruigrok TJH (1997) Climbing fiber collaterals contact neurons in the cerebellar nuclei that provide a GABAergic feedback to the inferior olive. Neuroscience 80:981–986

De Zeeuw CI, Wylie DR, Digiorgi PL, Simpson JI (1994) Projections of individual purkinje cells of identified zones in the flocculus to the vestibular and cerebellar nuclei in the rabbit. J Comp Neurol 349:428–447. doi: 10.1002/cne.903490308

De Zeeuw CI, Wylie DR, Stahl JS, Simpson JI (1995) Phase relations of Purkinje cells in the rabbit flocculus during compensatory eye movements. J Neurophysiol 74:2051–2064

Delvendahl I, Hallermann S (2016) The Cerebellar Mossy Fiber Synapse as a Model for High-Frequency Transmission in the Mammalian CNS. Trends Neurosci. doi: 10.1016/j.tins.2016.09.006

Dietrichs E, Bjaalie JG, Brodal P (1983) Do pontocerebellar fibers send collaterals to the cerebellar nuclei? Brain Res 259:127–131

Dietrichs E, Walberg F (1987) Cerebellar nuclear afferents—where do they originate? Anat Embryol (Berl) 177:165–172

Dreher J-C, Grafman J (2002) The roles of the cerebellum and basal ganglia in timing and error prediction: Cerebellar and striatal functions in timing and error prediction. Eur J Neurosci 16:1609–1619. doi: 10.1046/j.1460-9568.2002.02212.x

Falcon MI, Gomez CM, Chen EE, et al (2015) Early Cerebellar Network Shifting in Spinocerebellar Ataxia Type 6. Cereb Cortex bhv154. doi: 10.1093/cercor/bhv154

Fierro B, Palermo A, Puma A, et al (2007) Role of the cerebellum in time perception: A TMS study in normal subjects. J Neurol Sci 263:107–112. doi: 10.1016/j.jns.2007.06.033

Foscarin S, Ponchione D, Pajaj E, et al (2011) Experience-Dependent Plasticity and Modulation of Growth Regulatory Molecules at Central Synapses. PLoS ONE 6:e16666. doi: 10.1371/journal.pone.0016666

Freeman JH, Halverson HE, Poremba A (2005) Differential Effects of Cerebellar Inactivation on Eyeblink Conditioned Excitation and Inhibition. J Neurosci 25:889–895. doi: 10.1523/JNEUROSCI.4534-04.2005

Freeman JH, Rabinak CA (2004) Eyeblink conditioning in rats using pontine stimulation as a conditioned stimulus. Integr Physiol Behav Sci 39:180–191

Freeman JH, Steinmetz AB (2011) Neural circuitry and plasticity mechanisms underlying delay eyeblink conditioning. Learn Mem 18:666–677. doi: 10.1101/lm.2023011

Galliano E, De Zeeuw CI (2014) Questioning the Cerebellar Doctrine. In: Progress in Brain Research. Elsevier, pp 59–77

Gao Z, Proietti-Onori M, Lin Z, et al (2016) Excitatory Cerebellar Nucleocortical Circuit Provides Internal Amplification during Associative Conditioning. Neuron 89:645–657. doi: 10.1016/j.neuron.2016.01.008

Gao Z, van Beugen BJ, De Zeeuw CI (2012) Distributed synergistic plasticity and cerebellar learning. Nat Rev Neurosci 13:619–635. doi: 10.1038/nrn3312

Garcia KS, Steele PM, Mauk MD (1999) Cerebellar cortex lesions prevent acquisition of conditioned eyelid responses. J Neurosci 19:10940–10947

Gauck V, Jaeger D (2000) The Control of Rate and Timing of Spikes in the Deep Cerebellar Nuclei by Inhibition. J Neurosci 20:3006–3016

Gauck V, Jaeger D (2003) The contribution of NMDA and AMPA conductances to the control of spiking in neurons of the deep cerebellar nuclei. J Neurosci 23:8109–8118

Gebre SA, Reeber SL, Sillitoe RV (2012) Parasagittal compartmentation of cerebellar mossy fibers as revealed by the patterned expression of vesicular glutamate transporters VGLUT1 and VGLUT2. Brain Struct Funct 217:165–180. doi: 10.1007/s00429-011-0339-4

Geschwind DH, Perlman S, Figueroa KP, et al (1997) Spinocerebellar ataxia type 6: Frequency of the mutation and genotype-phenotype correlations. Neurology 49:1247–1251. doi: 10.1212/WNL.49.5.1247

Globas C, Bösch S, Zühlke C, et al (2003) The cerebellum and cognition. J Neurol 250:1482–1487. doi: 10.1007/s00415-003-0258-2

Gogolla N, Caroni P, Lüthi A, Herry C (2009) Perineuronal nets protect fear memories from erasure. Science 325:1258–1261

Gomez CM, Thompson RM, Gammack JT, et al (1997) Spinocerebellar ataxia type 6: gaze-evoked and vertical nystagmus, Purkinje cell degeneration, and variable age of onset. Ann Neurol 42:933–950

Gould BB, Graybiel AM (1976) Afferents to the cerebellar cortex in the cat: evidence for an intrinsic pathway leading from the deep nuclei to the cortex. Brain Res 110:601–611

Gould TJ, Steinmetz JE (1996) Changes in rabbit cerebellar cortical and interpositus nucleus activity during acquisition, extinction, and backward classical eyelid conditioning. Neurobiol Learn Mem 65:17–34

Grube M, Cooper FE, Chinnery PF, Griffiths TD (2010) Dissociation of duration-based and beat-based auditory timing in cerebellar degeneration. Proc Natl Acad Sci 107:11597–11601. doi: 10.1073/pnas.0910473107

Guo C, Witter L, Rudolph S, et al (2016) Purkinje Cells Directly Inhibit Granule Cells in Specialized Regions of the Cerebellar Cortex. Neuron 91:1–12. doi: 10.1016/j.neuron.2016.08.011

Hámori J, Somogyi J (1983) Differentiation of cerebellar mossy fiber synapses in the rat: A quantitative electron microscope study. J Comp Neurol 220:365–377. doi: 10.1002/cne.902200402

Happel MFK, Niekisch H, Castiblanco Rivera LL, et al (2014) Enhanced cognitive flexibility in reversal learning induced by removal of the extracellular matrix in auditory cortex. Proc Natl Acad Sci 111:2800–2805. doi: 10.1073/pnas.1310272111

Härtig W, Brauer K, Brückner G (1992) Wisteria floribunda agglutinin-labelled nets surround parvalbumin-containing neurons. NeuroReport 3:869–872

Heiney SA, Wohl MP, Chettih SN, et al (2014) Cerebellar-Dependent Expression of Motor Learning during Eyeblink Conditioning in Head-Fixed Mice. J Neurosci 34:14845–14853. doi: 10.1523/JNEUROSCI.2820-14.2014

Hesslow G (1994) Correspondence between climbing fibre input and motor output in eyeblink-related areas in cat cerebellar cortex. J Physiol 476:229–244

Hioki H, Fujiyama F, Taki K, et al (2003) Differential distribution of vesicular glutamate transporters in the rat cerebellar cortex. Neuroscience 117:1–6. doi: 10.1016/S0306-4522(02)00943-0

Hirono M, Watanabe S, Karube F, et al (2018) Perineuronal Nets in the Deep Cerebellar Nuclei Regulate GABAergic Transmission and Delay Eyeblink Conditioning. J Neurosci 38:6130–6144. doi: 10.1523/JNEUROSCI.3238-17.2018

Hoebeek FE, Witter L, Ruigrok TJH, De Zeeuw CI (2010) Differential olivo-cerebellar cortical control of rebound activity in the cerebellar nuclei. Proc Natl Acad Sci 107:8410–8415. doi: 10.1073/pnas.0907118107

Houck BD, Person AL (2015) Cerebellar premotor output neurons collateralize to innervate the cerebellar cortex: Collateral pathway in mouse cerebellum. J Comp Neurol n/a-n/a. doi: 10.1002/cne.23787

Husson Z, Rousseau CV, Broll I, et al (2014) Differential GABAergic and Glycinergic Inputs of Inhibitory Interneurons and Purkinje Cells to Principal Cells of the Cerebellar Nuclei. J Neurosci 34:9418–9431. doi: 10.1523/JNEUROSCI.0401-14.2014

Iozzo RV (1998) MATRIX PROTEOGLYCANS: From Molecular Design to Cellular Function. Annu Rev Biochem 67:609–652. doi: 10.1146/annurev.biochem.67.1.609

Ishikawa K, Fujigasaki H, Saegusa H, et al (1999) Abundant expression and cytoplasmic aggregations of α1A voltage-dependent calcium channel protein associated with neurodegeneration in spinocerebellar ataxia type 6. Hum Mol Genet 8:1185–1193

Ito M (1982) Cerebellar Control of the Vestibulo-Ocular Reflex--Around the Flocculus Hypothesis. Annu Rev Neurosci 5:275–297. doi: 10.1146/annurev.ne.05.030182.001423

Ito M (1984) The Cerebellum and Neural Control. New York: Raven Press

Ivarsson M, Svensson P (2000) Conditioned Eyeblink Response Consists of Two Distinct Components. J Neurophysiol 83:796–807. doi: 10.1152/jn.2000.83.2.796

Ivry RB (1996) The representation of temporal information in perception and motor control. Curr Opin Neurobiol 6:851–857

Ivry RB, Keele SW (1989) Timing functions of the cerebellum. J Cogn Neurosci 1:136–152

Ivry RB, Keele SW, Diener HC (1988) Dissociation of the lateral and medial cerebellum in movement timing and movement execution. Exp Brain Res 73:167–180

Ivry RB, Spencer RMC, Zelaznik HN, Diedrichsen J (2002) The cerebellum and event timing. Ann N Y Acad Sci 978:302–317

Jahanshahi M, Jones CRG, Dirnberger G, Frith CD (2006) The Substantia Nigra Pars Compacta and Temporal Processing. J Neurosci 26:12266–12273. doi: 10.1523/JNEUROSCI.2540-06.2006

Jahnsen H (1986) Electrophysiological characteristics of neurones in the guinea-pig deep cerebellar nuclei in vitro. J Physiol 372:129–147

Jakab RL, Hámori J (1988) Quantitative morphology and synaptology of cerebellar glomeruli in the rat. Anat Embryol (Berl) 179:81–88. doi: 10.1007/BF00305102

Jänke L, Loose R, Lutz K, et al (2000) Cortical activations during paced finger-tapping applying visual and auditory pacing stimuli. Cogn Brain Res 10:51–66

Jirenhed D-A, Bengtsson F, Hesslow G (2007) Acquisition, Extinction, and Reacquisition of a Cerebellar Cortical Memory Trace. J Neurosci 27:2493–2502. doi: 10.1523/JNEUROSCI.4202-06.2007

Jodice C, Mantuano E, Veneziano L, et al (1997) Episodic Ataxia Type 2 (EA2) and Spinocerebellar Ataxia Type 6 (SCA6) Due to CAG Repeat Expansion in the CACNA1A Gene on Chromosome 19p. Hum Mol Genet 6:1973–1978. doi: 10.1093/hmg/6.11.1973

Johansson F, Carlsson HAE, Rasmussen A, et al (2015) Activation of a Temporal Memory in Purkinje Cells by the mGluR7 Receptor. Cell Rep 13:1741–1746. doi: 10.1016/j.celrep.2015.10.047

Johansson F, Hesslow G, Medina JF (2016) Mechanisms for motor timing in the cerebellar cortex. Curr Opin Behav Sci 8:53–59. doi: 10.1016/j.cobeha.2016.01.013

Jörntell H, Ekerot C-F (2006) Properties of Somatosensory Synaptic Integration in Cerebellar Granule Cells In Vivo. J Neurosci 26:11786–11797. doi: 10.1523/JNEUROSCI.2939-06.2006

Kandel ER, Schwartz JH, Jessell TM (2000) Chapter 42: The cerebellum. In: Principles of Neural Science, 4th edn. McGraw-Hill Medical

Kandel ER, Schwartz JH, Jessell TM, et al (2013) Principles of Neural Science, 5th edn. McGraw-Hill Medical

Kano M, Watanabe T, Uesaka N, Watanabe M (2018) Multiple Phases of Climbing Fiber Synapse Elimination in the Developing Cerebellum. The Cerebellum 17:722–734. doi: 10.1007/s12311-018-0964-z

Kitai ST, McCrea RA, Preston RJ, Bishop GA (1977) Electrophysiological and horseradish peroxidase studies of precerebellar afferents to the nucleus interpositus anterior. I. climbing fiber system. Brain Res 122:197–214

Kleim JA, Freeman JH, Bruneau R, et al (2002) Synapse formation is associated with memory storage in the cerebellum. Proc Natl Acad Sci 99:13228–13231

Koch G, Oliveri M, Torriero S, et al (2007) Repetitive TMS of cerebellum interferes with millisecond time processing. Exp Brain Res 179:291–299. doi: 10.1007/s00221-006-0791-1

Koeppen A (2005) The pathogenesis of spinocerebellar ataxia. The Cerebellum 4:62–73. doi: 10.1080/14734220510007950

Krakauer JW, Shadmehr R (2006) Consolidation of motor memory. Trends Neurosci 29:58–64. doi: 10.1016/j.tins.2005.10.003

Kwok JCF, Carulli D, Fawcett JW (2010) In vitro modeling of perineuronal nets: hyaluronan synthase and link protein are necessary for their formation and integrity: Hyaluronan synthase and link protein in PNNs. J Neurochem no-no. doi: 10.1111/j.1471-4159.2010.06878.x

Kwok JCF, Dick G, Wang D, Fawcett JW (2011) Extracellular matrix and perineuronal nets in CNS repair. Dev Neurobiol 71:1073–1089. doi: 10.1002/dneu.20974

Lafarga M, Berciano MT, Blanco M (1984) The perineuronal net in the fastigial nucleus of the rat cerebellum: A Golgi and quantitative study. Anat Embryol (Berl) 170:79–85. doi: 10.1007/BF00319461

Lainé J, Axelrad H (1998) Lugaro cells target basket and stellate cells in the cerebellar cortex. NeuroReport 9:2399–2403

Lang EJ, Apps R, Bengtsson F, et al (2017) The Roles of the Olivocerebellar Pathway in Motor Learning and Motor Control. A Consensus Paper. The Cerebellum 16:230–252. doi: 10.1007/s12311-016-0787-8

Larsell O (1952) The morphogenesis and adult pattern of the lobules and tissues of the cerebellum of the white rat. J Comp Neurol 97:281–356

Lavond DG (2002) Role of the Nuclei in Eyeblink Conditioning. Ann N Y Acad Sci 978:93–105

Lavond DG, Hembree TL, Thompson RF (1985) Effect of kainic acid lesions of the cerebellar interpositus nucleus on eyelid conditioning in the rabbit. Brain Res 326:179–182

Lavond DG, Steinmetz JE (1989) Acquisition of classical conditioning without cerebellar cortex. Behav Brain Res 33:113–164

LeDoux MS, Hurst DC, Lorden JF (1998) Single-unit activity of cerebellar nuclear cells in the awake genetically dystonic rat. Neuroscience 86:533–545

Lee K-H, Egleston PN, Brown WH, et al (2007) The role of the cerebellum in subsecond time perception: evidence from repetitive transcranial magnetic stimulation. J Cogn Neurosci 19:147–157

Leergaard TB, Bjaarlie JG (2007) Topography of the complete corticopontine projection: From experiments to principal maps. Front Neurosci 1:211–223. doi: 10.3389/neuro.01.1.1.016.2007

Lewis JL, LoTurco JJ, Solomon PR (1987) Lesions of the Middle Cerebellar Peduncle Disrupt Acquisition and Retention of the Rabbit's Classically Conditioned Nictitating Membrane Response. Behav Neurosci 101:151–157

Llinás R, Baker R, Sotelo C (1974) Electrotonic coupling between neurons in cat inferior olive. J Neurophysiol 37:560–571

Lu H, Yang B, Jaeger D (2016) Cerebellar Nuclei Neurons Show Only Small Excitatory Responses to Optogenetic Olivary Stimulation in Transgenic Mice: In Vivo and In Vitro Studies. Front Neural Circuits 10:. doi: 10.3389/fncir.2016.00021

Maiz J, Karakossian MH, Pakaprot N, et al (2012) Prolonging the postcomplex spike pause speeds eyeblink conditioning. Proc Natl Acad Sci 109:16726–16730. doi: 10.1073/pnas.1214274109

Mangels JA, Ivry RB, Shimizu N (1998) Dissociable contributions of the prefrontal and neocerebellar cortex to time perception. Cogn Brain Res 7:15–39

Manto M, Bower JM, Conforto AB, et al (2012) Consensus Paper: Roles of the Cerebellum in Motor Control—The Diversity of Ideas on Cerebellar Involvement in Movement. The Cerebellum 11:457–487. doi: 10.1007/s12311-011-0331-9

Marr D (1969) A theory of cerebellar cortex. J Physiol 202:437–470

Marshall SP, Lang EJ (2009) Local Changes in the Excitability of the Cerebellar Cortex Produce Spatially Restricted Changes in Complex Spike Synchrony. J Neurosci 29:14352–14362. doi: 10.1523/JNEUROSCI.3498-09.2009

Mathy A, Ho SSN, Davie JT, et al (2009) Encoding of Oscillations by Axonal Bursts in Inferior Olive Neurons. Neuron 62:388–399. doi: 10.1016/j.neuron.2009.03.023

Matsuda S, Matsumoto H, Furubayashi T, et al (2015) The 3-Second Rule in Hereditary Pure Cerebellar Ataxia: A Synchronized Tapping Study. PLOS ONE 10:e0118592. doi: 10.1371/journal.pone.0118592

Matsuyama Z (1997) Molecular features of the CAG repeats of spinocerebellar ataxia 6 (SCA6). Hum Mol Genet 6:1283–1287. doi: 10.1093/hmg/6.8.1283

McCormick DA, Clark GA, Lavond DG, Thompson RF (1982) Initial localization of the memory trace for a basic form of learning. Proc Natl Acad Sci 79:2731–2735

McCormick DA, Lavond DG, Clark GA, et al (1981) The engram found? Role of the cerebellum in classical conditioning of nictitating membrane and eyelid responses. Bull Psychon Soc 18:103–105. doi: 10.3758/BF03333573

McCormick DA, Thompson RF (1984) Neuronal responses of the rabbit cerebellum during acquisition and performance of a classically conditioned nictitating membrane-eyelid response. J Neurosci 4:2811–2822

McCrea RA, Bishop GA, Kitai ST (1978) Morphological and electrophysiological characteristics of projection neurons in the nucleus interpositus of the cat cerebellum. J Comp Neurol 181:397–419. doi: 10.1002/cne.901810210

Meck WH, Penney TB, Pouthas V (2008) Cortico-striatal representation of time in animals and humans. Curr Opin Neurobiol 18:145–152. doi: 10.1016/j.conb.2008.08.002

Medina JF, Garcia KS, Mauk MD (2001) A Mechanism for Savings in the Cerebellum. J Neurosci 21:4081–4089. doi: 10.1523/JNEUROSCI.21-11-04081.2001

Medina JF, Nores WL, Mauk MD (2002) Inhibition of climbing fibres is a signal for the extinction of conditioned eyelid responses. Nature 416:4

Meyer K, Linker A, Rapport MM (1951) The production of monosaccharides from hyaluronic acid by beta-glucuronidase. J Biol Chem 192:275–281

Miall RC, Wolpert DM (1996) Forward models for physiological motor control. Neural Netw 9:1265–1279

Mojtahedian S, Kogan DR, Kanzawa SA, et al (2007) Dissociaton of conditioned eye and limb responses in the cerebellar interpositus. Physiol Behav 91:9–14. doi: 10.1016/j.physbeh.2007.01.006

Molineux ML, Mehaffey WH, Tadayonnejad R, et al (2008) Ionic Factors Governing Rebound Burst Phenotype in Rat Deep Cerebellar Neurons. J Neurophysiol 100:2684–2701. doi: 10.1152/jn.90427.2008

Mostofi A, Holtzman T, Grout AS, et al (2010) Electrophysiological Localization of Eyeblink-Related Microzones in Rabbit Cerebellar Cortex. J Neurosci 30:8920–8934. doi: 10.1523/JNEUROSCI.6117-09.2010

Najac M, Raman IM (2017) Synaptic excitation by climbing fibre collaterals in the cerebellar nuclei of juvenile and adult mice. J Physiol. doi: 10.1113/JP274598

Nieuwenhuys R, Voogd J, van Huijzen C (1988) The Human Central Nervous System, 3rd edn. Springer

Oakley DA, Russell IS (1972) Neocortical lesions and pavlovian conditioning. Physiol Behav 8:915–926. doi: 10.1016/0031-9384(72)90305-8

Oakley DA, Russell IS (1976) Subcortical nature of Pavlovian differentiation in the rabbit. Physiol Behav 17:947–954. doi: 10.1016/0031-9384(76)90013-5

Oakley DA, Russell IS (1975) Role of cortex in Pavlovian discrimination learning. Physiol Behav 15:315–321. doi: 10.1016/0031-9384(75)90099-2

Ohmae S, Medina JF (2015) Climbing fibers encode a temporal-difference prediction error during cerebellar learning in mice. Nat Neurosci 18:1798–1803. doi: 10.1038/nn.4167

Ohyama T, Nores WL, Medina JF, et al (2006) Learning-Induced Plasticity in Deep Cerebellar Nucleus. J Neurosci 26:12656–12663. doi: 10.1523/JNEUROSCI.4023-06.2006

Onuki Y, Van Someren EJW, De Zeeuw CI, Van der Werf YD (2015) Hippocampal-Cerebellar Interaction During Spatio-Temporal Prediction. Cereb Cortex 25:313–321. doi: 10.1093/cercor/bht221

Oscarsson O (1979) Functional units of the cerebellum - sagittal zones and microzones. Trends Neurosci 2:143–145. doi: 10.1016/0166-2236(79)90057-2

Palkovits M, Mezey É, Hámori J, Szentágothai J (1977) Quantitative histological analysis of the cerebellar nuclei in the cat. I. Numerical data on cells and on synapses. Exp Brain Res 28–28:. doi: 10.1007/BF00237096

Pedroarena CM, Schwartz C (2003) Efficacy and Short-Term Plasticity at GABAergic Synapses Between Purkinje and Cerebellar Nuclei Neurons. J Neurophysiol 89:704–715. doi: 10.1152/jn.00558.2002

Perrett SP, Ruiz BP, Mauk MD (1993) Cerebellar cortex lesions disrupt learning-dependent timing of conditioned eyelid responses. J Neurosci 13:1708–1718

Person AL, Raman IM (2011) Purkinje neuron synchrony elicits time-locked spiking in the cerebellar nuclei. Nature 481:502–505. doi: 10.1038/nature10732

Pickford J, Apps R (2017) Collateral impact: a dual role for climbing fibre collaterals to the cerebellar nuclei? J Physiol. doi: 10.1113/JP275091

Pizzorusso T, Medini P, Berardi N, et al (2002) Reactivation of Ocular Dominance Plasticity in the Adult Visual Cortex. Science 298:1248–1251. doi: 10.1126/science.1072699

Pollok B, Gross J, Kamp D, Schnitzler A (2008) Evidence for anticipatory motor control within a cerebello-diencephalic-parietal network. J Cogn Neurosci 20:828–840

Pugh JR, Raman IM (2008) Mechanisms of Potentiation of Mossy Fiber EPSCs in the Cerebellar Nuclei by Coincident Synaptic Excitation and Inhibition. J Neurosci 28:10549–10560. doi: 10.1523/JNEUROSCI.2061-08.2008

Pugh JR, Raman IM (2006) Potentiation of Mossy Fiber EPSCs in the Cerebellar Nuclei by NMDA Receptor Activation followed by Postinhibitory Rebound Current. Neuron 51:113–123. doi: 10.1016/j.neuron.2006.05.021

Pugh JR, Raman IM (2009) Nothing can be coincidence: synaptic inhibition and plasticity in the cerebellar nuclei. Trends Neurosci 32:170–177. doi: 10.1016/j.tins.2008.12.001

Racine RJ, Wilson DA, Gingell R, Sunderland D (1986) Long-term potentiation in the interpositus and vestibular nuclei in the rat. Exp Brain Res 63:. doi: 10.1007/BF00235658

Rancz EA, Ishikawa T, Duguid I, et al (2007) High-fidelity transmission of sensory information by single cerebellar mossy fibre boutons. Nature 450:1245–1248. doi: 10.1038/nature05995

Rao SM, Harrington DL, Haaland KY, et al (1997) Distributed neural systems underlying the timing of movements. J Neurosci 17:5528–5535

Reato D, Tara E, Khodakhah K (2016) Chapter 2: Deep Cerebellar Nuclei Rebound Firing In Vivo: Much Ado About Almost Nothing? In: The Neuronal Codes of the Cerebellum. Elsevier, p 283

Rowland NC, Jaeger D (2005) Coding of Tactile Response Properties in the Rat Deep Cerebellar Nuclei. J Neurophysiol 94:1236–1251. doi: 10.1152/jn.00285.2005

Ruigrok TJH (2011) Ins and Outs of Cerebellar Modules. The Cerebellum 10:464–474. doi: 10.1007/s12311-010-0164-y

Saute JAM, Donis KC, Serrano-Munuera C, et al (2012) Ataxia Rating Scales—Psychometric Profiles, Natural History and Their Application in Clinical Trials. The Cerebellum 11:488–504. doi: 10.1007/s12311-011-0316-8

Schmahmann JD (2010) The Role of the Cerebellum in Cognition and Emotion: Personal Reflections Since 1982 on the Dysmetria of Thought Hypothesis, and Its Historical Evolution from Theory to Therapy. Neuropsychol Rev 20:236–260. doi: 10.1007/s11065-010-9142-x

Schmitz-Hübsch T, Du Montcel ST, Baliko L, et al (2006) Scale for the assessment and rating of ataxia Development of a new clinical scale. Neurology 66:1717–1720

Schöls L, Krüger R, Amoiridis G, et al (1998) Spinocerebellar ataxia type 6: genotype and phenotype in German kindreds. J Neurol Neurosurg Psychiatry 64:67–73

Schonewille M, Gao Z, Boele H-J, et al (2011) Reevaluating the Role of LTD in Cerebellar Motor Learning. Neuron 70:43–50. doi: 10.1016/j.neuron.2011.02.044

Schreurs BG, Gusev PA, Tomsic D, et al (1998) Intracellular correlates of acquisition and long-term memory of classical conditioning in Purkinje cell dendrites in slices of rabbit cerebellar lobule HVI. J Neurosci 18:5498–5507

Sears LL, Steinmetz JE (1990) Acquisition of classically conditioned-related activity in the hippocampus is affected by lesions of the cerebellar interpositus nucleus. Behav Neurosci 104:681

Shinoda Y, Sugihara I, Wu H-S, Sugiuchi Y (2000) The entire trajectory of single climbing and mossy fibers in the cerebellar nuclei and cortex. In: Progress in brain research. Elsevier, pp 173–186

Shiotsuki H, Yoshimi K, Shimo Y, et al (2010) A rotarod test for evaluation of motor skill learning. J Neurosci Methods 189:180–185. doi: 10.1016/j.jneumeth.2010.03.026

Shutoh F, Ohki M, Kitazawa H, et al (2006) Memory trace of motor learning shifts transsynaptically from cerebellar cortex to nuclei for consolidation. Neuroscience 139:767–777. doi: 10.1016/j.neuroscience.2005.12.035

Slaker M, Churchill L, Todd RP, et al (2015) Removal of Perineuronal Nets in the Medial Prefrontal Cortex Impairs the Acquisition and Reconsolidation of a Cocaine-Induced Conditioned Place Preference Memory. J Neurosci 35:4190–4202. doi: 10.1523/JNEUROSCI.3592-14.2015

Solodkin A, Gomez CM (2011) Spinocerebellar ataxia type 6. Ataxic Disord 103:461–473

Solomon PR, Lewis JL, LoTurco JJ (1986) The role of the middle cerebellar peduncle acquisition and retention of the rabbit's classically conditioned nictitating membrane response. Bull Psychon Soc 24:75–78

Soong B, Liu R, Wu L, et al (2001) Metabolic Characterization of Spinocerebellar Ataxia Type 6. Arch Neurol 58:300. doi: 10.1001/archneur.58.2.300

Spencer RM, Zelaznik HN, Diedrichsen J, Ivry RB (2003) Disrupted timing of discontinuous but not continuous movements by cerebellar lesions. Science 300:1437–1439

Spencer RMC, Ivry RB (2013) Cerebellum and Timing. In: Manto M, Schmahmann JD, Rossi F, et al. (eds) Handbook of the Cerebellum and Cerebellar Disorders. Springer Netherlands, Dordrecht, pp 1201–1219

Spencer RMC, Ivry RB, Zelaznik HN (2005) Role of the cerebellum in movements: control of timing or movement transitions? Exp Brain Res 161:383–396. doi: 10.1007/s00221-004-2088-6

Spencer RMC, Verstynen T, Brett M, Ivry R (2007) Cerebellar activation during discrete and not continuous timed movements: An fMRI study. NeuroImage 36:378–387. doi: 10.1016/j.neuroimage.2007.03.009

Stoyas CA, La Spada AR (2018) Chapter 11 - The CAG–polyglutamine repeat diseases: a clinical, molecular, genetic, and pathophysiologic nosology. In: Handbook of Clinical Neurology. Eds: Geschwind, D.A., Paulson, H.L., Klein, C. Elsevier, pp 143–170

Suenaga M, Kawai Y, Watanabe H, et al (2008) Cognitive impairment in spinocerebellar ataxia type 6. J Neurol Neurosurg Psychiatry 79:496–499

Sugihara I (2011) Compartmentalization of the Deep Cerebellar Nuclei Based on Afferent Projections and Aldolase C Expression. The Cerebellum 10:449–463. doi: 10.1007/s12311-010-0226-1

Sugihara I, Shinoda Y (2007) Molecular, Topographic, and Functional Organization of the Cerebellar Nuclei: Analysis by Three-Dimensional Mapping of the Olivonuclear Projection and Aldolase C Labeling. J Neurosci 27:9696–9710. doi: 10.1523/JNEUROSCI.1579-07.2007

Sugihara I, Wu HS, Shinoda Y (1999) Morphology of single olivocerebellar axons labeled with biotinylated dextran amine in the rat. J Comp Neurol 414:131–148

Szapiro G, Barbour B (2007) Multiple climbing fibers signal to molecular layer interneurons exclusively via glutamate spillover. Nat Neurosci 10:735–742. doi: 10.1038/nn1907

Telgkamp P, Raman IM (2002) Depression of inhibitory synaptic transmission between Purkinje cells and neurons of the cerebellar nuclei. J Neurosci 22:8447–8457

Ten Brinke MM, Heiney SA, Wang X, et al (2017) Dynamic modulation of activity in cerebellar nuclei neurons during pavlovian eyeblink conditioning in mice. eLife 6:

Ten Brinke MM, Boele H-J, Spanke JK, et al (2015) Evolving Models of Pavlovian Conditioning: Cerebellar Cortical Dynamics in Awake Behaving Mice. Cell Rep 13:1977–1988. doi: 10.1016/j.celrep.2015.10.057

Teune TM, Van Der Burg J, Van Der Moer J, et al (2000) Topography of cerebellar nuclear projections to the brain stem in the rat. Prog Brain Res 124:141–172

Thach WT (1968) Discharge of Purkinje and cerebellar nuclear neurons during rapidly alternating arm movements in the monkey. J Neurophysiol 31:785–797

Thach WT (1967) Somatosensory receptive fields of single units in cat cerebellar cortex. J Neurophysiol 30:675–696. doi: 10.1152/jn.1967.30.4.675

Thürling M, Kahl F, Maderwald S, et al (2015) Cerebellar Cortex and Cerebellar Nuclei Are Concomitantly Activated during Eyeblink Conditioning: A 7T fMRI Study in Humans. J Neurosci 35:1228–1239. doi: 10.1523/JNEUROSCI.2492-14.2015

Timmann D, Daum I (2007) Cerebellar contributions to cognitive functions: A progress report after two decades of research. The Cerebellum 6:159–162. doi: 10.1080/14734220701496448

Tolbert DL, Bantli H, Bloedel JR (1976) Anatomical and physiological evidence for a cerebellar nucleo-cortical projection in the cat. Neuroscience 1:205–217

Uusisaari M, De Schutter E (2011) The mysterious microcircuitry of the cerebellar nuclei. J Physiol 589:3441–3457. doi: 10.1113/jphysiol.2010.201582

Uusisaari M, Knöpfel T (2011) Functional Classification of Neurons in the Mouse Lateral Cerebellar Nuclei. The Cerebellum 10:637–646. doi: 10.1007/s12311-010-0240-3

Uusisaari M, Obata K, Knopfel T (2007) Morphological and Electrophysiological Properties of GABAergic and Non-GABAergic Cells in the Deep Cerebellar Nuclei. J Neurophysiol 97:901–911. doi: 10.1152/jn.00974.2006

Uusisaari MY, Knöpfel T (2012) Diversity of Neuronal Elements and Circuitry in the Cerebellar Nuclei. The Cerebellum 11:420–421. doi: 10.1007/s12311-011-0350-6

van Baarsen KM, Grotenhuis JA (2014) The anatomical substrate of cerebellar mutism. Med Hypotheses 82:774–780. doi: 10.1016/j.mehy.2014.03.023

van der Want JJL, Wiklund L, Guegan M, et al (1989) Anterograde tracing of the rat olivocerebellar system with phaseolus vulgaris leucoagglutinin (PHA-L). Demonstration of climbing fiber collateral innervation of the cerebellar nuclei. J Comp Neurol 288:1–18. doi: 10.1002/cne.902880102

van Dorp S, De Zeeuw CI (2014) Variable timing of synaptic transmission in cerebellar unipolar brush cells. Proc Natl Acad Sci 111:5403–5408. doi: 10.1073/pnas.1314219111

van Dorp S, De Zeeuw CI (2015) Forward Signaling by Unipolar Brush Cells in the Mouse Cerebellum. The Cerebellum 14:528–533. doi: 10.1007/s12311-015-0693-5

van 't Spijker HM, Kwok JCF (2017) A Sweet Talk: The Molecular Systems of Perineuronal Nets in Controlling Neuronal Communication. Front Integr Neurosci 11:. doi: 10.3389/fnint.2017.00033

Voogd J, Glickstein M (1998) The anatomy of the cerebellum. Trends Cogn Sci 2:307–313

Voogd J, Marani E (2016) Gross anatomy of the cerebellum. In: Essentials of cerebellum and cerebellar disorders. Gruol D., Koibuchi N., Manto M., Molinari M., Schmahmann J., Shen Y. (eds.). Springer, Cham

Voogd J, Pardoe J, Ruigrok TJ, Apps R (2003) The distribution of climbing and mossy fiber collateral branches from the copula pyramidis and the paramedian lobule: congruence of climbing fiber cortical zones and the pattern of zebrin banding within the rat cerebellum. J Neurosci 23:4645–4656

Wang D, Fawcett J (2012) The perineuronal net and the control of CNS plasticity. Cell Tissue Res 349:147–160. doi: 10.1007/s00441-012-1375-y

Wang D, Smith-Bell CA, Burhans LB, et al (2018) Changes in membrane properties of rat deep cerebellar nuclear projection neurons during acquisition of eyeblink conditioning. Proc Natl Acad Sci 115:E9419–E9428. doi: 10.1073/pnas.1808539115

Watanabe M, Kano M (2011) Climbing fiber synapse elimination in cerebellar Purkinje cells: Climbing fiber synapse elimination. Eur J Neurosci 34:1697–1710. doi: 10.1111/j.1460-9568.2011.07894.x

Weber P, Bartsch U, Rasband MN, et al (1999) Mice Deficient for Tenascin-R Display Alterations of the Extracellular Matrix and Decreased Axonal Conduction Velocities in the CNS. J Neurosci 19:4245–4262. doi: 10.1523/JNEUROSCI.19-11-04245.1999

Weeks ACW, Connor S, Hinchcliff R, et al (2007) Eye-blink conditioning is associated with changes in synaptic ultrastructure in the rabbit interpositus nuclei. Learn Mem 14:385–389. doi: 10.1101/lm.348307

Weyer A, Abele M, Schmitz-Hübsch T, et al (2007) Reliability and validity of the scale for the assessment and rating of ataxia: A study in 64 ataxia patients. Mov Disord 22:1633–1637. doi: 10.1002/mds.21544

White JJ, Sillitoe RV (2017) Genetic silencing of olivocerebellar synapses causes dystonia-like behaviour in mice. Nat Commun 8:14912. doi: 10.1038/ncomms14912

Witter L, Canto CB, Hoogland TM, et al (2013) Strength and timing of motor responses mediated by rebound firing in the cerebellar nuclei after Purkinje cell activation. Front Neural Circuits 7:. doi: 10.3389/fncir.2013.00133

Witter L, Rudolph S, Pressler RT, et al (2016) Purkinje Cell Collaterals Enable Output Signals from the Cerebellar Cortex to Feed Back to Purkinje Cells and Interneurons. Neuron. doi: 10.1016/j.neuron.2016.05.037

Wolpert DM, Miall RC, Kawato M (1998) Internal models in the cerebellum. Trends Cogn Sci 2:338–347

Wulff P, Schonewille M, Renzi M, et al (2009) Synaptic inhibition of Purkinje cells mediates consolidation of vestibulo-cerebellar motor learning. Nat Neurosci 12:1042–1049. doi: 10.1038/nn.2348

Wylie DR, De Zeeuw CI, Digiorgi PL, Simpson JI (1994) Projections of individual purkinje cells of identified zones in the ventral nodulus to the vestibular and cerebellar nuclei in the rabbit. J Comp Neurol 349:448–463. doi: 10.1002/cne.903490309

Xue Y-X, Xue L-F, Liu J-F, et al (2014) Depletion of Perineuronal Nets in the Amygdala to Enhance the Erasure of Drug Memories. J Neurosci 34:6647–6658. doi: 10.1523/JNEUROSCI.5390-13.2014

Yabe I, Sasaki H, Takeichi N, et al (2003) Positional vertigo and macroscopic downbeat positioning nystagmus in spinocerebellar ataxia type 6 (SCA6). J Neurol 250:440–443. doi: 10.1007/s00415-003-1020-5

Yarden-Rabinowitz Y, Yarom Y (2017) *In vivo* analysis of synaptic activity in cerebellar nuclei neurons unravels the efficacy of excitatory inputs. J Physiol. doi: 10.1113/JP274115

Yeo CH, Hardiman MJ (1992) Cerebellar cortex and eyeblink conditioning: a reexamination. Exp Brain Res 88:623–638

Yeo CH, Hardiman MJ, Glickstein M (1986) Classical conditioning of the nictitating membrane response of the rabbit. IV lesions of the inferior olive. Exp Brain Res 63:81–92

Yeo CH, Hardiman MJ, Glickstein M (1985) Classical conditioning of the nictating membrane of the rabbit. I. Lesions of the cerebellar nuclei. Exp Brain Res 60:87–98

Zbarska S, Holland EA, Bloedel JR, Bracha V (2007) Inferior olivary inactivation abolishes conditioned eyeblinks: Extinction or cerebellar malfunction? Behav Brain Res 178:128–138. doi: 10.1016/j.bbr.2006.12.012

Zelaznik HN, Spencer RMC, Ivry RB (2002) Dissociation of explicit and implicit timing in repetitive tapping and drawing movements. J Exp Psychol Hum Percept Perform 28:575–588. doi: 10.1037//0096-1523.28.3.575

Zhang W, Linden DJ (2006) Long-Term Depression at the Mossy Fiber-Deep Cerebellar Nucleus Synapse. J Neurosci 26:6935–6944. doi: 10.1523/JNEUROSCI.0784-06.2006

Zheng N, Raman IM (2010) Synaptic Inhibition, Excitation, and Plasticity in Neurons of the Cerebellar Nuclei. The Cerebellum 9:56–66. doi: 10.1007/s12311-009-0140-6

Zhou H, Lin Z, Voges K, et al (2014) Cerebellar modules operate at different frequencies. eLife 3:. doi: 10.7554/eLife.02536

Zhuchenko O, Bailey J, Bonnen P, et al (1997) Autosomal dominant cerebellar ataxia (SCA6) associated with small polyglutamine expansions in the alpha1A-voltage-dependent calcium channel. Nat Genet 15:62–69

Chapter 2

Learning-related changes in synaptic inputs and encoding in cerebellar nuclei neurons during eyeblink conditioning

Robin Broersen, Daniela Carulli, Joost Verhaagen, Cathrin B. Canto* and Chris I. De Zeeuw*

* indicates equal contribution to last authorship

In preparation

2.1 Abstract

Orchestrated activity within the olivo-cerebellar circuit is essential for generating anticipatory eyelid movements during eyeblink conditioning. The cerebellar nuclei play a crucial role in this functional circuitry by integrating various synaptic inputs, ultimately providing the sole cerebellar output to downstream areas that control eyelid muscles. Although it has been shown that cerebellar nuclei neurons are involved in the encoding and consolidation of conditioned responses, the plasticity mechanisms underlying cerebellar learning have not yet been unraveled. Here, we show that during conditioning VGLUT1+ mossy fiber collaterals and gephyrin+ Purkinje cell terminals increase in the eyeblink-encoding part of the interposed nucleus (IpN). Although this increase in mossy fibers allows for eyelid movements to be evoked optogenetically, these afferents do not contribute to task-related IpN activity and associated eyelid behavior. Moreover, whole-cell recordings obtained from 25 naïve and trained IpN neurons show that changes in task-related membrane potential dynamics are carried mainly by Purkinje cell activity. Interestingly, we observed prolonged membrane potential transients following a corneal air puff, indicating that learning-related circuit changes also impact encoding of unconditioned responses. Together, our results suggest that the role of mossy fiber collaterals for learning-related IpN activity is limited.

2.2 Introduction

Pavlovian eyeblink conditioning (EBC) has been used for decades to investigate cerebellar associative-learning mechanisms. During EBC, learning to execute well-timed eyelid movements critically depends on physiological activity in the intact cerebellar lobule HVI and interposed nucleus (IpN) (Yeo et al. 1985; Lavond and Steinmetz 1989; Sears and Steinmetz 1990; Yeo and Hardiman 1992; Garcia et al. 1999; Attwell et al. 2001; Freeman et al. 2005). Interfering with IpN activity in conditioned animals affects learned behavior (Clark et al. 1984; Lavond et al. 1985; Bracha et al. 1994; Bao et al. 2000; Freeman and Rabinak 2004; Ohyama et al. 2006; Mojtahedian et al. 2007), whereas inactivating lobule HVI results in altered temporal profiles of eyelid responses (McCormick and Thompson 1984b; Perrett et al. 1993; Garcia et al. 1999). Hence, the IpN is an essential component of the cerebellar network for the expression of conditioned responses (CRs) and plasticity mechanisms at the level of the IpN are able to, at least partly, compensate for the absence of cerebellar cortical task-related input (Medina et al. 2001; Ohyama et al. 2006; Freeman and Steinmetz 2011).

Repeated pairing of co-terminating conditioned (CS; light) and unconditioned stimuli (US; corneal air puff) leads to the emergence of CRs. CS information reaches the IpN directly via excitatory mossy fiber (MF) collaterals and indirectly through inhibitory Purkinje cell (PC) axons (Kitai et al. 1977; Brodal et al. 1986; Dietrichs and Walberg 1987). US information arrives through climbing fibers (CFs), which powerfully excite PCs and also form direct excitatory collaterals to IpN (Courville et al. 1977; van der Want et al. 1989; De Zeeuw et al. 1997). Integration of both excitatory and inhibitory inputs forms the basis for the activity patterns of these cerebellar output neurons, which in turn control neural activity in downstream motor nuclei. The emergence of CRs temporally coincides with changes in cerebellar circuit physiology (McCormick and Thompson 1984b; Mostofi et al. 2010; Heiney et al. 2014b; Halverson et al. 2015), of which a pronounced feature is the reduction in Purkinje cell (PC) simple spike activity during the CS-US interval (Berthier and Moore 1986; Jirenhed et al. 2007; Ten Brinke et al. 2015). Since pauses in PC activity tightly controls spike activity in IpN neurons (Gauck and Jaeger 2000, 2003; Person and Raman 2011), this disinhibition may take full account for the resulting IpN spike patterns that controls downstream motor areas (McCormick and Thompson 1984b; Berthier and Moore 1990; Ten Brinke et al. 2017). Yet, IpN neurons show differential spike responses during the CS-US interval, where the majority shows spike activity increases ('facilitation') and a minor population shows spike decreases ('suppression) (Ten Brinke et al. 2017).

The contribution of afferent MF and CF collaterals to this task-related IpN activity remains obscure, although various forms of plasticity involving MFs and possibly CFs have been shown to take place during conditioning, such as structural changes in excitatory afferent inputs (Kleim et al. 2002; Weeks et al. 2007; Boele et al. 2013). Conditioning leads to increased intrinsic excitability in IpN neurons (Wang et al. 2018) and removal of plasticity-restricting perineuronal nets (PNNs) around these neurons (van 't Spijker and Kwok, 2017)

has been shown to enhance learning (Hirono et al. 2018). The nuclei are a prominent site for synaptic plasticity (Zhang and Linden 2006; Pugh and Raman 2006, 2008, 2009), although direct evidence for synaptic plasticity *in vivo* is still lacking due to the technical difficulty associated with obtaining whole-cell recordings in awake behaving animals (Lee and Lee 2017; Petersen 2017).

Our aim in this study was to find out (i) which structural changes in IpN afferent inputs take place during conditioning, (ii) what is the contribution of IpN afferent inputs to membrane potential (V_m) dynamics and resulting spike activity, and (iii) how does the V_m and spike representation of the CS and US change during learning. We show that during conditioning both excitatory MF collaterals, as well as inhibitory PC terminals are increased in eyeblink-encoding regions of the IpN. Optogenetic activation and silencing of MFs leads to eyelid movements after conditioning, but MF activation does not contribute to task-related IpN activity and associated eyelid movements. *In vivo* awake whole-cell recordings in behaving mice during EBC indicate that learning-related changes in PC activity predominantly accounts for changed V_m encoding in IpN neurons.

2.3 Materials and methods

2.3.1 Animals and ethics statement

All animal experimental procedures were conducted in accordance with the institutional animal welfare committees of the Erasmus Medical Center and/or the Netherlands Institute for Neuroscience (NIN-KNAW). Adult male C57Bl/6J mice were used for histology (N = 6 siblings; 3 conditioned/3 pseudo-conditioned, age at perfusion: 46 days), microstimulation experiments (N = 3, age: 3-6 weeks), optogenetic MF stimulation experiments (N = 13, age at first EBC training: 53.2 ± 8.0 days), extracellular recordings (same animals, age at recordings: 74.6 ± 10.8 days), and *in vivo* awake whole-cell recordings (N = 21, 11 conditioned/10 naïve, age 50.4 ± 14.5 days).

2.3.2 Surgical procedures

2.3.2.1 Pedestal surgery

Mice were anesthetized with isoflurane (5% induction, 1.8-2% maintenance; in 0.2 L/min O_2 and 0.2 L/min air) and placed in a stereotaxic frame where their body temperature was kept at 37 °C using a feedback-controlled heating-pad. Eyes were covered with antimicrobial ointment to prevent drying (Terra-Cortril, Pfizer). Skin covering the skull was shaved and a mid-sagittal incision of approximately 1 cm was made to expose the skull bone, after which local anesthesia was applied on the skin around the incision (10% Xylocaine,

AstraZeneca). Primer (Optibond All-In-One, Kerr) was applied on bone and treated with UV light. A 6 x 3 x 5.7 mm aluminum block ('pedestal') was attached to a stereotaxic arm for correct positioning, and attached to the skull bone with dental acrylic (Flowline, Hereaus Kulzer). Skin edges were attached to the dental acrylic using tissue glue (Histoacryl, Aesculap AG). Post-operative analgesia was given subcutaneously in the form of Meloxicam (0.4 mg/kg Metacam, AUV) and mice were placed under an IR-light while recovering from anesthesia. Mice were allowed to recover for at least two days following surgery.

2.3.2.2 Virus injection and optic fiber placement

First part of the surgery was performed as described above, except that a longer mid-sagittal incision was made until the edge of the occipital bone. Then, a stereotaxic arm was used to mark the location of entry to reach the lateral pontine nuclei (-3.8 to -4 mm from bregma, ±1 mm lateral to midline, -5.5 to -5.8 mm depth), comparable to previously used coordinates (Boele et al. 2013). Two small craniotomies were made using a dental drill (Foredom Drill K1070-2E, Blackstone Industries) and the dura was carefully broken using a fine forceps, to allow access into the brain. Mice were injected with rAAV2/hsyn-eArch3.0-eYFP (UNC Vector Core, lot # AV5229B) (N = 9) or with a mix of the former and rAAV1/Syn-chronos-GFP (UNC Vector Core, lot # AV6550) (N=4). In both cases, final solutions contained viruses that were diluted 4x. One µl virus-containing solution was injected in each hemisphere using either quartz capillary pipettes (30-40 µm tip diameter) connected to a Harvard injection pump (speed of 0.15 µl/min), or borosilicate glass pipettes connected to a Nanoject II Auto-Nanoliter Injector (Drummond Scientific, speed of approximately 2 ul/min). Following injection, the pipette was left in place for at least 2 minutes to allow diffusion and was then slowly retracted. Bilateral optic fibers (Ø200 µm, FT200UMT, Thorlabs) connected to ceramic zirconia ferrules (MM-FER2007C-2300, Precision Fiber Products) were lowered into the brain through the same injection track until a depth of 5 mm was reached to enable light delivery to the pontine nuclei. Fibers were attached to the skull bone using dental cement, after which pedestals were attached on the skull as described above. Dental cement was painted using silver conductive paint (RS Components) to reduce shine through of optogenetic light. Mice were allowed to recover at least 2 weeks before continuing with the experiments.

2.3.2.3 Craniotomy surgery

Mice were anesthetized with isoflurane (5% induction, 1.8-2% maintenance; in 0.2 L/min O_2 and 0.2 L/min air) and placed in a stereotaxic frame where their body temperature was kept at 37 °C using a feedback-controlled heating-pad. Eyes were protected and kept moist using eye drops (Duodrops, Ceva). Hairs in the neck were removed and an incision was made in the skin covering the neck muscles, after which local anesthesia was applied (10%

Xylocaine, AstraZeneca). Neck muscles were removed to expose the occipital bone and two square-shaped craniotomies were made bilaterally using a dental drill (Foredom Drill K1070-2E, Blackstone Industries). Position of craniotomy was above Crus II, to access the dorsolateral hump (DLH) and the IpN. A thin layer of primer was applied around the craniotomies and a recording bath was made using dental acrylic (Flowline and Charisma, Heraeus Kulzer). As soon as the recording bath was made, it was filled with 0.9% NaCl solution to keep the dura moist. Skin and muscles surrounding the bath were attached to the dental cement using tissue glue. Then, the dura in the craniotomy was carefully removed using a needle tip (30G x ½ inch, BD Microlance) and fine forceps (Dumont #7 curved, Fine Science Tools). Directly after removing the dura, the recording bath was cleaned with 0.9% NaCl solution and filled with a low viscosity silicone elastomer sealant (Kwik-cast, World Precision Instruments) to protect the brain tissue from the air. Mice were given post-operative analgesia subcutaneously (Meloxicam 0.4 mg/kg), placed under an IR-light during recovery and closely monitored for at least two hours before starting the recording session.

2.3.3 Eyeblink conditioning

2.3.3.1 Training eyeblink boxes

All mice were habituated for at least 3 days before starting behavioral trainings. Habituations and trainings were done in prefabricated sound- and light-isolating boxes (Neurasmus). During habituations mice were head-fixed to a horizontal bar and could freely walk on a cylindrical treadmill in the dark to get accustomed to the environment (Chettih et al. 2011). To head-fix mice with the least amount of stress, they were shortly anesthetized with isoflurane (5% in 0.5 L/min O_2 and 0.5 L/min air) after which they woke up in the box. Mice were habituated with increasing durations ranging from 15 minutes on day 1 to 60 minutes on day 5. Hairs under the left eyelid were removed during anesthesia on day 2. From day 3 onward a 1.5 x 0.5 x 0.7 mm neodymium magnet (Supermagnete) was placed under the left eye using super glue (Bison) and 20 CS only trials and 2 US only trials with an intertrial interval (ITI) of 10 ± 2 sec was presented to familiarize the mouse with the stimuli. The CS consisted of a 260 ms light delivered through a green/blue LED placed ~7 cm in front of the mouse. The US consisted of a 10 ms corneal air puff (35-40 psi) delivered through a P20 pipette tip positioned ~5 mm from the left eye, where the US airflow was controlled by a picospritzer (MPPI-3, ASI). Eyelid movements were recorded through a magnetic sensor that was placed above the left eye to record magnet position, also known as magnet distance measuring technique (MDMT) (Koekkoek et al. 2002).

Trainings lasted 5-10 days and involved one daily training session comprising 200 CS-US (paired) trials, 20 CS only (CS) trials and 20 US only (US) trials, presented as a 20x repeated sequence of 1US-10paired-1CS. Trials followed a standardized format of 0-500 ms baseline, 500-760 ms CS (paired and CS trials), 750-760 ms US (paired and US trials), 760-2000 ms

post-stimuli period. MDMT data was captured at 1017.26 Hz using custom-written LabVIEW (National Instruments) software (Koekkoek et al. 2002). Trainings were started at least 10 min after placing mice in the box to allow full recovery of isoflurane anesthesia. Trials were initiated only if the eyelid signal exceeded 75% of maximum eyelid opening.

2.3.3.2 Experimental eyeblink setup

Mice used for *in vivo* whole-cell electrophysiology were first trained as described above, after which they were transferred to an electrophysiology setup equipped with similar behavioral equipment. Mice were trained for at least 3 more days before starting electrophysiological recording sessions to ensure they reached maximum performance and mice were familiar with the environment. Eyelid position at this setup was acquired using a 250 fps CCD camera (scA640-120 gc, Basler) directed at the left eye that was illuminated with an IR-light. Camera frames were transformed into a continuous data vector sampled at 2441 Hz based on pixel thresholding of a region of interest overlaying the eye and the eyelid. CS/US stimuli were triggered under the control of custom-made software utilizing TDT System 3 (Tucker Davis Technologies) and NI-PXI (National Instruments) processors. US TTL pulse was given 13 ms earlier to correct for the delay between the picospritzer and air puff arrival at the cornea. Trials were initiated only if the eye was >75% opened. Mice were placed in the electrophysiology setup without isoflurane anesthesia, since no magnet under the eyelid was used. Instead, to avoid reflection of IR-light caused by the whiskers a thin layer of water-proof black mascara was applied on the left whiskers. Different training protocols were used to optimize trainings, but they all included 200 paired CS-US trials daily with an ITI between 10 and 12 ± 2 s.

2.3.4 Eyeblink data processing

2.3.4.1 MDMT data (box)

MDMT data was analyzed using custom LabVIEW software. In short, acquired data was subjected to several quality checks: (i) trials with an unstable baseline were removed (trials with values exceeding 5x SD of the baseline period), (ii) sessions in which >75% of trials were removed were excluded and (iii) sessions with large variation in UR amplitude (>0.5 x coefficient of variation (CV)) were excluded. CRs were detected as eyelid closures during the last 200 ms of the CS-US interval that exceeded 10% of average UR amplitude.

2.3.4.2 Camera data (setup)

Camera data was analyzed using custom-made MATLAB routines. In short, data was preprocessed by filtering with a Gaussian low-pass filter (50 Hz cutoff-frequency) and trials with unstable baselines (values >5 x SD of the baseline period) were excluded. CRs and EOs

were detected as eyelid closures and openings, respectively, during the last 200 ms of the CS-US interval that exceeded 5 x SD of the baseline period.

2.3.4.3 Eyeblink performance parameters

CR/EO percentage was calculated by dividing the number of CRs/EOs trials over the total amount of CR/EO-eligible trials, multiplied by 100. Fraction of eyelid closure (FEC) (or alternatively: CR/EO amplitude) was calculated as maximum values (or absolute minimum values for EOs) of the baseline-normalized signal during the CS-US interval, divided by the average UR amplitude. Amplitude at US onset was the value of the baseline-normalized signal at US onset (750 ms after trial start), divided by the average UR amplitude. CR or EO onset was manually detected on a trial-by-trial basis and was defined as the time point of the last minimum before a continuously rising signal (CR) or as the time point of the last maximum before a continuously decreasing signal (EO). Area under the curve (AUC) was calculated as the absolute integral of the baseline-normalized signal between CR/EO onset and US onset (750 ms after trial start). UR AUC was calculated similarly, but during the first 200ms following US onset.

2.3.5 Experimental techniques

2.3.5.1 Microelectrode stimulation and labeling

Microelectrode stimulation was performed as described previously (Heiney et al. 2014b; Ten Brinke et al. 2017). In short, a stereotaxic craniotomy surgery was performed in habituated mice as described above. An 80-µm-diameter platinum iridium monopolar electrode (100 KΩ; Alpha Omega) was lowered into the brain with a 43° angle until a depth of 1500-1600 µm was reached. Electrodes were advanced in steps of 100 µm and after each step, currents generated (ISO-flex Stimulus Isolater, A.M.P.I.) and were applied in the range of 1–15 µA (200 ms pulse trains; 250 µs biphasic pulses; 500 Hz). The depth at which reliable eyelid contractions could be observed with low current amplitudes (<10 µA) was identified as the eyeblink-encoding region of the IpN. Established coordinates of this region was subsequently targeted for electrophysiological recordings. To mark this area in the IpN, the electrode was retracted, coated with Evans Blue solution (5% in saline, Sigma-Aldrich) and reinserted using identical position and coordinates, to reach the depth of the eyeblink-encoding area in IpN. Mice were transcardially perfused using 4% paraformaldehyde (PFA, Sigma-Aldrich) in phosphate buffered saline (PBS) after a lethal dose of pentobarbital (Nembutal) and brains were collected for histology.

2.3.5.2 Optogenetics

Mice for optogenetic interference experiments were first trained in the eyeblink boxes as described above, after which they were subjected to optogenetic stimulation sessions on day -1, 5 and 10 (Fig 3J-L) on the experimental setup. Bilateral optogenetic activation and silencing of targeted pontocerebellar MFs was achieved by light-induced activation of chronos or eArch3.0, respectively. Light was delivered through optic fiber implants that were connected to LED light sources. Chronos was activated using 50-260 ms pulses of 465 nm light generated by a 5W LED (60 lm, LZ1-B200, LEDEngin) connected to a custom-made LED driver, as described previously (Witter et al. 2013). This resulted in a light output of 1-2.5 mW/mm^2 at the tip of the optic fiber. Activation of eArch3.0 for MF silencing was achieved using 110-550 ms pulses of 590 nm light, generated by a commercially available LED source (M590F1, Thorlabs). This resulted in a light output of >3 mW/mm^2 at the tip of the optic fiber, sufficient to effectively silence neurons as reported previously (Gao et al. 2016). LED sources were controlled by TTL pulses from a Multiclamp 700B amplifier (Axon Instruments) and used to synchronize electrophysiology and eyelid recordings. Effort was made to reduce shine through or escape of optogenetic light from the optic fibers as much as possible. Silver conductive paint was often reapplied on the dental cement and silver foil was positioned around the optic fibers and equipment.

2.3.5.3 In vivo electrophysiology

Whole-cell and extracellular recordings were made using glass electrodes with a tip diameter of 1-2 µm and a resistance of 4-8 MΩ. Electrodes were heat-pulled on a P-1000 micropipette puller (Sutter Instrument) from filamented borosilicate glass capillaries (1.5 mm OD, 0.86 mm ID, Harvard Apparatus). Electrodes were back-filled with intracellular solution, containing (in mM): 10 KOH, 3.48 $MgCl_2$, 4 NaCl, 129 K-Gluconate, 10 HEPES, 17.5 glucose 4 Na_2ATP, and 0.4 Na_3GTP (295 ± 305 mOsm; pH 7.2). For whole-cell recordings intracellular solution was supplemented with 0.5% neurobiotin (Vector Labs). Electrophysiological recordings were made using a Multiclamp 700B amplifier (Axon Instruments) and digitized at 100 or 50 kHz with a Digidata 1440 digitizer (Axon Instruments). Electrodes were mounted in a 43° angle on a pipette holder connected to a headstage (CV-7B, Axon Instruments) and were controlled by a micromanipulator (SM7, Luigs und Neumann).

During *in* vivo awake whole-cell recordings, electrodes were lowered along the anteroposterior axis with high pressure to a depth of 1500-1600 µm relative to brain surface, after which the pressure was lowered to 15-20 mbar. Then, electrodes were advanced in steps of 2 µm while monitoring the current during 10 mV steps at 33 Hz in voltage clamp mode. All neurons reached a seal resistance of at least 1 GΩ before whole-cell configuration was initiated. Several protocols were run shortly after break-in to characterize the neuron, *i.e.* a sealtest protocol (10 mV steps at -65 mV holding in voltage clamp) and a step protocol

(current between 200 and -200 pA) in current clamp mode after bridge balance compensation. After these protocols a continuous recording in current clamp was started synchronously with a continuous recording of the left eye, during which stimuli were given until the neuron was lost or the recording quality became insufficient. During *in vivo* extracellular recordings the protocol was similar, although the electrode was advanced in a continuous movement without current injection. We recorded when action potentials of a single neuron could be clearly identified and had amplitudes of >1 mV. *In vivo* awake whole-cell recordings were made during only 1 session with a duration of <4 hours. Extracellular recordings were made during 1-3 daily sessions, each with a duration of <4 hours.

2.3.5.4 EBC stimulus protocols during in vivo electrophysiology

For whole-cell recordings during EBC, naïve animals received US only, CS only and paired trials in a 1:1:1 ratio with a pseudorandomized order. Conditioned animals received repetitive sequences of 1US-5paired-1CS to maintain conditioned behavior throughout the experiment. Trials were given with an ITI of 12 ± 2 s, no threshold for eyelid opening was used to maximize the amount of recorded trials. For extracellular recordings during EBC, trials with optogenetic stimulation were alternated with trials without optogenetic stimulation, the latter of which were used to analyze CS and US IpN spike responses. Possible trial-types are shown in Fig 3K and L, and were presented in a pseudorandom order with a fixed ITI of 8 s. A minimum of 3 valid trials was used to include a certain trial-type in the population analysis.

2.3.6 Data analysis

2.3.6.1 In vivo electrophysiology

Data was processed in Clampfit (v10.5, Axon Instruments) and MATLAB (vR2011b, MathWorks). Access resistance (R_a) and membrane resistance (R_m) were estimated based on the peak amplitude of average current signal and the amplitude of the relaxation phase during a 10 mV voltage step, respectively. Membrane time constant (tau) was estimated by fitting a single exponential function on the average current signal between 80-10% of peak-to-relaxation amplitude of the same voltage step. The resting membrane potential was corrected for by the junction potential, which was previously determined to be -8.53 mV ± 0.87 mV (Canto et al. 2016). Data was imported in MATLAB and synchronized with eyelid recordings based on TTL timestamps. For V_m analysis, spikes were removed by cutting 5 ms of data centered on the spike peak-amplitude time and connecting the ends by linear interpolation. Data was then filtered with a Gaussian low-pass filter (10 kHz cutoff-frequency) and event-related data for each trial-type was collected based on eyelid movement classification (as described above). V_m normalization was relative to the baseline

(0-500 ms) of each trial. CS-evoked V_m responses were determined based on the average of paired and CS only trials during the last 200 ms of the CS-US interval. US-evoked V_m responses were determined based on the first 200 ms following US onset of US only trials. In few cases US only trials were not available, in which case paired NM or CR/EO trials were used.

Compound excitatory postsynaptic potentials (cEPSPs) are identified as depolarizations exceeding 3x SD of baseline, where compound inhibitory postsynaptic potentials (cIPSPs) are hyperpolarizations exceeding 3x SD of baseline. Amplitudes represent averages of the maximum (cEPSP) or minimum (cIPSP) values of normalized data within a set timeframe. AUC (arbitrary units, a.u.) is the integral of normalized data (values >0 for cEPSP, <0 for cIPSP) and represents response magnitude. Onsets of V_m responses were manually detected on a trial-by-trial basis, reflecting the last trough before a increasing signal (cEPSP onset) or last peak before a decreasing signal (cIPSP onset).

Spikes times were detected using Clampfit threshold search (whole-cell data), or using a custom-written MATLAB spike analysis program (B.H.J. Winkelman, Netherlands Institute for Neuroscience, Amsterdam) and sorted based on spike waveform characteristics (extracellular data). Only data with clear spikes from single units were analyzed. Based on spike times we calculated: spike frequency (= number of spikes / duration of time period), coefficient of variation of spiking (CV = standard deviation (all interspike intervals (ISIs) / average (all ISIs)) and average CV of two adjacent ISIs ($CV_2 = 2 \mid ISI_{n+1} - ISI_n \mid / (ISI_n + ISI_n+1)$). Spontaneous spike calculations for whole-cell data were based on periods of quiet wakefulness directly after the start of recording, before the first stimulus was presented (duration: 35.28 ± 42.08 s). For extracellular data, time periods between trials were used.

2.3.6.2 Inclusion criteria and properties whole-cell recordings

Recordings were discarded if access resistance >100 MΩ or if spike amplitude <10 mV. Neurons were identified based on occurrence of clear spikes (spontaneous or current-evoked). Only good traces with a non-drifting V_m were selected for further analysis. Although neurons were generally recorded without current injection, very few neurons received limited current (25-200 pA) to maintain V_m at original values directly after break-in. The remaining neurons were recorded in both hemispheres (naïve vs conditioned: 6/12 vs 8/13 ipsilateral). Recording depth (naïve vs conditioned: 1835.5 ± 220.9 µm vs 1757.7 ± 170.4 µm; $t(21) = 0.951$, $P = 0.353$, independent t-test) was consistent with the depth of the IpN when approached with a relative angle of 43°, with the entry point in crus II (Paxinos and Franklin 2004). Recordings had a duration of 149.6 s (median; range 32.2-1172.7 s) during which 16 trials (median; range 2-106 trials) were presented. Electrophysiological properties of whole-cell recorded neurons are reported in (table S1). Neurons between groups showed comparable spike frequencies (naïve: 31.7 ± 30.7 Hz, range 0-107.7 Hz, conditioned: 40.0 ± 39.4 Hz, range 0-96.5 Hz, $U = 25$, $P = 0.894$, Mann-Whitney U-test). Spike

frequencies of whole-cell recorded neurons were significantly lower than neurons recorded extracellularly (whole-cell: 36.0 ± 35.0 Hz, extracellular: 72.9 ± 35.4 Hz, U = 157, P < 0.001, Mann-Whitney U-test), demonstrating that extracellular recordings are targeted preferentially at faster spiking neurons. Whole-cell neurons showed comparable CV (naïve: 0.71 ± 0.60, range 0.14-2.29, conditioned: 1.08 ± 0.74, range 0.28-2.28, U = 22, P = 0.3, Mann-Whitney U-test) and CV_2 values (naïve: 0.58 ± 0.32, range 0.12-1.14 conditioned: 0.68 ± 0.39, range 0.24-1.33, t(20) = 0.706, P = 0.488, independent t-test) between groups. Spike parameters of whole-cell recorded neurons were determined based on 35.3 ± 42.1 s (range 10.3-158.0 s) of spontaneous activity per neuron after break-in.

2.3.6.3 Location of recorded neurons

To determine the location of recorded neurons, brains containing filled neurons were histologically processed (as described below). Due to the short duration of recordings and the fact that neurons generally died or were unable to reseal at the end of the recording, we could not identify clearly labeled neurons. However, we frequently observed diffuse fluorescent labeling of groups of neurons or glia cells located in the IpN (not shown). This was likely the result of pressure-injecting pipette solution while advancing during the whole-cell recordings session.

2.3.7 Histological procedures

Mice were anesthetized and transcardially perfused with 100 ml 4% paraformaldehyde in 0.12 M phosphate buffer. Brains were dissected and post-fixed overnight at 4°C, then cryoprotected in 0.12 M phosphate buffer containing 30% sucrose at 4°C, until they sank. Cerebella were cut on a cryostat into 25 µm-thick coronal or sagittal sections and collected in PBS. Primary antibodies were incubated overnight at 4°C in PBS containing 0.25% Triton X-100, and 5% fetal calf serum. Primary antibodies were: mouse anti-NeuN (Millipore, 1:500), chicken anti-GFP (Aves Labs, 1:700), mouse anti-calbindin (Swant, 1:1500), rabbit anti-VGLUT1 (Synaptic Systems, 1:1000), guinea pig anti-VGLUT2 (Synaptic Systems, 1:1000), mouse anti-gephyrin (Synaptic Systems, 1:500). After washing, sections were then incubated for 1 h at room temperature with one of the following fluorophore-conjugated secondary antibodies or streptavidin: donkey anti-mouse Cy3, goat anti-chicken Alexa Fluor 488 (ThermoFisher Scientific), donkey anti-guinea pig Cy3 (ThermoFisher Scientific), donkey anti-rabbit Alexa Fluor 647 (ThermoFisher Scientific), streptavidin-488 (ThermoFisher Scientific), streptavidin-Cy3 (Jackson Immunoresearch). For each immunohistochemical reaction, slices from all experimental conditions were processed together and incubation times kept constant. After processing, sections were mounted on microscope slides with Tris-glycerol supplemented with 10% Mowiol (Calbiochem).

2.3.7.1 Imaging

Fluorescent images were acquired using a confocal microscope (SP5 and SP8, Leica Microsystems). Confocal images were taken at a resolution of 1024x1024 dpi and 50 Hz speed. Lasers intensity, gain and offset were maintained constant in each analysis. Quantitative evaluations were made by a blind experimenter using Image J software. Adobe Photoshop 6.0 (Adobe Systems, San Jose, CA, USA) was used to adjust image contrast and assemble the final plates.

2.3.7.2 Quantification of density of glutamatergic terminals

To estimate the density of VGLUT1 and VGLUT2-positive axon terminals, at least three coronal sections containing the DLH or the IntA (Bregma: -6.00, -6.12) were selected for each animal (pseudo-conditioned mice, N = 3; conditioned mice, N = 3). A 0.5 um-thick confocal image/side in each section was captured under a 63x objective. The ''analyze particle'' function of ImageJ was used to estimate the density of boutons (number of terminals/mm^2) in each image, after selecting the automatic threshold to remove unwanted background information.

2.3.7.3 Quantification of gephyrin-positive puncta

Single 0.4 um thick-confocal images of the DLH or the IntA (right and left side) in coronal sections (Bregma: -6.00, -6.12) have been collected under a 63x objective with 2.5x zoom. At least three sections have been selected/mouse. On such images the density of gephyrin-positive puncta around the soma of excitatory neurons (identified by their size, i.e. > 240 um^2 – Uusisaari et al. 2007) has been evaluated by Image J and expressed as number/um neuronal membrane (pseudo-conditioned mice, N = 3; DHL, n = 53 neurons; IntA, n = 40 neurons; conditioned mice, N = 3; DLH right side, n = 35 neurons, DLH left side, n = 18 neurons; IntA right side, n = 19 neurons, IntA left side, n = 12 neurons).

2.3.8 Statistics

Statistical analysis was carried out using MATLAB (vR2011b, MathWorks), SPSS (v22, IBM) or GraphPad Prism 5 (GraphPad Software Inc.). Normality of distributions was assessed using Shapiro-Wilk test and, if normality was violated, non-parametric tests were performed. Statistical tests that were used are reported throughout the text.

Behavioral performance was analyzed using repeated-measures ANOVA (data from camera setup) or linear mixed models (data from MDMT setup) with the maximum likelihood method. Group and session/day was modelled as fixed effects, and %CR and FEC at US onset were modelled as dependent variables. We assessed the fit of the model by running the

analysis with the unstructured, diagonal and first-order autoregressive repeated covariance types, after which we choose the covariance type with the lowest Akaike's information criterion (AIC) value, which was in most cases the unstructured type. Data is shown as mean ± SD, unless indicated otherwise and $P < 0.05$ was considered to be statistically significant.

2.4 Results

2.4.1 Spike response patterns of eyeblink-encoding IpN neurons

To examine how IpN neurons encode conditioned eyeblink responses, we first established that we could reliably record from eyeblink-encoding neurons in awake behaving mice. We trained habituated head-fixed mice daily for 10 days using a protocol containing 200 paired CS (260 ms green LED) and US (10 ms corneal air puff) trials with co-terminating stimuli (N = 9; Fig 1A). Mice showed learning as an increase in CR percentage and fraction eyelid closure (FEC; 0 is fully open, 1 is fully closed) at US onset (Fig 1B, C; table 1). Stereotaxic coordinates for reaching the eyeblink-encoding IpN region were optimized by functional mapping through microelectrode stimulation in awake and trained (N = 3) animals (Heiney et al. 2014b; Ten Brinke et al. 2017)(Fig S1), after which these coordinates were consistently used to guide our glass recording electrodes. We started by characterizing spike response patterns of eyeblink-encoding IpN neurons in awake conditioned mice (Fig 1A). CS and US responses were recorded in 132 neurons with an average spontaneous spike frequency of 72.9 ± 35.4 Hz. During recordings mice showed robust conditioned eyelid behavior (CR percentage: 58.0 ± 30.6%, CR amplitude: 45.7 ± 35.4% of UR, CR onset after CS: 136.4 ± 184.3 ms).

CS spike responses were classified in 88 neurons (Fig 1D) and US spike responses were classified in 98 neurons (Fig 1G), based on spike frequency changes during the CS-US or US period, respectively. We observed CS responses in 45.5% and US responses in 78.6% of recorded IpN neurons. In line with previously used nomenclature, neurons showing frequency increases were classified as spike facilitation cells, and those showing frequency decreases were classified as spike suppression cells (Ten Brinke et al. 2017). Neurons in our dataset showed differential CS responses (facilitation: 29.5% (26/88), suppression: 15.9% (14/88), no response: 54.5% (48/88); Fig 1D-F) with minor differences in the distribution compared to previously published results (Ten Brinke et al., 2017: facilitation: 22.2%, suppression: 8.5%, no response: 69.3%; $P = 0.027$, Fisher's Exact test). The distribution of US responses was also comparable to the same study (facilitation: 50% (49/98; our data) vs 49.6%, suppression: 10.2% (10/98) vs 10.3%, facilitation and suppression: 18.4% (18/98) vs 28.5% and no response: 21.4% (21/98) vs 11.5%; $P = 0.051$, Fisher's Exact test; Fig 1G-J). Based on the coarse similarities in CS and US response distributions, we conclude that we correctly targeted eyeblink-encoding IpN neurons.

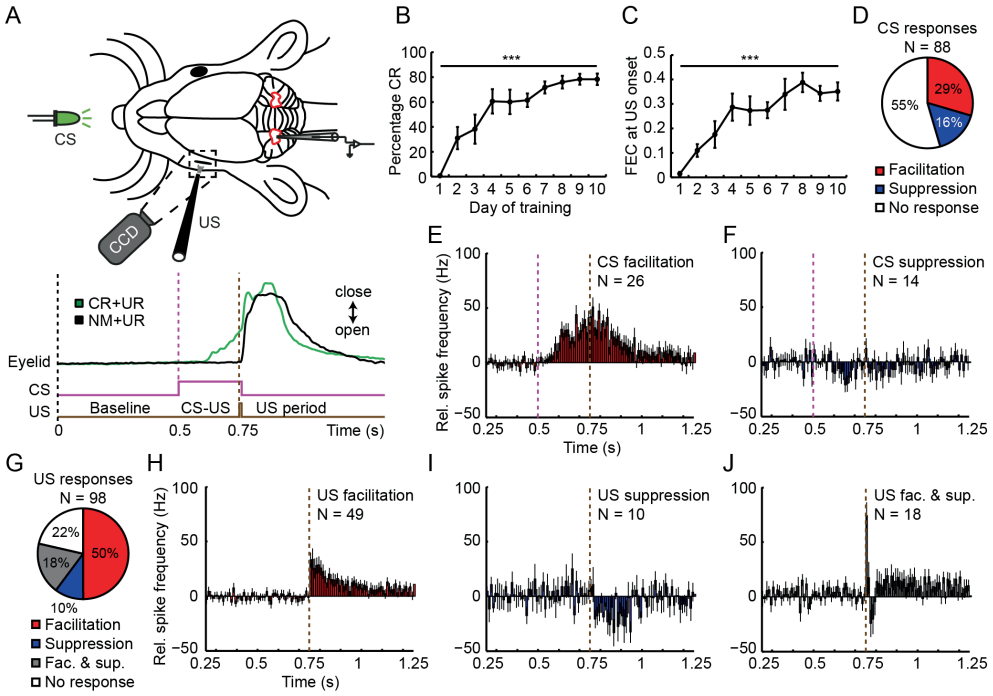

Fig 1. Activity of IpN neurons during eyeblink conditioning. (A) Extracellular recordings of IpN neurons in awake conditioned mice while eyelid movements were recorded. Eyelid closures during the interval between CS (260 ms LED light) and US (10 ms air puff) were identified as conditioned responses (CRs; green) and distinguished from no movement (NM; black) trials. (B, C) Mice showed a significant increase in percentage CR trials and fraction eyelid closure (FEC) at US onset during 10 days of training prior to recording sessions. (D) Distribution of neuronal CS-evoked spike responses in well-trained mice. (E, F) peristimulus time histogram (PSTH) showing relative (rel.) spike frequency changes during paired CS-US trials for (E) CS facilitation and (F) CS suppression neurons. (G) Distribution of neuronal US-evoked spike responses. (H-J) PSTH showing relative spike frequency changes following US for neurons showing US facilitation (H), US suppression (I) and US facilitation (fac.) & suppression (sup.) responses (J). Error bars represent SEM. PSTH bins are 10 ms. ***P<0.001

CS facilitation neurons showed peak frequency increases of 80.3 ± 38 Hz and CS suppression cells showed peak frequency decreases of -52.1 ± 23.3 Hz following the CS. Comparable spike frequency changes were observed after the US, where US facilitation neurons showed peak frequencies of 81.3 ± 54.2 Hz with an onset of <10 ms (Fig 1H). US suppression neurons showed peak frequency decreases of -50.7 ± 27 Hz after >20 ms following the US (Fig 1I). We also found neurons showing both US facilitation and suppression (Fig 1J), with a short-latency peak frequency increase of 103.3 ± 41.3 Hz and delayed a peak frequency decrease of -61.5 ± 34.3 Hz. These data suggest that direct excitatory axons evoked spike facilitation, whereas inhibitory axons evoked delayed spike suppression via a longer, multi-synaptic pathway. Previous studies have suggested that US-induced responses are conveyed via the olivo-cerebellar circuit, whereas conditioned

eyeblink responses are conveyed via the MF pathway (Freeman and Steinmetz 2011). There are strong indications that particularly the MF pathway undergoes learning-related structural changes (Kleim et al. 2002; Boele et al. 2013). As a next step we investigated learning-associated structural changes in IpN after conditioning in more detail.

Table 1. Learning performance during conditioning or pseudo-conditioning. RM: repeated-measures, GLMM: generalized linear mixed model, AR(1): first-order autoregressive model.

Group	Statistic, df	P-value	Statistical test
10 days conditioning	*Extracellular IpN recordings*		
CR percentage	F(3.098, 24.786) = 16.272	< 0.001	One-way RM ANOVA
FEC at US onset	F(4.139, 33.108) = 10.78	< 0.001	One-way RM ANOVA
Conditioned vs pseudo	*VGLUT1, VGLUT2, gephyrin*		
CR percentage			
Main-effect training	F(9, 40.452) = 13.941	< 0.001	GLMM (AR(1))
Main-effect group	F(1, 9.798) = 104.638	< 0.001	GLMM (AR(1))
Interaction training*group	F(9, 40.452) = 11.375	< 0.001	GLMM (AR(1))
FEC at US onset			
Main-effect training	F(9, 40.163) = 9.338	< 0.001	GLMM (AR(1))
Main-effect group	F(1, 15.301) = 50.729	< 0.001	GLMM (AR(1))
Interaction training*group	F(9, 40.163) = 8.514	< 0.001	GLMM (AR(1))
10 days conditioning	*In vivo* whole-cell recordings		
CR percentage	F(9, 59.703) = 4.876	< 0.001	GLMM (AR(1))
FEC at US onset	F(9, 60.234) = 4.845	< 0.001	GLMM (AR(1))

2.4.2 Conditioning induces an increase in VGLUT1+ and gephyrin+ puncta in the DLH

We studied changes in the number of excitatory and inhibitory terminals in the IpN in mice that were subjected to 10 days of conditioning (N = 3) or pseudo-conditioning (N = 3). Conditioned mice showed associative learning evident by an increase in CR percentage (N = 3) as opposed to pseudo-conditioned mice that did not learn (table 1). The IpN consists of two eyeblink-encoding regions: the anterior interposed nucleus (IntA) and dorsolateral hump (DLH), which were separately analyzed to enable identifying regional differences. The markers for excitatory synapses VGLUT1 and VGLUT2 were used to detect MF and CF terminals, since the former can express either VGLUT1 or VGLUT2 or both, and the latter expresses VGLUT2 only (Hioki et al. 2003). The marker gephyrin was used to detect inhibitory synapses. We investigated differences between groups (learning-related),

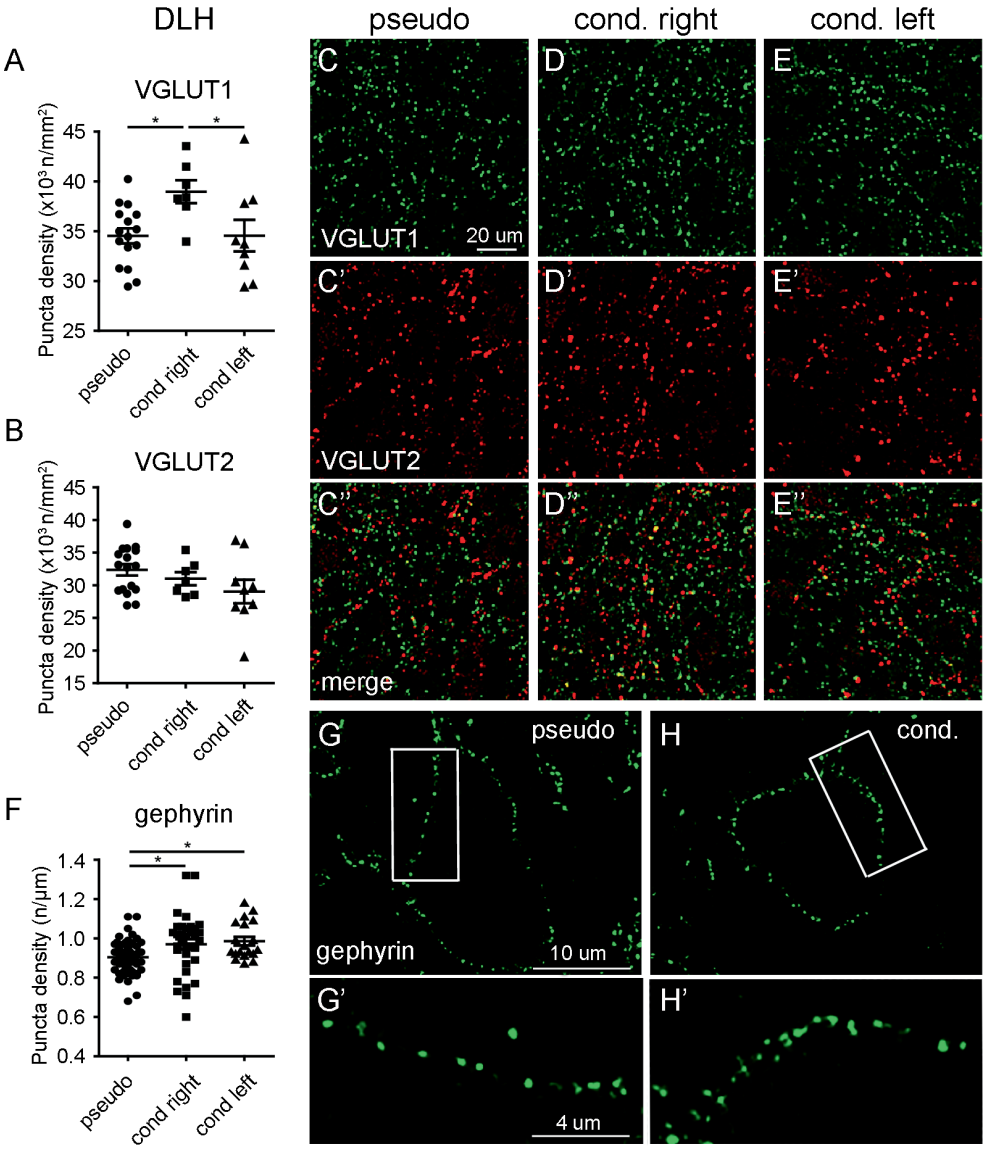

Fig 2. Increased density of VGLUT1+ and gephyrin+ puncta in DLH after EBC. (A) Increased density of VGLUT1+ puncta was observed in the right DLH in conditioned mice compared to the left side and pseudo-conditioned mice. (B) Density of VGLUT2+ puncta was unchanged after conditioning. (C-E'') VGLUT1 and VGLUT2 immunofluorescence in the DLH of pseudo-conditioned and conditioned mice (left and right). (F) Increased densities of gephyrin+ puncta in the bilateral DLH of conditioned mice was observed. (G-I') Immunofluorescence of gephyrin+ puncta on the neuronal membrane in the DLH. (H'-I') Magnified images the white squares indicated in H and I. Error bars represent SEM. *P<0.05, ***P<0.001

Table 2. Expression of VGLUT1, VGLUT2 and gephyrin in DLH and IntA. Cond.: conditioned, pseudo: pseudo-conditioned, DLH: dorsolateral hump, IntA: anterior interposed nucleus.

Condition	Statistic, df	P-value	Statistical test
VGLUT1			
DLH: pseudo vs cond. right vs cond. left	F(2, 29) = 4.155	**0.026**	One-way ANOVA
pseudo vs cond. right	N/A	**0.028**	Tukey *post-hoc*
pseudo vs cond. left	N/A	1	Tukey *post-hoc*
cond. right vs cond. left	N/A	0.054	Tukey *post-hoc*
IntA: pseudo vs cond. right vs cond. left	F(2, 30) = 2.022	0.15	One-way ANOVA
VGLUT2			
DLH: pseudo vs cond. right vs cond. left	F(2, 29) = 0.196	0.823	One-way ANOVA
IntA: pseudo vs cond. right vs cond. left	F(2, 26) = 0.053	0.949	One-way ANOVA
gephyrin			
DLH: pseudo vs cond. right vs cond. left	F(2, 104) = 5.468	**0.006**	One-way ANOVA
pseudo vs cond. right	N/A	**0.023**	Tukey *post-hoc*
pseudo vs cond. left	N/A	**0.021**	Tukey *post-hoc*
cond. right vs cond. left	N/A	0.873	Tukey *post-hoc*
IntA: pseudo vs cond. right vs cond. left	F(2, 67) = 0.416	0.662	One-way ANOVA

regions (DLH vs IntA) and hemispheres (contralateral vs ipsilateral, relative to air puff). We found that after 10 days of conditioning, mice showed an increased density of VGLUT1+ puncta in the contralateral DLH compared to pseudo mice (Fig 2A, C-E"; table 2). The density of VGLUT2+ puncta in the DLH was unchanged (Fig 2B; table 2), as well as the densities of VGLUT1+ and VGLUT2+ puncta in the IntA (Fig S2A, B, C-E"). This indicates that VGLUT1-positive MFs are upregulated during conditioning, in line with previously reported increases in MF varicosities predominantly in the contralateral IpN after conditioning (Boele et al. 2013).

We next compared the expression of gephyrin+ puncta on the postsynaptic side of the neuronal membrane in the DLH and IntA as a marker for inhibitory synapses (Fig 2G-H', S2G-H'), of which ~85% comes from PCs and ~15% from local interneurons (De Zeeuw and Berrebi 1995). We found a significantly increased density of gephyrin+ puncta in both the left and right DLH of conditioned mice compared to pseudo mice (Fig 2F), whereas expression of gephyrin in the IntA was comparable (Fig S2F). To find out whether PC axons or other inhibitory projections were increased, we used the expression of CALB+ puncta to identify PC axon terminals (Fig S3A). We quantified gephyrin+ puncta that were not

apposed to CALB+ puncta, thus representing inhibitory terminals other than from PCs. We found that conditioning did not significantly alter the percentage of gephyrin+/CALB- pairs on DLH neurons (naïve: 3.09 ± 1.49%, conditioned: 4.13 ± 3.1%; t(38) = 1.31, P = 0.20, independent t-test; Fig S3B), indicating that the increase gephyrin+ puncta was specifically due to an increase in PC synaptic terminals. Based on this evidence we conclude that during conditioning both excitatory MFs and inhibitory PCs increase in eyeblink-encoding regions of the IpN.

2.4.3 Optogenetic mossy fiber interference elicits eyelid movements only after learning

We next asked whether the learning-induced increases in excitatory MF terminals are also functional. To answer this question, we bilaterally transfected pontocerebellar MFs of the visual input-encoding lateral pontine nuclei (PN) (Leergaard and Bjaarlie 2007) with the optogenetic constructs chronos and/or eArch3.0. Using this approach, we were able to activate or silence MF fibers, respectively, through optic fibers implanted above the PN (Fig 3A). High densities of YFP and GFP co-labeled fibers were observed in PN and middle cerebellar peduncles ~5 weeks after injections (Fig 3B, B'). Throughout the cerebellum, co-labeled MF to granule cell synaptic boutons ('MF rosettes') were found (Fig 3C, C'). Transfection was specific to MFs, since no CF labeling was visible in the molecular layer of the cerebellar cortex. High densities of YFP and GFP co-expressing MFs were seen in both eyeblink-encoding IpN regions IntA and DLH (Fig 3D, D', E, E'), confirming that we had effectively transduced MF projections to the IpN and cerebellar cortex.

We first established that we could reliably modulate activity in MFs, by recording IpN spike activity during optogenetic stimulation. Chronos-evoked MF activation resulted in short-latency spike frequency changes in 75% of IpN neurons (54.2% facilitation, 12.5% suppression, 8.3% facilitation & suppression; Fig 3F), indicative of both mono- and polysynaptic spike frequency modulation. Optogenetic activation of eArch3.0, leading to MF silencing, caused IpN spike frequency changes in 48.6% of neurons (32.4% facilitation, 9.9% suppression and 6.3% facilitation & suppression), although spike changes were less abrupt than during MF activation (Fig 3H). We conclude that with our approach we could effectively modulate activity of MFs.

2.4.3.1 Optogenetic MF activation causes short latency eyelid closures in conditioned mice

Next, eyelid responses during MF activation were measured in mice in naïve state, after 5 (moderately trained mice), and after 10 days of conditioning (fully trained mice, Fig S4A). MF activation caused small eyelid closures in fully and moderately trained mice, but not in naïve mice (day 10: amplitude: 0.99 ± 0.55% of UR, peak latency: 68.5 ± 6.16 ms, t(3) = 3.598,

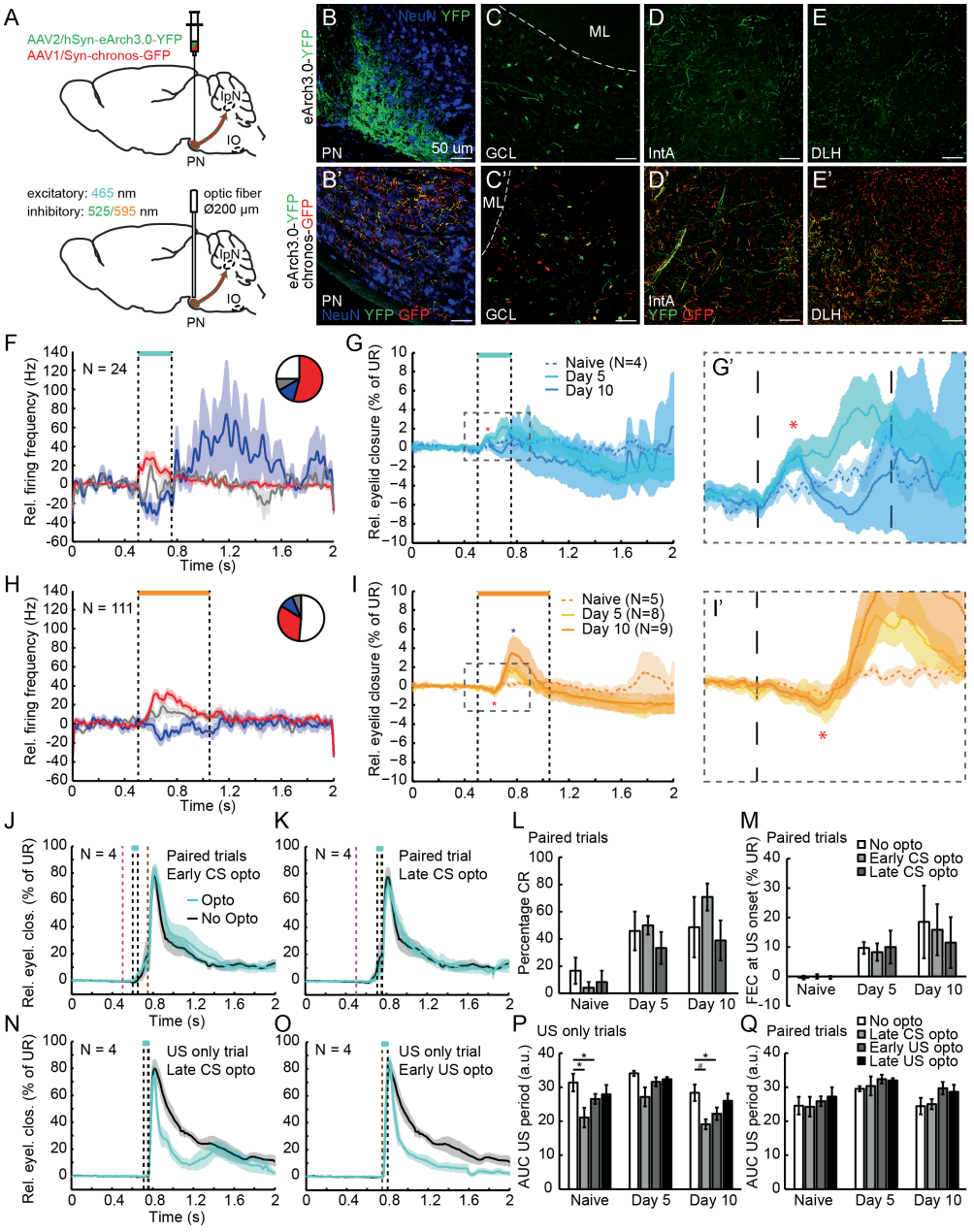

Fig 3. Optogenetic mossy fiber interference. (A) Viral injections in the bilateral PN leads to expression of optogenetic constructs for inhibitory and excitatory control of activity in pontocerebellar mossy fibers. (B-B') Expression of YFP and co-expression of YFP and GFP reporters in PN and middle cerebellar peduncle after injections shows intense co-labeling. (C-C') Labeled mossy fiber terminals are observed in the cerebellar GCL, whereas labeling in the ML is absent. (D-D', E-E') Intense co-labeling of mossy fibers in the IntA and DLH regions

of the cerebellar nuclei. (F) IpN spike activity changes during mossy fiber activation. (G) Optogenetic activation of mossy fibers leads to short-latency eyelid movements in conditioned mice (red asterisk). (G') magnified image of the grey square in G. (H) IpN spike activity changes during mossy fiber silencing. (I) Optogenetic silencing of mossy fibers leads to biphasic eyelid movements in conditioned mice, showing short-latency eyelid openings (red asterisk) and delayed eyelid closures (blue asterisk). (I) Magnified image of the grey square in I. (J, K) Mossy fiber activation at the time of onset (early CS opto) or during execution of CRs (late CS opto) does not influence (L) percentage CR trials or (M) FEC at US onset in naïve or (5 or 10-day) conditioned mice. (N, O) Mossy fiber activation right before (late CS opto) or during (early US opto) US arrival reduces UR magnitude (AUC) during (P) US only trials in naïve and conditioned mice, but not paired trials (Q). PN: pontine nuclei, IO: inferior olive, GCL: granule cell layer, ML: molecular layer, IntA: anterior interposed nucleus, DLH: dorsolateral hump. Error bars represent SEM. # indicates a trend, *P<0.05, **P<0.01, ***P<0.001

P = 0.037, two-tailed, one-sample t-test; day 5: amplitude with same latency: 0.92 ± 0.84% of UR, t(3) = 2.196, P = 0.058, one-tailed, one-same t-test; day 5 vs day 10: t(3) = -0.435, P = 0.693, paired t-test, Fig 3G, G', red asterisk). Eyelid closures with similar onset latencies were absent in naïve mice (-0.02 ± 0.38 ms; t(3) = -0.078, P = 0.471, one-tailed, one-same t-test) and were significantly lower than responses seen in both moderately and fully conditioned mice (vs day 10: t(3) = -6.854, P = 0.006, paired t-test; vs day 5: t(3) = -3.733, P = 0.033, paired t-test). This demonstrates that learning-associated sprouting of MFs (Kleim et al. 2002; Boele et al. 2013) enables general unspecific MF activation to elicit eyelid muscle-contractions only in moderately and fully conditioned mice but not in naïve animals. These data furthermore suggest that the observed MF sprouting could play a role in making general MF information selective for eyelid-specific movements.

2.4.3.2 Optogenetic MF silencing causes bidirectional eyelid movements

Eyelid responses to eArch3.0-evoked MF silencing were also measured in mice. In fully trained mice (N = 9), MF silencing caused significant eyelid openings (amplitude: -0.82 ± 0.45% of UR, t(8) = -5.508, P = 0.001, two tailed, one-sample t-test), with a peak latency of 129.9 ± 16.4 ms following stimulus onset (Fig 3I, I', red asterisk). In moderately conditioned mice (N = 8), MF silencing also induced significant eyelid openings at 129.9 ms after light onset (-0.71 ± 0.97% of US, t(7) = -2.076, P = 0.038, one-tailed, one-sample t-test), with comparable amplitudes (t(7) = -0.439, P = 0.674, paired t-test). Significant eyelid openings with a similar latency were absent in naïve mice (-0.34 ± 0.6% of US, t(4) = -1.256, P = 0.139, one-tailed, one-sample t-test). We conclude that MF silencing evoked eyelid movements only after learning-induced increases in MF terminals, consistent with the MF activation-induced eyelid closures as observed above.

Eyelid openings were followed by significant eyelid closures in 66.7% (6/9) in fully trained mice (amplitude: 7.1 ± 5.71% of US), peak latency: 279.3 ± 96.6 ms after light onset (Fig 3I blue asterisk). All moderately conditioned mice (8/8) showed significant eyelid closures with a peak latency of 254.4 ± 40.9 ms (amplitude: 2.54 ± 2.17% of US) and 60% (3/5) of naïve mice showed significant light-induced eyelid closures, although their peak time was

significantly later (amplitude: 1.41 ± 0.79% of UR, peak latency: 488.5 ± 102.8 ms; $\chi^2(2)$ = 6.433, P = 0.04, Kruskall-Wallis H test). The peak latency of these eyelid movements in moderately and fully conditioned mice is highly comparable to the time course of normal CRs during EBC (Fig 1A), suggesting that we evoked 'CR'-like responses during optogenetic MF silencing. It furthermore shows that we were unable to silence all pontocerebellar MFs. Because of these reasons we did not further employ MF silencing during the EBC paradigm.

2.4.4 MF activation does not facilitate CR, but affects UR only in unpaired US trials

We hypothesized that if MF collateral excitatory input to IpN neurons contributes to CRs, optogenetic MF activation during the CS-US interval would enhance CRs. Mice (N = 4) received 10 days of conditioning during which they learned (Fig 1B, C). Alternating sessions with MF activation were presented over the course of conditioning (Fig S4A, B). First, we established that we could alter IpN spike activity through MF activation during the task. Optogenetic MF activation during the CS-US period resulted in spike activity increases (Fig S4C, red arrowhead) or decreases (Fig S4D, blue arrowhead) in facilitation and suppression cells, respectively. MF activation right before the US led to a marginally significant reduction of US-evoked spike responses during paired trials (area under the curve (AUC) of first 200 ms after US: Z = 7, P = 0.063, Wilcoxon Signed Rank test; Fig S4E, red hashtag), but not in US only trials (AUC: t(5) = -0.033, P = 0.975, paired t-test; Fig S4F), although the spike activity profile appeared altered. MF activation right after US arrival did not alter US-evoked responses in paired (AUC: t(3) = 0.915, P = 0.428, paired t-test; Fig S4E) or US only trials (AUC: Z = 7, P = 0.465, Wilcoxon Signed Rank test; Fig S4G). Thus, optogenetic MF activation could alter task-related spike activity after the CS and US.

Next, we studied the effect of MF activation on eyelid behavior. Stimulation during the early (early CS; Fig 3J) phase of the CS-US interval (*i.e.* around CR onset) or late (late CS; Fig 3K) phase of the CS-US interval (during CR execution) did not influence percentage CR (Fig 3L; table 3) or FEC at US onset (Fig 3M; table 3). Early CS stimulation did also not influence CR onset (table 3). During stimulation, maximum eyelid movements were not significantly changed (table 3). Interestingly, MF activation around the US period significantly altered the UR. Stimulation right before and right after US arrival (Fig 3N, O) significantly reduced UR magnitude in naïve and fully conditioned mice, and showed a trend in moderately conditioned mice (Fig 3P; table 3). However, these effects were only present in US only and not in paired trials (Fig 3Q). These results suggest that MF activation can effectively change the UR, despite the trigeminal to motor nuclei projections being the main modulator of the reflexive UR. Previous studies that used IpN interference also led to diminished URs (Chapman et al. 1990; Bracha et al. 1994; Hesslow 1994).

Table 3. Statistics on behavioral parameters during optogenetic MF activation. RM: repeated-measures, FEC: fraction eyelid closure.

MF activation	Statistic, df	P-value	Statistical test
CR percentage			
Naïve	$\chi^2(2) = 1.4$	0.497	Friedman
5 days conditioning	$F(2, 6) = 1.114$	0.388	One-way RM ANOVA
10 days conditioning	$F(2, 6) = 1.35$	0.328	One-way RM ANOVA
FEC at US onset			
Naïve	$\chi^2(2) = 3.5$	0.174	Friedman
5 days conditioning	$F(2, 6) = 3.071$	0.121	One-way RM ANOVA
10 days conditioning	$\chi^2(2) = 3.5$	0.174	Friedman
CR onset - early CS opto			
5 days conditioning	$t(3) = 1.47$	0.238	Paired t-test
10 days conditioning	$t(2) = 0.47$	0.685	Paired t-test
Max response during opto			
Naïve			
No opto vs early CS opto	$t(3) = 0.769$	0.498	Paired t-test
No opto vs late CS opto	$t(3) = -0.277$	0.8	Paired t-test
5 days conditioning			
No opto vs early CS opto	$t(3) = 0.52$	0.639	Paired t-test
No opto vs late CS opto	$t(3) = 0.87$	0.936	Paired t-test
10 days conditioning			
No opto vs early CS opto	$t(3) = -2.156$	0.12	Paired t-test
No opto vs late CS opto	$Z = 4$	0.273	Wilcoxon Signed Ranks
AUC US period	**US only trials**		
Naïve	$F(3, 9) = 13.531$	**0.001**	One-way RM ANOVA
No opto vs late CS opto	$F(1, 3) = 24.547$	**0.016**	Simple contrast
No opto vs early US opto	$F(1, 3) = 10.775$	**0.046**	Simple contrast
No opto vs late US opto	$F(1, 3) = 6.251$	0.088	Simple contrast
5 days conditioning	$F(3, 9) = 3.17$	0.078	One-way RM ANOVA
10 days conditioning	$F(3, 9) = 6.548$	**0.012**	One-way RM ANOVA
No opto vs late CS opto	$F(1, 3) = 9.519$	0.054	Simple contrast
No opto vs early US opto	$F(1, 3) = 31.604$	**0.011**	Simple contrast
No opto vs late US opto	$F(1, 3) = 1.058$	0.379	Simple contrast
AUC US period	**Paired trials**		
Naïve	$F(3, 9) = 0.927$	0.467	One-way RM ANOVA
5 days conditioning	$F(3, 9) = 1.825$	0.213	One-way RM ANOVA
10 days conditioning	$F(3, 9) = 2.491$	0.126	One-way RM ANOVA

2.4.5 MFs are an unlikely candidate for short-latency US-evoked spike facilitation

Short-latency spike facilitation following the US (latency <10ms; Fig 1H, J) data (Ten Brinke et al. 2017) is likely caused through direct excitatory projections to IpN neurons, but which projections are responsible is unknown. Two possible candidates are collaterals from MFs and CFs, where the former has been favored based on the widespread expression of US-evoked responses in the DCN (Groenewegen and Voogd 1977). We hypothesized that if MFs are responsible for the US-evoked spike facilitation, partial optogenetic silencing of MFs during the US would reduce this activity. We recorded IpN spike responses in 52 neurons, while presenting alternating trials with MF silencing. Spike frequency changes following US was however not significantly altered during MF silencing (no opto: 78.6 ± 53.8 Hz, opto: 73.8 ± 45.5 Hz; Z = 52, P = 0.346, Wilcoxon Signed Rank test), suggesting that collaterals of CFs instead of MFs cause short-latency spike facilitation after the US.

2.4.6 Synaptic activity in IpN neurons underlying associative eyelid movements during EBC

Having established the limited contribution of structurally increasing MFs to IpN activity and CRs, we subsequently wanted to investigate how conditioned eyeblinks are synaptically encoded in IpN neurons. The reasoning is threefold: first, we found that functional MF and PC terminals increase during learning. Second, we showed that general MF stimulation after learning can evoke eyeblink-specific movements, as opposed to naïve animals where MF stimulation does not evoke any eye-related movements. Third, optogenetic MF stimulation during learning does not affect CRs significantly, which suggests that either (i) MF activity is not crucial for conditioned eyeblinks, (ii) that only partial MF activity is still enough to evoke well-timed CRs after learning, or (iii) next to MF activity PC synchrony has to occur to evoke MF-driven spiking (Wu and Raman 2017). We obtained *in vivo* whole-cell recordings of individual IpN neurons while mice performed EBC (Fig 1A). Both naïve and conditioned mice were recorded to study learning-associated changes in membrane potential (V_m) dynamics. To distinguish learned from voluntary behavior, three types of eyelid movements were identified: CRs, no movements (NMs) and eyelid openings (EOs; Fig 4A, purple trace), the latter of which has been reported to influence US-evoked spike responses (Ten Brinke et al. 2017). As expected, CRs were significantly more present in conditioned mice (0.8 ± 2.6% vs 72.9 ± 31.2% (conditioned), U = 120, P < 0.001, Mann-Whitney U test). EOs however were more frequently observed in naïve mice (37.0 ± 39.6% vs 1.0 ± 3.2%, U = 17.5, P = 0.003, Mann-Whitney U test; Fig 4B, C). Consequently, conditioned mice showed a higher FEC at US onset (-0.1 ± 0.16 vs 0.17 ± 0.16; U = 117, P < 0.001, Mann-Whitney U test; Fig 4D). This eyelid behavior corresponds to the robust learning that was observed during conditioning of these mice (Fig S5A, B; table 1).

2.4.6.1 IpN neurons show differential V_m encoding

We obtained V_m recordings of IpN neurons (n = 25) with distinct whole-cell properties (Methods; table S1) from awake behaving adult male mice during presentation of paired and unpaired trials (Fig S5C, D). In IpN neurons, V_m depolarizations can be evoked in multiple ways, *i.e.* through MF and CF collateral activity as well as reductions in tonic inhibition from PCs. Based on this nature, large depolarizations were called compound excitatory postsynaptic potentials (cEPSPs) since the exact contribution of inputs was unclear. Currents evoked by MF and CF collaterals are largely AMPA receptor-mediated and have a short rise time (Wu and Raman 2017; Najac and Raman 2017). Since synchrony or reductions in activity of PCs is necessary for MFs to drive IpN spike activity (Wu and Raman 2017), a likely scenario is a mutual contribution of both projections during the task. In contrast, IpN V_m hyperpolarizations can be evoked by increased synchronous inhibition from PCs (~85%) and local IpN interneurons (~15%) (De Zeeuw and Berrebi 1995; Gauck and Jaeger 2000; Telgkamp and Raman 2002; Pedroarena and Schwartz 2003; Witter et al. 2013). Accordingly, they were called compound inhibitory postsynaptic potentials (cIPSPs). In all of our recordings, we observed that neurons showing cEPSPs represent spike facilitation neurons (Fig 4F) and cIPSPs represent spike suppression neurons (Fig 4G). We further distinguished V_m responses that occurred during the CS-US interval as CS-cEPSPs or CS-cIPSPs, and after the US as US-cEPSPs or US-cIPSPs (Fig 4F, G).

2.4.6.2 Altered CS-cEPSP profiles after learning are likely caused by changes in PC activity

First, we classified IpN neurons based on V_m responses during the CS-US interval, where we found that 33.3% of neurons in naïve mice showed significant CS-evoked V_m responses, whereas this was 53.8% in conditioned mice (naïve vs conditioned; cEPSP: 25.0% vs 38.5%, cIPSP: 8.3% vs 15.4%, no response: 66.7% vs 46.2%, P = 0.629, Fisher's Exact test). The distribution of these responses is strikingly similar to our observed spike activity patterns described earlier (Fig 1D), which indicates that a similar population of IpN neurons was recorded both extra- and intracellularly. Next, to investigate learning-induced changes in V_m encoding, we compared CS-cEPSPs and CS-IPSPs between naïve and conditioned mice (Fig 4H-I'; table 4). We found that CS-cEPSPs had comparable amplitudes ($t(6) = 0.333$, P = 0.75, independent t-test) and onsets (U = 7, P = 1, Mann-Whitney U test). Interestingly, these similar V_m encoding properties underlie EOs in naïve and CRs in conditioned mice, where the absolute amplitude of eyelid movement was not different ($t(6) = -0.016$, P = 0.988, independent t-test; table 4). In contrast to naïve mice, where we observed transient CS-cEPSPs (Fig 4H, I; slope: -33.59 ± 3.13 mV/s, $t(2) = -18.556$, P = 0.003), conditioned mice showed sustained CS-cEPSPs (slope within dotted square: 7.49 ± 23.01 mV/s, $t(4) = 0.728$, P = 0.507, one-sample t-test; between groups: $t(6) = -2.98$, P = 0.025; independent t-test; Fig 4J).

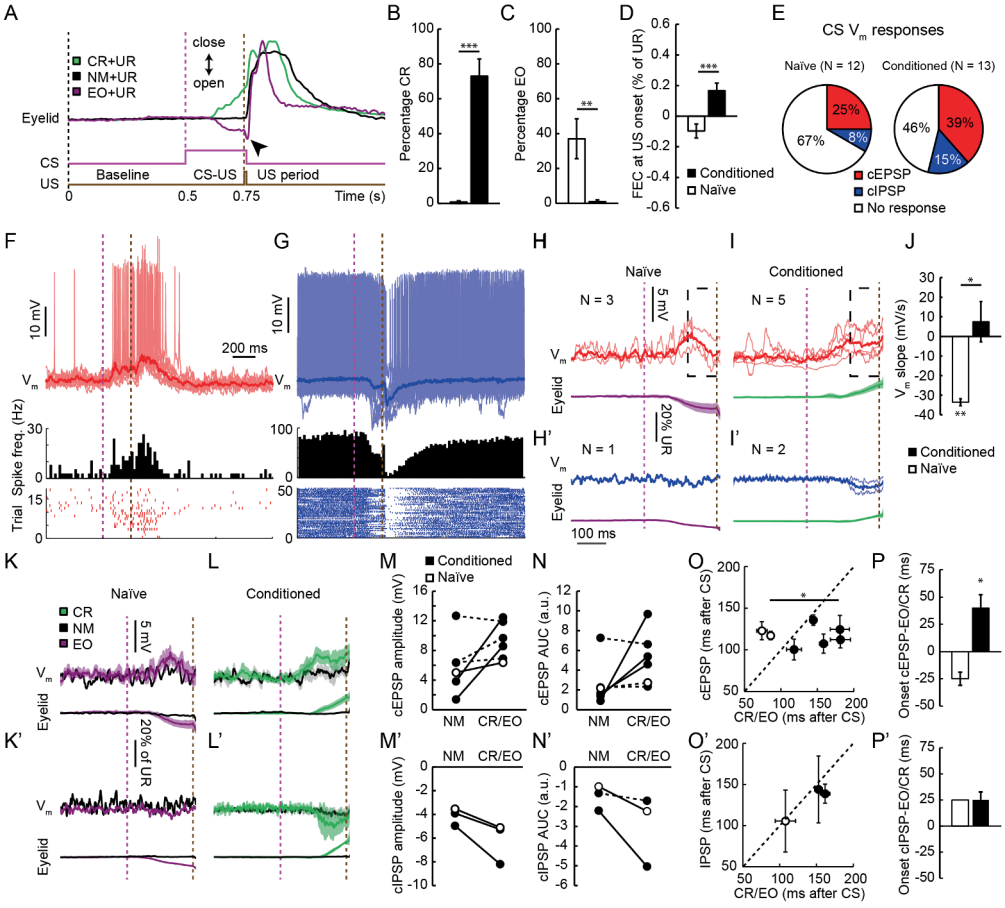

Fig 4. Membrane potential dynamics underlying CS-evoked eyelid responses during EBC. (A) CR, NM and EO trials were identified during the CS-US period. Occasionally the UR was preceded by a short-latency eyelid opening (black arrowhead). During CS only trials of recordings, conditioned mice showed more CRs (B) whereas naïve mice showed more EOs (C). This led to a higher FEC at US onset for conditioned mice (D). (E) IpN neurons show differential V_m responses following the CS, with more widespread encoding in conditioned mice. (F, G) CS-cEPSPs and CS-cIPSPs (below magenta line), as well as US-cEPSPs and CS-cIPSPs (below brown line) were distinguished as changes relative to the baseline, and these V_m responses coincided with spike facilitation and suppression responses, respectively. (H-I') Average CS-cEPSP and CS-cIPSP responses measured in naïve (H, H') and conditioned (I, I') mice during CS only and paired trials, with their associated eyelid movements. Note that eyelid movements represented mostly EOs and CRs in naïve and conditioned mice, respectively. CS-cEPSPs were transient in naïve, but sustained in conditioned mice, as measured by the slope of the traces within the black dotted square (J). (K-L') IpN neuronal V_m responses were dependent eyelid movements in both groups. Based on the amplitude or magnitude (AUC) of V_m responses, neurons specifically encoding eyelid movements were identified (red lines indicates significance). (O, P) CS-cEPSPs preceded the onset of CRs, but not of EOs. Onset of CS-cIPSPs was variable and occurred around movement onset (O'-P'). Error bars represent SEM. *P<0.05, **P<0.01, ***P<0.001

Additionally, in none of our recordings we were able to identify V_m dynamics that unambiguously represented activity from MF collaterals, although other inputs could have obscured the detection of these. These findings are consistent with reduced PC simple spike rates during the CS-US period that emerges during conditioning (Berthier and Moore 1986; Jirenhed et al. 2007; Ten Brinke et al. 2015) and indicate that learning-related changes in V_m are mainly carried by PCs. Consistent with the much smaller percentage of CS spike suppression cells reported here and earlier (Ten Brinke et al. 2017), we found too few CS-cIPSP neurons to compare V_m responses (Fig 4H', I').

Table 4. Characteristics of CS and US-evoked cEPSPs/cIPSPs and eyelid movements. RM: repeated-measures, FEC: fraction eyelid closure.

Group	CS/US	Response type	Amplitude (mV)	V_m onset (ms)	FEC (% of UR)
Conditioned	CS	cEPSP (N = 5)	3.67 ± 1.88	92.16 ± 27.99	8.65 ± 4.62
		cIPSP (N = 2)	-1.41 ± 1.03	136.2 (N=1)	3.75 ± 0.76
Naïve	CS	cEPSP (N = 3)	4.12 ± 1.81	94.61 ± 4.35	8.59 ± 5.02
		cIPSP (N = 1)	-1.29	80.1	4.89
Conditioned	US	cEPSP (N = 6)	9.11 ± 3.84	13.13 ± 7.76	70.16 ± 22.68
		cIPSP (N = 2)	-8.80 ± 0.09	13.15 ± 1.01	48.53 ± 8.34
Naïve	US	cEPSP (N = 9)	7.53 ± 3.40	11.38 ± 7.0	58.64 ± 22.78
		cIPSP (N = 1)	-3.02	17.27	32.26

2.4.6.3 Eyelid movements are caused by population activity, where IpN neurons encode movements differentially

To further investigate how V_m responses relate to eyelid movements, we separately studied V_m responses during CR, NM and EO trials. We found that V_m encoding neurons not necessarily showed larger synaptic responses in trials where movements occurred (Fig S6). In our dataset, 3/5 neurons in conditioned and 1/1 neuron in naïve mice specifically encode CRs and EOs through increased cEPSP amplitudes or/and AUC (Fig S6A and Fig 4K-N; uninterrupted lines indicate significance). In these neurons, cEPSPs during CR or EO trials were 5.73 ± 3.87 mV larger compared to NM trials. In a minority of neurons (2/5 in conditioned mice) movements did not influence the profile of CS-cEPSPs (Fig S6B and Fig 4K-N; dotted lines). Neurons showing CS-cIPSPs all showed increased V_m responses during CR or EO trials, where they showed 2.06 ± 1.02 mV larger response amplitudes (Fig S6C and 4K'-N'). These findings show that IpN neurons encode different aspects of the task, such as the CS in absence of eyelid movement, and that these heterogeneous responses at the population level give rise to conditioned eyelid movements.

2.4.6.4 Synaptic encoding precedes CRs but follows after EOs

Although IpN neurons encode both CRs and EOs, the importance and contribution of IpN output to these movements could be different since the former movements are conditioned and the latter movements are not. Logically, if movements depend on IpN output then IpN V_m encoding would precede movements. Therefore, we studied the latency of synaptic encoding in these neurons and resulting eyelid movements. We determined onsets (relative to CS onset) of both V_m responses and CRs (N = 7 neurons) and EOs (N = 3 neurons) in conditioned and naïve mice, respectively. First, we found differences in onsets of EOs and CRs, *i.e.* EO onsets were significantly earlier than CR onsets (EO: 89.2 ± 17.2 ms, CR: 156.8 ± 22 ms; t(8) = -4.686, P = 0.002, independent t-test), highlighting the different nature of eyelid movements. Next, in relation to movements, CS-cEPSP onset significantly preceded CR onset with a lead of 39.9 ± 27.4 ms (Z = 5, P = 0.043, Wilcoxon Signed rank test; Fig 4O, P). In contrast, CS-cEPSPs followed EO onset with a lag of 24.9 ± 8.5 ms. This effect was not evident in CS-cIPSP responses (Fig 4O', P'), although we did observe an increased variability in cIPSP onsets compared to cEPSP onsets (standard deviation (SD) cEPSP onset: 26.9 ± 12 ms, SD cIPSP onset: 66 ± 26.9 ms, t(8) = 3.798, P = 0.005, independent t-test), while movement onsets were comparably variable between recordings (mean difference (MD): 5.76ms, t(8) = 0.798, P = 0.448, independent t-test). Together, these findings show that CRs are synaptically encoded tens of milliseconds before movement output, whereas EOs are initialized before they are synaptically encoded in the IpN.

2.4.7 Synaptic activity in IpN neurons underlying unconditioned responses

Contrary to the CS, which is conveyed via the MF pathway, the US is conveyed through CFs originating in the IO (Freeman and Steinmetz 2011), where CF collaterals project to IpN neurons (Courville et al. 1977; van der Want et al. 1989; De Zeeuw et al. 1997). Since we found that PC axons change during learning, this could influence synaptic encoding of the US. Therefore, as a next step we asked whether these learning-related changes IpN afferents influence US encoding. In line with our findings from the spike data (Fig 1G), the vast majority of IpN neurons showed US-evoked synaptic responses. US-evoked V_m responses were observed in 83.3% of neurons in naïve and 69.2% of neurons in conditioned mice, where the distribution of responses was comparable between groups (naïve vs conditioned: cEPSP: 75.0% vs 46.2%, cIPSP: 8.3% vs 15.4%, cEPSP & cIPSP: 0% vs 7.7%, no response: 16.7% vs 30.8%; P = 0.497, Fisher's Exact test; Fig 5A). From this we conclude that the US is widely encoded with a high synaptic input/spike output translation in both naïve and conditioned mice.

2.4.7.1 US-evoked synaptic responses are more prolonged after conditioning

To test whether learning influenced synaptic encoding of the US, we quantified US-evoked cEPSPs in both naïve and conditioned mice (Fig 5B, C). We found that the half-width of US-cEPSPs was significantly increased in conditioned animals (conditioned vs naïve: 109.3 ± 79.6 ms vs 43.8 ± 46.7 ms, $t(12) = 2.184$, $P = 0.049$, independent t-test, data log-transformed), while mice showed comparable URs (FEC: $t(13) = 0.961$, $P = 0.354$, independent t-test; table 4, Fig 5B, C). Amplitude of US-cEPSPs was however comparable between groups ($t(13) = 0.839$, $P = 0.417$; table 4, Fig 5B, C). To further rule out that these prolonged US-cEPSPs were caused by changes in UR we correlated US-cEPSP AUC and UR AUC, however we did not find a significant correlation between these parameters (naïve: $r = -0.43$, $P = 0.244$; conditioned: $r = -0.6$, $P = 0.208$, Spearman correlation), suggesting that the magnitude of the US-cEPSP is not related to the UR. Together, we conclude that US-cEPSPs are more prolonged after conditioning; an effect that was not caused by differences in UR. Changes in US-cEPSPs could be the result of more PC inhibitory terminals, leading to a prolonged disinhibition of IpN neurons following synchronized US-evoked complex spike activity. This could serve as a mechanism to enhance learning, since prolonging the complex spike pause has been shown to facilitate learning (Maiz et al. 2012).

2.4.7.2 US is synaptically encoded following initiation of the UR

We further investigated the relation between the UR and IpN synaptic encoding, by comparing the onsets of V_m responses and URs (relative to US onset). We found that in 42.5 ± 23.4% of valid trials the UR was preceded by a short eyelid opening (Fig 4A, black arrowhead). These US-eyelid openings occurred equally often in naïve and conditioned mice ($t(8) = -1.278$, $P = 0.237$; independent t-test) with comparable amplitudes (naïve: 5.23 ± 4.04% of UR, conditioned: 1.16 ± 0.63% of UR, $t(4.197) = -2.227$, $P = 0.087$, independent t-test) and short latency (2.60 ± 1.03 ms). A likely cause for these eyelid movements is the pressure of the air puff, however on such small timescales their presence can introduce bias in our estimate of the UR. Nonetheless, the onset of the subsequent UR was 10.54 ± 3.63 ms. Furthermore, there was no difference in onsets of US-cEPSPs and US-cIPSPs (US-cEPSP: 15.22 ± 7.77 ms, US-cIPSP: 16.09 ± 2.77ms; $t(12) = -0.185$, $P = 0.856$; independent t-test), even though US-cIPSPs were most probably caused via a longer neuronal pathway and caused as a result of PC activity.

We then compared onsets of V_m responses and URs on a trial-by-trial basis. We found that URs started significantly earlier than US-cEPSPs or US-cIPSPs with a lead of 5.29 ± 8.74 ms, ($t(13) = -2.263$, $P = 0.041$, independent t-test) with no difference between naïve and conditioned mice ($t(12) = -0.850$, $P = 0.412$, independent t-test; Fig 5D, E). Although IpN activity can have a modulatory role during ongoing UR execution, V_m encoding of the US takes place with a small lag, as expected from the reflexive nature of the UR.

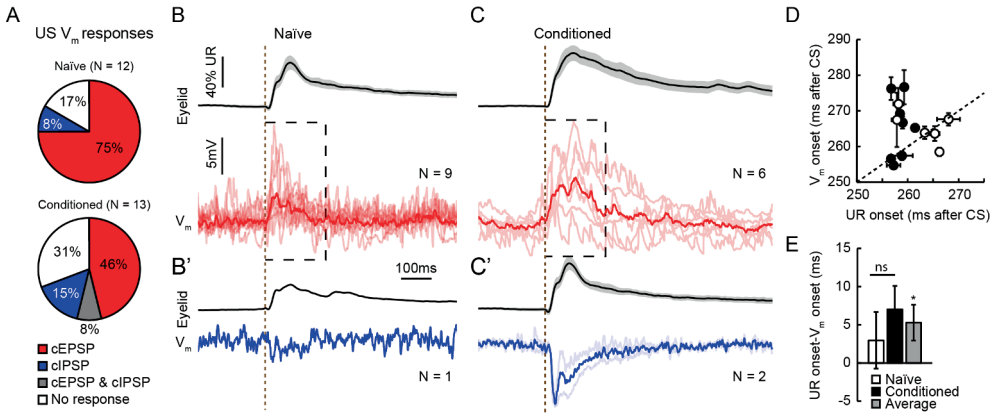

Fig 5. Membrane potential dynamics underlying US-evoked eyelid responses during EBC. (A) IpN neurons in naïve and conditioned mice show differential US-evoked V_m responses. (B, C) US-cEPSPs are more prolonged after conditioning. (B', C') US-cIPSPs were visually more pronounced in conditioned mice. (D, E) Onset of V_m responses was significantly later than UR onset, indicating that UR initiation is independent of IpN activity. Error bars represent SEM. *P<0.05

2.5 Discussion

In this study we presented several novel findings on neuronal encoding and plasticity mechanisms during cerebellar learning. We started by recording task-related spike responses in eyelink conditioned mice in the IpN, a part of the cerebellar nuclei that has been shown to be crucial for both the acquisition and expression of conditioned EBC behavior (Clark et al. 1984; Lavond et al. 1985; Yeo et al. 1985; Lavond and Steinmetz 1989; Sears and Steinmetz 1990; Bracha et al. 1994; Freeman and Rabinak 2004; Freeman et al. 2005; Ohyama et al. 2006; Mojtahedian et al. 2007). We showed that the heterogeneous population of IpN neurons (Uusisaari et al. 2007; Uusisaari and Knöpfel 2011, 2012) display differential spike responses during the task, in line with previously published response classifications (Ten Brinke et al. 2017), although we found minor differences in response distributions. Next, we investigated the structural changes occurring during EBC and we found that conditioning induces increases in both excitatory MFs and inhibitory PC projections to the DLH, an prominent eyeblink-encoding area of the IpN (Heiney et al. 2014b). To investigate the functional role of these changes we used partial optogenetic activation and inhibition of MFs, effectively inducing eyelid movements but only after conditioning. During EBC however MF activation did not result in altered performance, suggesting that direct excitatory MFs do not have an essential contribution to conditioned eyelid movements. MF activity did however influence the time course of the air puff-

induced UR, consistent with previous studies that reported changes in UR after IpN inactivation (Bracha et al. 1994; Wikgren and Korhonen 2001).

Having established that we could successfully target the eyeblink-encoding IpN, we then employed *in vivo* whole-cell recordings of IpN neurons in awake behaving mice to gain further insight in the ongoing synaptic activity during the task. This is an exceptionally challenging technique when performed in moving rodents and recordings are often short (Powell et al. 2015; Lee and Lee 2017; Petersen 2017). We found that conditioned mice exhibited sustained cEPSPs following the CS, whereas transient cEPSPs were observed in mice novel to the task. Since the temporal profile of these cEPSPs coincides with learning-induced reductions in PC simple spike frequency (Jirenhed et al. 2007; Ten Brinke et al. 2015), we propose that the change in synaptic encoding could be entirely caused by PCs where again, the contribution of MF collateral inputs seem neglectable. If these inputs would contribute to CRs, they would at least cause detectable CS-related synaptic currents in IpN neurons. However, we could not identify these MF-mediated synaptic currents, which would be primarily AMPA-receptor mediated and have a specific profile with a fast rise-time (Wu and Raman 2017; Najac and Raman 2017). In line with this assumption, blocking glutamatergic CF- and MF-mediated neurotransmission in the IpN only mildly affects conditioned performance (Aksenov et al. 2005), whereas blocking GABAergic PC-mediated neurotransmission completely abolishes performance (Aksenov et al. 2004). Together, these results all point towards the suggestion that the role of MFs in shaping IpN synaptic currents and spike output is relatively limited.

We furthermore compared synaptic encoding of conditioned versus 'voluntary' eyelid movements, where we found that the initiation of voluntary eyelid openings (mainly observed in naïve animals) did not rely on IpN activity, as onsets of cEPSPs followed movement onsets. Interestingly, the magnitude of these eyelid movements could correlate with associated cEPSPs, suggesting a role for the cerebellum in controlling ongoing movements as part of a wider neuronal network. A similar role could apply to its contribution to the UR, since IpN synaptic encoding lagged behind the UR, reflecting the direct trigeminal nerve to facial nucleus projections (Holstege et al. 1986; Pellegrini et al. 1995; van Ham and Yeo 1996) and possibly efference copy encoding in the cerebellum (Wolpert et al. 1998). Remarkable in this respect is our finding that synaptic encoding of the UR was prolonged after conditioning. Since US-evoked activity in the dorsal accessory olivary nucleus has been shown to diminish over the course of conditioning (Sears and Steinmetz 1991), it is likely that changes downstream cause prolonged US-cEPSPs. This could involve plasticity at the level of molecular layer interneurons, since these neurons are able to tightly control eyelid movements (Heiney et al. 2014a). It could also be a consequence increased MF and/or PC terminals, although the former would contradict the consensus that MFs are part of the CS and not the US pathway (Steinmetz et al. 1986, 1987; Freeman and Rabinak 2004). This consensus further appears to be compatible with our results showing that short-latency spikes following the US (Fig 1H, J) could not be diminished through MF silencing, thus pointing towards a role for CF collateral inputs.

However, whether prolonged cEPSPs has any functional significance for the UR remains questionable, since magnitudes of the UR and cEPSPs were not correlated. A possibility is that a prolonged post-complex spike pause in PCs underlies the observed prolonged IpN cEPSPs, although evidence lacks for such a mechanism so far. This would however be conceivable given that prolonging the complex spike pause can enhance EBC learning (Maiz et al. 2012).

If MFs do not directly contribute to CRs during physiological EBC behavior, why do they increase? Learning-associated sprouting of MFs has been reported several years ago already (Boele et al. 2013), although so far no other supporting studies had been published. Our results were independently obtained using the expression of VGLUT1 as a marker for MFs, instead of anterograde labeling. We could distinguish MFs from CFs since CFs only express VGLUT2 (Hioki et al. 2003). Interestingly, our results only show a MF increase in the contralateral IpN (relative to the air puff), whereas Boele et al. (2013) reported increased MFs in both hemispheres with a significantly *larger* increase in the contralateral hemisphere. It is possible that a significant ipsilateral increase in VGLUT1+ MFs remained undetected, since many non-eyeblink-encoding MFs could complicate quantification of these terminals. Yet, eyeblink-encoding neurons within the ipsilateral IpN are substantially more important for conditioned behavior (Freeman et al. 1995) and unilateral lesions of the ipsilateral IpN are sufficient to abolish CRs (Clark et al. 1984, 1992; Lavond et al. 1985). This raises the question as to why MFs are more increased in the contralateral IpN, while at the same time PC terminals are increased in both hemispheres. These questions remain to be answered, perhaps by studying MF expression in animals that have been bilaterally conditioned (both eyes receive US), or by comparing expression in left- or right-eye conditioned animals.

Despite their increase during conditioning, their precise function in the context of EBC remains uncertain. Several studies have shown that conditioned eyelid movements can be elicited solely by direct excitatory projections reaching the IpN, after inactivating the cerebellar cortex (McCormick and Thompson 1984a, b; Perrett et al. 1993; Ohyama et al. 2003, 2006). A conclusion is that these direct excitatory projections are sufficient for the expression of conditioned eyelid movements (although with a different temporal profile; see Ohyama et al. 2006). Such a result could occur however as a result of increased IpN excitability, since tonic inhibition from PCs in the cerebellar cortex in that case is reduced or absent. In physiological states, MF synaptic currents are small and possibly remain undetected because of constant V_m fluctuations, however in this excitable state MFs could evoke spike activity. Another possibility is that MFs facilitate plasticity mechanisms in the IpN. Such a role would fit considering the plasticity-inducing temporal order of excitation and inhibition during EBC (Pugh and Raman 2006, 2008, 2009; Zheng and Raman 2010). Mechanisms like the emergence of the CS-evoked complex spikes (Ohmae and Medina 2015; Ten Brinke et al. 2015) or IpN rebound potentiation (Alviña et al. 2009; Hoebeek et al. 2010; Witter et al. 2013) could furthermore enhance plasticity.

A potential caveat in our optogenetic approach is that we were unable to directly measure the effectivity of the eArch3.0-mediated MF silencing. Although measurements of IpN spike activity have unambiguously indicated that chronos-mediated MF activation was effective (Fig 3H), this remains uncertain for MF silencing, since this would require direct measurements of MF axons *in vivo*. For our observations, it is likely that the pathway through the cerebellar cortex contributed to the delayed spike activity changes that we observe (Fig 3H). Furthermore, the exact site of the visual relay center in the PN is uncertain, since studies have shown labeled corticopontine projections from visual areas in both lateral and medial PN regions (Aitkin and Boyd 1978; Glickstein et al. 1980, 1985; Albus et al. 1981; Leergaard and Bjaarlie 2007). Based on these studies we targeted primarily the lateral PN, but lesions in this region may not fully block visual CS-evoked CRs (Steinmetz et al. 1987). The wide transfection around the PN and labeling throughout the cerebellum indicates that we could target at least part of the visually-encoding MFs, although it is clear that this was not sufficient to prevent visual CS information to reach the cerebellum. 'CR'-like responses could still be evoked during MF silencing (Fig 3I), while studies have shown strong decreases in conditioned behavior after PN inactivation (Lavond et al. 1981; Bao et al. 2000). Another consideration is the possibility that light 'leakage' from the optic fibers may have been visually detected by the mouse, although great care was taken to prevent this effect by reducing the light shattering as much as possible. Whether this has influenced the reduced UR during MF activation remains to be determined.

Although *in vivo* whole-cell recordings in behaving mice may provide insight in synaptic encoding during EBC, the limitations of this technique need to be acknowledged. IpN neurons continuously receive and integrate many active inputs (Bengtsson et al. 2011; Canto et al. 2016; Yarden-Rabinowitz and Yarom 2017) meaning that the V_m is in a constant state of fluctuation (see Fig S5C, D). As a result, stimuli-evoked responses were likely to be variable, therefore requiring more trials for a reliable average. Subtle but significant V_m responses could have been masked by intertrial variability and have remained undetected. This in combination with the limited number of recordings with overall short durations may lead to undersampling, particularly when recording from a heterogeneous neuronal population such as in the IpN (Uusisaari et al. 2007; Uusisaari and Knöpfel 2011, 2012). Our experimental approach therefore focused on obtaining an adequate number of trials in current clamp mode while we allowed neurons to retain their physiological membrane voltage. A question that remains unanswered is: what is the exact contribution and temporal profile of excitatory and inhibitory inputs for shaping learned V_m responses? These questions could be answered by clamping the neuron at the reversal potential for inhibition or excitation, or alternatively by voltage clamp measurements during behavior. These techniques were however not feasible within this study. Furthermore, although shown *in vitro* (Canto et al. 2018; Wang et al. 2018), evidence for learning-related changes in intrinsic excitability *in vivo* remains to be discovered.

To conclude, our results demonstrate that EBC-associated changes in IpN are diverse and multifaceted, impacting both the structure and contribution of afferent inputs to the sub- and suprathreshold activity underlying conditioned behavior.

2.6 Acknowledgements

We are grateful to the following people for their technical contribution: J.W. Potters, H.J. Boele, S.K.E. Koekkoek, Z. Gao, M.M Ten Brinke, J.K. Spanke A.C.H.G. IJpelaar. We furthermore thank B. Winkelman, A. Court, C. Geelen, M. Mešković, G. Özel, M. Bouw, S.O. Stokman for their diverse contribution. We thank I. Duguid and P. Chadderton for their constructive comments on the *in vivo* awake whole-cell technique in our lab. This study was enabled by funding from Dutch Organization for Medical Sciences (ZonMw), Life Sciences, the ERC-advanced, CEREBNET and C7 programs of the European Community (CIDZ), and Boehringer Ingelheim Fonds.

2.7 Supplementary tables and figures

Table S1. Whole-cell electrophysiological properties of recorded neurons.

Group	ID	Mem. pot. (mV)	Spike amp. (mV)	Spike HW (ms)	Rs (MΩ)	Rmem (MΩ)	Cmem (pF)	Mem constant (τ; ms)
Naive	1	-67.86	24.21	0.49	63.05	52.56	73.87	2.12
	2	-32.55	15.20	1.57	74.57	493.61	4.09	0.26
	3	-53.63	27.51	0.93	29.15	184.07	21.65	0.54
	4	-44.45	26.29	0.97	28.30	162.54	38.24	0.92
	5	-44.21	32.09	0.3	31.55	26.36	163.45	2.35
	6	-49.7	27.66	1.00	37.71	179.21	44.24	1.38
	7	-44.05	22.91	1.44	46.53	272.96	31.82	1.26
	8	-51.07	27.72	1.55	35.44	316.68	4.56	0.15
	9	-50.67	14.86	2.15	62.11	255.35	32.60	1.63
	10	-57.66	51.75	1.33	30.20	854.75	16.98	0.50
	11	-40.48	48.88	0.98	20.57	1733.81	23.26	0.47
	12	-53.67	25.31	0.93	51.81	73.50	51.70	1.57
Mean ± SD		**-49.2 ± 9.0**	**28.7 ± 11.3**	**1.1 ± 0.5**	**42.6 ± 16.9**	**383.8 ± 481.9**	**42.2 ± 43.0**	**1.1 ± 0.7**
Conditioned	1	-43.9	29.54	0.3	43.05	68.31	75.84	2.00
	2	N/A	27.87	1.84	24.65	64.87	35.91	0.64
	3	-65.96	36.78	0.99	43.74	474.39	3.49	0.14
	4	-42.59	23.94	0.76	73.64	547.48	7.70	0.50
	5	-47.1	14.23	0.95	55.28	104.21	13.73	0.50
	6	-46.55	35.31	0.48	36.40	174.57	161.01	4.85
	7	-71.06	No spikes	No spikes	63.90	655.53	2.65	0.15
	8	-72.86	21.96	0.96	37.12	1015.51	18.74	0.67
	9	N/A	21.01	0.92	57.54	248.27	62.60	2.92
	10	N/A	17.78	0.56	51.31	103.49	103.50	3.55
	11	-57.51	38.87	2.1	39.56	800.78	2.71	0.10
	12	-44.78	18.16	0.47	61.24	247.40	485.63	23.84
	13	-69.78	22.2173	1.08	42.61	382.92	5.02	0.19
Mean ± SD		**-44.8 ± 32.8**	**25.6 ± 8.0**	**1.0 ± 0.5**	**48.5 ± 13.5**	**376.0 ± 305.5**	**75.3 ± 132.4**	**3.1 ± 6.4**

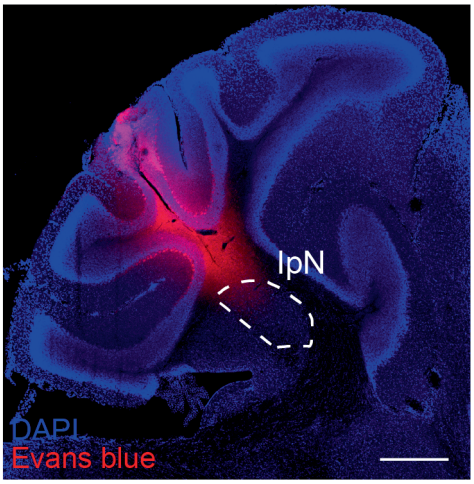

Fig S1. Microstimulation location. (A) Insertions of Evans Blue-coated microstimulation electrode revealed fluorescent labeling in the IpN. Same coordinates were used to guide glass electrodes for electrophysiological recordings.

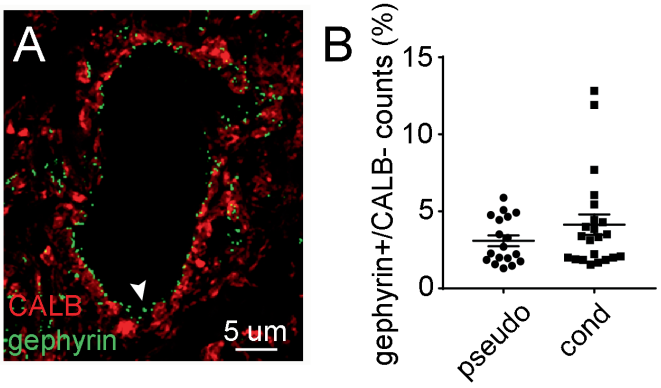

Fig S3. Gephyrin+ and CALB+ puncta expression in DLH. (A) Expression of postsynaptic gephyrin+ puncta relative to CALB+ PC terminals at the neuronal membrane. White arrowhead shows gephyrin+ puncta not apposed to a CALB+ PC terminal. (B) Conditioning did not lead to changes in gephyrin+/CALB- counts as a percentage of total gephyrin+ puncta. Error bars represent SEM.

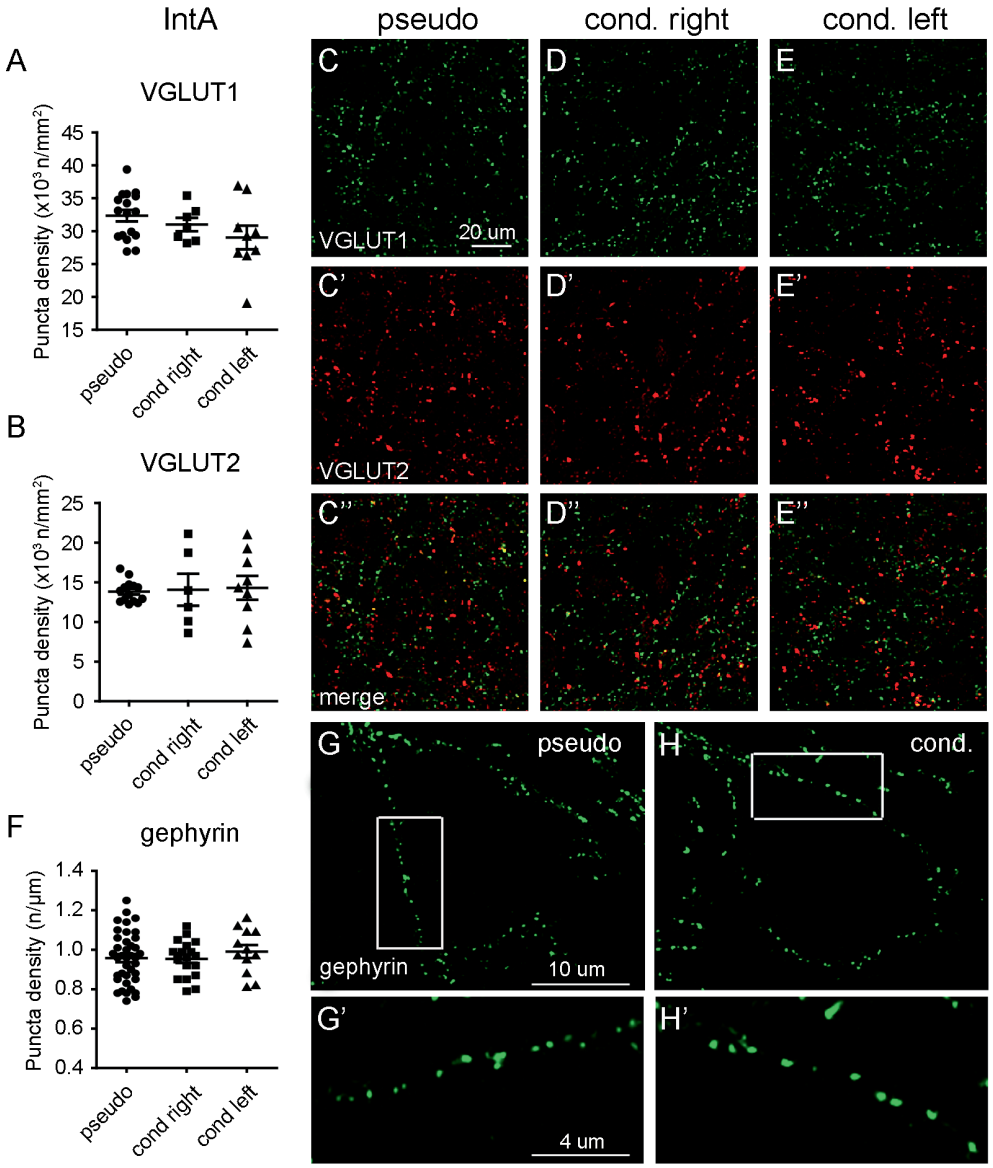

Fig S2. Density of VGLUT1+, VGLUT2+ and gephyrin+ puncta in IntA after EBC. (A, B) Density of VGLUT1+ puncta and VGLUT2+ puncta was unchanged after conditioning. (C-E'') Immunofluorescent labeling of VGLUT1+ and VGLUT2+ puncta in IntA in pseudo and conditioned mice (left and right). (F) Density of gephyrin+ puncta in IntA was also unchanged after conditioning (G-H) Immunofluorescent labeling of gephyrin+ puncta in IntA in pseudo and conditioned mice. (G'-H') Magnified images of gephyrin+ puncta in the white squares indicated in G and H. Error bars represent SEM.

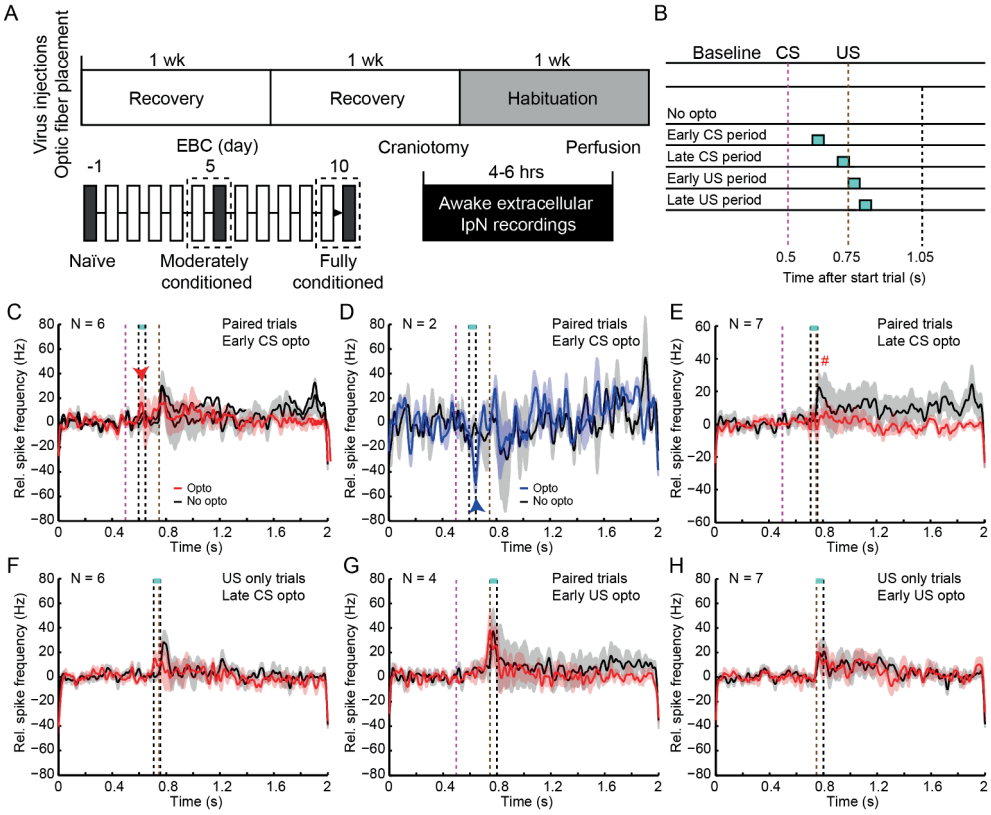

Fig S4. Optogenetic mossy fiber interference during EBC. (A) Timeline showing experiments with mossy fiber interference during EBC. Optogenetic interference sessions were done before training at day -1, at day 5 and at day 10. (B) Mossy fiber activation (50 ms) is employed at different periods during an EBC trial. (C, D) Mossy fiber activation (50 ms) during the CS-US period could induce a spike frequency increase (C; red arrowhead) and decrease (D; blue arrowhead) in spike facilitation (red traces) and suppression (blue traces) IpN neurons, respectively. (E, F) Mossy fiber activation right before US arrival could influence US-evoked spike responses in US only and paired trials. (G, H) mossy fiber activation right after US arrival did not influence US-spike responses. Error bars represent SEM. # indicates a trend, ***P<0.001

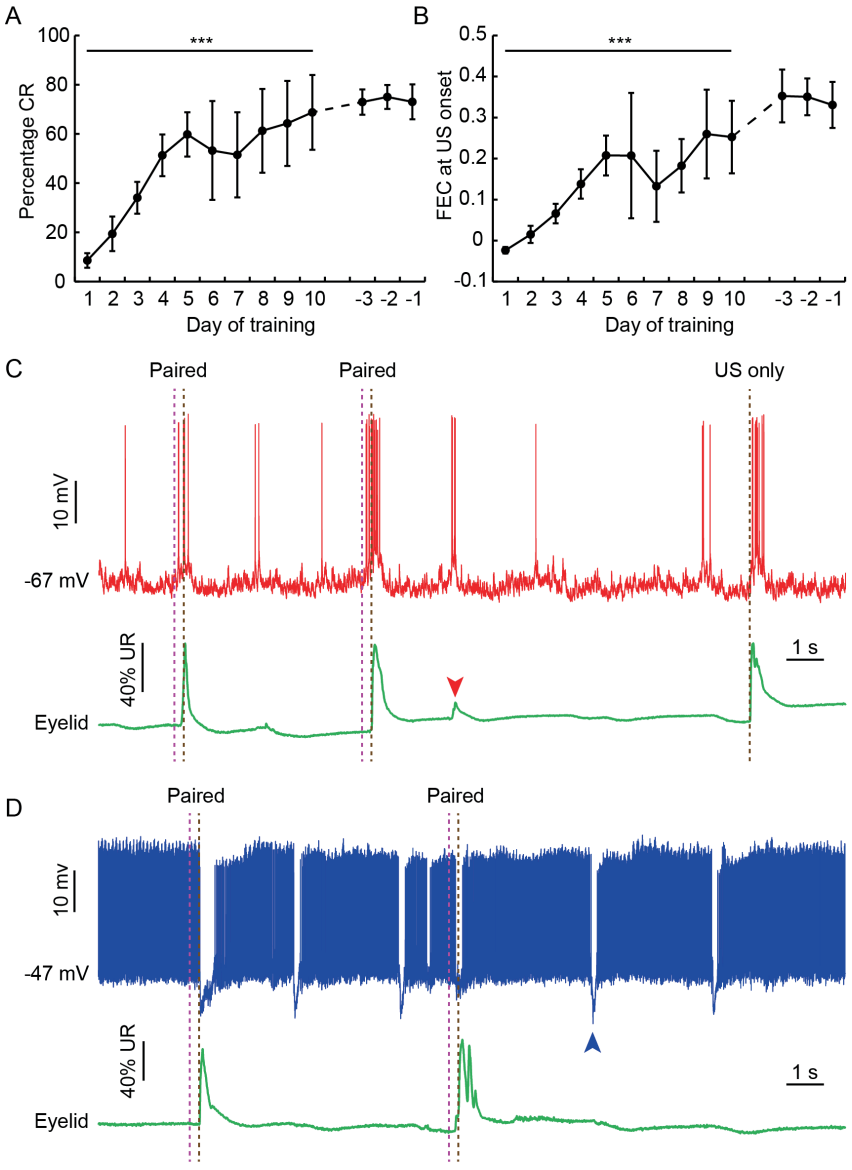

Fig S5. *In vivo* awake whole-cell recordings during EBC. Mice were subjected to conditioning for at least 10 days during which they showed an increase in (A) percentage CR trials and (B) FEC at US onset. Performance during the last three days before recordings are indicated at the right of the graphs, and show that mice were well-trained before recordings. (C, D) Example traces of *in vivo* awake whole-cell recording during which paired and US only trials were given. Red arrowhead indicates a spontaneous (voluntary) eyelid movements that elicited a cEPSP and spikes in this neuron. Blue trace in D shows a fast-spiking IpN neuron that shows task-related cIPSPs, as well as spontaneous cIPSPs (blue arrowhead). Error bars represent SEM. ***P<0.001

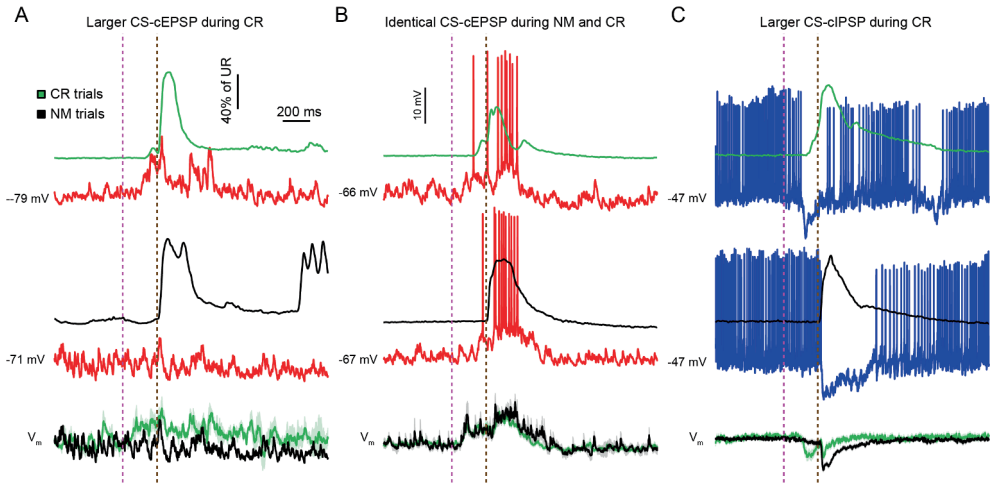

Fig S6. Encoding of conditioned eyelid movements in the V_m of IpN neurons. (A) IpN neuron showing higher CS-cEPSPs in CR trials (green average) compared to NM trials (black average) without spike activity. (B) IpN neuron showing identical CS-cEPSPs in CR trials and NM trials. Spike activity occurs both during the CS-US period and following the US. (C) IpN neuron showing CS-IPSPs on CR trials, but not on NM trials. Average US-cIPSP is diminished during CR trials (compared green and black V_m averages). Error bars represent SEM.

2.8 References

Aitkin LM, Boyd J (1978) Acoustic input to the lateral pontine nuclei. Hear Res 1:67–77

Aksenov D, Serdyunkova N, Irwin K, Bracha V (2004) GABA Neurotransmission in the Cerebellar Interposed Nuclei: Involvement in Classically Conditioned Eyeblinks and Neuronal Activity. J Neurophysiol 91:719–727. doi: 10.1152/jn.00859.2003

Aksenov DP, Serdyunkova N, Bloedel JR, Bracha V (2005) Glutamate Neurotransmission in the Cerebellar Interposed Nuclei: Involvement in Classically Conditioned Eyeblinks and Neuronal Activity. J Neurophysiol 93:44–52. doi: 10.1152/jn.00586.2004

Albus K, Donate-Oliver F, Sanides D, Fries W (1981) The distribution of pontine projection cells in visual and association cortex of the cat: An experimental study with horseradish peroxidase. J Comp Neurol 201:175–189. doi: 10.1002/cne.902010204

Alviña K, Ellis-Davies G, Khodakhah K (2009) T-type calcium channels mediate rebound firing in intact deep cerebellar neurons. Neuroscience 158:635–641. doi: 10.1016/j.neuroscience.2008.09.052

Attwell PJE, Rahman S, Yeo CH (2001) Acquisition of Eyeblink Conditioning Is Critically Dependent on Normal Function in Cerebellar Cortical Lobule HVI. J Neurosci 21:5715–5722. doi: 10.1523/JNEUROSCI.21-15-05715.2001

Bao S, Chen L, Thompson RF (2000) Learning- and cerebellum-dependent neuronal activity in the lateral pontine nucleus. Behav Neurosci 114:254–261. doi: 10.1037//0735-7044.114.2.254

Bengtsson F, Ekerot C-F, Jörntell H (2011) In Vivo Analysis of Inhibitory Synaptic Inputs and Rebounds in Deep Cerebellar Nuclear Neurons. PLoS ONE 6:e18822. doi: 10.1371/journal.pone.0018822

Berthier NE, Moore JW (1986) Cerebellar Purkinje cell activity related to the classically conditioned nictitating membrane response. Exp Brain Res 63:341–350

Berthier NE, Moore JW (1990) Activity of deep cerebellar nuclear cells during classical conditioning of nictitating membrane extension in rabbits. Exp Brain Res 83:44–54

Boele H-J, Koekkoek SKE, De Zeeuw CI, Ruigrok TJH (2013) Axonal Sprouting and Formation of Terminals in the Adult Cerebellum during Associative Motor Learning. J Neurosci 33:17897–17907. doi: 10.1523/JNEUROSCI.0511-13.2013

Bracha V, Webster ML, Winters NK, et al (1994) Effects of muscimol inactivation of the cerebellar interposed-dentate nuclear complex on the performance of the nictitating membrane response in the rabbit. Exp Brain Res 100:453–468

Brodal P, Dietrichs E, Walberg F (1986) Do pontocerebellar mossy fibres give off collaterals to the cerebellar nuclei? An experimental study in the cat with implantation of crystalline HRP-WGA. Neurosci Res 4:12–24

Canto CB, Broersen R, De Zeeuw CI (2018) Intrinsic excitement in cerebellar nuclei neurons during learning. PNAS 115:9824–9826

Canto CB, Witter L, De Zeeuw CI (2016) Whole-Cell Properties of Cerebellar Nuclei Neurons In Vivo. PloS One 11:e0165887

Chapman PF, Steinmetz JE, Sears LL, Thompson RF (1990) Effects of lidocaine injection in the interpositus nucleus and red nucleus on conditioned behavioral and neuronal responses. Brain Res 537:149–156

Chettih SN, McDougle SD, Ruffolo LI, Medina JF (2011) Adaptive Timing of Motor Output in the Mouse: The Role of Movement Oscillations in Eyelid Conditioning. Front Integr Neurosci 5:. doi: 10.3389/fnint.2011.00072

Clark GA, McCormick DA, Lavond DG, Thompson RF (1984) Effects of lesions of cerebellar nuclei on conditioned behavior and hippocampal neuronal responses. Brain Res 291:125–136

Clark RE, Lavond DG, Zhang AA (1992) Reversible lesions of the cerebellar interpositus nucleus during acquisition and retention of a classically conditioned behavior. Behav Neurosci 106:879–888

Courville J, Augustine JR, Martel P (1977) Projections from the inferior olive to the cerebellar nuclei in the cat demonstrated by retrograde transport of horseradish peroxidase. Brain Res 130:405–419

De Zeeuw CI, Berrebi AS (1995) Postsynaptic Targets of Purkinje Cell Terminals in the Cerebellar and Vestibular Nuclei of the Rat. Eur J Neurosci 7:2322–2333. doi: 10.1111/j.1460-9568.1995.tb00653.x

De Zeeuw CI, Van Alphen AM, Hawkins RK, Ruigrok TJH (1997) Climbing fiber collaterals contact neurons in the cerebellar nuclei that provide a GABAergic feedback to the inferior olive. Neuroscience 80:981–986

Dietrichs E, Walberg F (1987) Cerebellar nuclear afferents—where do they originate? Anat Embryol (Berl) 177:165–172

Freeman JH, Carter CS, Stanton ME (1995) Early cerebellar lesions impair eyeblink conditioning in developing rats: differential effects of unilateral lesions on postnatal day 10 or 20. Behav Neurosci 109:893

Freeman JH, Halverson HE, Poremba A (2005) Differential Effects of Cerebellar Inactivation on Eyeblink Conditioned Excitation and Inhibition. J Neurosci 25:889–895. doi: 10.1523/JNEUROSCI.4534-04.2005

Freeman JH, Rabinak CA (2004) Eyeblink conditioning in rats using pontine stimulation as a conditioned stimulus. Integr Physiol Behav Sci 39:180–191

Freeman JH, Steinmetz AB (2011) Neural circuitry and plasticity mechanisms underlying delay eyeblink conditioning. Learn Mem 18:666–677. doi: 10.1101/lm.2023011

Gao Z, Proietti-Onori M, Lin Z, et al (2016) Excitatory Cerebellar Nucleocortical Circuit Provides Internal Amplification during Associative Conditioning. Neuron 89:645–657. doi: 10.1016/j.neuron.2016.01.008

Garcia KS, Steele PM, Mauk MD (1999) Cerebellar cortex lesions prevent acquisition of conditioned eyelid responses. J Neurosci 19:10940–10947

Gauck V, Jaeger D (2000) The Control of Rate and Timing of Spikes in the Deep Cerebellar Nuclei by Inhibition. J Neurosci 20:3006–3016

Gauck V, Jaeger D (2003) The contribution of NMDA and AMPA conductances to the control of spiking in neurons of the deep cerebellar nuclei. J Neurosci 23:8109–8118

Glickstein M, Cohen JL, Dixon B, et al (1980) Corticopontine visual projections in macaque monkeys. J Comp Neurol 190:209–229. doi: 10.1002/cne.901900202

Glickstein M, May JG, Mercier BE (1985) Corticopontine projection in the macaque: The distribution of labelled cortical cells after large injections of horseradish peroxidase in the pontine nuclei. J Comp Neurol 235:343–359. doi: 10.1002/cne.902350306

Groenewegen HJ, Voogd J (1977) The parasagittal zonation within the olivocerebellar projection. I. Climbing fiber distribution in the vermis of cat cerebellum. J Comp Neurol 174:417–488. doi: 10.1002/cne.901740304

Halverson HE, Khilkevich A, Mauk MD (2015) Relating Cerebellar Purkinje Cell Activity to the Timing and Amplitude of Conditioned Eyelid Responses. J Neurosci 35:7813–7832. doi: 10.1523/JNEUROSCI.3663-14.2015

Heiney SA, Kim J, Augustine GJ, Medina JF (2014a) Precise Control of Movement Kinematics by Optogenetic Inhibition of Purkinje Cell Activity. J Neurosci 34:2321–2330. doi: 10.1523/JNEUROSCI.4547-13.2014

Heiney SA, Wohl MP, Chettih SN, et al (2014b) Cerebellar-Dependent Expression of Motor Learning during Eyeblink Conditioning in Head-Fixed Mice. J Neurosci 34:14845–14853. doi: 10.1523/JNEUROSCI.2820-14.2014

Hesslow G (1994) Inhibition of classically conditioned eyeblink responses by stimulation of the cerebellar cortex in the decerebrate cat. J Physiol 476:245–256

Hioki H, Fujiyama F, Taki K, et al (2003) Differential distribution of vesicular glutamate transporters in the rat cerebellar cortex. Neuroscience 117:1–6. doi: 10.1016/S0306-4522(02)00943-0

Hirono M, Watanabe S, Karube F, et al (2018) Perineuronal Nets in the Deep Cerebellar Nuclei Regulate GABAergic Transmission and Delay Eyeblink Conditioning. J Neurosci 38:6130–6144. doi: 10.1523/JNEUROSCI.3238-17.2018

Hoebeek FE, Witter L, Ruigrok TJH, De Zeeuw CI (2010) Differential olivo-cerebellar cortical control of rebound activity in the cerebellar nuclei. Proc Natl Acad Sci 107:8410–8415. doi: 10.1073/pnas.0907118107

Holstege G, Van Ham JJ, Tan J (1986) Afferent projections to the orbicularis oculi motoneuronal cell group. An autoradiographical tracing study in the cat. Brain Res 374:306–320. doi: 10.1016/0006-8993(86)90425-7

Jirenhed D-A, Bengtsson F, Hesslow G (2007) Acquisition, Extinction, and Reacquisition of a Cerebellar Cortical Memory Trace. J Neurosci 27:2493–2502. doi: 10.1523/JNEUROSCI.4202-06.2007

Kitai ST, McCrea RA, Preston RJ, Bishop GA (1977) Electrophysiological and horseradish peroxidase studies of precerebellar afferents to the nucleus interpositus anterior. I. climbing fiber system. Brain Res 122:197–214

Kleim JA, Freeman JH, Bruneau R, et al (2002) Synapse formation is associated with memory storage in the cerebellum. Proc Natl Acad Sci 99:13228–13231

Koekkoek SKE, Den Ouden WL, Perry G, et al (2002) Monitoring kinetic and frequency-domain properties of eyelid responses in mice with magnetic distance measurement technique. J Neurophysiol 88:2124–2133

Lavond DG, Hembree TL, Thompson RF (1985) Effect of kainic acid lesions of the cerebellar interpositus nucleus on eyelid conditioning in the rabbit. Brain Res 326:179–182

Lavond DG, McCormick DA, Clark GA, et al (1981) Effects of ipsilateral rostral pontine reticular lesions on retention of classically conditioned nictitating membrane and eyelid responses. Physiol Psychol 9:335–339. doi: 10.3758/BF03326990

Lavond DG, Steinmetz JE (1989) Acquisition of classical conditioning without cerebellar cortex. Behav Brain Res 33:113–164

Lee D, Lee AK (2017) In Vivo Patch-Clamp Recording in Awake Head-Fixed Rodents. Cold Spring Harb Protoc 2017:pdb.prot095802. doi: 10.1101/pdb.prot095802

Leergaard TB, Bjaarlie JG (2007) Topography of the complete corticopontine projection: From experiments to principal maps. Front Neurosci 1:211–223. doi: 10.3389/neuro.01.1.1.016.2007

Maiz J, Karakossian MH, Pakaprot N, et al (2012) Prolonging the postcomplex spike pause speeds eyeblink conditioning. Proc Natl Acad Sci 109:16726–16730. doi: 10.1073/pnas.1214274109

McCormick DA, Thompson RF (1984a) Cerebellum: Essential involvement in the classically conditioned eyelid response. Science 223:296–299

McCormick DA, Thompson RF (1984b) Neuronal responses of the rabbit cerebellum during acquisition and performance of a classically conditioned nictitating membrane-eyelid response. J Neurosci 4:2811–2822

Medina JF, Garcia KS, Mauk MD (2001) A Mechanism for Savings in the Cerebellum. J Neurosci 21:4081–4089. doi: 10.1523/JNEUROSCI.21-11-04081.2001

Mojtahedian S, Kogan DR, Kanzawa SA, et al (2007) Dissociaton of conditioned eye and limb responses in the cerebellar interpositus. Physiol Behav 91:9–14. doi: 10.1016/j.physbeh.2007.01.006

Mostofi A, Holtzman T, Grout AS, et al (2010) Electrophysiological Localization of Eyeblink-Related Microzones in Rabbit Cerebellar Cortex. J Neurosci 30:8920–8934. doi: 10.1523/JNEUROSCI.6117-09.2010

Najac M, Raman IM (2017) Synaptic excitation by climbing fibre collaterals in the cerebellar nuclei of juvenile and adult mice. J Physiol. doi: 10.1113/JP274598

Ohmae S, Medina JF (2015) Climbing fibers encode a temporal-difference prediction error during cerebellar learning in mice. Nat Neurosci 18:1798–1803. doi: 10.1038/nn.4167

Ohyama T, Nores WL, Mauk MD (2003) Stimulus generalization of conditioned eyelid responses produced without cerebellar cortex: implications for plasticity in the cerebellar nuclei. Learn Mem 10:346–354

Ohyama T, Nores WL, Medina JF, et al (2006) Learning-Induced Plasticity in Deep Cerebellar Nucleus. J Neurosci 26:12656–12663. doi: 10.1523/JNEUROSCI.4023-06.2006

Paxinos G, Franklin KBJ (2004) The Mouse Brain in Stereotaxic Coordinates, Second edition. Gulf Professional Publishing

Pedroarena CM, Schwartz C (2003) Efficacy and Short-Term Plasticity at GABAergic Synapses Between Purkinje and Cerebellar Nuclei Neurons. J Neurophysiol 89:704–715. doi: 10.1152/jn.00558.2002

Pellegrini JJ, Horn AKE, Evinger C (1995) The trigeminally evoked blink reflex. Exp Brain Res 107:166–180

Perrett SP, Ruiz BP, Mauk MD (1993) Cerebellar cortex lesions disrupt learning-dependent timing of conditioned eyelid responses. J Neurosci 13:1708–1718

Person AL, Raman IM (2011) Purkinje neuron synchrony elicits time-locked spiking in the cerebellar nuclei. Nature 481:502–505. doi: 10.1038/nature10732

Petersen CCH (2017) Whole-Cell Recording of Neuronal Membrane Potential during Behavior. Neuron 95:1266–1281. doi: 10.1016/j.neuron.2017.06.049

Powell K, Mathy A, Duguid I, Häusser M (2015) Synaptic representation of locomotion in single cerebellar granule cells. eLife 4:. doi: 10.7554/eLife.07290

Pugh JR, Raman IM (2008) Mechanisms of Potentiation of Mossy Fiber EPSCs in the Cerebellar Nuclei by Coincident Synaptic Excitation and Inhibition. J Neurosci 28:10549–10560. doi: 10.1523/JNEUROSCI.2061-08.2008

Pugh JR, Raman IM (2006) Potentiation of Mossy Fiber EPSCs in the Cerebellar Nuclei by NMDA Receptor Activation followed by Postinhibitory Rebound Current. Neuron 51:113–123. doi: 10.1016/j.neuron.2006.05.021

Pugh JR, Raman IM (2009) Nothing can be coincidence: synaptic inhibition and plasticity in the cerebellar nuclei. Trends Neurosci 32:170–177. doi: 10.1016/j.tins.2008.12.001

Sears LL, Steinmetz JE (1991) Dorsal accessory inferior olive activity diminishes during acquisition of the rabbit classically conditioned eyelid response. Brain Res 545:114–122

Sears LL, Steinmetz JE (1990) Acquisition of classically conditioned-related activity in the hippocampus is affected by lesions of the cerebellar interpositus nucleus. Behav Neurosci 104:681

Steinmetz JE, Logan CG, Rosen DJ, et al (1987) Initial Localization of the Acoustic Conditioned Stimulus Projection System to the Cerebellum Essential for Classical Eyelid Conditioning. Proc Natl Acad Sci U S A 84:3531–3535

Steinmetz JE, Rosen DJ, Chapman PF, et al (1986) Classical Conditioning of the Rabbit Eyelid Response With a Mossy-Fiber Stimulation CS: I. Pontine Nuclei and Middle Cerebellar Peduncle Stimulation. Behav Neurosci 100:878–887

Telgkamp P, Raman IM (2002) Depression of inhibitory synaptic transmission between Purkinje cells and neurons of the cerebellar nuclei. J Neurosci 22:8447–8457

Ten Brinke MM, Heiney SA, Wang X, et al (2017) Dynamic modulation of activity in cerebellar nuclei neurons during pavlovian eyeblink conditioning in mice. eLife 6:

Ten Brinke MM, Boele H-J, Spanke JK, et al (2015) Evolving Models of Pavlovian Conditioning: Cerebellar Cortical Dynamics in Awake Behaving Mice. Cell Rep 13:1977–1988. doi: 10.1016/j.celrep.2015.10.057

Uusisaari M, Knöpfel T (2011) Functional Classification of Neurons in the Mouse Lateral Cerebellar Nuclei. The Cerebellum 10:637–646. doi: 10.1007/s12311-010-0240-3

Uusisaari M, Obata K, Knopfel T (2007) Morphological and Electrophysiological Properties of GABAergic and Non-GABAergic Cells in the Deep Cerebellar Nuclei. J Neurophysiol 97:901–911. doi: 10.1152/jn.00974.2006

Uusisaari MY, Knöpfel T (2012) Diversity of Neuronal Elements and Circuitry in the Cerebellar Nuclei. The Cerebellum 11:420–421. doi: 10.1007/s12311-011-0350-6

van der Want JJL, Wiklund L, Guegan M, et al (1989) Anterograde tracing of the rat olivocerebellar system with phaseolus vulgaris leucoagglutinin (PHA-L). Demonstration of climbing fiber collateral innervation of the cerebellar nuclei. J Comp Neurol 288:1–18. doi: 10.1002/cne.902880102

van Ham JJ, Yeo CH (1996) Trigeminal Inputs to Eyeblink Motoneurons in the Rabbit. Exp Neurol 142:244–257. doi: 10.1006/exnr.1996.0195

Wang D, Smith-Bell CA, Burhans LB, et al (2018) Changes in membrane properties of rat deep cerebellar nuclear projection neurons during acquisition of eyeblink conditioning. Proc Natl Acad Sci 115:E9419–E9428. doi: 10.1073/pnas.1808539115

Weeks ACW, Connor S, Hinchcliff R, et al (2007) Eye-blink conditioning is associated with changes in synaptic ultrastructure in the rabbit interpositus nuclei. Learn Mem 14:385–389. doi: 10.1101/lm.348307

Wikgren J, Korhonen T (2001) Interpositus nucleus inactivation reduces unconditioned response amplitude after paired but not explicitly unpaired treatment in rabbit eyeblink conditioning. Neurosci Lett 308:181–184

Witter L, Canto CB, Hoogland TM, et al (2013) Strength and timing of motor responses mediated by rebound firing in the cerebellar nuclei after Purkinje cell activation. Front Neural Circuits 7:. doi: 10.3389/fncir.2013.00133

Wolpert DM, Miall RC, Kawato M (1998) Internal models in the cerebellum. Trends Cogn Sci 2:338–347

Wu Y, Raman IM (2017) Facilitation of mossy fibre driven spiking in the cerebellar nuclei by the synchrony of inhibition. J Physiol. doi: 10.1113/JP274321

Yarden-Rabinowitz Y, Yarom Y (2017) *In vivo* analysis of synaptic activity in cerebellar nuclei neurons unravels the efficacy of excitatory inputs. J Physiol. doi: 10.1113/JP274115

Yeo CH, Hardiman MJ (1992) Cerebellar cortex and eyeblink conditioning: a reexamination. Exp Brain Res 88:623–638

Yeo CH, Hardiman MJ, Glickstein M (1985) Classical conditioning of the nictating membrane of the rabbit. I. Lesions of the cerebellar nuclei. Exp Brain Res 60:87–98

Zhang W, Linden DJ (2006) Long-Term Depression at the Mossy Fiber-Deep Cerebellar Nucleus Synapse. J Neurosci 26:6935–6944. doi: 10.1523/JNEUROSCI.0784-06.2006

Zheng N, Raman IM (2010) Synaptic Inhibition, Excitation, and Plasticity in Neurons of the Cerebellar Nuclei. The Cerebellum 9:56–66. doi: 10.1007/s12311-009-0140-6

Chapter 3

Interplay between perineuronal nets in the cerebellar nuclei and Pavlovian eyeblink conditioning

Daniela Carulli*, Robin Broersen*, Cathrin B. Canto, Fred de Winter, Henk-Jan Boele, Barbara Hobo, Chris I. De Zeeuw and Joost Verhaagen

* indicates equal contribution

In preparation

3.1 Abstract

Perineuronal nets (PNNs) are assemblies of extracellular matrix molecules that enwrap some types of neurons and are involved in the regulation of plasticity and memory processes. PNNs are abundantly expressed in the deep cerebellar nuclei (DCN), but their precise role in cerebellar-dependent learning is unknown. We investigated the causal relationship between these PNNs and eyeblink conditioning (EBC), a form of associative learning that depends on plasticity in the olivo-cerebellar circuitry. PNNs in the EBC-associated parts of the DCN were reduced after 5 days of EBC, and were accompanied by a reduction of the chemorepulsive protein Semaphorin-3A. In addition, chondroitinase-induced enzymatic digestion of PNNs in the DCN facilitated EBC acquisition rates, but impaired both memory retention and relearning after extinction. Chondroitinase-treated DCN showed an increase in GABAergic terminals and a reduction in VGLUT1+ excitatory terminals. Furthermore, *in vivo* awake electrophysiological recordings of DCN neurons showed reduced spontaneous spike frequencies and increased spike irregularity. Together, these results implicate PNNs in the DCN as an important regulator for structural plasticity, and cerebellar-dependent learning and memory consolidation.

3.2 Introduction

Perineuronal nets (PNNs) are macro-molecular assemblies of extracellular matrix molecules, which form during postnatal development around some neuronal cell types throughout the central nervous system. They contribute to the end of critical periods (for a review: Kwok et al. 2011). Critical periods are temporary windows characterized by heightened levels of neuronal plasticity under the influence of external stimuli. PNNs are made of hyaluronan, chondroitin sulfate proteoglycans (CSPGs), link proteins and tenascin-R. Bound to PNN-CSPGs are the homeoprotein Otx2 and the chemorepulsive axon guidance molecule Semaphorin-3A (Sema3A). However, the role of Sema3A in PNNs is completely unknown (Vo et al. 2013; Dick et al. 2013; Carulli et al. 2013; de Winter et al. 2016). PNNs are not static structures. They can be physiologically modulated in conditions associated with plasticity, in both intact and injured brain. For example, mice reared in an enriched environment show a reduction of PNNs in parallel with increased plasticity (Sale et al. 2007; Foscarin et al. 2011). During injury-induced compensatory sprouting, PNN expression is strongly decreased (Carmichael et al. 2005; Carulli et al. 2013; Faralli et al. 2015).

Enzymatic digestion of CSPGs by chondroitinase (ch'ase) or genetic/pharmacological manipulation of PNN components, such as aggrecan, link protein-1 and Otx2, restore juvenile levels of plasticity and increase axonal sprouting (Pizzorusso et al. 2002; Massey et al. 2006; Galtrey et al. 2007; Frischknecht et al. 2009; Carulli et al. 2010; Beurdeley et al. 2012; Lee et al. 2017; Rowlands et al. 2018), pointing to a role of PNNs in stabilizing synaptic contacts and inhibiting the formation of new connections in the adult CNS. Recent evidence furthermore shows that PNNs play a crucial role in learning and memory. When PNNs are enzymatically reduced in the perirhinal cortex, memory of a familiar object is prolonged (Romberg et al. 2013; Yang et al. 2015). On the other hand, PNNs in the amygdala and in cortical areas have been shown to contribute to the consolidation of fear- and drug-associated memories (Gogolla et al. 2009; Xue et al. 2014; Slaker et al. 2015; Banerjee et al. 2017; Thompson et al. 2018). Accordingly, PNNs in the auditory cortex are transiently upregulated during auditory fear memory consolidation (Banerjee et al. 2017). PNNs in the deep cerebellar nuclei (DCN) have been shown to undergo modifications as a result of behavioral manipulation (Foscarin et al. 2011), although the exact role of these PNNs in associative learning, memory retention and DCN physiology remains to be clarified.

Associative learning during Pavlovian eyeblink conditioning (EBC) depends on different plasticity mechanisms in the olivo-cerebellar circuit (Tracy et al. 1998; Kleim et al. 2002; Jirenhed et al. 2007; Freeman and Steinmetz 2011; Gao et al. 2012; Boele et al. 2013; Canto et al. 2018; Wang et al. 2018). During EBC a neutral stimulus such as a LED light (conditioned stimulus, CS) is paired with an aversive corneal air puff (unconditioned stimulus, US), causing an eyelid closure (unconditioned response, UR). After repeated paired presentations of CS and US, animals learn to make an eyelid closure before arrival of the US (conditioned response, CR). This form of learning depends on activity in cerebellar lobule HVI (Yeo and Hardiman 1992; Garcia et al. 1999; Attwell et al. 2001), and the

dorsolateral hump (DLH) and anterior part of the interposed nucleus (IntA) (Yeo et al. 1985a; Lavond and Steinmetz 1989; Sears and Steinmetz 1990; Freeman et al. 2005). In well-trained animals inactivating these parts of the DCN abolishes learned performance (Bracha et al. 1994; Bao et al. 2000; Freeman and Rabinak 2004; Ohyama et al. 2006; Mojtahedian et al. 2007), but inactivation of lobule HVI leads to less severe effects and predominantly affects the timing of CRs (McCormick and Thompson 1984b; Perrett et al. 1993; Garcia et al. 1999). Thus, plasticity mechanisms at the level of the DCN play a role and can be sufficient for the expression of learned responses (Medina et al. 2000; Ohyama et al. 2006). Furthermore, in the DCN a learning-associated upregulation of synaptic terminals has been reported (Kleim et al. 2002; Boele et al. 2013) as well as changes in intrinsic excitability (Wang et al. 2018). Regulation of plasticity by PNNs in the DCN therefore may be an important mechanism for this type of cerebellar learning.

Here we investigated whether PNNs in the DCN are physiologically altered during EBC and vice versa, whether experimental interference with PNNs results in altered learning. We found that PNNs undergo learning-associated reductions only in conditioned, but not in control or pseudo-conditioned mice. This reduction coincided with lower Sema3A levels. Enzymatic digestion of PNNs enhanced learning performance, but impaired memory retention and reacquisition performance after extinction. Removal of PNNs led to changes in afferent synaptic terminals onto DCN neurons, *i.e.* the density of GABAergic terminals, including Purkinje cell (PC) terminals, was increased and the density of excitatory VGLUT1-positive terminals was decreased. To investigate the physiological effects, we performed *in vivo* awake recordings from DCN neurons and found decreased spontaneous spike frequencies and increase spike irregularity, in line with the increased number of PC terminals and reduced number of excitatory inputs. This study is the first to show (1) a bidirectional relationship between PNNs and associative cerebellar-dependent learning and (2) the physiological consequences of PNN removal in the DCN on activity in awake behaving mice.

3.3 Materials and methods

3.3.1 Ethical statement and conflicts of interest

All procedures were approved by the animal committee of the Royal Dutch Academy of Arts & Sciences (DEC-KNAW). All procedures adhered to the European guideline for the care and use of laboratory animals (Council Directive 86/6009/EEC). All authors declare no financial or non-financial conflict of interest.

3.3.2 Virus production

The green fluorescent protein (GFP) or the ch'ase gene was inserted into a lentiviral (LV) vector for long-term expression, containing the mouse phosphoglycerate kinase (PGK) promoter. The vector has been produced according to Zhao et al. (2011). Briefly, GFP or ch'ase transgene was subcloned into a transfer plasmid such that the transgene could be transcribed into a packageable RNA upon transfection into HEK293T cells along with non-recombining plasmids that express lentiviral and vesicular stomatitis virus (VSV-G) genes (Naldini et al. 1996; Dull et al. 1998). Each transfer plasmid specifies a vector RNA which contains, from 5' to 3', the RU5 fragment of the long terminal repeat (LTR), HIV-1 packaging signal in a Gag gene fragment, Rev response element, central polypurine tract/central termination sequence, PGK promoter with transgene, woodchuck hepatitis virus post-transcriptional regulatory element, and self-inactivating (SIN) 3' LTR. The vector RNAs are essentially identical except for the promoter, polylinker and transgene. The lentiviral vector was created with a transfer plasmid derived from pRRL via the SIN-W-PGK vector, with different polylinkers which includes an additional polypurine tract, and vector particles were generated by cotransfection with this plus two other plasmids (Déglon et al. 2000). Viral particles were concentrated by ultracentrifugation and the viral particle-containing pellet was resuspended in 0.1 M phosphate-buffered saline (PBS) pH 7.4 or in Dulbecco's modified Eagle's medium (DMEM), and stored at −80°C until further use. Viral titre was obtained by a p24 antigen ELISA assay (Perkin Elmer). The titre of LV-PGK-GFP was 3 x 10^{10} transducing units, the titre of LV-PGK-ch'ase was 1 x 10^{10} transducing units.

3.3.3 Virus injection and pedestal placement

Adult male C57Bl6/J mice (20-25 g) were deeply anesthetized using isoflurane (induction 5%, maintenance 2% in medicinal air) and eyes were protected from drying using antibacterial eye cream (Terra-Cortril, Pfizer). Body temperature was maintained at 37 °C using a temperature-controlled heating pad. A 1 cm longitudinal skin and muscle incision was made at the level of the occipital bone and the area was locally anesthetized (10% Xylocaine, AstraZeneca). Two small craniotomies were performed to expose the IV-V cerebellar lobule of the right and the left hemispheres. One µl of virus was injected into the interpositus nucleus in each side (+-2.0 mm lateral from midline, 2.0 mm depth, - 6.0 mm from Bregma) by a quartz capillary pipette (30-40 µm tip diameter) connected to a Harvard injection pump, with a speed of 0.15 µl/min. The pipette was left in place for 2 minutes after the injection and was then slowly retracted. Next, a continuation of the first incision was made in the skin covering the top of the skull and primer (Optibond All-In-One, Kerr) was applied on the skull and hardened out using UV-light. A small aluminum block was stereotaxically placed and attached on the bone using dental cement (Flowline, Heraeus Kulzer). The head skin was sutured and animals were given post-operative analgesia (0.4

mg/kg SC Meloxicam, Metacam, AUV). Mice were allowed to recover for at least 3 days following surgery.

3.3.4 Eyeblink conditioning

Adult male C57Bl6/J mice (20-25 g) were subjected to EBC using a camera setup or a setup based on magnetic distance measurement technique (MDMT setup) (Koekkoek et al. 2002). In the MDMT setup mice were placed in light and sound-proof boxes, whereas in the camera setup mice were placed in a faraday cage with curtains to create darkness. In both cases mice were first habituated for at least 5 days. During habituation mice were placed on a cylindrical treadmill (Fig 1A) with increasing durations (from 10 to 30 minutes). For mice trained in the MDMT setup, under isoflurane anesthesia hairs under the left eye were removed on day 3. From day 4 onward a small neodymium magnet (1.5 × 0.7 × 0.5 mm) was placed under the left eyelid using superglue (Bison) to allow detection of eyelid movements, thanks to a magnet sensor placed above the magnet, which detects changes in magnetic field. Ten minutes after closing the box, trainings were initiated. In the camera setup mice were placed on the treadmill without anesthesia and before fixation a thin layer of waterproof black mascara was applied on the left whiskers to prevent IR light reflection. For all mice, from day 4 onward a sequence of 10 CS only - 2 US only - 10 CS only trials was presented to make mice acquainted with the stimuli. US was a 10 ms corneal air puff (35-40 psi) delivered through a p20 pipette tip positioned ~5 mm from the left eye. CS was a 260 ms green (camera setup) or green/blue (MDMT setup) LED light positioned ~7 cm in front of both eyes (Fig 1A). US onset was 250 ms after CS onset, both stimuli co-terminated and stimuli were presented with an intertrial interval (ITI) time of 12 ± 2 sec (camera setup) or 10 ± 2 sec (MDMT setup). Trials were initiated only if the eye was more than ~75% opened. Eyelid movements in the camera set up were recorded using a 250 fps camera (scA640-120 gc, Basler) and the mouse eye was illuminated by an IR-light. Data was sampled at 2441 Hz and stimuli were triggered using TDT System 3 (Tucker Davis Technologies) and NI-PXI (National Instruments) processors. Eyelid movements in the MDMT set up were captured at 1000 Hz using custom-written LabVIEW (National Instruments) software (Koekkoek et al. 2002).

3.3.5 Experimental protocol

To study the effect of EBC on the morphology of PNNs in the DCN (Exp. 1), we randomly assigned mice to one of three groups: conditioned (N = 5), pseudo-conditioned (N = 5) or control (N = 6). Trainings for these experiments were done with the camera setup. Mice were housed individually for the duration of the experiment. Mice in the conditioned group received a sequence of 3 US only and 100 CS-US paired trials presented with an ITI of 12 ± 2 sec, 3 times per day for 5 consecutive days, totaling 15 training sessions. Mice in the

pseudo-random group received a sequence of 3 US only trials followed by a random sequence of 100 CS only and 100 US only trials 3 times a day for 5 days. Pseudo-random stimuli were presented with an ITI of 6 ± 2 sec to match the duration of the training of the conditioned group. To randomize trials we used the 'randi' function of MATLAB (MathWorks) and saved the order in one of three templates which we used in an alternating manner each session. Control mice received a pedestal and were left in the home cage for the duration of the experiment. All mice were at least P44 at the time of transcardial perfusion.

To study the effects of PNN digestion on EBC learning (Exp. 2) mice were randomly assigned to one of two groups: LV-GFP (N = 19) or LV-ch'ase (N = 17). LV-GFP mice received bilateral injections of LV-PGK-GFP and LV-ch'ase mice received injections of LV-PGK-ch'ase in the IntA nuclei as described above. One mouse in the LV-ch'ase group was excluded due to incomplete PNN digestion. After surgery, mice recovered for 14 days before initiation of habituation sessions as described above. Starting on day 21 after injections, mice were trained once a day for consecutive 5 days using the MDMT setup (*acquisition phase*). Each session consisted of 20 blocks of 1 US only - 10 CS-US paired - 1 CS only trials presented with an ITI of 10 ± 2 sec, totaling 20 US only, 20 CS only and 200 paired trials per session. Following acquisition trainings, memory retention (*retention phase*) was measured in mice that had showed robust learning during the acquisition phase (%CR >33.3% on the last training). Mice were subjected mice to retention sessions on day 3 (LV-GFP: N = 12; LV-ch'ase: N = 13), 7 (N = 12 and N = 14), 10 (N = 11 and N = 12), 14 (N = 7 and N = 7) and 21 (N = 3 and N = 4) after the last acquisition day. Retention sessions consisted of 5 blocks of 1 US only - 10 CS-US paired - 1 CS only trials presented, totaling 5 US only, 5 CS only and 50 paired trials. Following the retention session on day 21 mice were subjected to an extinction session (*extinction phase*) (LV-GFP: N = 3; LV-ch'ase: N = 4), during which 20 blocks of 1 US only - 11 CS only trials were presented, totaling 20 US only and 220 CS only trials. Then, after 3 days a short test session (1 US only - 10 CS only - 1 US only) was given to test the performance after extinction. Directly after this session a reacquisition session (*reacquisition phase*) was given, which in terms of protocol was equal to one acquisition session (see above). Mice were transcardially perfused following the last reacquisition session.

To investigate the effects of PNN removal on the physiological properties of IntA neurons (Exp. 3), mice were randomly assigned to a group receiving bilateral injections of LV-PGK-GFP (N = 6) or LV-PGK-ch'ase (N = 7) in the IntA nuclei (as described above). Two LV-ch'ase mice were excluded due to incomplete bilateral PNN digestion. In two other LV-ch'ase mice, neurons recorded in one hemisphere were excluded due to incomplete PNN digestion unilaterally. Habituations started between day 14 and 21 after injections. Mice received between 5 and 10 habituation sessions, after which mice were trained for 2 consecutive acquisition days (see acquisition phase Exp. 2). Directly following the second acquisition session, mice were used for *in vivo* awake electrophysiological recordings.

3.3.6 Eyeblink data analysis

Data acquired on the camera setup was analyzed using custom-written MATLAB (MathWorks) scripts. Data was filtered using a Gaussian 50 Hz lowpass filter and event-related data was gathered based on TTL timestamps indicating trial start and CS and US stimuli, which were also used to synchronize electrophysiological and behavioral data (Fig 1B). Trials were marked as unstable and were excluded if values during baseline (first 500 ms of trial) exceeded 5x SD of signal of baseline. To correct for the measurement bias during squinting following a US, all amplitudes were calculated relative to 66.7% of the average UR amplitude. UR amplitude was calculated as average of maxima during the first 450 ms following a US in US only trials (or paired trials if not available). CRs were defined as eyelid closures exceeding 10% of UR amplitude (Exp. 1) or >5x SD of baseline (Exp. 3) during 50-250 ms after CS onset. Data from the MDMT setup was similarly analyzed, although sessions were excluded if more than 75% of trials were invalid. CRs were defined as eyelid closures exceeding 10% of UR amplitude during 10-250 ms after CS onset.

3.3.7 *In vivo* electrophysiology

A bilateral craniotomy surgery was performed to access the IntA nuclei for extracellular recordings of single units. Mice were anesthetized using isoflurane and eyes were protected from drying using eye drops (Duodrops, Ceva). Body temperature was maintained at 37° C using a temperature-controlled heating pad guided by a rectal temperature probe. Skin in the neck was shaved and a 1 cm longitudinal incision was made to uncover the neck muscles. Muscles were locally anesthetized (10% Xylocaine, AstraZeneca) and removed to access the occipital bone. Two square craniotomies were made using a dental drill (Foredom Drill K1070-2E, Blackstone Industries) above Crus II, approximately 1.7 mm lateral to the midline. A thin layer of primer (Optibond All-In-One, Kerr) was applied around the craniotomies, hardened out with UV light, and a circular recording bath was created using dental cement (Flowline and Charisma, Heraeus Kulzer). Bath was filled with saline and the dura was removed covering the brain in both craniotomies. Bath was then filled with a low viscosity silicone elastomer sealant (Kwik-cast, World Precision Instruments) to prevent the brain from drying and the skin surrounding the bath was attached to the skull bone with tissue glue (Histoacryl). Post-operative analgesia was given by i.p. injection of meloxicam (0.4 mg/kg Metacam) and mice recovered for at least 2 hours before initiation of the recording session.

Extracellular recordings were performed using electrodes with a tip diameter of ~1 µm and a pipette resistance of 4-8 MΩ, heat-pulled from filamented borosilicate glass capillaries (1.5 mm OD, 0.86 mm ID, Harvard Apparatus) with a P-1000 micropipette puller (Sutter Instruments). Electrodes were filled with standard intracellular solution, containing (in mM): 10 KOH, 3.48 $MgCl_2$, 4 NaCl, 129 K-Gluconate, 10 hepes, 17.5 glucose 4 Na_2ATP, and 0.4 Na_3GTP (295 ± 305 mOsm; pH 7.2). Electrodes were attached to an electrode holder that

approached the brain surface in a 43° angle and movements were controlled by a micromanipulator (SM7, Luigs and Neumann). Recordings were amplified using a Multiclamp700B amplifier (Axon Instruments) and digitized on 100 kHz using a Digidata 1440 (Axon Instruments). Electrodes were lowered into the brain under high pressure till a depth of 1500 µm, after which the pressure was lowered to 15-20 mbar and the electrode was advanced in steps of 2 µm per second until individual spikes could be identified with >1 mV amplitudes. Then, an eyeblink protocol was presented consisting of 1 US only - 5 CS-US paired - 1 CS only trial for at least 80 trials or until spike amplitude became too low. The maximum duration of a recording session was 4 hours, after which mice were transcardially perfused for histology.

3.3.8 Electrophysiological data analysis

Spike times were obtained using a custom-written MATLAB spike analysis program (B.H.J. Winkelman, Netherlands Institute for Neuroscience, Amsterdam) and sorted based on spike waveform characteristics. In most recordings single units could be clearly identified, however recordings in which single units could not be unequivocally distinguished were excluded from analysis. Spontaneous spike characteristics were calculated based on 16.4 ± 7.8 seconds of recording while the mouse was in quiet wakefulness in the dark before start of EBC. We analyzed spike frequency (= number of spikes / duration of time period), coefficient of variation of spiking (CV = standard deviation (all interspike intervals (ISIs) / average (all ISIs)) and average CV of two adjacent ISIs ($CV_2 = 2 \mid ISI_{n+1} - ISI_n \mid / (ISI_n + ISI_n+1)$) as *in vivo* cell physiological parameters.

To classify spike responses to CS and US stimuli, we detect changes in spike frequency relative to the baseline period (0-500 ms before CS onset). Period for CS responses was 0-250 ms following CS onset and period for US responses was 0-250 ms following US onset. Behavioral and electrophysiological data were synchronized based on TTL pulses that were captured on all acquisition devices. Peristimulus time histograms (PSTHs) were generated using 20 ms bins and increases in spike frequency greater than 3x SD of the baseline period were defined as *spike facilitation cells* and decreases greater than 3x SD of the baseline period were defined as *spike suppression cells.* (Fig 9B, B').

3.3.9 Histological procedures

Mice were anaesthetized and transcardially perfused with 100 ml of 4% paraformaldehyde in 0.12 M phosphate buffer. Brains were dissected and postfixed overnight at 4°C, then cryoprotected in 0.12 M phosphate buffer containing 30% sucrose at 4°C, until they sank. Cerebella were cut on a cryostat into 25 µm-thick coronal or sagittal sections and collected in PBS.

Primary antibodies were incubated overnight at 4°C in PBS containing 0.25% Triton X-100, and 5% fetal calf serum. Primary antibodies were: mouse anti-NeuN (Millipore, 1:500), rabbit anti-Sema3A (Aviva, 1:200), chicken anti-GFP (Aves Labs, 1:700), mouse anti-calbindin (Swant, 1:1500), rabbit anti-VGAT (Synaptic Systems, 1:1000), rabbit anti-VGLUT1 (Synaptic Systems, 1:1000), guinea pig anti-VGLUT2 (Synaptic Systems, 1:1000), mouse anti-gephyrin (Synaptic Systems, 1:500). For Sema3A staining, sections were processed for immunofluorescence with the Tyramide Signal Amplification Biotin System (PerkinElmer) following the manufacturer's protocol. To visualize PNNs, sections were incubated in biotinylated *Wisteria floribunda* agglutinin (WFA; Sigma Aldrich, 20 µg/ml) for 2 h at room temperature. Sections were incubated for 1 h at room temperature with one of the following fluorophore-conjugated secondary antibodies or streptavidin: donkey anti-mouse Cy3, goat anti-chicken Alexa Fluor 488 (ThermoFisher Scientific), donkey anti-guinea pig Cy3 (ThermoFisher Scientific), donkey anti-rabbit Alexa Fluor 647 (ThermoFisher Scientific), streptavidin-488 (ThermoFisher Scientific), streptavidin-Cy3 (Jackson Immunoresearch). For each immunohistochemical reaction, slices from all experimental conditions were processed together and incubation times kept constant. After processing, sections were mounted on microscope slides with Tris-glycerol supplemented with 10% Mowiol (Calbiochem, LaJolla, CA). Histological preparations were examined under a Leica SP5 confocal microscope. Confocal images were taken at a resolution of 1024x1024 dpi and 50 Hz speed and each focal plane was 1 µm-thick. Lasers intensity, gain and offset were maintained constant in each analysis. Quantitative and morphometric evaluations were performed by using Image J software (see below). Adobe Photoshop 6.0 (Adobe Systems, San Jose, CA) was used to adjust image contrast and assemble the final plates.

3.3.9.1 Quantification of WFA intensity

Quantification of the staining intensity of PNNs following EBC or control treatment was performed in the DLH, in the most lateral part of the anterior interpositus (IntA) and in the dorsal part of the lateral nucleus in coronal sections on both sides. Sections were double labelled with NeuN antibodies and WFA, which is a general PNN marker, binding to sugar chains of the CSPGs (Härtig et al. 1992). Confocal images (1 um thick) of sections of the anterior DCN (6.00 to 6.24 mm caudal to Bregma) were acquired under a 63x objective. Analysis of WFA staining intensity around neurons with a visible NeuN+ nucleus was performed by ImageJ, as described in Foscarin et al. (2011). Briefly, for each analysed neuron the brightness intensity of WFA (range 0-255) (DLH: CTR n = 202; pseudo n = 146; conditioned n = 153; IntA: CTR n = 199; pseudo n = 138; conditioned n = 160; lateral nucleus: CTR n = 214; pseudo n = 168; conditioned n = 169) in 5-6 mice/condition (CTR, n = 6 mice; pseudo, n = 5 mice; conditioned, n = 5 mice) was measured by randomly selecting 15 pixels (approximately equidistant from each other) in the PNN surrounding the neuronal soma and calculating their average intensity. The background brightness, taken from a non-stained region of the cerebellar molecular layer, was subtracted from the brightness

measurements. Each net was assigned to one of three categories of staining intensity, ranging from the lowest to the highest value of WFA intensity: weak = 0-33%, medium = 34-66%, strong = 67-100% of maximum staining intensity. The average WFA staining intensity was also calculated. Quantification of PNN digestion after LV-ch'ase (N = 3) or LV-GFP (N = 3) injection was performed by evaluating WFA intensity in a selected area of the IntA (80,000 um^2) in 3 sections/mouse. The background brightness, taken from the molecular layer of a not-digested lobule, was subtracted from the measurements.

3.3.9.2 Quantification of Sema3A intensity

The analysis of Sema3A staining intensity was performed according to Carulli et al. (2013). Briefly, single 1 um-focal plane confocal images of the DLH were collected under a 63x objective. For each analysed neuron we measured by ImageJ the mean brightness intensity (range 0-255) of about 60 PNNs/animal (CTR, n = 65, conditioned, n = 59; number of animals: CTR, N = 6; conditioned, N = 5) by randomly selecting 15 pixels (approximately equidistant from each other) in the Sema3A staining surrounding the neuronal soma and calculating their average intensity. The outline of neuronal somata was delineated by PC terminals (identified by calbindin immunopositivity) impinging on the neuron. The background brightness, taken from a non-stained region of the cortical granule cell layer, was subtracted from the brightness measurements. Each net was then assigned to one of three categories of staining intensity, ranging from the lowest to the highest value of Sema3A intensity detected: weak = 0-33%, medium = 34-66%, strong = 67-100% of maximum staining intensity. The average Sema3A staining intensity was also calculated.

3.3.9.3 Quantification of gaps between VGAT-positive boutons

Single 0.5 um thick-confocal images of the IntA in sagittal sections have been collected under a 63x objective with 2x zoom. On such images, the intensity of VGAT staining around single DCN neurons has been plotted by using the ImageJ function "surface plot". In the plot the density (number/mm neuronal membrane) of "dips" with value < 40 a.u., followed by peaks > 100 a.u. has been quantified per each analyzed neuron (LV-PGK-GFP, n = 52 neurons from 5 mice; LV-PGK-ch'ase, n = 33 from 5 mice).

3.3.9.4 Quantification of gephyrin-positive puncta

Single 0.5 um thick-confocal images of the IntA in sagittal sections have been collected under a 63x objective with 3x zoom. On such images the density of gephyrin-positive puncta (number/um neuronal membrane) has been evaluated by ImageJ (LV-PGK-GFP, n = 26 neurons from 3 mice; LV-PGK-ch'ase, n = 23 from 4 mice).

3.3.9.5 Quantification of density of glutamatergic terminals

To estimate the density of VGLUT1 and VGLUT2-positive glutamatergic axon terminals, at least three sagittal sections (containing the IntA) were selected for each animal (N = 5 for LV-PGK-GFP; N = 4 for LV-PGK-ch'ase), and a 0.5 um-thick confocal image/section was captured under a 63x objective. The ''analyze particle'' function of ImageJ was used to estimate the density of boutons (number of terminals/mm^2) in each image, after selecting the automatic threshold.

3.3.10 Statistical analysis

All experiments were conducted in a blind manner. Histological quantification for Exp. 1 was performed blinded by coupling mice to IDs while keeping the groups unknown to the experimenter. Behavioral training (Exp. 2 and 3), histological quantification (Exp. 2) and electrophysiology (Exp. 3) were done blinded by having a third experimenter overseeing the mouse-group-ID coupling. Groups were revealed only after finishing all behavior trainings, histological steps or electrophysiology for each experimental question.

Statistical analysis was carried out by GraphPad Prism 5 (GraphPad Software Inc., La Jolla, CA, USA), SPSS version 22 (IBM) and MATLAB (R2011b, MathWorks). Normality of distributions was assessed using Shapiro-Wilk test and, if normality was violated, non-parametric tests were performed. Independent-samples Mann-Whitney U test was used to compare spontaneous spike characteristics. Chi-square test was used to compare the frequency distribution of WFA/Sema3A+ nets. One-way ANOVA or unpaired Student's t-test were used to compare the average staining intensity of WFA+ or Sema3A+ nets, respectively.

Behavioural performance was analysed using repeated-measures ANOVA (data from camera setup) or linear mixed models (data from MDMT setup) with the maximum likelihood method. Group and session/day were modelled as fixed effects, and %CR, CR amplitude and amplitude at US onset were modelled as dependent variables. We assessed the fit of the model by running the analysis with the unstructured, diagonal and first-order autoregressive repeated covariance types, after which we choose the covariance type with the lowest Akaike's information criterion (AIC) value, which was in most cases the unstructured type. Data is shown as mean ± SD, unless indicated otherwise and $P < 0.05$ was considered as statistically significant.

3.4 Results

Previous studies have shown that PNNs are decreased in conditions associated with plasticity in the adult brain, including following enriched environmental stimulation (Sale et al. 2007; Foscarin et al. 2011) or injury (Carmichael et al. 2005; Carulli et al. 2013; Faralli et al. 2015). Dynamic regulation of PNN expression is also reported during fear conditioning, with a transient upregulation of PNNs in the auditory cortex during auditory fear memory consolidation (Banerjee et al. 2017). To address whether structural changes occur in PNNs during EBC, we focused on PNN expression levels in the IntA and the DLH, which are the subnuclei of the cerebellum that are involved in EBC (Clark et al. 1992; Krupa et al. 1993; Krupa and Thompson 1997; Freeman et al. 2005; Freeman and Steinmetz 2011).

3.4.1 PNNs are altered during EBC

Mice were assigned to one of three groups: conditioned (cond), pseudo-conditioned (pseudo) and control (CTR). Conditioned and pseudo-conditioned mice received daily paired or unpaired training sessions while they were positioned head-fixed on a cylindrical treadmill (Fig 1A). Control animals remained in their home cage for the duration of the experiment, but just as the conditioned and pseudo-conditioned mice they received a pedestal (Fig 1C). We measured learning performance as the percentage of trials showing CRs and the amplitude of eyelid closure at the onset of US (Fig 1B). During training we found an increase in percentage CR over the course of training in the conditioned group, whereas pseudo-conditioned animals did not show learning (day: $F(1.971, 15.767) = 13.334$, $P<0.001$; group: $F(1, 8) = 17.332$, $P=0.003$; interaction: $F(1.971, 15.767) = 13.337$, $P<0.001$; Greenhouse-Geisser corrected repeated-measures ANOVA; Fig 1D). This increase was accompanied by an increase in eyelid closure at US onset in conditioned mice, but not in pseudo-conditioned mice (day: $F(1.746, 13.965) = 11.229$, $P=0.002$; group: $F(1, 8) = 14.523$, $P=0.005$; interaction: $F(1.746, 13.965) = 10.157$, $P=0.002$; Greenhouse-Geisser corrected repeated-measures ANOVA; Fig 1E).

Next, we quantified PNN expression levels in the IntA and the DLH as regions involved in EBC, and the lateral nucleus (Lat) as a control area. PNNs were detected by using the general PNN marker WFA (Härtig et al. 1992). Because WFA intensity shows a wide range of variability in the DCN, we divided PNNs according to their WFA staining intensity in three categories: strong/medium/weak WFA intensity (as in Foscarin et al. 2011). The percentage of strong/medium/weak nets in conditioned mice (on day 5 of training) was compared to that of control and pseudo-conditioned mice. Data have been collected from both the right and the left side, as axonal plasticity has been reported in both sides after EBC (Boele et al. 2013).

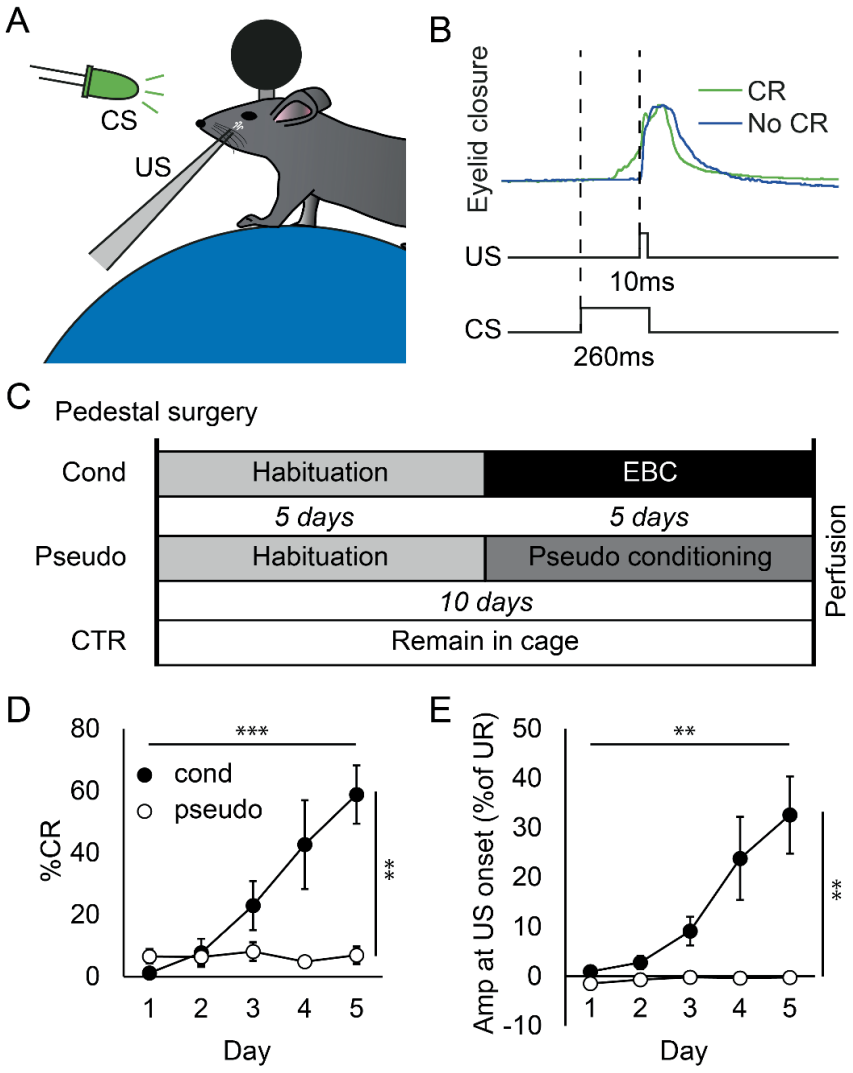

Fig 1. Experimental design and learning performance. (A) Mice were head-fixed on a cylindrical treadmill during training sessions. (B) Paired presentation of a CS (260 ms green LED light) and a US (10 ms corneal air puff) led to associative learning, measured as eyelid closures during the CS-US interval (green line; CR). (C) Mice were assigned to the conditioned (cond), pseudo-random (pseudo) or control (CTR) group. All mice received a pedestal, after which only the cond and pseudo group continued with habituation sessions and classical EBC (cond group) or unpaired presentation of CS and US (pseudo conditioning; pseudo group). Learning was observed in the cond group as an increase in percentage of trials with CRs (D) and an increased eyelid closure amplitude at the time of US onset (E), whereas pseudo animals did not show this. Error bars represent standard error of the mean (SEM). * $P < 0.05$, ** $P < 0.01$, *** $P < 0.001$

In control mice, the DLH displayed the highest number of strong nets (~ 80%), followed by the IntA (~65% of strong nets) and the Lat (~10% of strong nets), with an opposite distribution of weak nets (DLH: ~2%; IntA: ~8%; Lat: ~45%) (Fig 2B, C, F, I, L; DLH vs IntA: $X^2_2 = 23.83$ (n = 401), P<0.001; DLH vs Lat: $X^2_2 = 23.83$ (n = 416), P<0.001; IntA vs Lat: $X^2_2 = 123.50$ (n = 413), P<0.001). Pseudo-conditioned mice showed a frequency distribution similar to control mice (Fig 2C, D, F, G, I, J, L; CTR DLH vs pseudo DLH: $X^2_2 = 4.24$ (n = 348): P = 0.12; CTR IntA vs pseudo IntA: $X^2_2 = 3.13$ (n = 337), P = 0.21; CTR Lat vs pseudo Lat, $X^2_2 = 2.48$ (n = 382), P = 0.29), indicating that the presentation of conditioned and unconditioned stimuli in random order does not affect PNN expression. Interestingly, in conditioned mice, there was a remarkable decrease in the percentage of strong WFA+ nets in the DLH when compared to control and pseudo-conditioned mice (from ~ 85% to ~ 55%), which was accompanied by an increase in the percentage of medium nets (from ~ 15% to ~ 40%) and weak nets (from ~1% to ~5%) (Fig 2C-E, L; CTR DLH vs cond DLH: $X^2_2 = 31.97$ (n = 357), P<0.001; pseudo DLH vs cond DLH: $X^2_2 = 40.90$ (n = 299), P<0.001). Accordingly, the average WFA intensity in the DLH was significantly lower in conditioned mice when compared to control and pseudo-conditioned mice (Fig 2M; CTR: 209.34 +- 37.54 SD, pseudo: 218.86 +- 36.15 SD, conditioned: 176.25 +- 41.38 SD; one-way ANOVA, P<0.001, F(2, 498) = 52.3; Bonferroni post-hoc).

A strong PNN reduction has been also detected in the IntA of conditioned mice with respect to control and pseudo-conditioned mice. Strong PNNs decreased from ~ 65% to ~ 30%, while the percentage of medium and weak nets increased (from ~ 25% to ~ 50% and from ~ 8% to ~ 16%, respectively; Fig 2F-H, L; CTR vs cond mice, $X^2_2 = 39.30$ (n = 359), P<0.001; pseudo vs cond mice: $X^2_2 = 51.95$ (n = 298), P<0.001). Accordingly, the average WFA intensity in the IntA was significantly reduced in conditioned mice (Fig 2M; CTR: 182.83 +- 49.06 SD, pseudo: 194.55 +- 42.53 SD, cond: 152.26 +- 41.64 SD; one-way ANOVA, F(2, 494) = 36.19, P<0.001; Bonferroni post-hoc).

In the lateral nucleus, the effect of EBC on PNN expression was less remarkable. The percentage of weak nets shifted from 44% (in control mice) to 54%, with a 3% decrease in medium nets and a 7% decrease in strong nets (CTR vs cond mice, $X^2_2 = 7.03$ (n = 383), P<0.05). However, there was no significant difference in the frequency distribution of conditioned mice when compared to pseudo-conditioned mice (Fig 2I-L; $X^2_2 = 3.76$ (n = 337, P=0.15). The average WFA intensity was slightly lower in conditioned mice when compared to control and pseudo-conditioned mice (Fig 2M; CTR: 114.92 +- 51.41 SD, pseudo: 114.50 +- 45.13 SD, cond: 97.68 +- 46.56 SD; one-way ANOVA, F(2, 548) = 7.38, P<0.001; Bonferroni post-hoc).

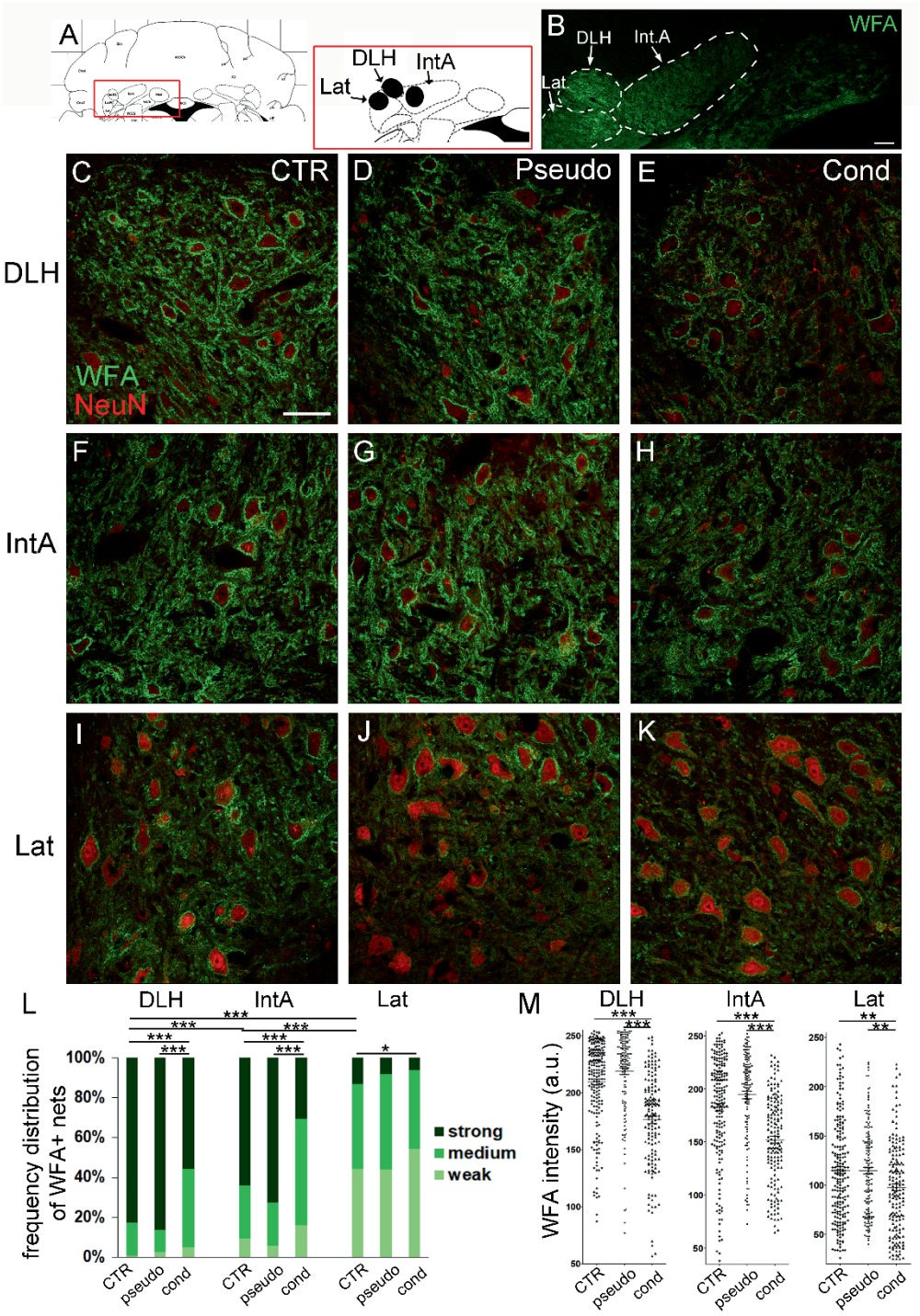
A
DLH
IntA
Lat
B
DLH
Int.A
Lat
WFA
C
CTR
D
Pseudo
E
Cond
DLH
WFA
NeuN
F
G
H
IntA
I
J
K
Lat
L
DLH
IntA
Lat
frequency distribution of WFA+ nets
100%
80%
60%
40%
20%
0%
strong
medium
weak
CTR
pseudo
cond
M
WFA intensity (a.u.)

Fig 2. PNNs are reduced during EBC. (A, B) The intensity of WFA+ nets was analysed in the dorsolateral hump (DLH), anterior interpositus (IntA) and lateral nucleus (Lat) of mice which were trained for 5 days (conditioned mice), in pseudoconditioned (pseudo) mice and in control (CTR) mice. The exact location of the analysis is represented by black circles in A, which shows a scheme of the cerebellum (Paxinos mouse brain atlas: Bregma: -6.12 mm). The distribution of WFA+ nets according to their intensity (strong/medium/weak) is different in the three nuclei in CTR mice (B, C, F, I, L). No difference has been detected in the frequency distribution of WFA+ nets between CTR and pseudo animals in either nucleus (C, D, F, G, I, J, L). A significant shift in the frequency distribution of WFA+ nets towards weakly and medium stained nets is present in the DLH and IntA of cond mice when compared to CTR and pseudo mice (C-H, L). A slight increase in the percentage of weakly stained PNNs was detected in the lateral nucleus of cond mice when compared to CTR mice (I-L). In M, single WFA+ nets are plotted according to their staining intensity (arbitrary units (a.u.): from 0 to 255). A significant decrease in the average staining intensity is found in all three nuclei in cond mice with respect to CTR and pseudo mice. In C-K, neuronal cell bodies are stained by anti-NeuN antibodies. Scale bars: 100 μm in B, 50 μm in C (also applies to D-K). Number of animals: CTR, N = 6; pseudo, N = 5; cond, N = 5. Number of neurons: DLH, CTR n = 202; pseudo n = 146; conditioned n = 153; IntA, CTR n = 199; pseudo n = 138; conditioned n = 160; Lat, CTR n = 214; pseudo n = 168; conditioned n = 169. * $P < 0.05$, ** $P < 0.01$, *** $P < 0.001$

3.4.2 Sema3A levels in PNN are reduced during EBC

Sema3A, a known chemorepulsive axon guidance molecule, has been recently found in the PNNs of many brain areas, but its role at present is not known (Vo et al. 2013). Sema3A has been found in all DCN subdivisions, where the majority of PNNs contain Sema3A and Sema3A staining intensity is directly correlated to the staining intensity of WFA (Carulli et al. 2013). Sema3A in DCN PNNs is reduced during enhanced structural plasticity, in both physiological and injury-induced conditions, suggesting a plasticity-inhibitory role of this molecule (Carulli et al. 2013). We asked whether the expression of Sema3A is also diminished during EBC. Because there was no difference in WFA levels between control and pseudo-conditioned mice, we investigated the effect of EBC on Sema3A expression with respect to control mice (Fig 3A-D). We evaluated the content of the protein in both the right and the left DLH, by defining the relative frequencies of nets showing weak, medium or strong Sema3A immunolabeling intensity (Fig 3E). We observed that the intensity of Sema3A+ PNNs was significantly reduced in conditioned mice when compared to control mice (Fig 3E, F; $X^2_2 = 18.42$ (n = 124), $P < 0.001$; average intensity: CTR = 119.42 +- 48.90, conditioned = 84.10 +- 36.61, Student's t-test $t_{122} = 4.5$, $P < 0.001$).

3.4.3 Expression of ch'ase enhances eyeblink learning

Previous data show that the digestion of PNNs in the DCN by ch'ase induces a higher learning performance at the end of the training period in eyeblink conditioned mice (Hirono et al. 2018). Those data suggest that the observed physiological decrease in WFA and Sema3A levels in conditioned mice may play a causal role in the manifestation of the behavior. To study whether robust PNN digestion in the DCN further boosts memory formation in the eyeblink conditioned paradigm, we overexpressed ch'ase in the DCN by means of lentiviral vectors (Bosch et al. 2012; Burnside et al. 2018).

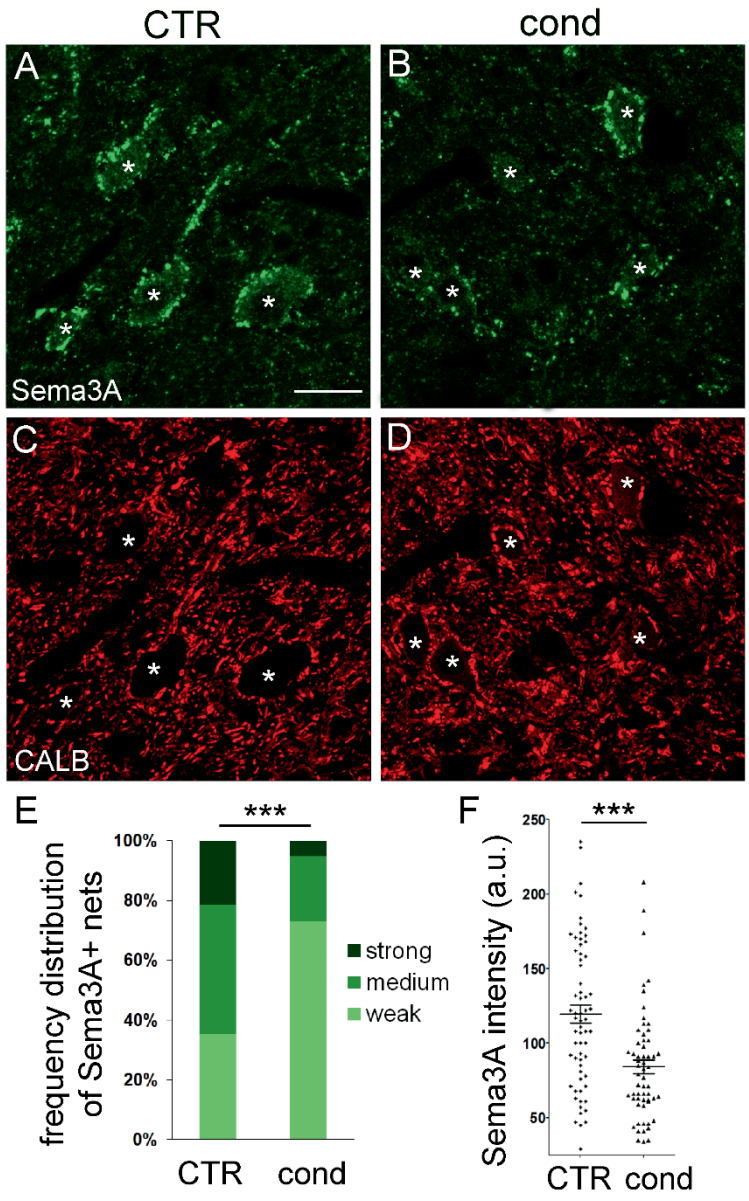

Fig 3. Sema3A staining intensity is reduced during EBC. A and B show Sema3A staining around neurons of the DLH in CTR and cond mice, respectively. Neuronal cell bodies are revealed thanks to the presence of PC terminals (stained by anti-cabindin antibodies) around them (C, D), and are indicated by asterisks (A-D). E shows the frequency distribution of Sema3A+ nets in the DLH of CTR and cond mice. In F, the single Sema3A+ nets are plotted according to their staining intensity (arbitrary units (a.u.)). Scale bar: 30 µm in A (also applies to B-D). Number of animals: CTR, N = 6; cond, N = 5. Number of neurons: CTR, n = 65, cond, n = 59. *** $P < 0.001$

Mice were then subjected mice to daily eyeblink training sessions (Fig 4A). Lentivirus overexpressing GFP (LV-PGK-GFP) has been used as control virus. Strong GFP levels have been detected as early as one week post-injection, and up to 7 weeks after injection. Both DCN neurons and glial cells were transduced, together with glial cells in the white matter and neurons and glial cells in the cerebellar cortex (Fig 4B). Lentivirus overexpressing ch'ase (LV-PGK-ch'ase) virtually completely abolished WFA staining in the injected areas (~95% decrease in WFA staining), encompassing the IntA and DLH (Fig 4C-E), and in some cases affecting also part of the lateral nucleus and medial nucleus, as well as the cerebellar cortex areas close to the DCN. Qualitative observations revealed that the extent of PNN digestion was comparable in animals sacrificed at short (2 weeks after injection) and long (7 weeks after injection) time points.

We asked whether the robust removal of PNNs affected learning performance. We found that mice injected with LV-ch'ase learned significantly better than mice with lentivirus mediated-GFP expression (Fig 4F-H). In particular, both LV-ch'ase and LV-GFP animals showed a significant increase in percentage CR over the course of training, but LV-ch'ase mice learned significantly faster and better (day: $F(4, 34.657) = 46.051$, $P<0.001$; group: $F(1, 35.083) = 6.214$, $P=0.018$; interaction: $F(4, 34.657) = 3.234$, $P=0.023$). This effect was confirmed by a significantly higher %CR at day 5 of acquisition (mean difference (MD) = -21.43, $t(33) = -2.352$, $P=0.025$; Fig 4F). Amplitudes of CRs increased during the training, but were significantly increased in LV-ch'ase mice (day: $F(4, 34.388) = 7.91$, $P<0.001$; group: $F(1, 35.325) = 5.006$, $P=0.032$; interaction: $F(4, 34.388) = 3.721$, $P=0.013$; Fig 4G). Moreover, the average eyelid closure at US onset based on all paired trials was significantly higher for LV-ch'ase mice than for LV-GFP mice (day: $F(4, 34.925) = 30.031$, $P<0.001$; group: $F(1, 35.11) = 5.302$, $P=0.027$; interaction: $F(4, 34.925) = 2.03$, $P=0.112$; Fig 4H). Together, these results indicate that viral mediated ch'ase overexpression in the IntA and DLH accelerates and ameliorates cerebellar-dependent learning.

3.4.4 Removal of PNNs reduces memory retention

A proposed role of PNNs is to facilitate the stabilization of synapses and removal of PNNs has been shown to impair the consolidation of memory (Gogolla et al. 2009; Xue et al. 2014; Banerjee et al. 2017; Thompson et al. 2018). We hypothesized that long-term removal of PNNs would disrupt stabilization of synapses, resulting in decreased memory retention. To test this hypothesis, we compared memory retention over a period of 21 days of LV-ch'ase and LV-GFP mice that showed learning during the acquisition phase (%CR > 33.3%; Fig 5), excluding the mice that did not learn from further analysis as non-learners (Fig 5A; dotted lines). Since we wanted to measure memory retention specifically, sessions were designed to contain 25% of the amount of trials of an acquisition session in order to induce some degree of reacquisition of the learned behavior, which depended on savings (Medina et al. 2001). As a result, mice did not fully unlearn the behavior at the end of the retention period.

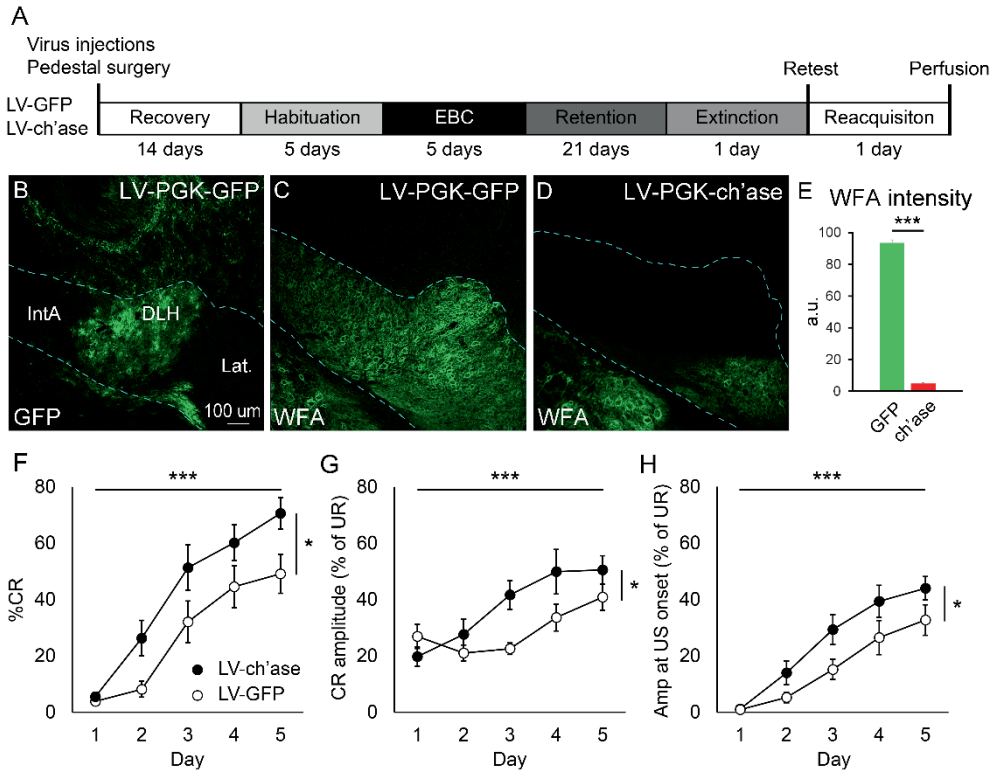

Fig 4. Effect of LV-PGK-GFP and LV-PGK-ch'ase injections in the DCN on EBC performance. (A) Timeline showing experimental design and duration of every phase. Days in between phase are not shown. (B) LV-PGK-GFP efficiently transduces neurons and glial cells in the DCN (dashed line), as well as in the cerebellar cortex. (C-E) The DCN mice are characterized by strong PNNs as visualized by WFA immunolabeling. Ch'ase injections targeted at the IntA effectively removed PNNs (D, E). (F-H) Behavioral performance was calculated as %CR, CR amplitude and amplitude at US onset from paired trials and was compared between LV-GFP and LV-ch'ase mice. For all parameters we found an increase over days, as well as significant difference between groups or an interaction effect. * $P < 0.05$, *** $P < 0.001$. Error bars represent SEM.

The following results should be seen as pilot data and should therefore be interpreted with care, since the number of mice per retention day is variable and in some cases relatively low (see methods for N at each time point). We found that over the course of retention days there was a significant decrease in %CR, as well as a significant interaction effect, indicating that only LV-ch'ase animals showed a significant decrease in performance during the retention phase (retention day: $F(4, 8.488) = 13.608$, $P=0.001$; group: $F(1, 23.106) = 2.735$, $P=0.112$; interaction: $F(4, 8.488) = 22.769$, $P<0.001$; Fig 5A). CR amplitude did not significantly change over the retention days or was different between groups, although the interaction between group and days showed an interesting trend (retention day: $F(4, 74.902) = 1.396$, $P=0.244$; group: $F(1, 58.502) = 0.169$, $P=0.683$; interaction: $F(4, 74.902) = 2.367$,

P=0.06, AR(1) type; Fig 5D). Supporting the reduction in %CR over days, the average amplitude at US onset reduced significantly over retention days and there was a trend towards a difference between groups (retention day: F(4, 76.785) = 4.58, P=0.002; group: F(1, 37.034) = 3.838, P=0.058; interaction: F(4, 76.785) = 1.568, P=0.191, AR(1) type; Fig 5G). These data strongly indicate that consolidation of acquired memory was disrupted after removal of PNNs, which led to less savings and as a result less memory retention over time.

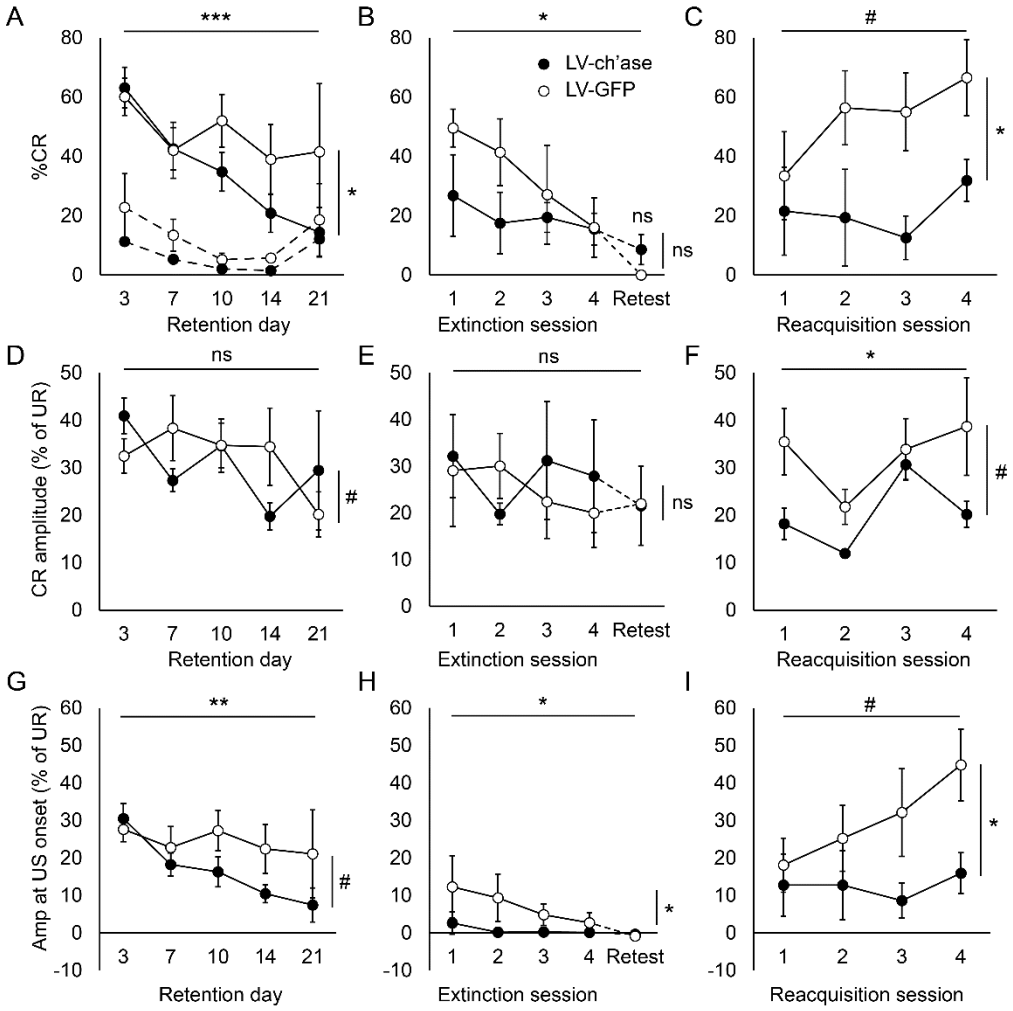

Fig 5. Eyeblink performance of trained LV-ch'ase and LV-GFP during the retention, extinction and reacquisition phase. (A, D, G) Behavioral performance was measured as %CR, CR amplitude and amplitude at US onset of paired trials. We found a significant interaction effect indicating that only LV-ch'ase mice showed a decreased %CR over the retention phase. Mice that did not reach at least 33.3% CR on the last acquisition session were excluded (dotted lines in A). CR amplitude and amplitude at US onset showed a trend towards an interaction effect, but did not reach significance. (B, E, H) Performance for the same three behavioral metrics during the extinction phase for CS only trials. All extinction sessions were given in close succession on the same day. Then, three days after the extinction, a short retest was given to test the effectiveness of the extinction. A significant reduction in both %CR and amplitude at US onset was observed during the extinction, with the addition of an interaction effect for the latter parameter. %CR of the retest was not significantly different from 0, suggesting successful extinction. (C, F, I) To test learning after extinction between groups, mice were subjected to four reacquisition sessions given in close succession on the same day. Results were analyzed from paired trials Significant and near-to-significant increases were measured for all parameters, indicating that learning occurred during the reacquisition phase. Significant interaction effects were seen for %CR and amplitude at US onset, suggesting that LV-GFP mice learned better during reacquisition. # indicates a trend, but no significance, * $P < 0.05$, ** $P < 0.01$, *** $P < 0.001$. Error bars represent SEM.

3.4.5. Removal of PNNs impairs memory reacquisition after extinction

The rate at which memory is reacquired after extinction depends on the strength of previously stabilized synaptic contacts (Medina et al. 2001). We hypothesized that if memory consolidation was impaired after PNN removal as a result of a failure to stabilize synaptic contacts, the rate of relearning during reacquisition would be reduced. To test this hypothesis, we first subjected mice (LV-GFP: N = 3 and LV-ch'ase: N = 4) to an extinction phase during which CS only and US only trials (ratio 11:1) were presented (Fig 5B, E, H). The four extinction sessions each consisted of 55 CS only and 5 US only trials, and they were given directly following each other on the same day. We then analyzed the eyelid responses on CS only trials as a metric of performance. We found a significant decrease in %CR over sessions (session: $F(4, 23.285) = 3.798$, $P=0.016$; group: $F(1, 8.676) = 1.029$, $P=0.338$; interaction: $F(4, 23.285) = 1.198$, $P=0.338$, AR(1) type; Fig 5B). The amplitude at US onset also showed a significant decrease over sessions in addition to a difference between groups (extinction session: $F(4, 8.764) = 5.192$, $P=0.02$; group: $F(1, 17.442) = 10.197$, $P=0.005$; interaction: $F(4, 8.764) = 3.086$, $P=0.076$, diagonal type; Fig 5H). CR amplitude did not show any change over sessions or between groups (extinction session: $F(4, 22.219) = 0.346$, $P=0.844$; group: $F(1, 9.542) = 0.008$, $P=0.931$; interaction: $F(4, 22.219) = 1.483$, $P=0.241$, AR(1) type; Fig 5E). To confirm that mice had delearned after extinction we tested performance on CS only trials three days later, showing that %CR of all LV-GFP mice was 0 and %CR was not different from 0 of LV-ch'ase mice ($t(3) = 1.686$, $P=0.19$, one-sample t-test). Based on these results we conclude that all mice had delearned.

Subsequent to the retest mice were given four short training sessions (25% of an acquisition training) to measure how quickly they relearned (Fig 5C, F, I). Over those sessions we found a significant interaction between group and sessions and a trend over sessions (session: $F(3, 2.342) = 13.825$, $P=0.05$; group: $F(1, 6.028) = 1.425$, $P=0.277$; interaction: $F(3, 2.342) = 16.579$, $P=0.041$; Fig 5C). CR amplitude changed significantly over the sessions, and showed a trend

for a group and interaction effect (reacquisition session: F(3,13.719) = 13.326, P<0.001; group: F(1,6.471) = 127.158, P=0.056; interaction: F(3,13.719) = 3.175, P=0.058, AR(1) type; Fig 5F). The amplitude at US onset showed a significant interaction-effect and a trend towards an increase over sessions (reacquisition session: F(3,19.874) = 2.675, P=0.075; group: F(1,7.14) = 2.749, P=0.14; interaction: F(3,19.874) = 3.161, P=0.047, AR(1) type; Fig 5I). These preliminary data indeed suggest that removal of PNNs result in reduced consolidation of the memory trace, which prevented mice from showing quick relearning after extinction.

3.4.6 Removal of PNNs leads to an increased number of PC terminals and decreased number of glutamatergic terminals on DCN neurons

To investigate whether ch'ase affects DCN neuronal connectivity, we examined morphological changes of GABAergic and glutamatergic terminals. There are two types of GABAergic afferents in the DCN, namely from PCs and from local inhibitory interneurons (Uusisaari and Knöpfel 2008), accounting for 85% and 15% of the GABAergic input on the DCN, respectively (De Zeeuw and Berrebi 1995). Interestingly, it has been shown that ch'ase injection in the cerebellar cortex induces sprouting of PC axon collaterals (Corvetti and Rossi 2005). To visualize GABAergic terminals in the DCN we used anti-vGAT and anti-gephyrin antibodies, which stain GABA pre-synaptic and post-synaptic elements, respectively (Fig 6). To visualize glutamatergic terminals, we used anti-VGLUT1 and anti-VGLUT2 antibodies. Mossy fibre terminals express VGLUT1 or VGLUT2 or both. Climbing fibre terminals express VGLUT2 (Hioki et al. 2003).

Four weeks following LV-ch'ase injections, VGAT+ terminals in the IntA, including PC terminals (revealed by calbindin-immunopositivity), appeared more numerous around DCN neurons (Fig 6A-K). Indeed, the number of gaps between VGAT+ synaptic boutons was strongly decreased when compared to LV-GFP-injected mice (GFP: 161.29+- 6.24 sem gaps/mm neuronal membrane; n = 52 neurons; ch'ase: 86.24 +- 7.33 sem, n = 33 neurons; Student's t-test $t_{83} = 7.0$, $P < 0.001$) (Fig 6K). Increased GABAergic input on ch'ase-treated DCN neurons has been confirmed by evaluating the number of gephyrin+ puncta around DCN neuronal somata. More numerous gephyrin+ puncta were found in ch'ase mice with respect to GFP-mice (GFP: 0.88 +- 0.02 sem puncta/um neuronal membrane, n = 26 neurons; ch'ase: 1.00 +- 0.03 sem, n = 23 neurons; Student's t-test $t_{47} = 3.69$, $P < 0.001$) (Fig 6L-P).

Interestingly, an opposite effect of ch'ase on glutamatergic terminals has been observed. Four weeks following LV-ch'ase injection, we found that the number of VGLUT1+ terminals was reduced (GFP: 35170.61 +- 1008.04 sem terminals/mm^2; ch'ase: 29786.38 +- 1114.02 sem; Student's t-test $t_7 = 3.58$, $P < 0.01$), while the number of VGLUT2+ terminals was unaffected (GFP: 28569.69 +- 1263.90 sem terminals/mm^2; ch'ase: 28511.12 +- 932.87 sem; Student's t-test $t_7 = 0.03$, $P = 0.97$) (Fig 7).

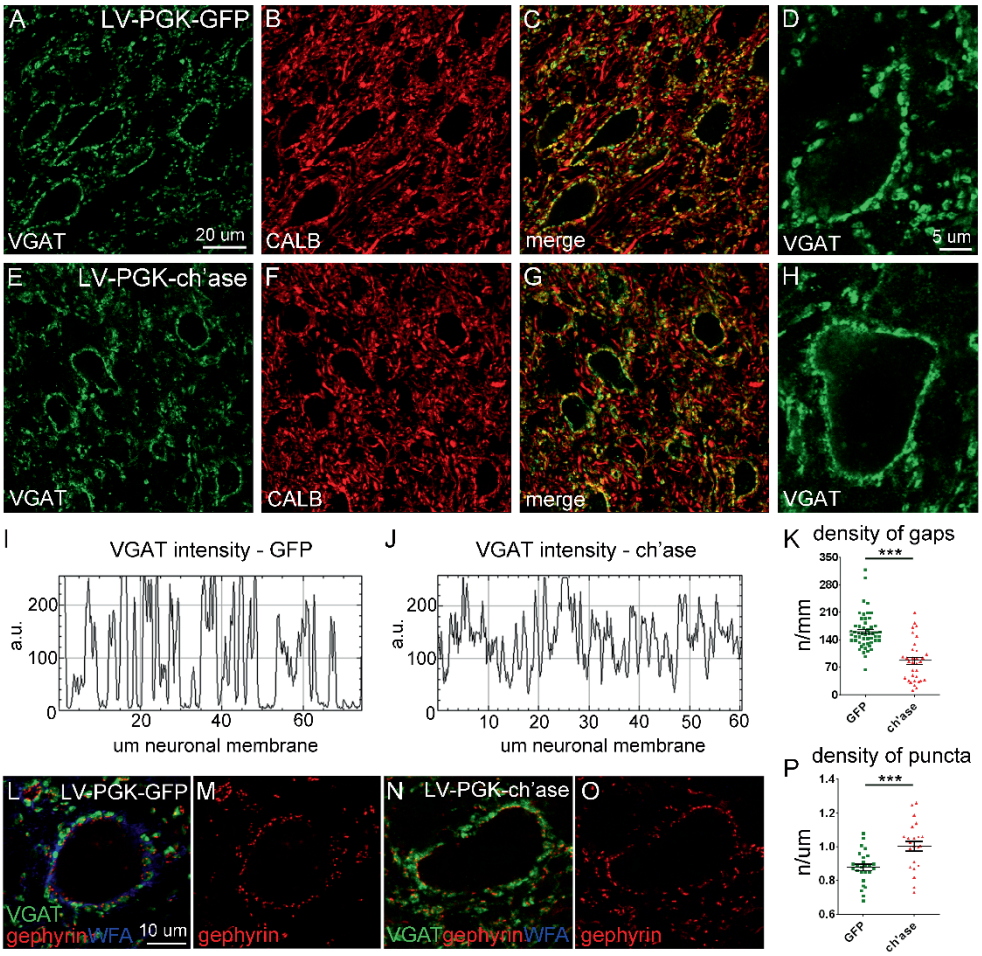

Fig 6. Effect of ch'ase on inhibitory projections in DCN. (A-H) Immunolabeling in the IntA for VGAT and calbindin (CALB), markers of inhibitory boutons and PCs, respectively. Co-expression of these fluorescent markers allowed for identification of discrete synaptic terminals belonging to PCs around individual IntA neurons in LV-PGK-GFP and LV-PGK-ch'ase mice. (I, J) Plots showing intensity of VGAT fluorescence along the neuronal membrane of IntA neurons in LV-PGK-GFP and LV-PGK-ch'ase mice (see D and H for exemplifying pictures). High values indicate VGAT-positive structures and dips indicate space between terminals (gaps). Quantification of gap density revealed that VGAT+ structures were more abundant after ch'ase treatment (K). For further quantification of the number of GABAergic synapses a combination of VGAT and gephyrin immunolabeling was used (L-O). Quantification of gephyrin-positive puncta revealed an increase in GABAergic synapses after ch'ase. Error bars represent SEM. *** $P < 0.001$

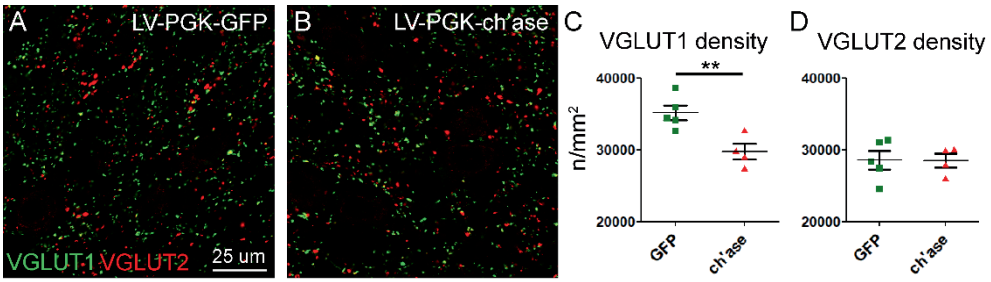

Fig 7. Effect of ch'ase on excitatory projections in DCN. A and B show immunolabeling of VGLUT1 and VGLUT2-positive terminals in the IntA in LV-PGK-GFP (N=5; A) and LV-PGK-ch'ase (N=4; B) injected mice. (C, D) Quantification of these puncta revealed that the VGLUT1 density was reduced after ch'ase, whereas VGLUT2 density remained unchanged. Error bars represent SEM ** P < 0.01

3.4.7 Removal of PNNs leads to altered spike activity of DCN neurons in awake behaving mice

A recent *in vitro* study has reported an increased frequency of inhibitory postsynaptic potentials (IPSPs) in DCN neurons after ch'ase, indicating that PNN removal enhances GABAergic transmission in the DCN (Hirono et al. 2018). Based on those data and our observed changes in synaptic terminals of PCs after ch'ase, we hypothesized that DCN neurons would show altered spike properties *in vivo* after PNN removal. To test this hypothesis, we made extracellular single unit recordings targeted at the IntA and DLH in awake behaving animals during EBC (Fig 8A, B). Mice injected with LV- GFP or LV-ch'ase were trained for two days to be able to identify task-related CS-encoding neurons, after which their neuronal spike properties were compared (Fig 9). In contrast to our previous results, on average LV-GFP injected mice (N=6) showed a higher eyeblink performance on day 2 of training and during the experimental recordings than LV-ch'ase mice (N=5) (Fig 8C-E). Percentage CR was significantly higher during both sessions (training 2: U = 0, P=0.004, MWU test; Exp: t(8) = 5.650, P<0.001, independent t-test; Fig 8C), CR amplitude was higher on training 2 (training 2: t(4.018) = -4.988, P=0.007, independent t-test; Exp: U = 6, P=0.222, MWU test; Fig 8D) and the amplitude at US onset was higher during the experiment (training 2: t(9) = 1.973, P=0.08; Exp: t(4.788) = 3.520, P=0.018, independent t-test; Fig 8E).

Extracellular DCN recordings were obtained from LV-GFP (n=35 cells) and LV-ch'ase (n=38 cells) mice (Fig 8A). Cells recorded in hemispheres where PNNs were not fully digested were excluded. Neuronal responses to paired CS-US presentation were classified in order to identify task-related activity. In line with published studies we found both neurons that increased and neurons that decreased their spike frequency during the CS-US period (Fig 9B, B'), representing spike *facilitation* and spike *suppression* cells, respectively (Berthier and Moore 1990; Ten Brinke et al. 2017). In LV-ch'ase mice 8 cells (21.1%) showed facilitation responses and 30 cells (78.9%) showed no response. In LV-GFP mice 18 cells (51.4%) showed

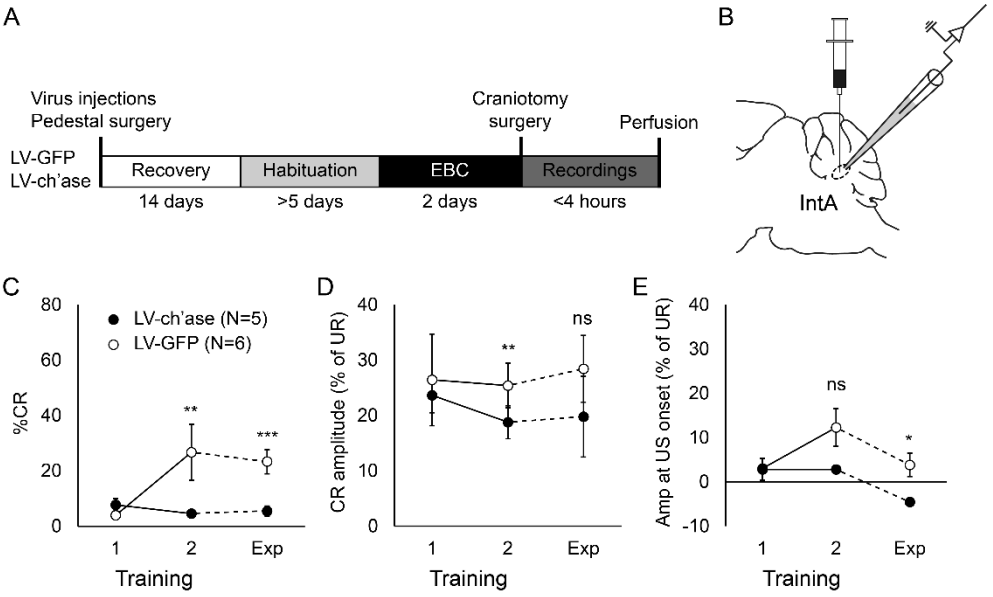

Fig 8. Virus injections for electrophysiology and behavioural performance. (A, B) Mice were stereotaxically injected in the IntA with LV-GFP or LV-ch'ase and received a pedestal. After two weeks of recovery a short EBC training was given. Subsequent to the second EBC training, a craniotomy surgery was performed and after at least 2 hours of recovery, a session of <4 hours of *in vivo* awake extracellular recordings was performed targeted at neurons in the IntA and DLH (B). (C, D, E) Behavior during the two trainings and during the recording session ('Exp'). In contrast to our previous results, LV-GFP animals showed improved performance on day 2, whereas LV-ch'ase animals did not. Error bars represent SEM. * P < 0.05, ** P < 0.01, *** P < 0.001

spike facilitation, 5 cells (14.3%) showed spike suppression, 11 cells (31.4%) showed no response and 1 cell (2.9%) showed both facilitation and suppression responses. The higher proportion of CS-responding cells in LV-GFP are in agreement with the higher eyeblink performance during the experiment in these animals (Fig 8C-E). Spontaneous spike activity during quiet wakefulness prior to the presentation of stimuli of all recorded cells was compared between groups (Fig 9C-E), showing that the firing frequency in LV-ch'ase mice was significantly lower (LV-GFP: 53.8 ± 31.4 Hz; LV-ch'ase: 35.6 ± 31.3 Hz; U = 465, P=0.027, MWU-test; Fig 9C). No difference in CV (LV-GFP: 0.58 ± 0.25; LV-ch'ase: 0.8 ± 0.6; U = 730, P=0.343, MWU-test; Fig 9D) or CV_2 values (LV-GFP: 0.5 ± 0.14; LV-ch'ase: 0.54 ± 0.21; t(64.86) = -0.821, P=0.415, independent t-test; Fig 9E) was found between groups. Then we compared the same metrics between groups, but only for CS-responding cells (*i.e.* all except 'no response' cells; Fig 9F-H). The significant decrease in firing frequency was maintained or even stronger (LV-GFP: 55.5 ± 28.3 Hz; LV-ch'ase: 22.7 ± 22.2 Hz; t(30) = 2.971, P=0.006; Fig 9F) and we found a trend towards an increased CV value (LV-GFP: 0.52 ± 0.15; LV-ch'ase: 0.77 ± 0.29; t(8.268) = -2.274, P=0.052; Fig 9G), although this did not reach significance. The CV_2 value remained comparable between groups (LV-GFP: 0.49 ± 0.12; LV-ch'ase: 0.58 ± 0.18; t(30) = -1.651, P=0.109; Fig 9H).

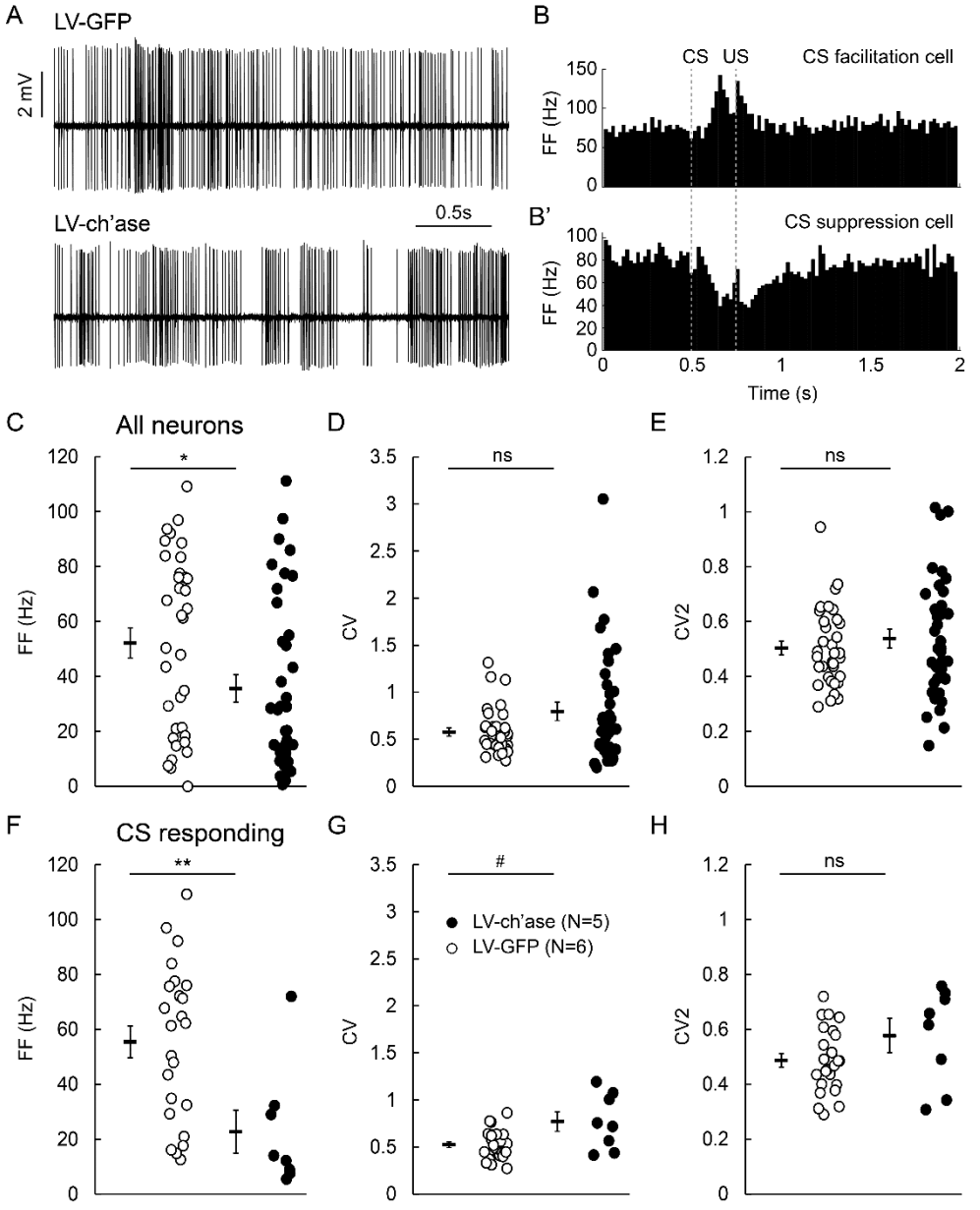
A
LV-GFP
2 mV
LV-ch'ase
0.5s
B
CS US
CS facilitation cell
FF (Hz)
B'
CS suppression cell
Time (s)
C
All neurons
*
FF (Hz)
D
ns
CV
E
ns
CV2
F
CS responding
**
FF (Hz)
G
#
LV-ch'ase (N=5)
LV-GFP (N=6)
CV
H
ns
CV2

Fig 9. Spontaneous spike activity of IntA and DLH neurons after PNN digestion. (A) Representative traces of cells in awake behaving LV-GFP (upper trace) and LV-ch'ase mice (lower trace). (B, B') Cells were characterized based on changes in firing frequency (FF) during the period between CS and US presentation (between grey dotted lines). Compare baseline FF (0-0.5 sec) to FF between dotted lines (CS-US period): CS facilitation cells show increases in FF (B) whereas CS suppression cells show reductions in FF (B'). Note that both cells also show responses after the US. (C-E) Comparison of all recorded neurons in LV-GFP and LV-ch'ase neurons revealed a significantly reduced FF in LV-ch'ase mice (C), whereas CV and CV_2 values were comparable (D, E). When comparing the FF of CS-responding neurons, the difference in FF remained (F). In addition, we found a trend in CV value where spike activity in LV-ch'ase tends to be more irregular (G), although CV_2 values remained similar. Error bars represent SEM. # indicates a trend, but no significance, * $P < 0.05$, ** $P < 0.01$

In summary, these results indicate that ch'ase-mediated PNN digestion leads to changes in spike activity of IntA and DLH neurons involved in EBC, *i.e.* a lower spontaneous spike frequency and possibly an elevated spike irregularity, in awake mice in quiet wakefulness.

3.5 Discussion

In the present study we have investigated the relationship between PNNs in the DCN and Pavlovian EBC, a type of cerebellar-dependent associative learning that strongly depends on both cerebellar cortex and DCN function (Bracha et al. 1994; Freeman et al. 1995; Attwell et al. 2001; Freeman and Steinmetz 2011; Heiney et al. 2014). We found that conditioned mice showed reduced PNNs compared to controls or mice that were pseudo-conditioned after five days of training. This reduction was most prominent in the IntA and DLH, areas that have been shown to be involved in EBC (Clark et al. 1992; Krupa et al. 1993; Krupa and Thompson 1997; Freeman et al. 2005; Freeman and Steinmetz 2011). PNN reductions in the DLH coincided with a reduced presence of Sema3A, a PNN component known to be dynamically expressed during plasticity (Foscarin et al. 2011; Carulli et al. 2013).

In addition, when we enzymatically degraded PNNs by virally expressing ch'ase in the DCN we observed a pronounced acceleration of learning. A recent report has described comparable findings (Hirono et al. 2018) and both this report and our findings suggest that removal of PNNs allows for enhanced plasticity in the DCN leading to accelerated learning. Over the course of memory retention sessions lasting up to 21 days during which mice were intermittently retrained using short training protocols, we observed that mice with digested PNNs showed memory decline. We propose that in these mice synaptic contacts formed during the acquisition phase have not been stabilized and that the memory trace has not been consolidated due to the absence of PNNs. In line with this idea, we found that after extinction sessions after which all learned behavior was abolished, mice with intact PNNs relearned faster than mice with digested PNNs. Relearning on such short timespan has been proposed to rely largely on savings (Medina et al. 2001) and presumably the previously formed and stabilized synapses facilitated this process. At a cellular level ch'ase was shown

to result in a decrease in the density of VGLUT1+ terminals. VGLUT1 mRNA is strongly expressed in pontine neurons (Allen Brain Atlas) which relay the CS to the cerebellum (Gould et al. 1993; Freeman and Steinmetz 2011), thus mossy fiber terminals involved in EBC likely express VGLUT1+. EBC is accompanied by increased sprouting of pontine mossy fibers (Boele et al. 2013) and increased number of VGLUT1+ boutons (see **Chapter 2**). The observed reduction in VGLUT1+ terminals 4 weeks after LV-ch'ase injection may explain the inability of ch'ase-treated mice to retain EBC memory. In addition, ch'ase induces an increase in the number of PC terminals, possibly as a result of reduced Sema3A content, since this has been shown to correlate with the number of PC synapses (Carulli et al. 2013).

The consequences of ch'ase treatment on the stability of synaptic terminals have been previously assessed in other brain regions. An increased number of GABAergic terminals has been found in the hippocampus and the visual cortex following ch'ase (Donato et al. 2013; Lensjø et al. 2017). In contrast, ch'ase induces a decrease in the number of parvalbumin+ inputs in the prefrontal cortex (Sullivan et al. 2018) and a reduction in glutamatergic inputs in the medial entorhinal cortex (Lensjø et al. 2017). Altogether, those data point to differential effects of ch'ase in distinct brain areas, which may depend on the specific properties of the neuronal sub-populations and the organization of the neuronal network.

We found that PNN removal also alters the spike properties of DCN neurons in awake behaving mice. DCN neurons showed lower spontaneous firing frequencies and increased spike irregularity, a likely consequence of increased PC innervation since these cells form the main type of inhibitory input to DCN neurons (Telgkamp and Raman 2002; Pedroarena and Schwartz 2003). This would support earlier *in vitro* findings advocating for increased GABAergic transmission in the DCN after PNN depletion (Hirono et al. 2018). However, part of this effect could have been caused by a decreased density of excitatory VGLUT1-positive terminals, although the density of PC terminals onto DCN neurons is far higher (Chan-Palay 1977; Palkovits et al. 1977; De Zeeuw and Berrebi 1995). The effects of PNN digestion on other types of cerebellar behavior such as locomotion remain elusive.

The finding that learning can be facilitated by enhancing plasticity mechanisms directly at the level of the DCN is remarkable, because long-term depression (LTD) at the parallel fiber to PC synapse has been generally put forward as primary mediator for eyeblink learning (Medina et al. 2000; Yamazaki and Tanaka 2009). Many lesion studies have shown that learning does not take place after inactivation of the cerebellar cortex (Yeo et al. 1985b; Perrett et al. 1993; Garcia et al. 1999). However, targeted lesions of the cerebellar cortex after learning does not completely abolish CS-evoked eyelid movements but primarily affects their timing (McCormick and Thompson 1984a; Ohyama et al. 2006), suggesting that plasticity in the DCN does play a role during eyeblink learning. It has been hypothesized that during the initial stages of learning plasticity in the cerebellar cortex is particularly important, whereas during later stages of learning the memory trace shifts towards the

DCN (Doyon et al. 2002; Shutoh et al. 2006). Since the evidence comes from both vestibulo-ocular reflex adaptation and motor sequence learning, it seems reasonable to extrapolate this hypothesis to EBC. To fully dissect the contribution of cerebellar cortex versus nuclei plasticity, both high spatial and temporal specificity has to be achieved by combining cell-specific transgenic approaches with DREADDs or optogenetics tools. This is however beyond the scope of this study.

An interesting observation in this study is that mice that were injected with LV-GFP or LV-ch'ase for the electrophysiology experiments (Exp. 3) showed learning rates that contrasted with our earlier findings (Exp. 2), that is, LV-GFP mice learned better. The low number of animals per group (LV-ch'ase: N = 5 and LV-GFP: N = 6) may have allowed for individual differences to contribute to the unanticipated effect. Moreover, the effect is based on a short training period (two days) and the direction of the effect could potentially have changed over the course of additional training days. Since considerably more mice were used to test for the behavioral effect of PNN digestion in Exp. 2 (LV-ch'ase: N = 17 and LV-GFP: N = 19) and supporting findings have been published (Hirono et al. 2018) we do not see the obligation to reconsider our conclusions from Exp. 2. The low amount of learning in LV-ch'ase mice did however simultaneously lower the number of CS-responding IntA/DLH neurons that could be identified in these mice, since spiking activity in these neurons is correlated with the amplitude of CRs (Ten Brinke et al. 2017). Despite this, we obtained sufficient neurons to localize our *in vivo* physiology findings to task-related DCN neurons.

One could argue that a potential caveat of this study is the nature of the control virus used in Exp. 2 and 3 (LV-PGK-GFP). The virally expressed ch'ase protein was secreted by neurons after synthesis, and digested CSPGs in the extracellular space, whereas the GFP was not secreted. Overexpression of GFP can influence cell physiology and can eventually be toxic (Ansari et al. 2016), which, although highly unlikely, could have biased our results. A better control condition would therefore be to use an inactive variant of ch'ase that is excreted in a similar way as the active protein. This virus was unfortunately not available to us at that time. Another important consideration is the low number of animals that was measured for part of the retention, extinction and reacquisition phases. In order to corroborate our findings we will complement our data with newly tested mice. These experiments are currently in progress and will contribute to the quality of the study.

This study raises several questions that are important for our understanding of the mechanisms by which PNN digestion facilitates cerebellar learning and memory. We have studied changes in PNNs during five days of daily EBC trainings, which could be considered the initial phase of this learning paradigm. Studies often use training protocols consisting of ten (or more) days and our own unpublished results show that it is particularly the CR amplitude that increases after the first five days. Recently obtained pilot data show that PNNs are indistinguishable from control conditions after ten days of trainings, which suggests that the changes in PNNs are transient and an intact PNN is essential for stabilization of newly formed synapses. In this regard, it would be highly interesting to see

whether the combination of a short-lasting removal of PNNs at the beginning of training and PNN re-formation at the end of training would result in an overall better learning rate and memory retention. Neither this study, nor the study by Hirono and colleagues are able to show evidence for this, since both LV-PGK-ch'ase and ch'ase ABC lyase are active for at least ten days after injection (Lin et al. 2007). Finally, an important question that follows from this study is which PNN molecules are responsible for the observed effects. We showed that Sema3A, a potential chemorepulsive candidate in this respect (Carulli et al. 2013; de Winter et al. 2016), was reduced after five days of training. However to exactly determine whether a reduced Sema3A content is sufficient for learning facilitation, experiments have to be conducted where Sema3A content is reduced while other PNN components remain unchanged. One way to do this experimentally is to interfere with binding sites of Sema3A in PNNs (Vo et al. 2013; Dick et al. 2013). Using adeno-associated vectors overexpressing an inactive form of the Sema3A receptor neuropilin-1 (AAV8-CMV-NP1-Y297A) with adeno-associated vectors overexpressing GFP (AAV8-CMV-GFP) as control virus, our labs have started experiments to tackle exactly this question.

3.6 Acknowledgements

We are grateful to the following people for their technical contribution: J.W. Potters, H.J. Boele, S.K.E. Koekkoek, Z. Gao, M.M Ten Brinke, J.K. Spanke A.C.H.G. IJpelaar. We furthermore thank B. Winkelman, A. Court, C. Geelen, M. Mešković, G. Özel, M. Bouw, S.O. Stokman for their contribution to this study.

3.7 References

Ansari AM, Ahmed AK, Matsangos AE, et al (2016) Cellular GFP Toxicity and Immunogenicity: Potential Confounders in in Vivo Cell Tracking Experiments. Stem Cell Rev Rep 12:553–559. doi: 10.1007/s12015-016-9670-8

Attwell PJE, Rahman S, Yeo CH (2001) Acquisition of Eyeblink Conditioning Is Critically Dependent on Normal Function in Cerebellar Cortical Lobule HVI. J Neurosci 21:5715–5722. doi: 10.1523/JNEUROSCI.21-15-05715.2001

Banerjee SB, Gutzeit VA, Baman J, et al (2017) Perineuronal Nets in the Adult Sensory Cortex Are Necessary for Fear Learning. Neuron 95:1–11. doi: 10.1016/j.neuron.2017.06.007

Bao S, Chen L, Thompson RF (2000) Learning- and cerebellum-dependent neuronal activity in the lateral pontine nucleus. Behav Neurosci 114:254–261. doi: 10.1037//0735-7044.114.2.254

Berthier NE, Moore JW (1990) Activity of deep cerebellar nuclear cells during classical conditioning of nictitating membrane extension in rabbits. Exp Brain Res 83:44–54

Beurdeley M, Spatazza J, Lee HHC, et al (2012) Otx2 Binding to Perineuronal Nets Persistently Regulates Plasticity in the Mature Visual Cortex. J Neurosci 32:9429–9437. doi: 10.1523/JNEUROSCI.0394-12.2012

Boele H-J, Koekkoek SKE, De Zeeuw CI, Ruigrok TJH (2013) Axonal Sprouting and Formation of Terminals in the Adult Cerebellum during Associative Motor Learning. J Neurosci 33:17897–17907. doi: 10.1523/JNEUROSCI.0511-13.2013

Bosch KD, Bradbury EJ, Verhaagen J, et al (2012) Chondroitinase ABC promotes plasticity of spinal reflexes following peripheral nerve injury. Exp Neurol 238:64–78. doi: 10.1016/j.expneurol.2012.08.003

Bracha V, Webster ML, Winters NK, et al (1994) Effects of muscimol inactivation of the cerebellar interposed-dentate nuclear complex on the performance of the nictitating membrane response in the rabbit. Exp Brain Res 100:453–468

Burnside ER, De Winter F, Didangelos A, et al (2018) Immune-evasive gene switch enables regulated delivery of chondroitinase after spinal cord injury. Brain 141:2362–2381. doi: 10.1093/brain/awy158

Canto CB, Broersen R, De Zeeuw CI (2018) Intrinsic excitement in cerebellar nuclei neurons during learning. PNAS 115:9824–9826

Carmichael ST, Archibeque I, Luke L, et al (2005) Growth-associated gene expression after stroke: evidence for a growth-promoting region in peri-infarct cortex. Exp Neurol 193:291–311. doi: 10.1016/j.expneurol.2005.01.004

Carulli D, Foscarin S, Faralli A, et al (2013) Modulation of semaphorin3A in perineuronal nets during structural plasticity in the adult cerebellum. Mol Cell Neurosci 57:10–22. doi: 10.1016/j.mcn.2013.08.003

Carulli D, Pizzorusso T, Kwok JCF, et al (2010) Animals lacking link protein have attenuated perineuronal nets and persistent plasticity. Brain 133:2331–2347. doi: 10.1093/brain/awq145

Chan-Palay V (1977) Cerebellar dentate nucleus. Organization, cytologyand transmitters. Springer Berl 126:275–280

Clark RE, Lavond DG, Zhang AA (1992) Reversible lesions of the cerebellar interpositus nucleus during acquisition and retention of a classically conditioned behavior. Behav Neurosci 106:879–888

Corvetti L, Rossi F (2005) Degradation of Chondroitin Sulfate Proteoglycans Induces Sprouting of Intact Purkinje Axons in the Cerebellum of the Adult Rat. J Neurosci 25:7150–7158. doi: 10.1523/JNEUROSCI.0683-05.2005

de Winter F, Kwok JCF, Fawcett JW, et al (2016) The Chemorepulsive Protein Semaphorin 3A and Perineuronal Net-Mediated Plasticity. Neural Plast 2016:1–14. doi: 10.1155/2016/3679545

De Zeeuw CI, Berrebi AS (1995) Postsynaptic Targets of Purkinje Cell Terminals in the Cerebellar and Vestibular Nuclei of the Rat. Eur J Neurosci 7:2322–2333. doi: 10.1111/j.1460-9568.1995.tb00653.x

Déglon N, Tseng JL, Bensadoun J-C, et al (2000) Self-Inactivating Lentiviral Vectors with Enhanced Transgene Expression as Potential Gene Transfer System in Parkinson's Disease. Hum Gene Ther 11:179–190. doi: 10.1089/10430340050016256

Dick G, Tan CL, Alves JN, et al (2013) Semaphorin 3A Binds to the Perineuronal Nets via Chondroitin Sulfate Type E Motifs in Rodent Brains. J Biol Chem 288:27384–27395. doi: 10.1074/jbc.M111.310029

Donato F, Rompani SB, Caroni P (2013) Parvalbumin-expressing basket-cell network plasticity induced by experience regulates adult learning. Nature 504:272–276. doi: 10.1038/nature12866

Doyon J, Song AW, Karni A, et al (2002) Experience-dependent changes in cerebellar contributions to motor sequence learning. Proc Natl Acad Sci 99:1017–1022

Dull T, Zufferey R, Kelly M, et al (1998) A Third-Generation Lentivirus Vector with a Conditional Packaging System. J Virol 72:9

Faralli A, Dagna F, Albera A, et al (2015) Modifications of perineuronal nets and remodelling of excitatory and inhibitory afferents during vestibular compensation in the adult mouse. Brain Struct Funct 221:3193–3209. doi: 10.1007/s00429-015-1095-7

Foscarin S, Ponchione D, Pajaj E, et al (2011) Experience-Dependent Plasticity and Modulation of Growth Regulatory Molecules at Central Synapses. PLoS ONE 6:e16666. doi: 10.1371/journal.pone.0016666

Freeman JH, Carter CS, Stanton ME (1995) Early cerebellar lesions impair eyeblink conditioning in developing rats: differential effects of unilateral lesions on postnatal day 10 or 20. Behav Neurosci 109:893

Freeman JH, Halverson HE, Poremba A (2005) Differential Effects of Cerebellar Inactivation on Eyeblink Conditioned Excitation and Inhibition. J Neurosci 25:889–895. doi: 10.1523/JNEUROSCI.4534-04.2005

Freeman JH, Rabinak CA (2004) Eyeblink conditioning in rats using pontine stimulation as a conditioned stimulus. Integr Physiol Behav Sci 39:180–191

Freeman JH, Steinmetz AB (2011) Neural circuitry and plasticity mechanisms underlying delay eyeblink conditioning. Learn Mem 18:666–677. doi: 10.1101/lm.2023011

Frischknecht R, Heine M, Perrais D, et al (2009) Brain extracellular matrix affects AMPA receptor lateral mobility and short-term synaptic plasticity. Nat Neurosci 12:897–904. doi: 10.1038/nn.2338

Galtrey CM, Asher RA, Nothias F, Fawcett JW (2007) Promoting plasticity in the spinal cord with chondroitinase improves functional recovery after peripheral nerve repair. Brain 130:926–939. doi: 10.1093/brain/awl372

Gao Z, van Beugen BJ, De Zeeuw CI (2012) Distributed synergistic plasticity and cerebellar learning. Nat Rev Neurosci 13:619–635. doi: 10.1038/nrn3312

Garcia KS, Steele PM, Mauk MD (1999) Cerebellar cortex lesions prevent acquisition of conditioned eyelid responses. J Neurosci 19:10940–10947

Gogolla N, Caroni P, Lüthi A, Herry C (2009) Perineuronal nets protect fear memories from erasure. Science 325:1258–1261

Gould TJ, Sears LL, Steinmetz JE (1993) Possible CS and US pathways for rabbit classical eyelid conditioning: electrophysiological evidence for projections from the pontine nuclei and inferior olive to cerebellar cortex and nuclei. Behav Neural Biol 60:172–185

Härtig W, Brauer K, Brückner G (1992) Wisteria floribunda agglutinin-labelled nets surround parvalbumin-containing neurons. NeuroReport 3:869–872

Heiney SA, Wohl MP, Chettih SN, et al (2014) Cerebellar-Dependent Expression of Motor Learning during Eyeblink Conditioning in Head-Fixed Mice. J Neurosci 34:14845–14853. doi: 10.1523/JNEUROSCI.2820-14.2014

Hioki H, Fujiyama F, Taki K, et al (2003) Differential distribution of vesicular glutamate transporters in the rat cerebellar cortex. Neuroscience 117:1–6. doi: 10.1016/S0306-4522(02)00943-0

Hirono M, Watanabe S, Karube F, et al (2018) Perineuronal Nets in the Deep Cerebellar Nuclei Regulate GABAergic Transmission and Delay Eyeblink Conditioning. J Neurosci 38:6130–6144. doi: 10.1523/JNEUROSCI.3238-17.2018

Jirenhed D-A, Bengtsson F, Hesslow G (2007) Acquisition, Extinction, and Reacquisition of a Cerebellar Cortical Memory Trace. J Neurosci 27:2493–2502. doi: 10.1523/JNEUROSCI.4202-06.2007

Kleim JA, Freeman JH, Bruneau R, et al (2002) Synapse formation is associated with memory storage in the cerebellum. Proc Natl Acad Sci 99:13228–13231

Koekkoek SKE, Den Ouden WL, Perry G, et al (2002) Monitoring kinetic and frequency-domain properties of eyelid responses in mice with magnetic distance measurement technique. J Neurophysiol 88:2124–2133

Krupa D, Thompson J, Thompson RF (1993) Localization of a memory trace in the mammalian brain. Science 260:989–991. doi: 10.1126/science.8493536

Krupa DJ, Thompson RF (1997) Reversible inactivation of the cerebellar interpositus nucleus completely prevents acquisition of the classically conditioned eye-blink response. Learn Mem 3:545–556. doi: 10.1101/lm.3.6.545

Kwok JCF, Dick G, Wang D, Fawcett JW (2011) Extracellular matrix and perineuronal nets in CNS repair. Dev Neurobiol 71:1073–1089. doi: 10.1002/dneu.20974

Lavond DG, Steinmetz JE (1989) Acquisition of classical conditioning without cerebellar cortex. Behav Brain Res 33:113–164

Lee HHC, Bernard C, Ye Z, et al (2017) Genetic Otx2 mis-localization delays critical period plasticity across brain regions. Mol Psychiatry 22:680–688. doi: 10.1038/mp.2017.1

Lensjø KK, Christensen AC, Tennøe S, et al (2017) Differential Expression and Cell-Type Specificity of Perineuronal Nets in Hippocampus, Medial Entorhinal Cortex, and Visual Cortex Examined in the Rat and Mouse. eneuro 4:ENEURO.0379-16.2017. doi: 10.1523/ENEURO.0379-16.2017

Lin R, Kwok JCF, Crespo D, Fawcett JW (2007) Chondroitinase ABC has a long-lasting effect on chondroitin sulphate glycosaminoglycan content in the injured rat brain. J Neurochem 0:071116233414006-??? doi: 10.1111/j.1471-4159.2007.05066.x

Massey JM, Hubscher CH, Wagoner MR, et al (2006) Chondroitinase ABC Digestion of the Perineuronal Net Promotes Functional Collateral Sprouting in the Cuneate Nucleus after Cervical Spinal Cord Injury. J Neurosci 26:4406–4414. doi: 10.1523/JNEUROSCI.5467-05.2006

McCormick DA, Thompson RF (1984a) Cerebellum: Essential involvement in the classically conditioned eyelid response. Science 223:296–299

McCormick DA, Thompson RF (1984b) Neuronal responses of the rabbit cerebellum during acquisition and performance of a classically conditioned nictitating membrane-eyelid response. J Neurosci 4:2811–2822

Medina JF, Garcia KS, Mauk MD (2001) A Mechanism for Savings in the Cerebellum. J Neurosci 21:4081–4089. doi: 10.1523/JNEUROSCI.21-11-04081.2001

Medina JF, Nores WL, Ohyama T, Mauk MD (2000) Mechanisms of cerebellar learning suggested by eyelid conditioning. Curr Opin Neurobiol 10:717–724

Mojtahedian S, Kogan DR, Kanzawa SA, et al (2007) Dissociaton of conditioned eye and limb responses in the cerebellar interpositus. Physiol Behav 91:9–14. doi: 10.1016/j.physbeh.2007.01.006

Naldini L, Blömer U, Gallay P, et al (1996) In Vivo Gene Delivery and Stable Transduction of Nondividing Cells by a Lentiviral Vector. Sci New Ser 272:263–267

Ohyama T, Nores WL, Medina JF, et al (2006) Learning-Induced Plasticity in Deep Cerebellar Nucleus. J Neurosci 26:12656–12663. doi: 10.1523/JNEUROSCI.4023-06.2006

Palkovits M, Mezey É, Hámori J, Szentágothai J (1977) Quantitative histological analysis of the cerebellar nuclei in the cat. I. Numerical data on cells and on synapses. Exp Brain Res 28–28:. doi: 10.1007/BF00237096

Pedroarena CM, Schwartz C (2003) Efficacy and Short-Term Plasticity at GABAergic Synapses Between Purkinje and Cerebellar Nuclei Neurons. J Neurophysiol 89:704–715. doi: 10.1152/jn.00558.2002

Perrett SP, Ruiz BP, Mauk MD (1993) Cerebellar cortex lesions disrupt learning-dependent timing of conditioned eyelid responses. J Neurosci 13:1708–1718

Pizzorusso T, Medini P, Berardi N, et al (2002) Reactivation of Ocular Dominance Plasticity in the Adult Visual Cortex. Science 298:1248–1251. doi: 10.1126/science.1072699

Romberg C, Yang S, Melani R, et al (2013) Depletion of Perineuronal Nets Enhances Recognition Memory and Long-Term Depression in the Perirhinal Cortex. J Neurosci 33:7057–7065. doi: 10.1523/JNEUROSCI.6267-11.2013

Rowlands D, Lensjø KK, Dinh T, et al (2018) Aggrecan Directs Extracellular Matrix-Mediated Neuronal Plasticity. J Neurosci 38:10102–10113. doi: 10.1523/JNEUROSCI.1122-18.2018

Sale A, Maya Vetencourt JF, Medini P, et al (2007) Environmental enrichment in adulthood promotes amblyopia recovery through a reduction of intracortical inhibition. Nat Neurosci 10:679–681. doi: 10.1038/nn1899

Sears LL, Steinmetz JE (1990) Acquisition of classically conditioned-related activity in the hippocampus is affected by lesions of the cerebellar interpositus nucleus. Behav Neurosci 104:681

Shutoh F, Ohki M, Kitazawa H, et al (2006) Memory trace of motor learning shifts transsynaptically from cerebellar cortex to nuclei for consolidation. Neuroscience 139:767–777. doi: 10.1016/j.neuroscience.2005.12.035

Slaker M, Churchill L, Todd RP, et al (2015) Removal of Perineuronal Nets in the Medial Prefrontal Cortex Impairs the Acquisition and Reconsolidation of a Cocaine-Induced Conditioned Place Preference Memory. J Neurosci 35:4190–4202. doi: 10.1523/JNEUROSCI.3592-14.2015

Sullivan CS, Gotthard I, Wyatt EV, et al (2018) Perineuronal Net Protein Neurocan Inhibits NCAM/EphA3 Repellent Signaling in GABAergic Interneurons. Sci Rep 8:. doi: 10.1038/s41598-018-24272-8

Telgkamp P, Raman IM (2002) Depression of inhibitory synaptic transmission between Purkinje cells and neurons of the cerebellar nuclei. J Neurosci 22:8447–8457

Ten Brinke MM, Heiney SA, Wang X, et al (2017) Dynamic modulation of activity in cerebellar nuclei neurons during pavlovian eyeblink conditioning in mice. eLife 6:

Thompson EH, Lensjø KK, Wigestrand MB, et al (2018) Removal of perineuronal nets disrupts recall of a remote fear memory. Proc Natl Acad Sci 115:607–612. doi: 10.1073/pnas.1713530115

Tracy JA, Thompson JK, Krupa DJ, Thompson RF (1998) Evidence of plasticity in the pontocerebellar conditioned stimulus pathway during classical conditioning of the eyeblink response in the rabbit. Behav Neurosci 112:267–285. doi: 10.1037//0735-7044.112.2.267

Uusisaari M, Knöpfel T (2008) GABAergic synaptic communication in the GABAergic and non-GABAergic cells in the deep cerebellar nuclei. Neuroscience 156:537–549. doi: 10.1016/j.neuroscience.2008.07.060

Vo T, Carulli D, Ehlert EME, et al (2013) The chemorepulsive axon guidance protein semaphorin3A is a constituent of perineuronal nets in the adult rodent brain. Mol Cell Neurosci 56:186–200. doi: 10.1016/j.mcn.2013.04.009

Wang D, Smith-Bell CA, Burhans LB, et al (2018) Changes in membrane properties of rat deep cerebellar nuclear projection neurons during acquisition of eyeblink conditioning. Proc Natl Acad Sci 115:E9419–E9428. doi: 10.1073/pnas.1808539115

Xue Y-X, Xue L-F, Liu J-F, et al (2014) Depletion of Perineuronal Nets in the Amygdala to Enhance the Erasure of Drug Memories. J Neurosci 34:6647–6658. doi: 10.1523/JNEUROSCI.5390-13.2014

Yamazaki T, Tanaka S (2009) Computational Models of Timing Mechanisms in the Cerebellar Granular Layer. The Cerebellum 8:423–432. doi: 10.1007/s12311-009-0115-7

Yang S, Cacquevel M, Saksida LM, et al (2015) Perineuronal net digestion with chondroitinase restores memory in mice with tau pathology. Exp Neurol 265:48–58. doi: 10.1016/j.expneurol.2014.11.013

Yeo CH, Hardiman MJ (1992) Cerebellar cortex and eyeblink conditioning: a reexamination. Exp Brain Res 88:623–638

Yeo CH, Hardiman MJ, Glickstein M (1985a) Classical conditioning of the nictating membrane of the rabbit. I. Lesions of the cerebellar nuclei. Exp Brain Res 60:87–98

Yeo CH, Hardiman MJ, Glickstein M (1985b) Classical conditioning of the nictitating membrane response of the rabbit. II. Lesions of the cerebellar cortex. Exp Brain Res 60:99–113

Zhao R-R, Muir EM, Alves JN, et al (2011) Lentiviral vectors express chondroitinase ABC in cortical projections and promote sprouting of injured corticospinal axons. J Neurosci Methods 201:228–238. doi: 10.1016/j.jneumeth.2011.08.003

Chapter 4

Early trajectory prediction in elite athletes

Cullen B. Owens, Casper de Boer, Giulia Gennari, Robin Broersen, Johan J. Pel, Brian Miller, Wesley Clapp, Ysbrand D. Van der Werf, and Chris I. De Zeeuw (2018)

The Cerebellum, 17 (6), p 766–776

4.1 Abstract

Cerebellar plasticity is a critical mechanism for optimal feedback control. While Purkinje cell activity of the oculomotor vermis predicts eye movement speed and direction, more lateral areas of the cerebellum may play a role in more complex tasks, including decision-making. It is still under question how this motor-cognitive functional dichotomy between medial and lateral areas of the cerebellum plays a role in optimal feedback control. Here we show that elite athletes subjected to a trajectory prediction, go/no-go task manifest superior sub-second trajectory prediction accompanied by optimal eye movements and changes in cognitive load dynamics. Moreover, while interacting with the cerebral cortex both the medial and lateral cerebellar networks are prominently activated during the fast feedback stage of the task, regardless of whether or not a motor response was required for the correct response. Our results show that cortico-cerebellar interactions are widespread during dynamic feedback and that experience can result in superior task-specific decision skills.

4.2 Introduction

The cerebellum is an important site of plasticity for motor learning and part of a larger network consisting of both cortical and subcortical brain areas that support functions such as adaptation of movements, temporal processing (Roitman and Shadlen 2002) and spatiotemporal prediction (Onuki et al. 2015). Increasing evidence has surfaced indicating that the cerebellum may also moderate cognitive control in both humans and animals when strict temporal processing is required (Timmann and Daum 2007; Rahmati et al. 2014; Baumann et al. 2014). It has been said that hitting a major league fastball is one of the most biologically challenging tasks for a human to accomplish. It requires years or even decades to execute at the highest level, and requires millisecond level precision in neurocomputational terms. In less than 500 milliseconds (ms) the batter must watch the ball coming out of the pitcher's hand (preparatory period), recognize the pattern of the seams on the ball and interpolate the spin (pattern recognition), and then integrate that information with the expected trajectory and speed of the pitch (timed trajectory prediction) in order to determine whether it will pass through the strike zone or not (a Go/NoGo decision). If the ball appears to pass through the strike zone, the batter must make fast and accurate motor adjustments with bat in hand to make proper contact with the ball (online motor control). Therefore, the act of hitting in baseball consists of discrete trials that require several categorically different sequential cognitive and motor processes in a very short amount of time. Specifically, hitting a baseball can be divided into two main subtasks of a different nature. The first 225 ms is considered a Go/No-Go timed decision-making task, since the batter has to decide in this time window whether or not to swing. The latter part of the pitch trajectory is considered a motor control and timing task, because the batter has to make fast motor adjustments to contact the ball accurately (Adair 2015). Given this clear segregation, baseball is an attractive model for dissecting the differential impact of various temporal cues on perception, decision-making and sensorimotor control.

There is ample scientific evidence that elite athletes develop task specific skills in perception, cognition and motor control (Miller and Clapp 2011; Muraskin et al. 2015). For example, well-practiced baseball players show improved reaction times in a Go/No-Go task with stationary cues. They also show an increased ability to extrapolate the momentum of a visually occluded moving target (Kida et al. 2005; Nakamoto et al. 2014). Furthermore, expert cricket batsmen making predictive saccades during the pitch show they make better use of early flight information (Land and McLeod 2000). However, in these examples the relationship between psychophysical and neurophysiological demands is less well understood. Although it has been posited that elite athletes may bias the right action earlier and that elite athlete action selection is superior, it has to our knowledge not been shown how psychophysical and neurophysiological computations may facilitate superior performance in sequence; i.e., from preparatory period, to trajectory prediction to decision making, and finally to action selection. We chose to investigate the parametrical space of this sequence and the functional neural network that might mediate it.

4.3 Materials and methods

4.3.1 Participants

In total, 10 male baseball field players (mean age 17.4) defined as having seen > 5000 live game pitches from the AAA national youth team of the Royal Netherlands Baseball and Softball Federation (KNBSB) and 10 male age-matched non-baseball players (mean age 18.3); ($t(18) = 0.952$, $P = 0.354$)) were included. Experts and controls were excluded from the study if they reported playing video games more than five hours per week, had any known motor problems, or did not have normal or corrected-to-normal vision. In the latter case, subjects' vision was tested using a standard eye chart. Prior to measurements, a written informed consent was obtained from all subjects. In the case of subjects under the age of 18, signed informed consent was obtained from both parents. The study was approved by the medical ethical committee of Erasmus MC, Rotterdam (MEC-2012-524). One control and one expert subject were excluded from pupillary response analysis and one expert subject was excluded from initiation of hand movement analysis due to insufficient quality of data.

4.3.2 Study design

All subjects performed a simple Reaction Time Task (RTT) and a Trajectory Prediction Task (TPT), divided across four blocks in a fixed order. Subjects first performed 50 trials of the RTT on measurement setup 1, and then 3 blocks of 80 trials of TPT on measurement setup 2. Both setups were situated in a temperature controlled dark room and all subjects were given a few minutes of rest between blocks.

4.3.3 Reaction Time Task

Measurement setup 1 was used to calculate the reaction time. The RTT consisted of a 25-inch monitor (IIyama, Nagano, Japan, 60 Hz) and a keyboard. During RTT subjects placed their head on a chin-rest in front of the screen at a distance of 460 mm, which resulted in a visual angle of 59 x 36 degrees (width x height). The subjects saw a video demo of the task prior to the measurements, and they were instructed to press the space bar of a keyboard as quickly as possible when the visual stimulus (a white ball with red seams on a black background) appeared. Each subject received a total of 50 trials with a short break after 25 trials. During each trial the stimulus was displayed for 500 ms with random intertrial intervals between 1.5 and 4 seconds. The maximum allowed reaction time was 750 ms and key presses in the first 125 ms were considered catch trials. For each RTT trial, reaction time was calculated as the time between stimulus presentation and pressing the keyboard (excluding the catch time trials). After each trial, the subject's reaction time was presented above the stimulus to motivate the subject to decrease their reaction time.

4.3.4 Trajectory Prediction Task

Measurement setup 2 consisted of a combination of a 32-inch touch screen (ELO Touchsystems, Leuven, Belgium), a 3D infrared motion capture system (Vicon Model, Oxford, United Kingdom), and an infrared eye tracking system (Chronos Vision, Berlin, Germany). Eye and hand movements were recorded at a rate of 200 Hz. The exact specifications of this setup have been published (de Boer et al. 2013). Subjects placed their head on a chin-rest in front of the screen at a distance of 460 mm, resulting in a visual angle of 75 by 46 degrees (width x height). Prior to the measurements, all subjects received verbal instructions followed by a series of practice runs, with a maximum of 20 trials.

In this task (Fig 1) subjects were instructed to fixate on a black cross, located at a 20 degrees vertical visual angle above the center of the screen. After a variable fixation period, the cross was replaced by a solid black circle that immediately started moving from the location of the cross toward a target area (10 x 10 degrees) at the bottom of the screen in a straight-line trajectory. If subjects anticipated the stimulus would end up inside the target area (Go trial), they were instructed to touch the screen as quickly as possible with their dominant index finger and hold it there. If subjects anticipated the stimulus would end up outside the target area (No-Go trial), subjects were instructed not to touch the screen. It was emphasized that subjects had to touch and hold the position on the screen before the stimulus reached its final position. After the stimulus had reached its final position, visual feedback on trial performance (correct or incorrect) was presented for 500 ms.

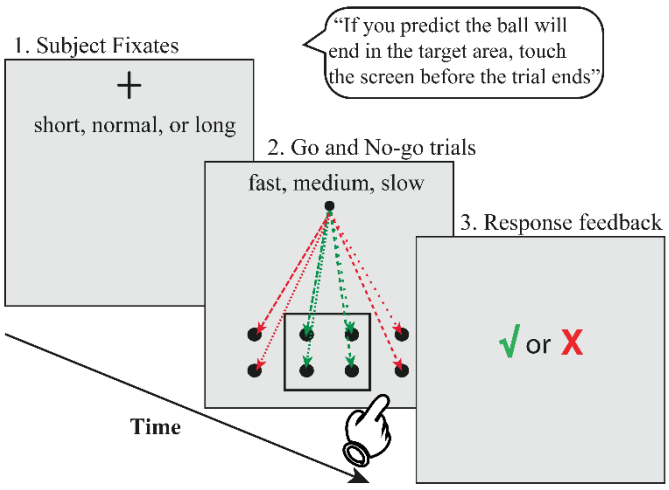

Fig 1. Trajectory prediction task. A fixation cross appeared with a variable duration (390 ms, 890 ms, or 1900 ms), followed by either a fast (385 ms), medium (485 ms) or slow (585 ms) moving stimulus to one of 8 final locations, within (green dotted lines; go trials) or outside the target square (red dotted lines; no-go trials). Fixation duration and stimulus speed and trajectory were pseudo-randomly intermixed. A screen touch (and hold) in go trials (hit) and no-touch in no-go trials (correct rejection) resulted in a correct response (green check). A red X appeared after an incorrect response. Each subject performed three blocks of 80 trials on the behavioral task.

The following parameters were pseudo-randomly varied and counterbalanced within each block. Four final locations were designated as 'Go' trials and four locations were designated as 'No-Go' trials (final locations outside the target area on both sides). Three stimulus flight speeds were designated (385 ± 5, 485 ± 5 or 585 ± 5 ms) and were presented 24 times per speed (three times per final location). A stimulus flight time of 985 ms (probe) was used eight times in total (one time per final location). Presentation time of the fixation cross was either 390 ± 5, 890 ± 5, or 1900 ± 5 ms. Each fixation duration was applied 24 times per block. During stimulus flight speeds of 985 ms (8 trials) a fixation duration of 1000 ms was applied. Neighboring final locations were equidistant vertically and horizontally to each other, forming a 4 by 2 grid. All final locations were targeted ten times per block. All stimuli varied ± 5 ms in duration due to an asynchrony between the stimulus presentation rate (200 Hz, synchronized with the eye-tracking system and the motion detection system) and the screen refresh rate (60 Hz). For brevity we refer to each flight speed as 390 ms (fast), 490 ms (medium) and 590 ms (slow), and we refer to each presentation time of the fixation cross as 390 ms (short), 890 ms (normal) and 1900 ms (long).

4.3.5 Data processing and outcome parameters

At least ten reliable trials were required in order for an outcome parameter to be included in final analysis. Seven eye movement outcomes, two hand outcomes, and eight pupil outcomes were calculated. Otherwise, the subject was excluded from the analysis.

Total tracking time is the total time per trial (in ms and as percentage of the total trial time) during which gaze was < 8 degrees from the stimulus. Mean gaze to stimulus distance (GSD) is the mean distance (in degrees) between the subject's gaze and position of the stimulus during the part of the trial that is defined as 'tracking'. Eye response time is defined as the time between stimulus onset and first saccade onset (gaze velocity exceeding 50 degrees/second). The primary saccade amplitude is defined as the degrees of the first saccadic eye movement. The fixation error is the mean number of degrees from the fixation cross across the entire fixation period. Hand response time is the time between stimulus onset and index finger velocity exceeding 20 degrees/second. Touch time is the time between stimulus onset and touching the screen. Trial performance calculated as percentage of correct or incorrect trials is classified as a hit (correct Go trials), miss (incorrect Go trials), correct rejection (correct No-Go trials) or false alarm (incorrect No-Go trials). For pupillary responses, we calculated mean diameters for baseline (first 100ms of the fixation period (in millimeters)), end of the fixation period (last 100 ms) and end of the stimulus presentation (last 100ms). We calculated the slope of diameter change at all three periods as well; this was done for all periods (overall), during the fixation period only, and during the stimulus flight only. Finally, we calculated the latency to peak response (maximal pupil diameter within the trial) and the peak size change (difference between maximal diameter within the whole trial and baseline diameter). Eye and hand traces were

visualized using custom MATLAB (Mathworks, Natick, MA, USA) software. Using these visualizations, each trial was manually checked while the rater was blind to subject and group. In each trial, x- and y-coordinates of the eye movements, gaze and hand velocity, and task evoked pupillary response were plotted in relation to the stimulus onset and subject's screen touch. All trials that did not allow reliable analysis (e.g. due to blinking or noisy signal) were removed.

4.3.6 Statistical analysis

To assess for normality of distributions we used the Shapiro-Wilk test. For distributions where normality could be assumed, we tested for differences in all outcome parameters between experts and controls using univariate ANOVA tests with group as between-subjects variable and block, final location, fixation duration, and speed as within-subjects variable. To test for a within-subject effect of block on each parameter, repeated measures ANOVA tests were used. Post-hoc Bonferroni-corrected and independent samples t-tests were used to more closely examine differences between groups and within individual blocks. For comparisons where data were not normally distributed, we used the Mann-Whitney U-test. In all statistical tests, significance level was set at 0.05. All statistical testing was performed in IBM SPSS Statistics 21. T-tests are two-way unless stated otherwise. Results are calculated as mean ± standard deviation (SD), unless stated otherwise and figures display standard error of the mean (SEM).

4.3.7 fMRI procedure

We used an adapted version of our novel timed, trajectory prediction task for fMRI investigation. For the MRI implementation of the task, we restricted the presentation of the stimuli to two speeds only, i.e. fast (370 +/-20 milliseconds) and medium (500 +/-10 milliseconds), to maintain sufficient power for event-related analysis. We also increased the number of trials from 80 trials per block to 96 trials per block. All other stimuli parameters were the same as that described in the behavioral study. We recruited six male right-handed participants (2 expert baseball players and 4 novices) from the same cohort as in the behavioral study.

Subjects were lying in the MRI scanner in a supine position. The visual stimuli were provided by using an LCD projection onto a screen standing behind the MR scanner; the image of this projection was visible through a mirror attached to the head coil above the subjects' eyes. Responses of the right hand were acquired using a four-button MR-compatible response box (Current Design, HHSC-1x4-CL). Every subject performed three runs of the task, with 48 Go and 48 No-go trials each.

4.3.8 fMRI imaging parameters and acquisition

Functional and structural MR scans were recorded using a 3T scanner (Philips, 3.0-Tesla Achieva) at the Spinoza Center, University of Amsterdam. For functional MRI scans, whole-brain functional T2*-weighted MRI data were acquired using a gradient-echo planar imaging (EPI) sequence (55 transverse slices with 0 mm gap, ascending slice acquisition; voxel size 2.5 × 2.5 × 2.5 mm^3; repetition time (TR) 3179 ms, echo time (TE) 29.93 ms; flip angle 80°; field of view (FOV) 200 × 200 mm^2). For co-registration purposes, we acquired T1-weighted MR images (220 slices; TR 8.2 ms; TE 3.8 ms; inversion time 670.4ms; FOV 240 × 188 mm^2, matrix size 240 × 187; flip angle 8°; voxel size 1 × 1 × 1 mm^3). Head movements were minimized by restraining the subject's head using sponge cushions inside the 32-channel head-coil.

4.3.9 fMRI Analysis

All pre-processing and analysis steps were done using FSL 5.08 (FMRIB's Software Library, www.fmrib.ox.ac.uk/fsl). In brief, we performed skull-stripping of the T1 images using BET, filtered the functional images using a 100-second high-pass filter and smoothed them with a 5-mm full-width at half maximum (FWHM) Gaussian kernel. We performed event-related general linear modeling (GLM) at first level on the three blocks per subject, using FEAT (FMRI Expert Analysis Tool) Version 6.00, part of FSL. Our first analysis investigated brain activation patterns associated with the different response types, i.e. go and no-go responses. In the model we used hits, correct rejections, misses and false alarms as events. We modeled the events for the duration of the stimulus. Using these events, we constructed the following contrasts: 'correct hits – misses' (go contrast), 'correct rejections – misses' (no-go contrast). We generated first-level GLM analyses contrasting the responses to fast vs. medium stimuli, across the combination of correct hits and correct rejections, by creating a 'fast – medium' contrast. In addition, we generated separate 'fast - medium' contrasts for the correct hits and correct rejection stimuli, respectively.

Activation maps were co-registered to the individual T1 scan using BBS and then brought into standard space using linear warping with 12 degrees of freedom. We then carried each of the three different types of first-level analyses into second level using a fixed-effects higher-level analysis for the three runs per subject, thereby constructing single-subject activation maps. These images were then carried into third-level mixed-effects analyses using FLAME1+2 to be maximally sensitive to meaningful effects in small numbers of subjects, so as to obtain group averages via a one-sample t-test. The main effects of activation are reported at a z-threshold of 2.3 with cluster correction at $P < 0.01$. All images conform to neurological convention, i.e. the left side is left in the image.

4.4 Results

4.4.1 Experts perform better only under the most challenging conditions

We first investigated subjects' overall performance, i.e. percentage of correct trials, over all three blocks. Both experts and controls improved their overall performance over blocks of trials ($F(1,18) = 21.042$, $P < 0.001$)). *Post-hoc* Bonferroni corrected tests showed that performance in block 2 (mean difference (MD) = 7.2, $P = 0.033$) and block 3 (MD = -10.2, $P = 0.001$) was better than performance in block 1. We found no interaction effect between block and group on overall performance, indicating that both experts and controls performed better in blocks 2 and 3 compared to block 1. However, experts performed better than controls in block 3 (MD = -6.70, $t(18) = -2.435$, $P = 0.026$), but not in block 1 or 2 (Fig 2A). At the most challenging temporal constraints, *i.e.* when fixation time prior to the trial was short, experts performed on average 6.2% better ($t(18) = 2.154$, $P = 0.023$). In trials where stimulus speed was fast, experts performed on average 7.2% better ($t(18) = 1.917$, $P = 0.035$) (Fig 2B).

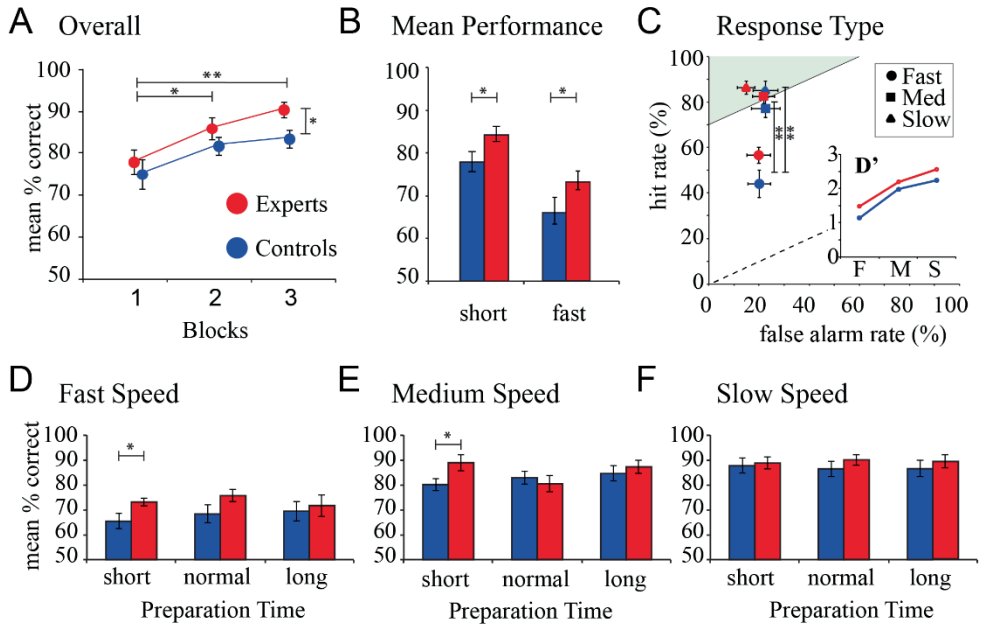

Fig 2. Performance. (A) Overall group average performance over 3 blocks of 80 trials. Subjects improved from block 1 to block 2 and block 1 to block 3. Experts performed significantly better than controls on block 3. (B) Experts perform better on average during the shortest fixation duration and at the fastest flight times. (C) Experts do better than controls as flight speed decreases by increasing hit rate with a higher D' score (inset F=fast, M=medium, S=slow). (D, E, F) When all blocks are compiled and broken down by fixation duration and flight time, experts perform better at the short fixation duration of the fast (D) and medium (E) flight times, but not the slow. (* = $P < 0.05$; ** = $P < 0.01$) *(N=10/group).* Numbers represent means and SEM.

We also tested what type of responses contributed to task performance relevant to flight speed and group. Subjects had a better performance at slow and medium flight speeds compared to fast flight speeds due to increased hit responses ($F(2,54) = 44.157$, $P < 0.001$) rather than reduced false alarms ($F(2,54) = 0.592$, $P = 0.557$) (Fig 2C). *Post-hoc* Bonferroni-corrected tests showed that hit rate was lower in trials with fast stimulus speeds compared to trials with medium stimulus speeds ($MD = -0.294$, $P < 0.001$) and slow stimulus speeds ($MD = -0.346$, $P < 0.001$). Differences between groups was also reflected in the D' measure; a statistical measure in signal detection theory to quantify how a system distinguishes signal from noise. We found experts with higher D' scores overall (controls: 1.14, 1.99, 2.25; experts: 1.48, 2.19, 2.57), and both groups show reductions in hits rather than increased false alarms when the flight speed increases, highlighting the impact of flight speed on stimulus sensitivity rather than specificity (Fig 2C inset).

Finally, we were interested to see how groups differed in all nine trial variations. Here we compiled performance over all three blocks, measuring performance during all combinations of preparation times *and* stimulus flight speeds. When preparation times were short, experts performed better during fast (controls: 65.4 ± 3.1%, experts: 73.1 ± 1.6%, $t(18) = -2.216$, $P = 0.040$) (Fig 2D) and medium (Fig 2E) flight speeds (controls: 80.2 ± 2.5%, experts: 88.9 ± 3.2%, $t(18) = -2.145$, $P = 0.046$). These differences did not hold for other combinations (Fig 2D-F).

4.4.2 Fast decision-making was associated with activation of cerebellar areas

Using fMRI, we first investigated which brain areas were engaged during our task. We hypothesized that shorter durations allotted for the go/no-go decision would recruit cerebellar areas when exogenous temporal cues varied (Coull and Nobre 2008). We found that a faster stimulus speed, contrasted with medium speed, was associated with a large cluster in the medial cerebellum (vermis), right lateral cerebellar cortex (Crus I) ($Zmax = 4.01$) and the left inferior parietal lobe ($Zmax = 4.19$) (Fig 3A, B, Table 1). When contrasting only hit responses during fast and medium stimuli speeds, we observed clusters of activity in the medial and right lateral cerebellum ($Zmax = 3.81$) (Fig 3C, Table 1). When contrasting only correct rejections during fast and medium stimulus speeds, we observed differential activity in the vermis and bilateral cerebellar cortex crus I and II ($Zmax = 4.19$), in addition to the bilateral inferior parietal lobe ($Zmax = 3.96$), bilateral somatomotor cortex ($Zmax = 4.07$), left frontal operculum ($Zmax = 4.1$), and middle frontal gyrus ($Zmax = 4.25$) (Fig 3D. Table 1). These results indicate that our task recruits both medial and lateral cerebellar regions that are co-active with a network of cortical areas when temporal conditions change, regardless of whether or not a motor response is required for the correct response.

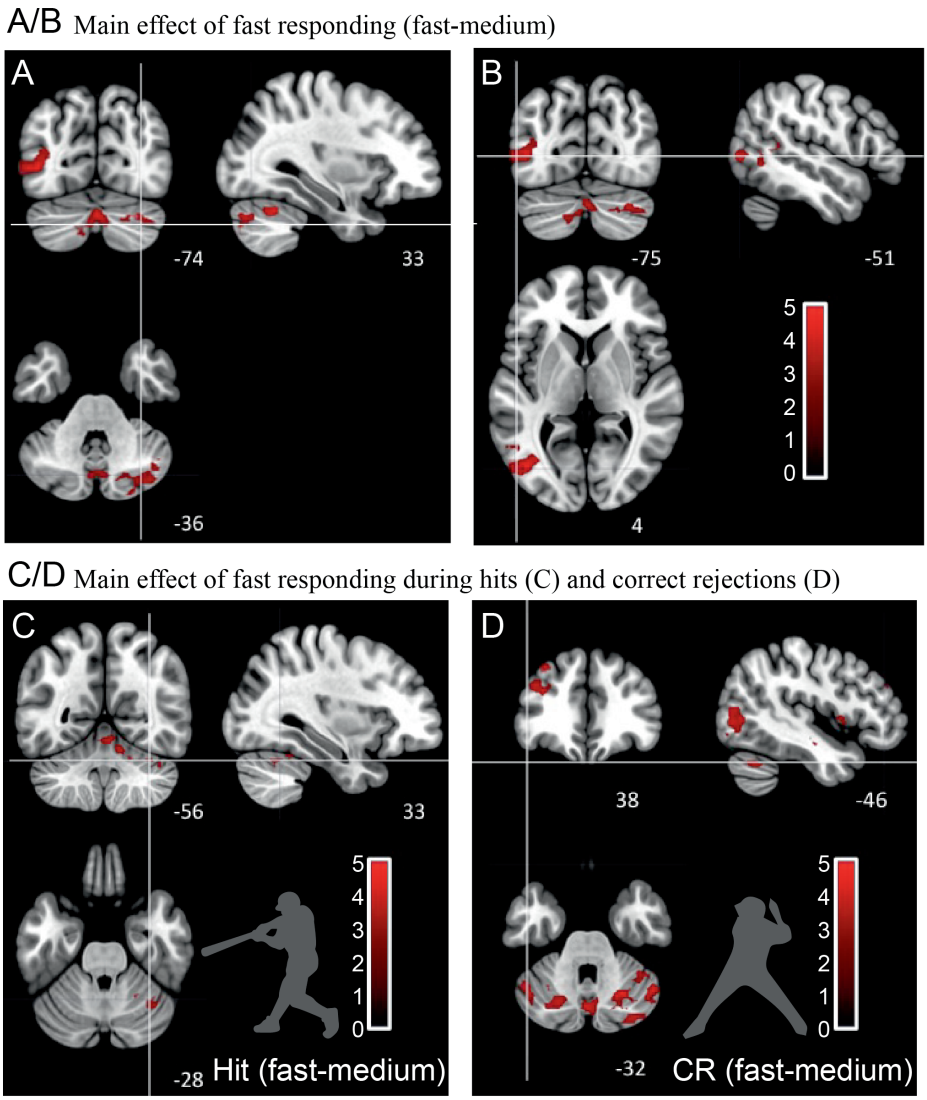

Fig 3. fMRI. The main effect of fast responding is shown in panels A/B. Fast responding is associated with medial and lateral cerebellum. When contrasting BOLD response during fast vs. medium stimuli, across combined hits and correct rejections, differential activity was associated with medial cerebellum (vermis), right lateral cerebellum (Crus areas) and left inferior parietal lobe (and Table 1). (C) BOLD response differences of hit trials between medium and fast flight speed. Cerebellar vermis and right cerebellar cortex (area I-VII, crus I) showed a large significant cluster (Zmax = 3.81; x = 6, y = -54, z = -12). Images were thresholded at z > 2.3 cluster corrected at P = 0.01; only the vermis and right cerebellum exceeded the significance threshold. (D) BOLD response differences of correct rejections between fast and medium flight speed in six large clusters including cerebellar vermis, right cerebellar cortex (area I-VII, crus I) (Zmax = 4.19); left putamen, left frontal operculum (Zmax = 4.1); left and right temporo-occipital cortex, inferior parietal lobule (Zmax = 4.22 and 3.96); bilateral superior parietal gyrus, intraparietal sulcus (Zmax = 4.07); and middle frontal gyrus (Zmax = 4.25) *(N=6).*

4.4.3 Experts show cognitive efficiency when preparation time is short

We found task-evoked pupillary responses (TEPRs) to be a reliable measure with consistent baselines between groups at all experimental periods. An increase in pupil size diameter from baseline to the end of the fixation period ($F(2,18) = 16.710$, $P = 0.003$) and between the end of the fixation period to end of the flight time was found ($F(2,18) = 10.694$, $P = 0.01$), with no significant group differences (Fig 4A). Interestingly, during the short fixation trials pupil diameter of experts reached its peak earlier than that of controls at fast ($MD = 55$, $t(16) = 2.183$, $P = 0.044$) and medium ($MD = 95$, $t(16) = 2.328$, $P = 0.033$), but not slow ($MD = 58$, $t(16) = 1.147$, $P = 0.268$) flight speeds (Fig 4B). Experts also showed a shallower slope of dilation during ball flight at the fastest flight speed ($MD = 0.153$, $t(16) = 2.301$, $P = 0.035$) (Fig 4C), but not at the medium or slow flight speed ($MD = 0.087$, $t(16) = 1.251$, $P = 0.229$; $MD = 0.028$, $t(16) = 0.311$, $P = 0.760$), indicating that pupil diameters of experts increase less abruptly once the fast stimulus has appeared. These data show how expert pupil dilation, although comparable to that of controls in size, occurs faster prior to stimulus onset suggesting a more prompt mental engagement that coincides with the preparatory signal.

Since experts mobilize cognitive resources earlier at short fixations and fast flight speeds, while the slope of change asymptotes during the stimulus, longer fixation times might exert an additional cognitive load upon them. Indeed, we found that during trials with long fixation durations experts showed a longer latency to peak at all flight speeds fast ($MD = -306$, $t(16) = -2.522$, $P = 0.012$, one-tailed), medium ($MD = -265$, $t(16) = -2.086$, $P = 0.026$, one-tailed) and slow ($MD = -317$, $t(16) = -2.047$, $P = 0.028$, one-tailed)) (Fig 4D). Moreover, at the long fixation trials experts have a steeper overall slope (fixation time + flight speed) at the slow flight speed ($MD = -0.045$, $t(16) = -1.985$, $P = 0.032$), but not the medium or fast flight speed ($MD= -0.006$, $t(16) = -0.241$, $P = 0.813$; $MD = 0.004$, $t(16) = 0.100$, $P = 0.921$). Finally, there were no group differences in peak pupil dilation and slope of pupil dilation at the medium fixation.

4.4.4 Experts show greater recruitment of cognitive resources during false alarms

To investigate the relation between pupil size and response types we arranged and analyzed trials by hits, misses, correct rejections and false alarms. We found a main effect of response type ($F(3,45) = 14.534$, $P < 0.001$) as well as an interaction between response type and group ($F(3,45) = 4.707$, $P = 0.006$), suggesting that the extent to which pupil size changes is a function of the response depending on the group. Contrasts revealed that greater pupil dilation occurred with hits compared to misses ($F(1,15) = 24.795$, $P < 0.001$) and with false alarms compared to correct rejections ($F(1,15) = 15.722$, $P = 0.001$), but not misses compared to correct rejections ($F(1,15) = 3.670$, $P = 0.075$) (Fig 4E). These response type differences may be due to movement preparation and action associated with hits and false alarms. Interestingly, experts showed larger peak dilation for false alarms compared to hits relative

to controls (F(1,15) = 0.027, P = 0.007), suggesting the highest level of arousal during incorrect No-Go trials.

Table 1. Z-max results contrasting all fast and slow trials, fast and slow hits, and fast and slow correct rejections.

Area	Size	Zmax	x	y	z
Figure 3A/B fast - medium					
Cerebellar vermis, bilateral cerebellar cortex VI, VII, crus I,	1047	4.01	0	-72	-32
Left temporo-occipital cortex, inferior parietal lobule	639	4.19	-44	-76	6
Figure 3C Hits fast-medium					
Cerebellar vermis, right cerebellar cortex I-VII, crus I	344	3.81	6	-54	-12
Figure 3D Correct rejections fast - medium					
Vermis and bilateral cerebellar cortex I-IX, Crus I, Crus II	2170	4.19	6	-58	-40
Left putamen, left frontal operculum	967	4.1	-26	6	4
Left temporo-occipital cortex, inferior parietal lobule	925	4.22	-40	-74	2
Bilateral superior parietal gyrus, intraparietal sulcus	837	4.07	12	-62	50
Right temporo-occipital cortex, inferior parietal lobule	537	3.96	54	-58	4
Middle frontal gyrus	364	4.25	-34	36	42

We found a main effect of response type on pupil dilation slope over the whole trial (fixation and stimulus) (F(2,30) = 5,195, P = 0.011), which is in line with the finding that the steepness of the slope describing pupil dilation across the entire trial varied depending on the choice the subject was about to make. However, there was no interaction between response type and group in this respect. Contrasts revealed that pupil change across the whole trial was significantly different when comparing hits to misses (F(1,15) = 10.033, P = 0.006) and hits to correct rejections (F(1,15) = 66.797, P < 0.001), while differences between dilation slopes associated with false alarms and those associated to the other response types were not significant (Fig 4F).

Additionally, the main effect of response type on pupil dilation during the fixation period only, was also significant (F(2,30) = 3.329, P = 0.028), suggesting that the steepness of the pupil dilation slope during fixation time depends on the response subjects *will* choose during the trial. There was no interaction between response type and group. Contrasts revealed that change in pupil dilation within the fixation period was steeper for hits relative to misses (F(1,15) = 11.695, P = 0.004), correct rejections (F(1,15) = 24.295, P < 0.001) and false alarms (F(1,15) = 4.920, P = 0.042) (Fig 4G).

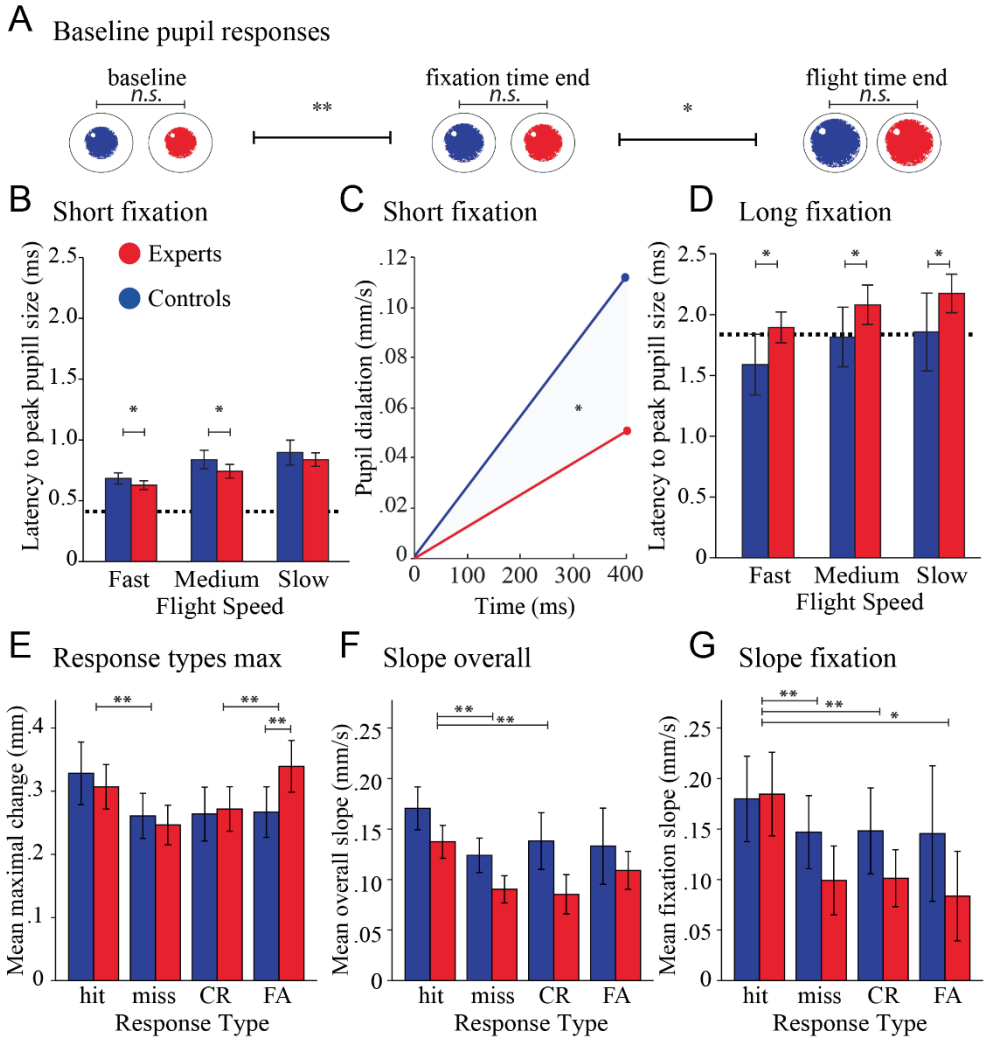

Fig 4. Pupillary responses. (A) Subject pupil dilation increased progressively, but did not differ between groups at the different time points; baseline period, end of fixation time, or end of flight time. (B) During trials with the short fixation, experts reached peak pupil dilation earlier than controls on the fast and medium flight speeds, but not slow. (C) Pupil dilation slope during flight on trials with the short fixation and fast flight speed; consistent with peak latencies, expert pupil diameter enlarged less abruptly during flight time. (D) During trials with the long fixation, experts reached peak pupil dilation later than controls on all flight speeds. (E-F) *hit* (correct go trials/all go trials); *miss* (incorrect go trials/all go trials) correct rejections (*CR*) (correct no-go trials/all no-go trials) false alarms (*FA*) (incorrect no-go trials/all no-go trials) (E) Experts showed larger dilations during false alarms relative to controls. (F) The slope of the change in pupil dilation across the whole trial (fixation plus flight time) was different when comparing hits to misses and hits to correct rejections. (G) When considering fixation intervals only, the slope of pupil dilation depended on the response subjects chose at the end of the trial. Dashed line indicates stimulus onset *(N=9/group)*.

These results could not be confounded by motor preparation or action, because the data were only taken during presentation of the fixation cross, the durations of which were pseudo-randomly distributed.

4.4.5 Experts show precise, cost-efficient eye movements

Next, we measured eye movements and we found that distance between gaze and stimulus (GSD) during the trials showed an interaction-effect between flight speed and group ($F(5,59) = 4.012$, $P = 0.024$; ANOVA) (Fig 5A). During the fastest flight speed, experts tracked the stimulus for a lower percentage of the trial duration ($F(1,54) = 4.733$, $P = 0.034$) (Fig 5B). These results indicate that during the most challenging trials experts keep their gaze closer to the stimulus initially, but track the stimulus for less of the trial.

To rule out that differences in reaction time contributed to our results, we compared performance of both groups on a simple reaction time task (RTT). We did not find significant differences in reaction time between experts (310 ± 1.88 ms) and controls (312 ± 2.29 ms; $t(18) = 0.264$, $P = 0.26$). All motoric measures including saccade onset, initiation of hand movements, and task reaction time adapted to faster temporal parameters, but did not differ between groups.

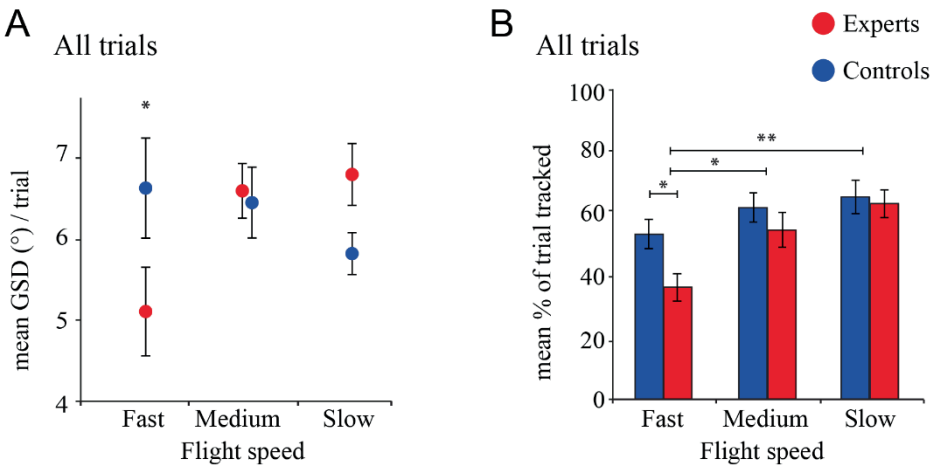

Fig 5. Eye Movements. (A) Expert mean gaze-stimulus distance (GSD) was shorter at the fast flight speed and increased as flight speed decreased, while control mean GSD decreased as flight time decreased, showing an interaction between group and flight speed (B) Tracking measures (see methods) showed a significantly larger percentage of the trial tracked by controls during the fastest flight times. We also found the mean percent of the trial tracked increased as stimulus speed decreased from the fast to medium and the fast to slow flight speed *(N=10/group).*

We also calculated the distance of the subjects' gaze to the fixation cross at the end of the fixation time (and therefore start of the stimulus movement), so as to determine whether subjects kept their gaze on the fixation cross prior to trial start (fixation error). We found no effect of fixation duration on fixation error ($F(3,53) = 0.456$, $P = 0.714$), but did find an interaction effect of fixation duration and group on fixation error ($F(3,54) = 3.587$, $P = 0.019$). When we compared experts and controls at each fixation duration parameter, we found fixation error was smaller in experts only in trials with the long fixation duration ($t(9) = 3.874$, $P = 0.024$). These data are in line with the pupillary response results on the long fixation durations, described above.

4.5 Discussion

We developed a novel trajectory prediction, go/no-go task with the aim of modeling temporal parameters from a hitter's perspective in baseball so that the response time window reflected a 90, 80, or 70 mile/hour fastball. The first part of a real pitch necessitates pattern and trajectory prediction followed by a go/no-go decision, while the latter part of the pitch requires precise motor control and timing (Adair 2015) (Fig 6A). In our task, subjects were instructed to predict whether a downward-moving stimulus would terminate inside (go trial) or outside (no-go trial) a visible target area on a computer screen. Task difficulty changed by manipulating the duration of temporal cues; three initial fixation intervals, followed by three stimulus speeds pseudo-randomly intermixed. We found medial and lateral cerebellum was activated when contrasting fast trials with medium trials. We also found that experts performed the best at the most difficult parameters, short preparation time and fast stimulus speed. Expert performance measures were accompanied by closer gaze-stimulus distance and shorter tracking during ball flight. At short preparation times, experts exhibit earlier and faster pupillary response and at long preparation times, longer pupillary response compared to controls. Finally pupil response showed a main effect of performance related to responses that require a motor response (Hits and False Alarms). These main effects also showed an interaction suggesting experts show greater recruitment of cognitive resources during false alarms (Fig 6B).

4.5.1 Cortico-cerebellar networks

We observed cerebellar network activation during both motor and non-motor responses, suggesting that the cerebellar role in our task cannot be attributed to the motor response alone. Experts showed pronounced performance differences, coinciding with distinct eye movement and pupil dynamics. These findings could reflect tuning of large cortico-cerebellar networks in experts, which in effect allows for quick cognitive preparation to make fast decisions. Recent evidence suggests that baseball players show expertise-level

differences in cognitive processing and differences in structural connectivity, supporting functional connectivity and modulatory attention (Muraskin et al. 2016).

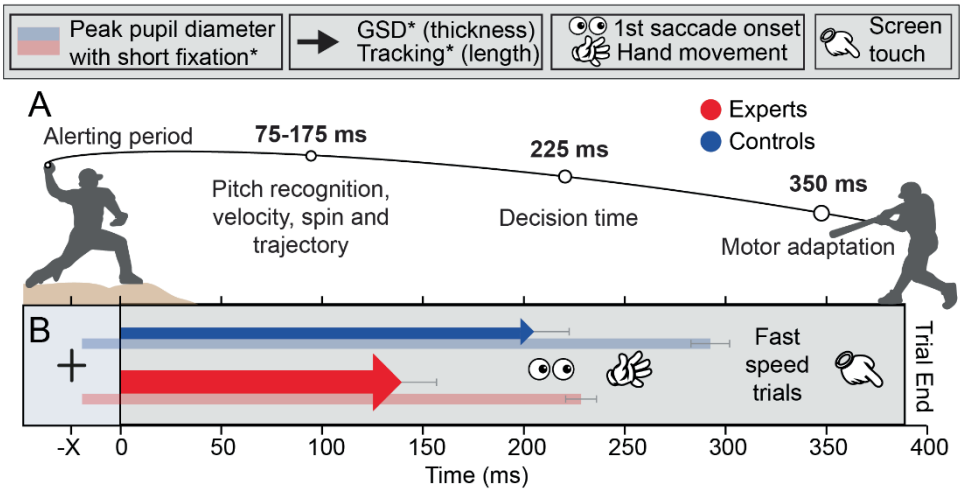

Fig 6. Summary and temporal dynamics. (A) Upper panel: temporal dynamics of a professional baseball pitch. (B) Group averages of psychophysical responses at the short preparation and fast stimulus speed trials including significant differences in stimulus tracking (arrow length), gaze to stimulus distance (arrow thickness), and peak pupil dilation (transparent bars). Saccade onset, hand movements, and screen touch reaction times did not differ between groups.

There is evidence that the basal ganglia (BG) is associated with action selection (Schmidt et al. 2013), whereas the cerebellum is more commonly associated with action preparation and execution (Gaidica et al. 2018). When we broke down our data into response types, we found that as flight speed increased, both groups' hit rates significantly decreased while false alarm rates stayed the same. Therefore, in our task, the difference in response windows from 585 millisecond to 485 or 385 millisecond response windows resulted in subjects' decreased hits and increased misses, indicating increased demands on action execution over action selection. When we analyzed pupil response broken down into response types we found overall, larger peak pupil dilation in trials where action preparation occurred (hits and false alarms) and that experts had a larger peak dilation during false alarms when compared to controls suggesting a higher level of arousal during incorrect No-Go trials. These data indicated to us that action preparation and initiation may influence our group differences in this task to a greater extent than action selection. This evidence also supports our fMRI findings where when contrasting the same response types (Hits or False Alarms) with differing flight speeds (fast and medium) we found both medial and lateral cerebellar activation. Recent alternative BG hypotheses posit that BG controls a time varying signal that controls speed-accuracy tradeoff and that its activity reflects the commitment to a decision (Thura and Cisek 2017). However, transient increases in deep

cerebellar nuclei activity precede and are time-locked to saccades (Ohmae et al. 2017) or limb movements in a simple reaction time task (Thach 1975), both functions evident during our task.

Furthermore, cerebellar Purkinje cell simple spike activity has been found to signal visual events and encode target motion and direction in similar visually guided tasks (Miles et al. 2006; Herzfeld et al. 2015), facilitating direct and active integration between perceptual and motor demands (Zimmermann et al. 2011). To this extent, there is growing evidence that subcortical circuits may provide a short-cut to drive motor actions prior to visual information reaching awareness (Spering and Carrasco 2015). Given that the lateral cerebellum was activated during correct rejections, our data provide evidence that the cerebellum is also involved in the decision process of the initiation of movements, rather than online movement control alone. Although we did not find activation of BG in our fMRI results, we were interested in neural networks involved in the dynamic feedback in the task over the response types themselves. Overall, we conclude that experience in elite sports allows for early activation of arousal systems to precisely tune cortico-cerebellar pathways, resulting in distinct physiological responses required for coping with sub-second decisions.

4.5.2 Timing

In baseball, a batter must take into account several pieces of information for trajectory interpolation. Since we did not ask our subjects to make an overt duration estimate of each trial, our task did not involve explicit timing, but rather implicit timing. Although baseball players are also constantly performing an explicit timing task where they must deliberately and exactly time their swing of the bat to coincide with the speed and trajectory of the ball, we chose to exclude this real world scenario from the equation, allowing our subjects to decide anywhere within the time of the trial. Still, the feedback response in our task might have contributed to both explicit and implicit learning (Taylor et al. 2014). Moreover, implicit timing, such as that employed by a batter when observing the angle and movement of the pitchers arm, might be used to predict the forthcoming duration of the stimulus, in a different way than the batter interprets speed based on the perceptual increase in size of the ball approaching (Coull and Nobre 2008).

Although the three fixation durations employed in the current task were not predictable at first, after time it might have been possible to implicitly learn their duration since there were only three. Pupil responses function as reporter indicators for dynamic, intensive aspects of human cognition where the amplitude is proportional to task complexity, allowing one to discriminate individual differences in resource availability and investment (van der Meer et al. 2010). Experts performed better than controls when fixation presentation was short and stimulus speed was fast, while they activated cognitive resources faster during these trials. When fixation was long however, they performed

similarly but delayed activation of cognitive resources. These results indicate that experts may rely more heavily on endogenous alerting temporal cues than controls.

Optimal feedback control theory attributes a forward model to account for accurate prediction of sensory outcomes from motor commands, such as those for eye movements and hand movements. Such sensory predictions are then integrated in order to estimate the state of the body in the world (state estimation). For a particular estimated state the system must adjust the gains of sensorimotor feedback loops so movements optimally balance costs and rewards for maximum gain or performance (Yarrow et al. 2009). We found that all subjects adjusted eye, hand and touch latency relative to our temporal cues during the trial (flight speed) and these adjustments were strikingly similar across groups. However, experts performed more accurately with earlier cognitive engagement, suggesting experts exhibited optimal preparation skills but similar motor control for this task.

4.5.3 Summary and functional implications

We have highlighted variable contributions of temporal cues to identify potential visuo-motor and perceptual differences in a population of elite athletes playing a popular sport. Given that experts exhibited superior performance when decision time was short and preparation time was limited, we purport that the arousal systems of experts may precisely tune the relevant cortico-cerebellar pathways to optimize their psychophysical responses, allowing them to cope with changing task conditions. Indeed, evidence indicates pupil size is associated with the locus coeruleus, superior colliculus and anterior cingulate cortex and may be crucial for synchronizing arousal states to facilitate behavior (Joshi et al. 2016). The finding that experts track the ball for less time, but do so more accurately while performing better at the fastest flight speed, may also provide a clue as to how they cope with real-world challenging conditions in their sport. Possibly, experts' increased exposure to these temporal constraints allows for faster adaptation of eye movements. Cerebellum and the superior colliculus provide directional drive of the eyes, while the cerebellum keeps track of the progress of the saccade toward the target and ends saccades by cutting off drive from the superior colliculus (Quaia et al. 1999). Purkinje cell simple spike activity has been found to signal visual events and encode target motion in a visually guided reaching task (Miles et al. 2006), facilitating direct and active integration between perceptual and motor tasks (Zimmermann et al. 2011). Intriguingly, accumulating reports argue that the retinocollicular pathway could provide a short-cut to drive motor actions, such as fast orienting eye movements to targets of interest, before visual information reaches awareness (Spering and Carrasco 2015). Within our task, this network may be primed in experts in order to make a fast decision accounting for less tracking and at the same time, a better performance on the fastest flight speeds. The retinogeniculate pathway through primary visual cortex (V1) is specialized for feature based motion perception, while the retinocollicular pathway that bypasses V1 is thought to be specialized for detecting motion energy (Azzopardi and Hock 2011).

Taken together, the current study may have multiple and widespread implications toward better neural training methods for elite athletes. Additionally, modeling other sports with control of similar single trial tasks and populations with parametrically diverse cognitive skills may further facilitate a mechanistic understanding to improve rehabilitation for clinical populations.

4.6 Acknowledgements

The authors wish to thank Robert Eenhoorn, Martijn Nijhoff, Evert-Jan ‘t Hoen and the players and families of the Royal Netherlands Baseball and Softball Federation for organizing and volunteering research subjects, and Bas Koekkoek and Peter Holland for excellent advice and technical assistance. This work was supported by funds for C.I.D.Z. from the Dutch Organization for Fundamental Research (ALW and MAGW), ZonMw, EU-CEREBNET, EU-ERC(POC) and Neuroscouting, LLC.

4.7 References

Adair RK (2015) The Physics of Baseball. HarperCollins

Azzopardi P, Hock HS (2011) Illusory motion perception in blindsight. Proc Natl Acad Sci USA 108:876–881. doi: 10.1073/pnas.1005974108

Baumann O, Borra RJ, Bower JM, et al (2015) Consensus Paper: The Role of the Cerebellum in Perceptual Processes. MCER 14:197–220. doi: 10.1007/s12311-014-0627-7

Coull J, Nobre A (2008) Dissociating explicit timing from temporal expectation with fMRI. Current Opinion in Neurobiology 18:137–144. doi: 10.1016/j.conb.2008.07.011

de Boer C, van der Steen J, Schol RJ, Pel JJ (2013). Repeatability of timing of eye-hand coordinated movements across different cognitive tasks. J Neurosci Methods 218:131-8. doi: 10.1016/j.jneumeth.2013.05.011

Gaidica M, Hurst A, Cyr C, Leventhal DK (2018) Distinct Populations of Motor Thalamic Neurons Encode Action Initiation, Action Selection, and Movement Vigor. J Neurosci 0463–18. doi: 10.1523/JNEUROSCI.0463-18.2018

Herzfeld DJ, Kojima Y, Soetedjo R, Shadmehr R (2015) Encoding of action by the Purkinje cells of the cerebellum. Nature 526:439–442. doi: 10.1038/nature15693

Joshi S, Li Y, Kalwani RM, Gold JI (2016) Relationships between Pupil Diameter and Neuronal Activity in the Locus Coeruleus, Colliculi, and Cingulate Cortex. Neuron 89:221–234. doi: 10.1016/j.neuron.2015.11.028

Kida N, Oda S, Matsumura M (2005) Intensive baseball practice improves the Go/Nogo reaction time, but not the simple reaction time. Brain Res Cogn Brain Res 22:257–264. doi: 10.1016/j.cogbrainres.2004.09.003

Land MF, McLeod P (2000) From eye movements to actions: how batsmen hit the ball. Nat Neurosci 3:1340–1345. doi: 10.1038/81887

Miles OB, Cerminara NL, Marple-Horvat DE (2006) Purkinje cells in the lateral cerebellum of the cat encode visual events and target motion during visually guided reaching. The Journal of Physiology 571:619–637. doi: 10.1113/jphysiol.2005.099382

Miller BT, Clapp WC (2011) From vision to decision: the role of visual attention in elite sports performance. Eye Contact Lens 37:131–139. doi: 10.1097/ICL.0b013e3182190b7f

Muraskin J, Dodhia S, Lieberman G, et al (2016) Brain dynamics of post-task resting state are influenced by expertise: Insights from baseball players. Hum Brain Mapp. doi: 10.1002/hbm.23321

Muraskin J, Sherwin J, Sajda P (2015) Knowing when not to swing: EEG evidence that enhanced perception-action coupling underlies baseball batter expertise. NeuroImage 123:1–10. doi: 10.1016/j.neuroimage.2015.08.028

Nakamoto H, Mori S, Ikudome S, et al (2014) Effects of sport expertise on representational momentum during timing control. Atten Percept Psychophys 77:961–971. doi: 10.3758/s13414-014-0818-9

Ohmae S, Kunimatsu J, Tanaka M (2017) Cerebellar Roles in Self-Timing for Sub- and Supra-Second Intervals. J Neurosci 37:3511–3522. doi: 10.1523/JNEUROSCI.2221-16.2017

Onuki Y, Van Someren EJW, De Zeeuw CI, Van der Werf YD (2015) Hippocampal-cerebellar interaction during spatio-temporal prediction. Cereb Cortex 25:313–321. doi: 10.1093/cercor/bht221

Quaia C, Lefèvre P, Optican LM (1999) Model of the control of saccades by superior colliculus and cerebellum. Journal of Neurophysiology 82:999–1018.

Rahmati N, Owens CB, Bosman LWJ, et al (2014) Cerebellar potentiation and learning a whisker-based object localization task with a time response window. J Neurosci 34:1949–1962. doi: 10.1523/JNEUROSCI.2966-13.2014

Roitman JD, Shadlen MN (2002) Response of neurons in the lateral intraparietal area during a combined visual discrimination reaction time task. J Neurosci 22:9475–9489.

Schmidt R, Leventhal DK, Mallet N, et al (2013) Canceling actions involves a race between basal ganglia pathways. Nature Publishing Group 16:1118–1124. doi: 10.1038/nn.3456

Spering M, Carrasco M (2015) Acting without seeing: eye movements reveal visual processing without awareness. Trends in Neurosciences 38:247–258. doi: 10.1016/j.tins.2015.02.002

Taylor JA, Krakauer JW, Ivry RB (2014) Explicit and Implicit Contributions to Learning in a Sensorimotor Adaptation Task. Journal of Neuroscience 34:3023–3032. doi: 10.1523/JNEUROSCI.3619-13.2014

Thach WT (1975) Timing of activity in cerebellar dentate nucleus and cerebral motor cortex during prompt volitional movement. Brain Research 88:233–241.

Thura D, Cisek P (2017) The Basal Ganglia Do Not Select Reach Targets but Control the Urgency of Commitment. Neuron 95:1160–1170.e5. doi: 10.1016/j.neuron.2017.07.039

Timmann D, Daum I (2007) Cerebellar contributions to cognitive functions: a progress report after two decades of research. MCER 6:159–162. doi: 10.1080/14734220701496448

van der Meer E, Beyer R, Horn J, et al (2010) Resource allocation and fluid intelligence: insights from pupillometry. Psychophysiology 47:158–169. doi: 10.1111/j.1469-8986.2009.00884.x

Yarrow K, Brown P, Krakauer JW (2009) Inside the brain of an elite athlete: the neural processes that support high achievement in sports. Nat Rev Neurosci 10:585–596. doi: 10.1038/nrn2672

Zimmermann E, Burr D, Morrone MC (2011) Spatiotopic Visual Maps Revealed by Saccadic Adaptation in Humans. Current Biology 21:1380–1384. doi: 10.1016/j.cub.2011.06.014

Chapter 5

Action perception recruits the cerebellum and is impaired in spinocerebellar ataxia patients

Abdel R. Abdelgabar*, Judith Suttrup*, Robin Broersen*, Ritu Bhandari*, Samuel Picard, Christian Keysers#, Chris I. De Zeeuw#, Valeria Gazzola#

*, # indicate equal contribution to first and last authorship

Submitted
Preprint available on BioRxiv: doi: 10.1101/480293

5.1 Abstract

Our cerebellum has been proposed to generate prediction signals that may help us plan and execute our motor programs. However, to what extent our cerebellum is also actively involved in perceiving the action of others remains to be elucidated. Using fMRI, we show here that observing goal-directed hand actions of others bilaterally recruits cerebellar Lobules VI, VIIb and VIIIa. Moreover, whereas healthy subjects (n = 31) were found to be able to discriminate subtle differences in the kinematics of observed limb movements of others, patients suffering from spinocerebellar ataxia type 6 (SCA6; n = 21) were severely impaired in performing such tasks. Our data suggest that the human cerebellum is actively involved in perceiving the kinematics of the hand actions of others and that SCA6 patients' deficits include a difficulty in perceiving the actions of other individuals. This finding alerts us to the fact that cerebellar disorders can alter social cognition. Given that impairments in social cognition have been reported to be one of the most debilitating consequences of neurological disorders, this finding may be relevant to improving the quality of life of patients and their families.

5.2 Introduction

The ability to perceive hand actions of others plays a key role in our ability to learn fine motor skills from conspecifics and interact successfully with them in cooperative and competitive settings. C*erebral* cortical regions involved in motor control, including the premotor cortex and inferior parietal cortex where mirror neurons were found in the monkey (di Pellegrino et al. 1992; Gallese et al. 1996; Rizzolatti et al. 1996; Kohler et al. 2002; Keysers et al. 2003; Fogassi et al. 2005; Rozzi et al. 2008), and the primary somatosensory cortex (SI) (Gazzola and Keysers 2009; Caspers et al. 2010; Keysers et al. 2010), have been shown to be necessary for extracting subtle information from the observed kinematics of hand actions (Urgesi et al. 2014; Keysers et al. 2018). A powerful task to reveal the impact of disturbing these cortical regions requires participants to judge the weight of an object lifted by another individual. This task depends on the ability to transform subtle kinematic cues into a weight estimate. Perturbing activity in the premotor cortex and SI disrupts the ability to perceive the weight (Pobric et al. 2006; Valchev et al. 2017), suggesting a causal role of premotor and somatosensory region in action perception.

The cerebellum is a key partner of these neocortical brain regions during motor control, where its role is well established (Kelly and Strick 2003; Gao et al. 2018). It is perhaps not surprising that some have speculated that the cerebellum may also play a role in the perception and prediction of the kinematics of observed hand actions. Specifically, it has been proposed that the cerebellum could leverage its forward models (*i.e.* neural computations that transform motor signals into expected sensory consequences) to predict the actions of others (Miall 2003; Wolpert et al. 2003; Fuentes and Bastian 2007; Gazzola and Keysers 2009; Rizzolatti and Sinigaglia 2010; Sokolov et al. 2017). Although this proposal is intuitively appealing, we still have little evidence for the cerebellum being a reliable and even necessary node of the action observation network (Sokolov et al. 2017). This is because fMRI evidence for its recruitment during action observation is mixed, and very few neuro-modulation or lesion studies have explored the impact of cerebellar disruptions on hand action observation.

With a few exceptions, imaging studies on action perception have typically focused on the involvement of the neocortex, leaving the information about cerebellar activity limited to what the field of view of fMRI of these studies usually included, *i.e.* the dorsal cerebellum (*e.g.* Aziz-Zadeh 2006; Gazzola et al. 2007a, b; Catmur et al. 2008; Gazzola and Keysers 2009; Agnew et al. 2012; Brunner et al. 2014; Plata Bello et al. 2014; Di Cesare et al. 2015; Jelsone-Swain et al. 2015; Thomas et al. 2018). Several other experimental studies fail to observe cerebellar activation to hand action observation (Iacoboni et al. 1999, 2001; Buccino et al. 2004; Orr et al. 2008; Rocca and Filippi 2010; Jastorff et al. 2012; Sasaki et al. 2012; Horan et al. 2014). This inconsistency is also reflected in meta-analyses of action observation studies, with some finding no (Caspers et al. 2010) or very limited cerebellar activations (Molenberghs et al. 2012), and others finding several clusters (Van Overwalle et al. 2014). In their extensive meta–analysis, Van Overwalle et al. found that only 28% of the reviewed

studies investigating action observation report cerebellar activity. The degree to which these inconsistencies depend on data-acquisition and data-analysis pipelines not optimized for the cerebellum is difficult to estimate *post-hoc*, and experiments that optimize methods for the cerebellum, assess the reliability of activations in individual participants, and assess replicability across studies are required. Part I of the current manuscript will therefore present four fMRI experiments that map and replicate the recruitment of cerebellar voxels during hand action observation using MRI acquisition and analysis methods optimized for the cerebellum. These studies highlight that lobules VI and VIII are consistently recruited by action observation.

However, to establish whether the cerebellum causally contributes to hand action observation, its activity must be perturbed and the impact on action perception measured. Unfortunately, only two studies have taken that route so far. First, Sokolov et al. (2010) showed that four patients with tumors in the left lateral cerebellum (but not those with lesions in the vermis) were impaired in their ability to detect whether a point-light walking motion was embedded in random dot motion of that locomotor activity. However, the motor control of routine walking and of skilled hand actions is fundamentally different, as demonstrated by the fact that lesioning the pyramidal tract that transmits the cortical output to the spinal cord leaves routine treadmill walking unaltered (Eidelberg and Yu 1981), but severely impairs skilled hand actions (Forssberg et al. 1999; Duque et al. 2003; Hermsdörfer et al. 2003). Second, Cattaneo et al. (2012) tested the involvement of the cerebellum in the perception of action sequences. They showed eight participants affected by cerebellar ischemia sets of four still photographs taken during an action (*e.g.* opening a bottle and pouring a glass of water). One out of the four pictures was not fitting the temporal sequence of the action, and the task was to identify which one was the intruder. They found the performance of five of the cerebellar patients to be below the range of the sixteen healthy controls. While this study does not explore the processing of the subtle kinematic cues, it provides the first evidence that cerebellar impairments can affect the ability of participants to identify acts not belonging to a particular action sequence.

However, while dozens of studies in hundreds of participants establish that premotor and parietal regions of the neocortex are necessary for the optimal perception of observed actions (Urgesi et al. 2014; Keysers et al. 2018), the necessary role of the cerebellum in hand action observation hinges on a single study with 8 patients. In part II of the current study we therefore aim to provide new evidence for a contribution of the cerebellum to action perception, and the first evidence for its role in processing subtle kinematic cues during hand action perception. To this aim, we tested the ability of 21 patients with spinocerebellar ataxia of subtype 6 (SCA6) to detect the weight of a box by observing the kinematics of a hand lifting the box in a video setting. SCA6 is a rare late-onset neurodegenerative disorder characterized by ataxia and associated with a loss of Purkinje cells in the cerebellum. A Voxel-based morphology study points to loss of gray matter in the hemispheres of lobule VI (Rentiya et al. 2017) as being the primary cause of the upper limb ataxia – adjacent to regions in which we find cerebellar activations to action observation in part I. Task

performance was compared with that of 31 age-matched controls. Participants were tested in (i) a condition in which a sleeve on the actor's arm occluded muscle shape information, forcing participants to focus on the arm's kinematics to judge the weight of the box (Sleeve condition), and in (ii) a condition in which the sleeve was removed to reveal information on the appearance of muscle contractions, which complements the arm's kinematic information (NoSleeve). Comparing the two groups in the Sleeve condition will reveal whether the cerebellum is necessary for kinematic processing. Comparing the gain in performance across the two conditions (*i.e.* the NoSleeve-Sleeve performance difference) across groups will reveal whether the cerebellum is necessary to extract additional information from biological shape.

The two main aims of our work are therefore to establish: (a) whether and where hand action observation reliably activates the cerebellum and (b) whether perturbations of cerebellar functioning impair the ability to process the kinematic and/or shape of observed actions.

5.3 Materials and methods

5.3.1 General overview of the experiments and participants (Table 1)

Experiment #1 was aimed at localizing cerebellar activity to action observation using different analysis pipelines, and at comparing the results between pipelines and to those found in the literature. Experiment #2 and #3 tested the replicability of the results of Experiment #1 on two independent samples of participants, and on a different MRI scanner. Experiment #4 tested the impact of the weight discrimination task on the previously identified action observation network, and Experiment#5 was aimed at directly testing the involvement of the cerebellum in action perception by comparing the accuracy in weight estimation between SCA6 patients and matched controls. All tested healthy participants had a normal or corrected to normal vision, and none had a history of neurological conditions or treatments. The participants tested in the MRI also met MRI safety requirements.

The SCA6 patient group was recruited in collaboration with the department of Neurology at the Erasmus MC Rotterdam. The severity of disease progression was clinically assessed by a licensed neurologist using the Scale of the Assessment and Rating of Ataxia (SARA) (Schmitz-Hubsch et al. 2006; Saute et al. 2012). SARA includes 8 items (gait, stance, sitting, speech disturbance, finger chase, nose-finger test, fast alternating hand movements and heel-shin slide) reflecting neurological manifestations of cerebellar ataxia (Weyer et al. 2007). SARA scores range from 0 to 40, with higher scores corresponding to higher progression. The average SARA score for our patients group (N_{SARA} = 17) was 11.38 ± 5.75 (SD; range: 2 to 21.5). The thirty-one healthy participants that were recruited as control group, matched the SCA6 group for age ($t_{(50)}$ = 0.96, P = 0.34), handedness (SCA6: 19 right

handed and 2 left handed, Controls: 27 right and 4 left handed, Yates corrected $X^2 = 0$, P = 0.94) and gender (SCA6 15f:6m, ctrl 15f:16m, Yates corrected $X^2 = 1.86$, P = 0.17). However, our patient group contained numerically fewer males, an issue that is addressed in control analyses. Controls did not receive a clinical assessment.

All participants signed an informed consent in accordance with the declaration of Helsinki. The fMRI study protocols were approved by the medical ethical committee of the University of Groningen (METc2012/380), the ethics review board of the University of Amsterdam (2015-BC-4697), the Academic Medical Center of Amsterdam (W15_243#15.0288), and the clinical study protocol was approved by the Medical Ethical Committee of the Erasmus MC Rotterdam (MEC-2013-095).

5.3.2 Stimuli, tasks and paradigms

Action observation task (Fig 1A). During the observation task participants watched 39 unique movies of a human right hand interacting with objects displayed on a table (ActionOBS). The 39 control movies displayed a hand movement without a meaningful object interaction (CtrlOBS). Exp. #1 and 2 also contained a third static condition, in which the hand rested close to the object (Arnstein et al. 2011; Valchev et al. 2016). This static condition was not included in Exp. 3, and therefore not included in the group analyses. Conditions were randomized across participants and presented using the Presentation® software (Version 18.0, Neurobehavioral Systems, Inc., Berkeley, CA, www.neurobs.com) in a single fMRI run. Participants were instructed to pay close attention to the movies shown.

Weight discrimination task (WD, Fig 1B): Participants performed a two-alternative forced-choice task, in which at every trial, participants had to choose in which of the two presented videos the heaviest object was lifted. The 4 seconds video-clips showed a human arm lifting an object. In order to avoid participants to deduce the weight from object movement only (e.g. differences in object shaking during the lifting phase), a black panel occluded both the object and the hand from vision. To disentangle whether the contribution of cerebellum mainly comes from computation of action kinematics or from arm shape information, two versions of the task were created: (i) in half of the trials, the arm lifting the object was sleeved thus making the kinematic of the arm the only information available to perform the task (Sleeve); (ii) in the other half, the arm was uncovered thus allowing both kinematic and shape information to be used (NoSleeve; Fig 1B). During the video recording, the actor was instructed to lift one of three weights (2850 g, 900 g and 180 g) within 4 seconds. A metronome was used to time the lift, and a reference line was marked on the wall in front of the actor to help maintaining the same lifting height throughout all videos. The actor was aware of the object weight to avoid hesitation in the lifting. Videos were recorded using a digital video camera (Sony DSRPDX10P) and edited using Adobe Premiere Pro (Version CS5, Adobe System Incorporated, San Jose, USA).

Table 1. Experiments overview. From left to right: the acronym of each experiment (AO = action observation; AOrep = action observation replication; SCA6 = spinocerebellar ataxia type 6; WD = weight discrimination; SARA = Scale of the Assessment and Rating of Ataxia); the number of participants included in the analyses and their characterization (number in brackets indicate the number of initially recruited participants); the average age of the group, its standard deviation and range in brackets; the number of females and males within each group of included participants; the technique involved in the experiment; the task used for each experiment; the aim of each experiment. All groups of participants are independent except the ones marked with *, in which the same 25 participants underwent both the passive observation and the weight estimation task in separate sessions. In Exp. #1, four participants were excluded from the statistical analysis: two due to excessive head motion (displacement of more than the 3.5 mm voxel dimension), one reported sleepiness, and one because of image distortion. In Exp. #5, two participants were excluded from the weight lifting task because pre-symptomatic, and two more were excluded from the correlation with SARA because did not have SARA scores.

Exp.	Nº Subj incl., (recruited) Subj. type	Mean Age ± SD [range]	Gender F, M	Technique	Task	Experimental aim
Exp. #1, AO	31 (35) healthy	23±4 [19-40]	21, 10	fMRI	Action observation	Localize cerebellar voxels responding to action observation
Exp. #2, AOrep1	25* (25) healthy	25.2±4 [19-32]	13, 12	fMRI	Action observation	Replicability of cerebellar activations to action observation
Exp. #3, AOrep2	23 (23) healthy	25.5±3.6 [21-33]	11, 12	fMRI	Action observation	Replicability of cerebellar activations to action observation
Exp. #4, WD	25* (23) healthy	25.2±4 [19-32]	13, 12	fMRI	Weight estimation	Localize cerebellar activations to the weight discrimination task and compare them with Exp. #1-3
Exp. #5, SCA6	19_{WD}, and 17_{SARA} (21) SCA6	62±7 [49-80]; 60.8±7 [49-68]	WD 14, 5 SARA 12, 5 Total 15, 6	Behav + eye tracking (N=4)	Weight estimation	Investigate whether cerebellar deficits are reflected in decreased accuracy in perception
	31 healthy	61±7 [43-74]	15, 16	Behav + eye tracking (N=7)	Weight estimation	

Clips showing the same lifted weight were never paired. In half of the trials the heaviest object was lifted first, in the other half as second. The order was randomized in Psychopy2 (Peirce 2009). After the second clip, the task instruction was presented until the subject indicated his/her response. Before the beginning of the task participants performed four training trials. Some minor task differences were present between Exp#4 and #5 (Fig 1B).

Exp. #5 (behavior). Participants gave the response by pressing the arrow keys on a standard QWERTY keyboard using their right hand. Ninety-six trials were presented in total, and participants had the option to take a short voluntary break after the first half of the trials.

Exp. #4 (fMRI). Participants indicated their responses by means of a MRI compatible button box. Participant used their left hand to select the first clip and their right hand to select the second. Stimuli were presented using Presentation® software. For the fMRI experiment, a numerosity task was additionally introduced and intermixed with the weight discrimination task. Participants had to estimate and compare the number of moving dots shown in video 1 and 2 instead of weight. The movement of the dots followed the kinematic of the arm presented in the Sleeve and NoSleeve conditions, but the arm was not visible. Since an error occurred in the randomization of this condition, and this task was not

performed by the SCA6 group, the numerosity condition was not included in the group analyses. Seventy-two trials were presented in total (24 for each of the three conditions).

5.3.3 fMRI data acquisition

All MRI data sets included an anatomical scan. Exp. #1 then included one functional scan of the action observation task. Exp. #2 and 3 aimed at comparing the effect of different numbers of simultaneous slice acquisition on task based fMRI, and included four and five functional scans of action observation respectively. The results of this comparison are the subject of a separate manuscript. Because participants of Exp. #1 only saw the movies once, we only included the first view of the action observation task, independently of the number of simultaneously acquired slices. Exp. #4 included two functional runs of the weight lifting task. These two runs were randomly presented between the four observation runs of Exp. #2. The scanning parameters were chosen to achieve a coverage of the entire cerebrum and cerebellum (Table S1).

5.3.4 Localization of cerebellar activations, impact of different analysis pipelines and replicability

The impact of different pipelines on cerebellar task-based responses was analyzed on data from Exp. #1. The four considered pipelines mainly differed in the order in which the pre-processing and first level subject statistics were computed, and in the normalization template. Because the comparison revealed a no clear advantage of using pipelines optimized for the cerebellum compared to the traditional one, the method and results of this comparison are presented in the supplementary material.

All the analyses included in the main text therefore follow the traditional approach which includes: slice-time correction, realignment of functional images to the computed mean, co-registration of the anatomical image to the mean, whole brain normalization to the MNI template (final voxel size: 2 × 2 × 2 mm) based on the parameter generated during the segmentation of the co-register anatomy, a smoothing with a 6 mm FMHW Gaussian kernel followed by a general linear model (GLM). Analyses testing the possibility of activation leakage between the anterior cerebellum and the temporal cortex due to smoothing are reported in the supplementary material.

For Exp. #1 to 3, the GLM included two standard box car predictors that modelled the ActionOBS and CtrlOBS video presentation. Exp. #1-2 also included a predictor modelling the static conditions. All predictors were convolved with the canonical hemodynamic response function (HRF). The last six regressors of no interest included the displacements and rotations along the three axes, determined during image realignment. The ActionOBS-CtrlOBS contrast was computed at the subject-level to generate action specific activations

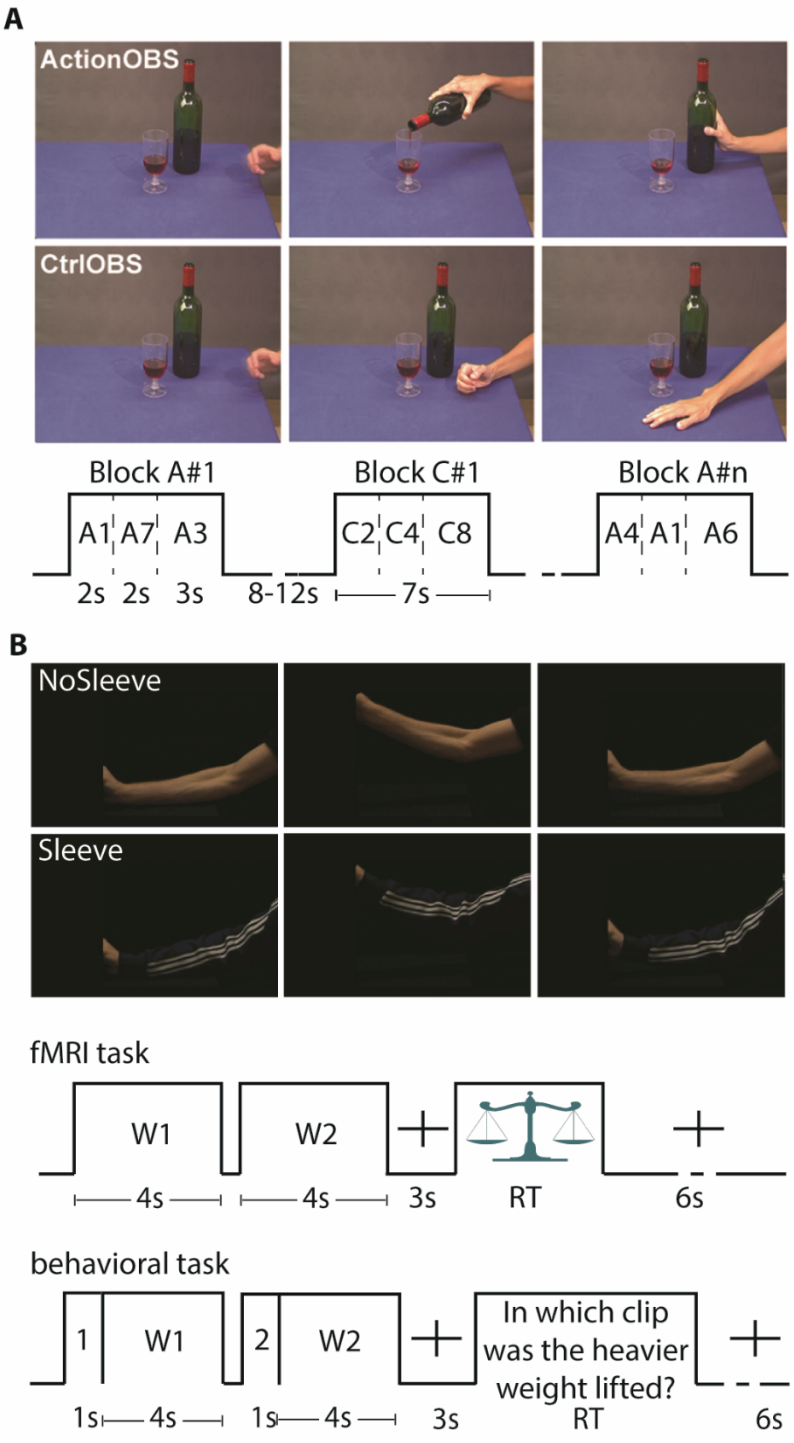
A
ActionOBS
CtrlOBS
Block A#1
Block C#1
Block A#n
A1 A7 A3
C2 C4 C8
A4 A1 A6
2s 2s 3s
8-12s
7s
B
NoSleeve
Sleeve
fMRI task
W1
W2
4s
4s
3s
RT
6s
behavioral task
1
W1
2
W2
In which clip was the heavier weight lifted?
1s
4s
1s
4s
3s
RT
6s

Fig 1. Experimental tasks. (A) Action observation task. Example of one out of the 39 possible actions and its control, followed by the task structure. Ctrl = control. OBS = observation. A = action. C = control. The ActionOBS and CtrlOBS movies were grouped in blocks of 7 seconds. Each block contained three actions from the same condition, with a total of 13 blocks for each condition. Blocks were separated by a fixation cross for a random period of 8 to 12 seconds, displayed on a background that was visually similar to the table. (B) Weight discrimination task. Frame extracted from the NoSleeve (top) and Sleeve (bottom) weight lifting condition, followed by the trial structure for the fMRI (top) and behavioral experiments (bottom). In the fMRI task the window of time participants were requested to answer was indicated by a weighing scale. In the behavioral task clips were preceded by the number 1 or 2 denoting whether it was the first or second clip of the pair. The sentence following the video was translated from Dutch for illustration purposes. RT = participant's reaction time.

for observation. Analyses of variance on the ActionOBS-CtrlOBS contrast values from Exp. #1-3 were also implemented to directly compare the results of the three experiments to each other (within-subjects ANOVA) as well as to baseline (one-way ANOVA).

All analyses were run in SPM8 and 12 (Wellcome Trust Centre for Neuroimaging, UCL, UK) using Matlab 7.14 (The MathWorks Inc., Natick, USA) with a bounding box size adjusted to include the entire cerebellum [-90 -126 -72; 91 91 109], complemented by custom Matlab scripts. Unless specified otherwise, all analyses were estimated within the cerebellar mask using the cerebellar anatomical map from the Anatomy toolbox (http://www.fz-juelich.de/ime/spm_anatomy_toolbox) (Geyer et al. 1996, 1999, 2000; Amunts et al. 1999; Grefkes et al. 2001; Geyer 2004; Eickhoff et al. 2005, 2006, 2007; Caspers et al. 2006; Choi et al. 2006). The Anatomy toolbox was also used to define regions of interests, and guide anatomical descriptions of clusters of activity.

Unless specified otherwise, all statistical maps were thresholded at $p_{FWE} < 0.05$ with a minimal cluster size of 10 voxels. We chose peak-level FWE-correction, because we wished to (i) interpret activation of individual voxels, and, motivated by the inconsistencies of cerebellar activations in the literature, (ii) to limit the risks of Type I errors.

In order to investigate the consistency in location of voxels responding to action observation between participants and studies, we computed consistency maps (Gazzola and Keysers 2009), and Supplementary method 1.2). However, as the consistency maps cannot confirm that voxels responding to action observations are present in all participants, we counted the number of activated voxels within each participant. This counting was done separately for the four cerebellar anatomical regions of interest (left and right lobule VI, and VIIb/VIIIa), and for the cerebellum as a whole. To compare the reliability of cerebellar activations with that of the cortex, the counting was done for three additional cortical regions, typically associated with the action observation network (Gazzola and Keysers 2009; Caspers et al. 2010; Molenberghs et al. 2012): the premotor area BA44, the inferior parietal complex PF and the primary somatosensory cortex SI.

5.3.5 Localization of the weight discrimination task

The GLM of Exp. #4 included eight boxcar predictors: three modelled the video presentation (*i.e.* from the beginning of Video 1 to the end of Video 2) associated to the Sleeve, NoSleeve and Numerosity conditions; two captured the participants responses at the time the weighting scale was presented separately for the left and right hand; one captured text information given to our participants at the beginning and the end of the each session; one included button presses that happened outside the response window; and one included the four videos used for training (only for the first session). The six head motion parameters were again added as covariate of no interest. Analyses of variance were used to compare the Sleeve and NoSleeve conditions to each other (within-subjects ANOVA), and to baseline (one-way ANOVA). As for Exp. #1-3, unless specified otherwise, the ANOVAs were computed within the cerebellar mask, at $p_{FWE} < 0.05$.

To test whether the videos used for the weight estimation task elicited activity in the areas to be found active for general action observation, an additional GLM was computed within a binary mask obtained by the global null conjunction of Exp. #1, 2 and #3 [$Exp\#1_{ActionOBS\text{-}CtrlOBS}$ OR $Exp\#2_{ActionOBS\text{-}CtrlOBS}$ OR $Exp\#3_{ActionOBS\text{-}CtrlOBS}$] ($t_{FWE} = 2.06$) from the one-way ANOVAs that included the ActionOBS-CtrlOBS from all three experiments. Results are shown at $p_{FWE} < 0.05$.

5.3.6 Analyses of behavioral data

Task performance scores were calculated as proportion of correct responses. We checked their normality using the Lilliefors test. Performance for the Sleeve and for the NoSleeve-Sleeve difference were normally distributed (both $P > 0.12$). The performance in the NoSleeve condition and the average score of Sleeve and NoSleeve violated normality (both $P < 0.002$). Accordingly, we used nonparametric tests as our main approach, and parametric analyses (ANOVAs and Bayesian analyses) were only used to supplement analyses for the Sleeve and NoSleeve-Sleeve difference.

To make sure the deficits in action perception did not occur because of visual tracking problems, eye tracking data were collected from four patients and seven healthy subjects; these control data as well as the methods for eye tracking are presented in the supplementary material.

5.3.7 Data availability

Data will be available online on zenodo upon acceptance of the manuscript.

5.4 Results

5.4.1 Localization of action observation activations in the cerebellum and their reliability

Using fMRI we found that viewing goal directed hand actions compared to control stimuli (ActionOBS-CtrlOBS) in Exp. #1 bilaterally recruited cerebellar Lobules VI, VIIb and VIIIa (Table 2, Fig 2A and S1). Overlapping cerebellar activity observed in our experiments with the meta-analysis of Van Overwalle and colleagues (Van Overwalle et al. 2014) (blue clusters of Fig 2A, and Supplementary results) reveals that only a small portion of the right lobule VI is common among the two studies. To test whether the limited overlap is due to subtracting our control condition, we overlapped the meta-analysis map with a global null conjunction of our conditions (*i.e.* ActionOBS OR CtrlOBS, $p_{FWE} < 0.05$, $t = 2.8$). The overlap remained limited to right Lobule VI (Fig 2B).

Considering this inconsistency, we (1) replicated the experiment on a different scanner in two new groups of participants and (2) explored how many of our participants had activations in the cerebellum. Replicating the analysis in new participants confirmed the cerebellar recruitment, despite differences in scanning location and parameters (Fig 2C-E, Table 2-3). Looking at individual participants revealed that all but four (all from Exp. #1) of the 79 participants had significant activations to the ActionOBS-CtrlOBS contrast when tested at $P < 0.001$ ($t = 3.1$) within the cerebellum (blue circles in Fig 2G). The majority (68/79, 86.1%) additionally had >10 voxels activated (Fig 2G and first 5 columns of Table S4) and most had at least 10 voxels in each of the cerebellar lobules identified in the group (ROIs encompassing lobule VI or lobule VIIb+VIIIa). A binomial distribution indicates that finding 10 or more voxels significant by chance at $P = 0.001$ in a ROI of 2085 voxels (the largest ROI we have) is highly unlikely ($P < 2x10^{-5}$).

To compare the reliability of cerebellar activations with those of the cerebrum, we took three regions consistently associated with the action observation system, Brodmann area (BA) 44, the PF complex and SI (Keysers and Gazzola 2009; Caspers et al. 2010; Molenberghs et al. 2012), and counted activated voxels in these regions subject by subject (Table S4, last 6 columns). Chi^2 tests comparing the proportion of participants with zero voxels activated in the 4 cerebellar and 6 cerebral regions using Fisher's exact test in R indicated that for Exp#1 and#2 the proportion with zero voxels activated was larger in the cerebellum (Exp1, $P = 0.001$; Exp2, $P = 0.004$; Exp3, $P = 0.86$).

Table 2. Cerebellar activations to ActionOBS-CtrlOBS for Exp. #1 to #3. Regions with ActionOBS-CtrlOBS≥4.31 labelled using SPM Anatomy Toolbox. Results are shown at $p_{FWE} < 0.05$ with cluster size >10 voxels. From left to right: the cluster size in number of voxels, the number of voxels falling in a cyto-architectonic area, the percentage of the cluster that falls in the cyto-architectonic area, the hemisphere (L = left; R = right), the name of the cyto-architectonic area when available or the anatomical description, the percentage of the area that is activated by the cluster, the t values of the peaks associated with the cluster followed by their MNI coordinates in mm.

Cluster size	# Voxels in cyto	% Cluster	Hem	Cyto or anatomical description	% Area	Peak Information T	x	y	z
Exp. #1 ActionOBS-CtrlOBS p_{FWE}<0.05, t=4.31									
655	523	79.8	R	Lobule VI (Hem)	29	9.06	28	-54	-26
						7.72	20	-70	-22
	61.8	9.4	R	Area FG4	12.6	5.60	24	-44	-18
	14.4	2.2	R	Lobule VIIa crusI (Hem)	0.4				
	11.9	1.8	R	Area hOc3v [V3v]	1.4				
	11.9	1.8	R	Area FG1	4.8				
340	328.6	96.7	L	Lobule VI (Hem)	17.5		-28	-54	-26
						6.20	-20	-68	-24
249	103.4	41.5	R	Lobule VIIIa (Hem)	14.2	6.38	28	-60	-54
						6.08	20	-66	-54
						5.51	30	-54	-52
	97.1	39	R	Lobule VIIb (Hem)	14.8	8.23	16	-76	-50
	24.1	9.7	R	Lobule VIIIb (Hem)	3.4				
	12.9	5.2	R	Lobule VIIIa (Verm)	6.1				
162	85.9	53	L	Lobule VIIIa (Hem)	11.3	7.18	-22	-62	-52
	51.9	32	L	Lobule VIIb (Hem)	7.6	6.68	-18	-70	-50
						6.59	-16	-74	-48
	22	13.6	L	Lobule VIIIb (Hem)	3.6				
Exp. #2 ActionOBS-CtrlOBS p_{FWE}<0.05, t=4.31									
398	131.3	33	R	Lobule VIIIb (Hem)	18.3	8.66	20	-58	-52
	105.1	26.4	R	Lobule VIIIa (Hem)	14.5	8.10	12	-70	-48
	50.4	12.7	R	Lobule IX (Hem)	7.2				
	38.4	9.6	R	Lobule VIIb (Hem)	5.9	8.28	16	-72	-52
	20.5	5.2	R	Lobule VIIIa (Verm)	9.8				
262	205.9	78.6	R	Lobule VI (Hem)	11.4	7.69	30	-50	-24
						5.03	20	-68	-22
	44.9	17.1	R	Area FG4	9.2				
	10.4	4	R	Area FG3	1.6				
153	67.1	43.9	L	Lobule VIIIa (Hem)	8.8	7.53	-16	-66	-48
						4.78	-24	-52	-50
	53.4	34.9	L	Lobule VIIIb (Hem)	8.8	5.31	-18	-58	-52
126	94.8	75.2	L	Lobule VI (Hem)	5.1	7.01	-30	-48	-22
						5.40	-26	-56	-18
	23.4	18.6	L	Area FG4	4				
Exp. #3 ActionOBS-CtrlOBS p_{FWE}<0.05, t=4.31									
514	433.8	84.4	L	Lobule VI (Hem)	23.2	8.45	-26	-52	-18
						6.72	-18	-68	-22
	43.3	8.4	L	Area FG4	7.3				
	15.8	3.1	L	Lobule V (Hem)	2.2				
	12.9	2.5	L	Area FG3	1.6				
452	372.8	82.5	R	Lobule VI (Hem)	20.7	6.89	28	-52	-22
						5.96	18	-70	-22
						5.88	20	-68	-24
	61.3	13.6	R	Area FG4	12.5				
402	139.9	34.8	R	Lobule VIIIa (Hem)	19.3	8.34	26	-58	-54
	99.8	24.8	R	Lobule VIIIb (Hem)	13.9	5.32	18	-52	-50
	76.5	19	R	Lobule VIIb (Hem)	11.7	8.88	14	-74	-50
	22.6	5.6	R	Lobule VIIIa (Verm)	10.8				
85	47.8	56.2	L	Lobule VIIIa (Hem)	6.3	6.19	-10	-74	-50
	32.5	38.2	L	Lobule VIIb (Hem)	4.8				
75	35.1	44.5	L	Lobule VIIIa (Hem)	4.6	6.11	-22	-58	-46
						6.10	-32	-52	-50
	24.8	31.3	L	Lobule VIIIb (Hem)	4.1				

Table 3. Comparison between Exp #1, #2 and #3 in number of voxel and peak distance per cluster of activity. For each of the four cerebellar clusters, and for each experiment separately, the number of voxels surviving $p_{FWE} < 0.05$ for the contrast ActionOBS-CtrlOBS is reported. The fourth column reports the number of voxels counted within the conjunction of the three experiments. The last row indicates the number of cerebellar voxels not falling within the region of interest. Columns 5-7 indicate the minimum Euclidean distance between the activation-peaks identified belonging to the four clusters by the Anatomy toolbox for SPM.

	Number of voxels				Min Euclidean distance		
	Exp1	**Exp2**	**Exp3**	**Exp1&2&3**	**Exp1,Exp**	**Exp1,Exp**	**Exp2,Exp**
Lob VI R	336	115	454	88	2.0	2.0	2.0
Lob VI L	537	216	391	202	7.5	2.8	4.0
LobVIIIa/VIIb R	148	84	130	20	4.5	2.8	3.5
LobVIIIa/VIIb L	223	198	265	120	4.9	6.3	7.2
OutsideROIs	179	344	299	56			

When combining all three experiments, the difference in proportion became highly significant ($P < 0.001$), with the cerebral ROIs hosting significant voxels in a larger proportion of participants than the cerebellar ROIs. Consistency maps indicated that the right Lobule VI hosted the most consistently activated voxel with 30 participants having significant activations in that specific voxel (Fig 2F).

In summary we find that our task reliably activates the cerebellum at the individual and group level, and across scanning location and pipelines. Despite the high reliability of our task the results however only overlap with those in the literature in a small part of right Lobule VI, and remain less reliable than cerebral activations.

5.4.2 Cerebellar activation to the weight discrimination task

Observing an arm lifting an object to judge its weight activates several regions of the cerebellum (Fig 3A, B and Table 4, $p_{FWE} < 0.05$, $t = 2.8$). The responses to lifting movements overlap with the ALE-meta-analysis maps (Van Overwalle et al. 2014) beyond Lobule VI, in bilateral Lobule VIIa crus I. Computing the GLM of the weight discrimination experiment within the global null mask of the previous three experiments shows that all clusters observed in Exp. #1-3 were activated by the observation of lifting movement (Fig 3C,D, Table 4).

What aspect of action observation is processed in the cerebellum? By disentangling the activity common to the Sleeve and NoSleeve conditions mentioned above (Conjunction Sleeve & NoSleeve) from that specific to the NoSleeve condition (NoSleeve-Sleeve), we can attempt to identify regions involved in kinematic and shape processing, respectively. The eye-tracking maps from the control participants show that the two conditions are indeed explored differently (Fig S2A). When the arm was covered participants focused similarly on the proximal and distal part of the arm ($t_{(12)} = 1.523$, $P = 0.154$) but if no sleeve was present participants focused significantly more on the proximal part of the arm ($t_{(12)} = -9.482$, $P < 0.001$) that reveals shape information in the upper arm musculature.

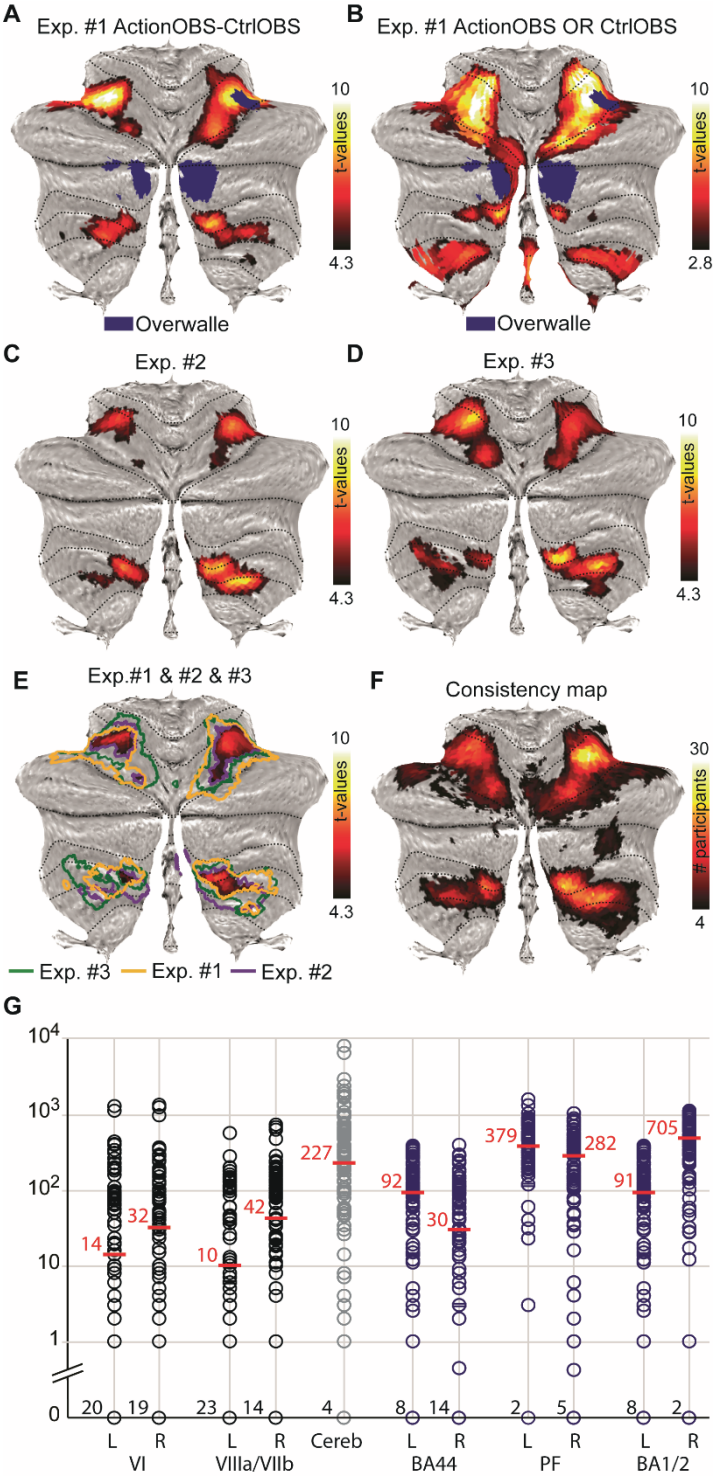
A
Exp. #1 ActionOBS-CtrlOBS
10
t-values
4.3
Overwalle
B
Exp. #1 ActionOBS OR CtrlOBS
10
t-values
2.8
Overwalle
C
Exp. #2
10
t-values
4.3
D
Exp. #3
10
t-values
4.3
E
Exp.#1 & #2 & #3
10
t-values
4.3
Exp. #3
Exp. #1
Exp. #2
F
Consistency map
30
participants
4
G
10^4
10^3
10^2
10
1
0
14
32
10
42
227
92
30
379
282
91
705
20
19
23
14
4
8
14
2
5
8
2
L
R
L
R
Cereb
L
R
L
R
L
R
VI
VIIIa/VIIb
BA44
PF
BA1/2

Fig 2. Reliability of cerebellar action observation activations. (A-B). In blue the maps presented by Van Overwalle and colleagues in 2014, and the results of the ActionOBS-CtrlOBS contrast of Exp. #1 in the hot color scale in (A) and of the global null conjunction ActionOBS OR CtrlOBS for Exp. #1 in (B), both at $p_{FWE} < 0.05$. (C-D) ActioOBS-CtrlOBS related activity for Exp. #2 and #3 respectively. $p_{FWE} < 0.05$, t = 4.3. (E) Activations common to Exp. #1-3. Yellow, blue and green contours indicate the borders of the clusters shown in A, C and D to facilitate the qualitative comparison. (F) Consistency map computed on the smoothed data for the ActionOBS-CtrlOBS ($p_{unc} < 0.001$, t = 3.1) contrast across the three experiments. The hot scale indicates the number of participant for which a particular voxel was significantly activated by the ActionOBS-CtrlOBS contrast. (G) Circles indicate the number of voxel a given subject had in each of the four cerebellar clusters (first four columns, black circles), in total in the cerebellum (fifth column, gray circles), and in three cortical regions also commonly activated by the ActionOBS-CtrlOBS constrast. The median is indicated by the red lines and numbers. Data are presented on a logarithmic scale and the number of participants having no voxels in a particular cluster is indicated on the x-axis.

Table 4. Cerebellar activations to the weight discrimination task. Results are shown at $p_{FWE} < 0.05$ with cluster size >10 voxels. Conventions as in Table 2.

Cluster size	#Voxels in cyto	% Cluster	Hem	Cyto or anatomical description	% Area	Peak Information			
						T	x	y	z
Sleeve OR NoSleeve, pFWE<0.05, t>2.8									
6254	898.6	14.4	L	Lobule VI (Hem)	48	7.02	-8	-76	-28
						6.87	-6	-78	-24
						6.22	-30	-58	-30
	797.1	12.7	R	Lobule VI (Hem)	44.2	6.86	28	-64	-24
						6.37	36	-46	-32
	793.3	12.7	L	Lobule VIIa crusI (Hem)	26.1	7.09	-36	-64	-30
						7.07	-40	-64	-32
						6.33	-44	-58	-28
	573.9	9.2	R	Lobule VIIa crusI (Hem)	17.7				
	373	6	L	Lobule VIIIa (Hem)	49	6.73	-8	-72	-46
	296.8	4.7	L	Lobule VIIb (Hem)	43.7				
	230.3	3.7	R	Lobule VIIIa (Hem)	31.7				
	199.9	3.2	L	Lobule VIIa crusII (Hem)	12.2				
	169.6	2.7	R	Lobule VIIb (Hem)	25.9	6.09	30	-64	-50
	146.1	2.3	R	Lobule VIIIa (Verm)	69.7				
	132.6	2.1	L	Lobule VIIIb (Hem)	21.9				
	130.8	2.1	L	Lobule VIIIa (Verm)	88.3				
	121.3	1.9	L	Lobule IX (Hem)	19.5				
	73.1	1.2	R	AreaFG3	11.2				
	72.6	1.2	R	Lobule VIIa crusII (Hem)	5.1				
	69.4	1.1	R	Lobule VIIIb (Hem)	9.7				
	64.4	1	L	Lobule VI (Verm)	30.7				
	59.6	1	R	Lobule VI (Verm)	25.7				
	46.5	0.7	R	Area FG4	9.5				
	46.3	0.7	R	Lobule IX (Hem)	6.6				
	42.5	0.7	R	Area FG2	13.1				
	38.1	0.6	R	Area FG1	15.3				
	36	0.6	L	Lobule VIIb (Verm)	117.6				
	33.6	0.5	L	Lobule VIIIb (Verm)	54.5				
	32.5	0.5	R	Lobule VIIIb (Verm)	45.1				
	31.9	0.5	R	Lobule VIIb (Verm)	97.3				
	24.3	0.4	L	AreaFG3	2.9				
	17.5	0.3	R	Lobule VIIa crusII (Verm)	30.8				
	16.9	0.3	R	Area hOc4v [V4(v)]	2.7	6.23	36	-74	-22
	14.3	0.2	L	Area FG2	2.8				

Sleeve OR NoSleeve, masked with Exp. #1-3, pFWE<0.05, t>2.4									
585	451.8	77.2	R	Lobule VI (Hem)	25	6.95	28	-64	-24
						5.83	34	-46	-32
						5.64	30	-54	-32
						4.82	24	-72	-22
						4.26	16	-72	-22
	56.9	9.7	R	Area FG4	11.6	5.1	32	-50	-22
	33.4	5.7	R	AreaFG3	5.1	5.2	36	-40	-26
						4.72	40	-46	-26
	16.4	2.8	R	Area FG2	5	5.91	44	-58	-26
	12.6	2.2	R	Area FG1	5.1	6.04	34	-60	-20
	11.1	1.9	R	Lobule VIIa crusI (Hem)	0.3				
393	93.8	23.9	R	Lobule VIIIa (Hem)	12.8	4.36	28	-60	-52
	72.3	18.4	R	Lobule VIIIb (Hem)	10				
	59.7	15.2	R	Lobule VIIb (Hem)	9	5.39	28	-64	-52
						4.82	26	-66	-50
						4.61	24	-68	-48
	57.4	14.6	R	Lobule VIIIa (Verm)	27.1	4.6	6	-72	-38
						6.13	10	-72	-44
	32	8.2	R	Lobule IX (Hem)	4.5	5.03	16	-56	-46
						4.55	14	-54	-50
	11.2	2.9	R	Lobule VIIb (Verm)	34	4.92	0	-76	-34
390	348.5	89.4	L	Lobule VI (Hem)	18.6	5.57	-26	-68	-24
						4.91	-32	-52	-30
						4.64	-36	-46	-28
						4.59	-34	-48	-26
						2.91	-24	-50	-24
	16	4.1	L	AreaFG3	1.9				
	10	2.6	L	Lobule VIIa crusI (Hem)	0.3	5.48	-44	-54	-30
						4.73	-38	-52	-34
262	111.5	42.6	L	Lobule VIIIa (Hem)	14.6	6.81	-8	-72	-46
						4.89	-28	-52	-50
						5.41	-22	-60	-48
	72.4	27.6	L	Lobule VIIIb (Hem)	11.9				
	27.1	10.4	L	Lobule VIIb (Hem)	4	5.69	-20	-72	-48
						5.65	-22	-70	-46
						5.49	-22	-66	-44
Sleeve AND NoSleeve, pFWE<0.05, t>4.5									
1742	418.1	24	L	Lobule VIIa crusI (Hem)	13.8	7.09	-36	-64	-30
						7.07	-40	-64	-32
	338.8	19.4	L	Lobule VI (Hem)	18.1	7.02	-8	-76	-28
						6.87	-6	-78	-24
						6.22	-30	-58	-30
	194.6	11.2	L	Lobule VIIIa (Hem)	25.6	6.73	-8	-72	-46
	179.3	10.3	L	Lobule VIIb (Hem)	26.4				
	52.5	3	R	Lobule VIIb (Hem)	8	6.09	30	-64	-50
	51.4	2.9	L	Lobule VIIa crusII (Hem)	3.1				
	37.4	2.1	L	Lobule VIIIa (Verm)	25.3				
	32.5	1.9	R	Lobule VIIIa (Hem)	4.5				
	31.9	1.8	L	Lobule VI (Verm)	15.2				
	29.6	1.7	R	Lobule VIIIa (Verm)	14.1	6.06	10	-72	-44
	27.6	1.6	L	Lobule VIIb (Verm)	90.2	5.93	-22	-70	-44
	24.1	1.4	R	Lobule VI (Verm)	10.4				
	22.6	1.3	L	Lobule IX (Hem)	3.6				
	20.1	1.2	L	Lobule VIIIb (Hem)	3.3				
	16.1	0.9	R	Lobule VI (Hem)	0.9				
	13.8	0.8	L	Area FG2	2.7				
	13.3	0.8	R	Lobule VIIa crusII (Hem)	0.9	6.33	-44	-58	-28
	10.3	0.6	R	Lobule VIIb (Verm)	31.3				

593	307.8	51.9	R	Lobule VI (Hem)	17.1	6.86	28	-64	-24
						6.37	36	-46	-32
						5.68	32	-54	-34
						5.5	24	-76	-20
	178.4	30.1	R	Lobule VIIa crusI (Hem)	5.5	5.67	38	-62	-30
	33.3	5.6	R	Area FG2	10.2	5.99	40	-68	-22
						5.88	44	-60	-26
	29.3	4.9	R	AreaFG3	4.5	5.42	36	-40	-28
	25.3	4.3	R	Area FG1	10.2	5.98	34	-60	-20
	11.3	1.9	R	Area hOc4v [V4(v)]	1.8	6.23	36	-74	-22
Sleeve AND NoSleeve, masked with Exp. #1-3 pFWE<0.05, t>3.9									
321	237.1	73.9	R	Lobule VI (Hem)	13.1	6.95	28	-64	-24
						5.83	34	-46	-32
						5.64	30	-54	-32
						4.82	24	-72	-22
						4.26	16	-72	-22
	27	8.4	R	AreaFG3	4.1	5.2	36	-40	-26
						4.72	40	-46	-26
	21.9	6.8	R	Area FG4	4.5	5.1	32	-50	-22
	16.4	5.1	R	Area FG2	5	5.91	44	-58	-26
	10	3.1	R	Lobule VIIa crusI (Hem)	0.3				
210	93.4	44.5	L	Lobule VIIIa (Hem)	12.3	6.81	-8	-72	-46
						5.41	-22	-60	-48
	44	21	L	Lobule VIIIb (Hem)	7.3	5.69	-20	-72	-48
					4	5.65	-22	-70	-46
						5.49	-22	-66	-44
	27.1	12.9	L	Lobule VIIb (Hem)		4.89	-28	-52	-50
127	38.3	30.1	R	Lobule VIIIa (Verm)	17.9	6.13	10	-72	-44
						4.6	6	-72	-38
	26.4	20.8	R	Lobule VIIIa (Hem)	3.6	4.36	28	-60	-52
	26.3	20.7	R	Lobule VIIb (Hem)	3.9	5.39	28	-64	-52
						4.92	0	-76	-34
						4.82	26	-66	-50
						4.61	24	-68	-48
70	52.4	74.8	L	Lobule VI (Hem)	2.8	4.91	-32	-52	-30
						4.64	-36	-46	-28
						4.59	-34	-48	-26
66	64.4	97.5	L	Lobule VI (Hem)	3.4	5.57	-26	-68	-24
15	11.4	75.8	R	Lobule IX (Hem)	1.6	5.03	16	-56	-46
						4.55	14	-54	-50

Results from the fMRI data indicate that in contrast to the conjunction that revealed consistent cerebellar involvement for kinematic processing, at FWE correction at peak level nothing survive for both the Sleeve-NoSleeve and the NoSleeve-Sleeve contrast within the cerebellum ($t = 4.42$, $P > 0.05$), while 22 voxels in the fusiform area FG4 become apparent for the contrast NoSleeve-Sleeve when the analyses is run for the whole brain ($t = 5.4$, $P < 0.05$). Accordingly, the cerebellum is significantly recruited by the kinematic cues common to both conditions (Fig 3), but not by the differential shape cue that the NoSleeve-Sleeve contrast situates in the ventral visual stream instead.

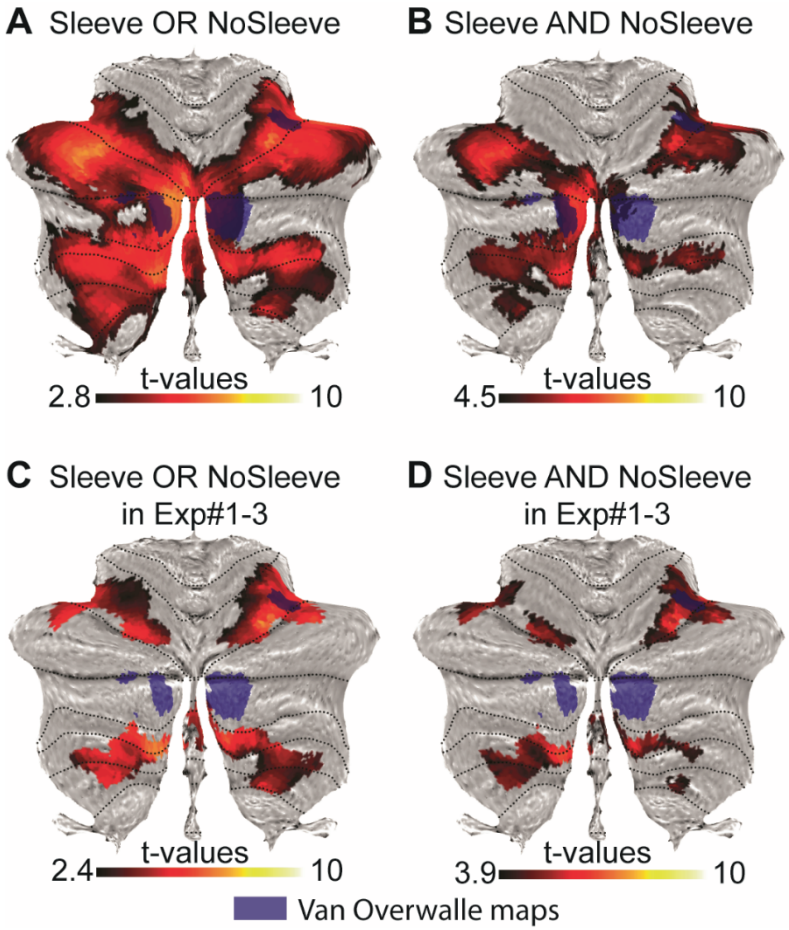

Fig 3. fMRI results of the weight discrimination task. (A) Voxels significantly activated by either the Sleeve (only kinematic information available) or the NoSleeve (both kinematic and shape information) condition (global null conjunction in SPM at $p_{FWE} < 0.05$, t = 2.8, min 10 vx). In blue the clusters identified by Van Overwalle et al. 2014, as responding to action perception. (B) Voxels activated by both (conjunction-conjunction in SPM) by the NoSleeve and Sleeve conditions ($p_{FWE} < 0.05$; t = 4.5, min 10 voxels). (C) Same as in (A) but within the clusters of activation found in Exp. #1 to #3 (Exp.#1 > 0 OR Exp.#2 > 0 OR Exp.#3 > 0). Results are shown at $p_{FWE} < 0.05$, t = 2.8, min 10 voxel. (D) Same as in (C) but within the clusters of activation found in Exp. #1 to #3 ($p_{FWE} < 0.05$; t = 3.9, min 10 voxels). All activations are shown on the flat map of the cerebellum offered by the SUIT toolbox.

5.4.3 Cerebellar contribution to action perception

The Mann-Whitney U test on task performance revealed a significant difference between SCA6 and controls for the Sleeve condition ($N_{SCA6} = 21$; $N_{ctrl} = 31$; U = 199.5; P < 0.009), in which participants depend on the kinematic information (Fig 4A). The same test revealed

that the gain of performance in the NoSleeve compared to the Sleeve condition (i.e. NoSleeve performance – Sleeve performance) did not differ significantly across groups (N_{SCA6} = 21; N_{ctrl} = 31; U = 274.5; P > 0.34). Not surprisingly, the two groups therefore also differed when the total performance was considered, including both the Sleeve and NoSleeve trials (N_{SCA6} = 21; N_{ctrl} = 31; U = 183; P < 0.004). Using d' instead of percent correct led to similar conclusions. To explore whether our pattern of findings, which included a significant group difference for the Sleeve condition and a lack of significant group difference in the gain of performance, was evidence that the cerebellum contributes to kinematic but not shape processing in our experiment, we performed a Bayesian t-test in JASP. The Bayes factors in favour of the alternative hypothesis Ctrl > SCA6 were BF = 14.7 (Sleeve) and BF = 0.19 (NoSleeve-Sleeve performance). Accordingly, we have strong evidence for a group difference in kinematic processing (Sleeve), and moderate evidence for a lack of difference for shape processing (NoSleeve-Sleeve).

To explore if this group difference in the performance could be due to the less than ideal matching on gender, we performed two further analyses. First, we performed a parametric ANOVA on the performance in the Sleeve condition with 2 Groups (SCA6 vs Ctrl) x 2 Genders. The interaction of Gender x Group was not significant ($F_{(1,48)}$ = 2.66, P = 0.11), suggesting that the group difference does not depend on gender. Second, we created control groups that were exactly matched in gender to the SCA6 group by sub-selecting 6 males out of the 16 available in the control group, keeping all the 15 females. There are 8008 ways to subsample 6 males out of 16, and for each of them, we calculated the p-value for the group difference in total performance using the Mann-Whitney U one tailed test. The median p-value across the 8008 subsamples was P = 0.016 and 7675 of the 8008 (96%) had P < 0.05 (Fig 4B). This confirms that compared to the majority of randomly subsampled, gender matched control groups, the SCA6 group shows impaired performance in our task.

To explore whether there is a significant association between the severity of the degenerative disorder and the performance in our task, we calculated the Spearman rank order correlations between the total performance score and the SARA score for the 17 patients for which we do have the SARA score (Fig 4C). We found that the association is significant: R = -0.55, $t_{(15)}$ = -2.54, P < 0.022.

Finally, to explore whether the perceptual impairment we observe in SCA6 patients would also be visible in implicit measures, we added eye tracking in our last participants (4 SCA6 and 7 controls), which did not show any significant group difference (Supplementary results 2.3). Given the small sample size only large group differences could have been detected, however, the qualitatively similar pattern in the two groups suggests that SCA6 did not severely alter how subjects explored the stimuli in space and time.

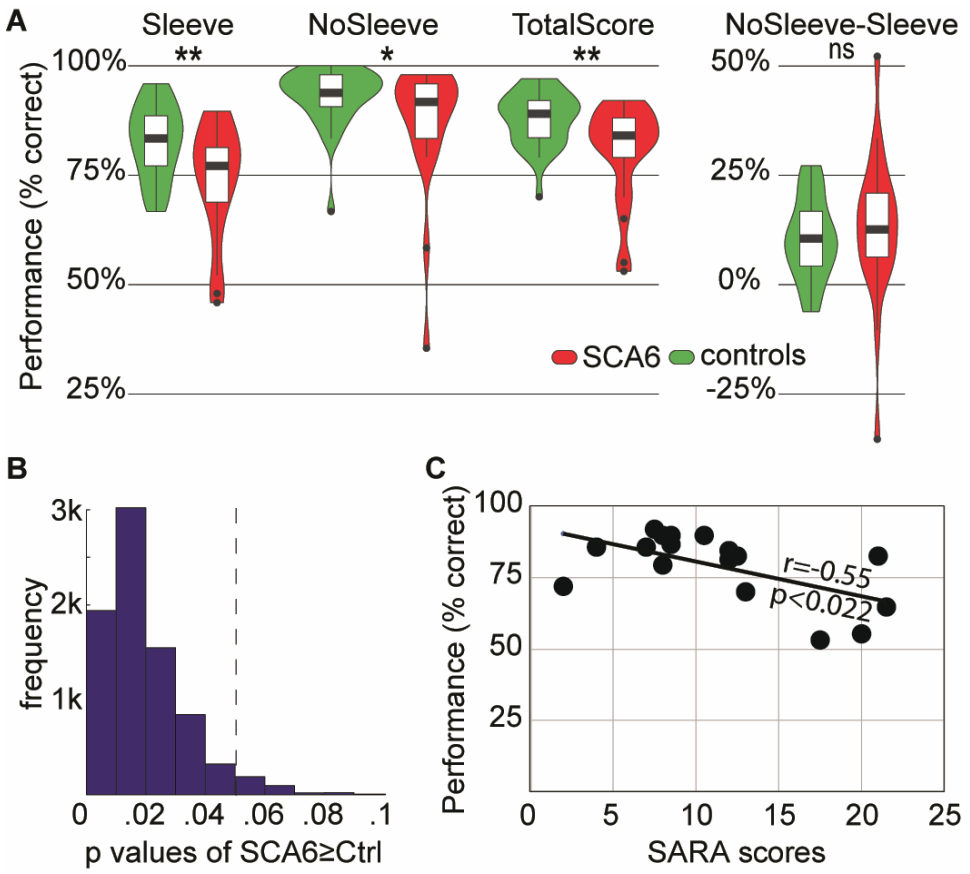

Fig 4. Weight discrimination task in SCA6 and healthy subjects. (A) Violin plot of the performance (percent correct responses) in the weight-discrimination task for the 21 SCA6 patients (red) and 31 controls (green) for the different conditions. *:P < 0.05, **:P < 0.01 using Mann-Witney U-tests to compare SCA6 vs controls group in each condition. (B) Distribution of p-values obtained from the 8008 possible subsamples of gender matched control groups, again using the Mann-Whitney U test to compare the total score (Sleeve and NoSleeve trials together) across groups. (C) The significant negative association between symptom severity (SARA) and total score in the weight perception task. The r-value reflects the non-parametric Spearman rank-order correlation. Higher SARA scores reflect more severe symptoms and predict more perceptual impairment.

5.5 Discussion

Our primary aims were (a) to explore whether and where the cerebellum is robustly activated by the observation of other individual's hand actions, of others, and (b) whether disrupting the cerebellum leads to significant impairments in hand action observation.

Regarding activations, using scanning parameters that include the entire cerebellum (both in terms of field of view during acquisition and bounding box during analysis) we found that across three studies and a total of 79 participants, the cerebellum was consistently recruited by the contrast between goal-directed hand actions and meaningless movements of the hand close to an object. Single subject analyses confirmed that the cerebellum was recruited in all but 4 participants. More specifically, we find that activity is reliably induced in the lateral hemispheres of lobule VI, and in a cluster including Lobules VIIb and VIIIa. All these activations are bilateral. Without using smoothing, it is apparent that the dorsal cluster in Lobule VI is distinct from activity in the ventral visual pathway, and is thus not the result of bleeding of activity from visual neocortical regions. Each of these clusters were found to be activated in the majority of individual participants. Together these results provide strong evidence that the cerebellum is consistently recruited by hand action observation.

This raises the question of why former studies failed to consistently report cerebellar activations. Our comparison of pipelines identifies two potential reasons: (i) up to SPM8, the default bounding box for analyses prevented the identification of some of the cerebellar clusters, and (ii) most studies focusing on the cerebrum have to choose between a larger field of view (i.e. more spatial coverage) vs. a shorter acquisition time (i.e. increased task sensitivity), which often ends in favoring a smaller field of view therefore cutting out the cerebellum in at least some participants. At the second level of analysis, if part of the cerebellum is missing in the field of view for some of the participants, this region is entirely removed from the search volume on which statistical analyses are computed across all subjects. This may have further reduced the consistency with which cerebellar activity is reported. Finally, a comparison between the number of participants activating our cerebellar ROIs compared to classic cerebral ROIs such as premotor area BA44 or inferior parietal complex PF, showed that the cerebellar ROIs indeed are slightly less reliably recruited, providing an additional factor. Overall, our three studies provide clear evidence that with proper measurement procedures and analyses pipelines, cerebellar recruitment during hand action observation can be demonstrated. The finding that these same regions are also activated when using a different, weight judgement task (Exp. #4) in our sample shows that this consistency does not depend on a specific task.

It is interesting that the specific locations of consistent activations in our study are overlapping with or adjacent to regions that have been associated with the sensorimotor control of hand actions in the cerebellum (Schlerf et al. 2015). One of our foci was localized in the anterior part of lobule VI, which is associated with the primary sensorimotor map of

finger motions in the cerebellum (Grodd et al. 2001; Schlerf et al. 2015). Our second focus was localized in the posterior inferior lobule VIIb expanding into lobule VIIIa. Its location is spatially adjacent to the secondary sensorimotor finger map (Grodd et al. 2001; Schlerf et al. 2015). This is in line with the notion that cerebro-cerebellar loops involved in fine kinematic control of hand actions may also serve as a valuable system to process fine kinematics of observed actions (Miall 2003; Wolpert et al. 2003; Fuentes and Bastian 2007; Gazzola and Keysers 2009; Rizzolatti and Sinigaglia 2010; Sokolov et al. 2017).

To explore whether the cerebellum is necessary for extracting information from the kinematics of the hand actions of others, we tested whether patients with SCA6 are impaired in a weight-lifting task that has been shown to depend on precise processing of hand movement kinematics (Hamilton et al. 2007). Our results indicate that SCA6 patients are indeed impaired in their kinematic processing as borne out by a group difference in the Sleeve condition that impoverishes muscle shape information. This impairment was more pronounced in patients with more severe SCA6 symptoms. Interestingly, when we analysed the data of the paradigms without the sleeves, we found that muscle shape processing appears to be preserved, as Bayesian statistics confirmed that the patients benefited from the additional muscle shape as much as the controls did. These results complement the results of the only other study that has, to our knowledge, examined the impact of cerebellar damage in action observation (Cattaneo et al. 2012) in that the two studies probed different aspects of hand action observation. In the task of Cattaneo, participants viewed four still frames of an action, and had to decide which was not part of that action. Solving that task does not require fine kinematic analyses, but an understanding of whether a particular hand-object interaction would be appropriate to achieve a particular goal. In our task, all movies show a hand successfully lifting an object, and performance thus depends on analysis of kinematics. That SCA6 patients were impaired in the Sleeve condition, in which kinematics was the primary cue, but could benefit from additional muscle shape, highlights that cerebellar degeneration particularly impairs kinematic processing. Moreover, these findings dovetail with our fMRI results, which show consistent cerebellar activity for the kinematic stimuli but not for the additional shape information provided in the NoSleeve condition.

As the cerebellum is involved in eye movement control, we were concerned that patients may be compromised in their ability to follow the movements of the arm with their gaze. However, our control data obtained from a small number of SCA6 patients does not suggest severe impairments in how our patients deploy their gaze. Future studies could include fMRI of SCA6 patients to explore where in the cerebellum degeneration alters task-related activity, and whether this includes regions associated with gaze-control. A previous voxel-based morphometry (VBM) study points to a loss of gray matter in the hemispheres of lobule VI as the primary cause of upper limb ataxia triggered by SCA6 (Rentiya et al. 2017), which is in close vicinity to and partly overlaps with regions in which we find cerebellar activations to action observation, but is lateral relative to the sections of lobule VI mostly associated with eye movements (Fig S3).

Because interfering with one node of the action observation network is known to disrupt the activity in the other connected nodes (Valchev et al. 2016), this should not be taken as evidence that the cerebellar activity, per se, is necessary for the processing of observed actions. It could be that SCA6 disrupted activity in other connected brain regions that in turn are necessary for the conscious report of weight. Instead, our findings should be interpreted at the network level, to suggest that the cerebellum is a necessary node in a network that contributes to optimal perception and interpretation of observed hand actions.

In the light of our findings we believe that it is time to consider the cerebellum a reliable and necessary component of the network that allows us to process the kinematics of observed hand actions. Clinically, one of the core complaints of many stroke survivors and their spouses are impairments in social cognition (Hillis 2014). These social sequelae are often not on the radar of neurological staff. We hope that by showing that SCA6 patients have deficits in perceiving the kinematics of the actions performed by other individuals – deficits that gets worse with the severity of the disease - our results contribute to an increased awareness of the social consequences of neurological disorders affecting the cerebellum. Being impaired in perceiving what other individuals around us do is likely to impact the way we related to others and thereby reduce our wellbeing.

5.6 Acknowledgements

We thank Filippo Migliorati and Rajat Thomas for their support during data analysis. We thank Marc Thioux, Anita Sibeijn-Kuiper, Judith Streurman and Teresa De Sanctis for help in acquiring the MRI data. We thank Jessica Willems, Esther Brusse, Henk-Jan Boele, Ruben van der Giessen, Cullen B. Owens for facilitating the experiments with SCA6 patients and performing neurological examinations. We thank the Spinoza Center Amsterdam and the Neuroimaging Center at the UMCG for contributing scan time for the fMRI data acquisition. We finally thank F. Van Overwalle for providing the mirror-maps from his meta-analysis (Van Overwalle et al. 2014).

5.6.1 Author contribution

Funding was obtained by V. Gazzola, C. Keysers, C. De Zeeuw and R. Bhandari. The experiment was conceived by V.Gazzola, C. De Zeeuw and C. Keysers together with A. Abdelgabar and J. Suttrup. FMRI data were collected by J. Suttrup (Exp.#1) and R. Bhandari (Exp.#2-4) with facilitation from V.Gazzola. Behaviuoral data on healthy volunteers and SCA6 patients were collected by A. Abedlgabar, R. Broersen and S. Picard with faciliation of C. De Zeeuw. Data analysis was performed by J. Suttrup, R. Bhandari, A. Abdelgabar, R.

Broersen and V. Gazzola, with suggestions from C. Keysers and C. De Zeuuw. The manuscript was written by J. Suttrup, A. Abdelgabar, R. Broersen and V. Gazzola, with extensive input from C. Keysers and comments from all the other authors.

5.6.2 Funding

This work was supported by the Netherlands Organization for Scientific Research (056-13-017, NIHC to C. Keysers., VENI 451-09-006 to V. Gazzola, VIDI 452-14-015 to V. Gazzola), the Brain and Behavior Research Foundation (NARSAD young investigator 22453 to V. Gazzola), the BIAL foundation (Research Project 255/16 to R. Bhandari), the European Research Council of the European Commission (ERC-StG-312511 to C.K.; ERC-Adv and ERC-PoC C.I. De Zeeuw), as well as the Dutch agencies for fundamental and medical research (NWO-ALW and Zon-Mw; C.I. De Zeeuw).

5.6.3 Competing interests

The authors declare to have no competing interests.

5.7 Supplementary methods

5.7.1 Impact of different analysis pipelines

Four pipelines were computed and compared to test the effect of different spatial normalization procedures. The analyses were done in SPM8 (Wellcome Trust Centre for Neuroimaging, UCL, UK) and complemented with customized Matlab scripts (Matlab 7.14; The MathWorks Inc., Natick, USA). Common to all, data pre-processing included: slice time correction of functional images using the bottom slice, located in the posterior cerebellum, as a reference slice; realignment and co-registration of the T1-weighted anatomical to the mean functional image. Below a description of the steps that followed for each pipeline separately. Table S2 more schematically illustrates the analysis steps used for the four pipelines. For Exp. #1, the acquisition plane was tilted by 30-45° from the AC-PC plane to cover the entire cerebellum.

Pipeline I: WB_MNInorm_GLM. As commonly done in fMRI analyses, the whole brain (WB) functional images were brought to MNI space before computing the GLM, using the normalization (norm) parameter generated during segmentation of the anatomical image (final voxel size: 2 × 2 × 2 mm). We manually adjusted the SPM8 bounding box settings to [-90 -126 -72; 91 91 109] to cover the entire cerebellum.

Pipeline II: WBcut_MNInorm_GLM. Same as for Pipeline I but without adjustment of the bounding box, which was left to the default SPM8 settings [-78 -112 -50; 78 76 85]. This allowed us to identify which part of the activation was left out in previous studies focusing on the cortex.

Pipeline III: Cereb_GLM_SUITnorm. A template for cerebellar-specific normalization using a high-resolution atlas of the human cerebellum (Cereb) is available in the literature (SUIT, (Diedrichsen 2006; Diedrichsen et al. 2009), and it has been shown to improve the alignment of anatomical landmarks and increase average t-values for cerebellar functional data sets (Diedrichsen 2006). The SUIT template is in MNI space, but it is based on a group of 20 participants in order to create an average anatomical template with enough anatomical details to account for the small size of cerebellar functional regions (Diedrichsen 2006). In pipeline III, following the method suggested by (Diedrichsen 2006), after co-registration, the functional images were directly fed into the subject-level general linear models. Resulting contrast images were subsequently normalized to the SUIT-space, by first isolating the cerebellum from the T1 images using an automated algorithm from the SUIT toolbox (www.icn.ucl.ac.uk/motorcontrol/imaging/suit.html). This step resulted in a cropped anatomical image covering the cerebellum and adjacent cortical regions, which was normalized into SUIT cerebellar space. The transformation parameters obtained during the normalization were then used to normalize the contrast images resulting from the first level GLM (final voxel size: 2 × 2 × 2 mm).

Pipeline IV: WB_GLM_MNInorm. The Cereb_GLM_SUITnorm pipeline differs from traditional whole brain pipelines not only in the normalization template but also in the moment at which normalization is computed: after vs. prior to the GLM. In order to assess the impact of this difference, pipeline IV was run with the same temporal order used in pipeline III: the first level GLM used the co-registered functional images, and the normalization to the MNI whole brain template was applied on the contrast images resulting from the GLM. Normalization parameters were calculated during the segmentation of the whole-brain T1 anatomical image (final voxel size: 2 × 2 × 2 mm). In order to include the entire cerebellum, the bounding box was manually adjusted to [-90 -126 -72; 91 91 109].

Smoothing, using a 6 mm FMHW Gaussian kernel, was applied to each pipeline after normalization. Although spatial smoothing is routinely applied in the neuroimaging literature, it poses the possibility of leakage of activation between the anterior cerebellum and the temporal cortex. We therefore report our results with and without the 6 mm FMHW Gaussian filter for our WB_MNInorm_GLM pipeline, which is closest to traditional MRI analysis in the literature. The impact of smoothing on leakage between cortical and cerebellar activation is also investigated by comparing cerebellar activity resulting from whole brain analyses run on either smoothed or unsmoothed data.

The same general linear models was applied to each pipeline. Two standard box car predictors modelled the ActionOBS, CtrlOBS and static conditions, and were convolved with the canonical hemodynamic response function (HRF). The last six regressors of no interest included the displacements and rotations determined during image realignment. The ActionOBS-CtrlOBS contrast was computed at the subject-level to generate action specific activations for observation, and tested against zero with a one-sample t-test at the group level. The static condition was modelled at the first level, but for the purpose of this study, not analyzed at the second level.

The choice of the statistical threshold at which to report the group results is not trivial. First, we want to be able to compare multiple activation maps resulting from different preprocessing pipelines. Second, correction algorithms based on random field theory require a certain amount of smoothness (Brett et al. 2004), which is not given using unsmoothed data sets. All statistical maps thus are thresholded at $p_{FWE} < 0.05$ and have minimal cluster size of 10 voxels. We chose peak-level FWE-correction because we wished to (i) interpret activation of individual voxels, and, motivated by the inconsistencies of cerebellar activations in the literature, (ii) limit the risks of Type I errors.

Anatomical descriptions of cerebral activity were guided by the probabilistic cytoarchitectonic maps (Geyer et al. 1996, 1999, 2000; Amunts et al. 1999; Grefkes et al. 2001; Geyer 2004; Eickhoff et al. 2005, 2006; Caspers et al. 2006; Choi et al. 2006) implemented in the anatomy toolbox for SPM (http://www.fz-juelich.de/ime/spm_anatomy_toolbox) (Eickhoff et al. 2005, 2006, 2007).

To investigate the impact of different pipelines, we used unsmoothed contrast images resulting from the 1st-level analysis of action observation data after setting them to identical image dimensions (91 × 109 × 91) using the ImCalc function. The contrast images were then fed to group-level, one-sample t-test, GLM models (ActionOBS-CtrlOBS > 0), one for each pipeline. Voxels missing in any of the four pipelines were excluded for the analysis with exception of the voxels missing due to the bounding box size, which were coded with 0, such that differences between the pipelines could also be evaluated in the inferior posterior cerebellum. The t-values from the four group-level t-values cerebellar maps were summed up using the NIfTI toolbox (version 1.25). In line with (Diedrichsen 2006), in order to compare the results of the four pipelines without biasing the comparison a priori to any specific pipeline, we selected from the sum of the four t-maps, the location of the 5 percent of voxels with the highest t-value sums as voxels of interest. The pipelines were then compared using a repeated-measures ANOVA design that considers each voxel of interest as a 'subject', and each pipeline a repeated measurement of this 'subject' (i.e. voxel). We then planned to perform t-tests that compare each of the pipelines against the WB_MNInorm_GLM pipeline, because the whole brain analysis is most frequently used in the neuroimaging literature.

5.7.2 Consistency maps

To generate the consistency maps, the normalized, smoothed single-subject t-maps of action observation (ActionOBS-CtrlOBS > 0) from Exp.#1-3 were thresholded at the t-value corresponding to $p_{unc} < 0.001$ (T = 3.1), which binarizes the images. All single-subject maps were then added together to generate the group-level consistency map, showing for each voxel the number of participants for which the voxel was significantly activated by action observation. The number of participants needed to show that a voxel is activated more consistently than expected by chance, was calculated using a cumulative binomial distribution with 31 repetitions and an associated probability of 0.001. The resulting probability was Bonferroni corrected using the number of voxels in the search volume (170675 for the whole brain). Thus, a voxel activated by four or more participants can be considered above chance (Gazzola and Keysers 2009).

5.7.3 Eye-tracking data acquisition and analysis

Eye tracking measures of 4 patients (mean age 60.4y ± 10.6 SD; mean SARA score: 10.88 ± 8.37 SD) and 7 control participants (mean age 63.5y ± 5.7 SD) were collected during the weight discrimination task using the EyeLink® 1000 system (SR Research Ltd., Mississauga, Ontario, Canada) at 500Hz. Participants sat up straight behind a desk and kept their head placed on a Head Support (SR Research Ltd., Mississauga, Ontario, Canada), providing support for the chin and forehead during the entire task. Task stimuli were presented using PsychoPy2 (v1.84, UON, UK)(Peirce 2009) on a 19 inch TFT monitor (UltraSharp 1907FP,

Dell, TX, USA) with 300x380cm dimensions, a resolution of 1280x1080 pixels and at a refresh rate of 55Hz. Distance between participants' eyes and screen was 593 ± 22.8 mm and room background light was minimized during the task. The presented clips appeared in the middle of the presentation screen and covered 720x480 pixels. A 9-point calibration and validation was executed before starting the experiment. PsychoPy2 sent text messages to be registered in EyeLink at the beginning and end of each pair of clips for synchronization purposes.

EyeLink EDF files were converted into MATLAB-compatible (MathWorks, USA) variables using the 'edf2mat' script (JN van der Geest, Dept of Neurosci, Erasmus MC, Rotterdam) and were further analysed using custom-written MATLAB code. Data was obtained on eye-related events (i.e. blinks, fixations and saccades) by using default gaze parser settings (EyeLink 1000 User's Manual, SR Research, Ontario, Canada). Data was filtered using a Gaussian lowpass filter with a 50Hz cutoff frequency and was converted from pixels to visual degrees, using X and Y resolution values as calculated by EyeLink. We synchronized eye movement recordings with start of each pair of clips based on message event timestamps corresponding to start of the pair of clips. Then, for each clip we visually determined periods in which object lifting-associated arm movement occurred and we quantified eye-related parameters of events occurring during those periods, comparing SCA6 patients and controls. Parameters included number of saccades, blinks and fixations, duration of blinks and fixations (in milliseconds), saccade peak velocity (in visual degrees/second), saccade amplitude (in visual degrees) and distance in the horizontal and vertical plain (calculated on trial basis during 'fixation periods', representing smooth pursuit and drift). All of these parameters were calculated based on clip periods where arm movement occurred. To make a distinction between distal and proximal part of the arm, we decided on a x-coordinate (pixel 380 from left side movie) based on movies where a arm without sleeve was visible. We took into account arm movement dynamics during the movie and attempted to encompass deformations of the brachior radialis muscle during lifting in the proximal part of the arm (right side of the movie) and movements of the hand and wrist in the distal part of the arm (left side). The same x-coordinate was used for every movie analysed in both Sleeve and NoSleeve conditions.

Heat plots (Fig S2A, B) were generated based on matrices where values represented summation of gaze positions for each datapoint *during the period of arm movement*, separating Sleeve versus NoSleeve conditions. Matrices were processed using a 2-D circular averaging filter with a radius of 3 in replicate boundary setting, converted into a grayscale image and thresholded using an alphamask, so that values higher than 0.002 (on a scale of 0-1) were plotted with 75% opacity using colormap 'jet' on top of a two merged representative frames from movies in the Sleeve and NoSleeve conditions, showing begin and end-position of a lift movement. Gaze position over time was calculated from gaze positions in the V and H axis of all subjects per group (Fig S2C, D). Distance along both axis was calculated by summation of the absolute difference between sampling points during the task (Fig S2E - H). Figures were further processed in Illustrator CS6 (Adobe, USA).

The different eye tracking measures of patients and controls have been compared using pairwise independent two sample t-tests. While not being a prominent feature, previous studies have found abnormalities in saccades for SCA6 patients (Gomez et al. 1997; Buttner et al. 1998; Christova et al. 2008), based on this a priori hypothesis we have performed one-tailed tests for all saccade metrics. We have used FDR correction as a more lenient multiple comparisons correction method as opposed to the more conservative Bonferroni correction, to increase our sensitivity to group differences.

Eye tracking measurements have been performed on a subset of patients and controls, to check whether these subsets are representative for their respective groups we performed the main Group analysis on task performance. There were no significant performance differences between controls and their eye tracker subgroup ($F(1,36) = 0.6655$, $P = 0.420$, $\omega 2 = 0.0038$) nor between patients and the eye tracker patient subgroup ($F(1,22) = 1.3605$, $P = 0.256$, $\omega 2 = 0.0097$).

5.8 Supplementary Results

5.8.1 Effect of different analysis pipelines on cerebellar activation during action observation

When we mapped the activations triggered by viewing goal directed hand actions compared to control stimuli (ActionOBS-CtrlOBS) with a traditional pipeline and a bounding box encompassing the whole cerebellum, we found four main clusters of activation. Fig S1A and Table S3 locate these clusters in the bilateral Lobule VI, VIIIa and VIIb. When the smaller SPM8 default bounding box was used the activations in Lobule VIIIa were not visible as they were not included in the search volume used in the analyses (Fig S1B).

Analyzing the data with the specific cerebellar normalization and the procedure proposed by (Diedrichsen 2006; Diedrichsen et al. 2009) results in the same clusters of activity identified with the traditional approach (Fig S1C and Table S3). When the average top 5% of t-values is compared between the traditional and cerebellar specific pipeline (Fig S1E), no significant difference is observed between the two approaches ($P > 0.95$, $t = -0.06$). Bayesian paired sample t-test confirms that there is evidence for the two pipelines to give equal results ($BF_{10} = 0.043$; https://jasp-stats.org/). To investigate the impact of running the GLM in the subject space, instead of on normalized data, as it is done in the cerebellar optimized pipeline, we re-calculated the whole brain analysis following the same order of pre-processing. While at visual inspection the maps look very similar (Fig S1D), the top 5% t-values is significantly lower ($P < 0.002$, $t = 3.14$). Fig S1E also indicates a significant drop of t-values ($P < 0.001$, $t = 11.8$) when the small bounding box is used, likely due to part of the active voxels not included in the statistical computation.

In summary, these results indicate that as long as the whole cerebellum is included in the analyses, activations are preserved across different analysis pipelines. Additionally, in our data set, no clear advantage is observed when using the pipeline optimized for the cerebellum compared to the traditional one, possibly due to improvement of co-registration and normalization algorithms in the newer SPM releases, which do not make the specific adjustments for the cerebellum anymore necessary.

5.8.2 Effect of spatial smoothing on cerebellar activation during action observation

Because the dorsal cerebellum is located close to the ventral temporal lobe, one concern in reporting cerebellar activations from whole brain analyses is that smoothing could make activations of the ventral visual stream bleed into the cerebellum. Comparing results computed on unsmoothed and smoothed data indicates that spatial smoothing increases the number of super-threshold voxels during action observation (ActionOBS-CtrlOBS > 0) in the cerebellum by 168%, from 350 to 939 voxels, given the same t-value threshold of t = 5.8 (corresponding to the most stringent t value resulting from FWE of whole brain smoothed and unsmoothed results). However, smoothing caused clusters that are separated when using unsmoothed data to merge into a single cluster (arrow in Fig S1F). In particular, the merging happened within the right cerebellar lobule VI, and bilaterally between the cerebellar lobule VIIb and VIIIa. Results on the unsmoothed data confirm cerebellar activations in all previously identified clusters, including the dorsal lobule VI, supporting the notion that activations are not the result of smoothing leading to a bleeding of activation from ventral visual cortex onto the adjacent cerebellum (Fig S1G). Despite unsmooth results confirming the extensive cerebellar activation on the lobule VI, the cluster still belong to a bigger cluster encompassing the fusiform gyrus, making a clear attribution of voxels at the border to the fusiform or the cerebellum more difficult, which is evident in some of the tables. Additionally, 80% of the lobut VI cluster reported by (Van Overwalle et al. 2014) falls within the fusiform regions (FG4 in particular), suggesting that smoothing might have had a bigger impact on the meta-analysis maps computation.

5.8.3 Eye movements during the weight discrimination task

In the Sleeve condition, subjects from both groups focussed equally on the distal and proximal part of the arm (Ctrl: $t_{(12)} = 1.523$, P = 0.154; SCA6: $t_{(6)} = -0.802$, P = 0.453; Fig S2A and B, left panels). In the NoSleeve condition both groups focussed significantly more on the proximal muscles of the lower arm (Ctrl: $t_{(12)} = -9.482$, $p < 0.001$; SCA6: $t_{(6)} = -4.238$, P = 0.005; Fig S2A and B, right panels). There was no group difference in either condition (Sleeve: $t_{(9)} = 1.112$, P = 0.295; NoSleeve: $t_{(9)} = -0.197$, P = 0.848).

There were no significant group differences in any of the following parameters: number of saccades (t_7 = 2.17, P = 0.197), Saccade peak velocity (t_7 = 2.32, P = 0.197), saccade amplitude (t_6 = 1.45, P = 0.327), duration of blinks (t_5 = -0.15, P = 0.995), time lost blinking (t_9 = 0.33, P = 0.995), duration of fixations (t_6 = 1.72, P = 0.327), duration of fixation (t_8 = -1.6, P = 0.327).

We next investigated whether the trajectory of eye movement over time differed across groups. (Fig S2C). We did not observe any differences between groups for the Sleeve (V: $t_{(9)}$ = 0.163, P = 0.874; H: $t_{(9)}$ = 0.727, P = 0.486; Fig D2E and F) and NoSleeve condition (V: $t_{(9)}$ = 0.03, P = 0.977; H: $t_{(9)}$ = 0.762, P = 0.465; Fig S2G and H).

5.9 Supplementary tables and figures

Table S1. Scanning parameters across fMRI experiments. MB = multi band (i.e. number of simultaneously acquired slices), S = sense factor. TR = repetition time in msec. Exp. = experiment.

		Groningen, NL, Exp. #1	**SPINOZA, Amsterdam, NL** **Exp. #2 & #4**				**SPINOZA, Amsterdam, NL** **Exp. #3**				
Anatomical acquisition parameters	Sequence	3D-spoiled T1-weighted	T1-weighted				T1-weighted				
	Slices	170	170				250				
	Resolution (mm)	256x256	240x222				256 x256				
	Field of view (mm)	232	240 x 240 x 170				240x256x250				
	Voxel size (mm)	1x1x1	1x1x1				1x1x1				
Functional acquisition parameters	Sequence	T2*-weighted	T2*-weighted				T2*-weighted				
	Slices		MB1S2 Exp#2&4	MB2S 2	MB3S 2	MB4S 2	MB1S 2	MB1S 2	MB2S 2	MB4S1.5	MB4S 2
	Nº of slices	41	40	40	39	40	44	36	44	44	44
	Echo time (ms)	28	27.6	27.6	27.6	27.6	30	30	30	30	30
	Thickness (mm)	3.5	3.5	3.5	3.5	3.5	2.7	3.3	2.7	2.7	2.7
	Gap (mm)	NO	0.34	0.34	0.34	0.34	0.27	0.33	0.27	0.27	0.27
	Flip angle	70	72.9	72.9	72.9	72.9	79	75	64	51	50
	Repetition time	2000	2060	1230	760	570	2450	2000	1220	700	630
	Resolution	64x62	80x157				80x78				
	Field of view (mm)	224	240 x 240 x 153.65				TR[2450,1220,700,630]=216x216x130.4 TR[2000]=240x240x130.3				
	Voxels size (mm)	3.5x3.5x3.5	3.0x3.0x3.0				TR[2450,1220,700,630]=2.7x2.7xx2.7 TR[2000]=3.0x3.0x3.3				
	Number of volumes acquired	345	360 Exp.#2; 325 and 326 for session 1 and 2 of Exp. #4				200	245	400	700	780

Table S2. Schema of the temporal order of processing steps and bounding box size for the four processing pipelines testing the effect of different normalization parameters in Exp. #1. Each column details the order of processing steps used in a specific pipeline. All pipelines start with core preprocessing including: centering of the anatomical image to the anterior commissure, slice timing, realignment of all EPI images to one another. Finally, the T1 image is coregisted to the mean EPI image. Only then do the different pipelines start to differ. The acronym of the different pipelines is constructed using the following elements. WB: whole-brain. Cereb: Cerebellum specific analysis. GLM: general linear model, referring to the first level of analysis. SUIT: spatially unbiased atlas template. MNI: MNI brain template. norm: normalization.

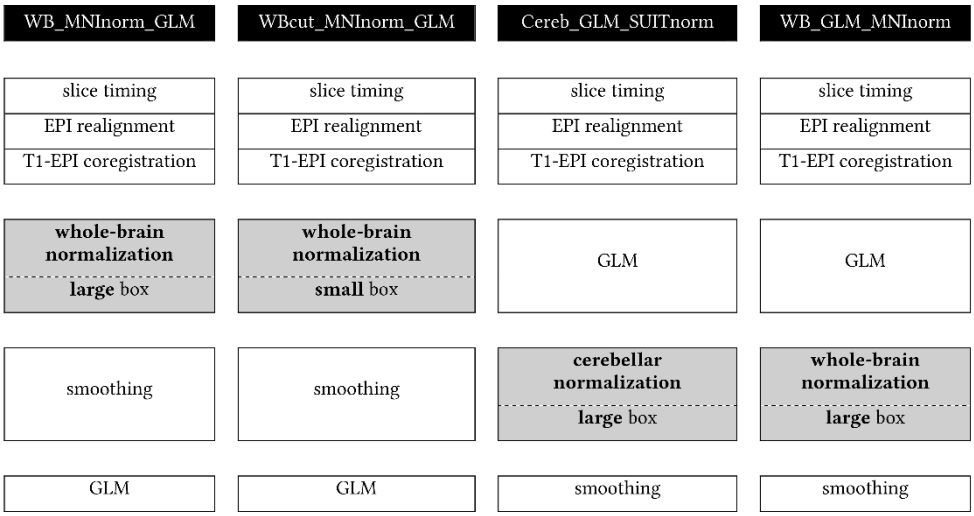

Table S3. Cerebellar activations to ActionOBS-CtrlOBS for the WB_MNInorm_GLM and the Cereb_GLM_SUITnorm pipelines. Regions with ActionOBS-CtrlOBS≥5.4. Only clusters with minimum 10 voxels are reported. Clusters are described using SPM Anatomy Toolbox. From left to right: the cluster size in number of voxels, the number of voxels falling in a cyto-architectonic area, the percentage of the cluster that falls in the cyto-architectonic area, the hemisphere (L = left; R = right), the name of the cyto-architectonic area when available or the anatomical description, the percentage of the area that is activated by the cluster, the t values of the peaks associated with the cluster followed by their MNI coordinates in mm.

Cluster size	# Voxels in cyto	% Cluster	Hem	Cyto or anatomical description	% Area	Peak Information			
						T	x	y	z
Exp. #1,WB_MNInorm_GLM pipeline, ActionOBS-CtrlOBS p_{FWE}<0.05, t=5.8, min. 10 voxels									
138	130.8	94.7	R	Lobule VI (Hem)	7.2	9.41	30	-56	-24
						8.13	32	-50	-30
						6.96	38	-48	-28
						6.95	30	-46	-24
100	66.6	66.6	L	Lobule VIIIa (Hem)	8.8	7.48	-26	-60	-52
						6.41	-20	-64	-56
	27.8	27.8	L	Lobule VIIb (Hem)	4.1	7.68	-12	-74	-48
	4.5	4.5	L	Lobule VIIIb (Hem)	0.7				
94	83	88.3	R	Lobule VIIb (Hem)	12.7	9.28	18	-78	-52
						9.13	14	-76	-48
						8.63	16	-74	-46
79	77.5	98.1	L	Lobule VI (Hem)	4.1	12.22	-28	-54	-24
						6.24	-34	-52	-28
47	43.1	91.8	R	Lobule VI (Hem)	2.4	10.13	22	-72	-22
47	45.8	97.3	R	Lobule VIIIa (Hem)	6.3	7.84	24	-64	-54
						7.03	30	-60	-52
						6.5	18	-68	-54
Exp. #1, Cereb_GLM_SUITnorm pipeline, ActionOBS-CtrlOBS p_{FWE}<0.05, t=5.4, min. 10 voxels									
214	199.1	93	R	Lobule VI (Hem)	11	9.18	30	-56	-24
						8.25	22	-72	-22
						7.48	32	-52	-28
						6.72	26	-66	-20
159	110.4	69.4	L	Lobule VIIIa (Hem)	14.5	7.97	-26	-58	-54
						7.62	-24	-60	-52
						7.11	-20	-62	-58
	25.4	16	L	Lobule VIIb (Hem)	3.7	8.35	-16	-74	-52
						8.05	-14	-72	-48
	21.1	13.3	L	Lobule VIIIb (Hem)	3.5	8.44	-20	-60	-48
118	97.4	82.5	R	Lobule VIIb (Hem)	14.9	8.35	16	-74	-46
						7.93	14	-76	-52
						7.78	12	-76	-48
						7.68	18	-78	-54
	14.1	12	R	Lobule VIIIa (Hem)	1.9				
101	99	98	L	Lobule VI (Hem)	5.3	11.04	-28	-54	-24
						7.35	-24	-56	-28
						6.08	-28	-60	-22
72	65.6	91.1	R	Lobule VIIIa (Hem)	9	8.17	24	-64	-54
						7.56	26	-60	-56
Exp. #1, WB_GLM_MNInorm pipeline, ActionOBS-CtrlOBS p_{FWE}<0.05, t=5.4, min. 10 voxels									
102	91.4	89.6		Lobule VIIb (Hem)	14	9.3	18	-78	-52
						8.97	14	-76	-48
						8.52	16	-74	-46
101	96.3	95.3		Lobule VI (Hem)	5.3	9.3	30	-56	-24
						8.06	32	-50	-30
						7.1	36	-50	-30
						6.91	30	-46	-24
94	61.6	65.6	left	Lobule VIIIa (Hem)	8.1	7.52	-26	-60	-52
					4	6.4	-26	-64	-56
					0.7	6.16	-22	-64	-56
	27	28.7	left	Lobule VIIb (Hem)		7.74	-14	-74	-48
73	71.5	97.9		Lobule VI (Hem)	3.8	12.49	-28	-54	-24
42	41.5	98.8		Lobule VIIIa (Hem)	5.7	7.74	24	-64	-54
						7.02	30	-60	-52
						6.54	18	-68	-54
39	35.9	92		Lobule VI (Hem)	2	10.13	22	-72	-22
						7	26	-66	-20

Table S4. Number of activated cerebellar voxel. Median of activated voxels for the ActionOBS-ActionCtrl contrast for each experiment individually (Exp1-3) and when considered as a group (All; N = 79), for each of the four anatomically defined cerebellar clusters identified at the group level (but separately for each hemisphere: L, left; R, right). Results are also reported for the whole cerebellum (Cereb), and for cortical areas activated by the same contrast and of similar volume (PF L, PF R, BA44L, BA44R). Percentage of participants having no voxels (% zeros) in any of the region of interest, and the percentage of those having at more than 10 voxels (% > 10) are also reported. The size, in number of voxels, of each ROI is indicated under the ROI name in the first line.

		VI L	VI R	VIIIa/ VIIb L	VIIIa/ VII R	Cereb	PF L	PF R	BA44 L	BA44 R	BA1/2 L	BA1/2 R
		2085	2041	1640	1588	21127	2205	2337	869	607	1101	1349
median	**Exp1**	14	47	4	5	208	517	373	115	41	115	501
	Exp2	4	10	9	54	186	244	146	89	20	88	254
	Exp3	67	50	8	82	384	450	282	91	72	91	705
	All	14	31	7	44	224	379	282	92	30	92	485
% zeros	**Exp1**	25.8	25.8	45.2	29.0	12.9	0.00	0.00	12.9	19.4	12.90	0.00
	Exp2	32.0	24.0	28.0	12.0	0.0	0.00	8.00	4.0	20.0	4.00	4.00
	Exp3	17.4	21.7	26.1	17.4	0.0	8.70	13.04	13.0	13.0	13.04	4.35
	All	25.3	24.1	34.2	20.3	5.1	2.53	6.33	10.1	17.7	10.13	2.53
% >10	**Exp1**	51.6	58.1	38.7	45.2	77.4	100.0	93.55	83.9	67.7	83.87	100.00
	Exp2	40.0	48.0	48.0	84.0	88.0	96.00	84.00	92.0	60.0	92.00	92.00
	Exp3	60.9	69.6	47.8	73.9	95.7	91.30	82.61	73.9	78.3	73.91	91.30
	All	50.6	58.2	44.3	65.8	86.1	96.20	87.34	83.5	68.4	83.54	94.94

Fig S1 (page 172). Effect of different analysis pipelines on cerebellar activation to action observation. (A-D) Cerebellar activations ($p_{FWE} < 0.05$) for the four pipelines displayed on flat maps of the cerebellum. Color code in (A) identifies the different cerebellar lobules (Diedrichsen and Zotow 2015). (E) For each of the four pipelines (A-D), the graphs shows the mean top 5% of t-values, and indicates the significant differences between the traditional pipeline (A) and the other three (B-D). *p < 0.002, **p < 0.001, ns = not significant. (F) As in (A) on the uncolored flat-map and on a sagittal slice. When smoothing is applied, the cerebellar cluster marked with the black arrow is part of a temporal lobe cluster. When smoothing is not applied as in (G) the cluster is clearly cerebellar. (G) Same as in (A) and (F) but computed on unsmoothed data.

Fig S2 (page 173). Task-related eye movement dynamics. (A, B) Heatplots based on spatial gaze intensity, identifying IRs during arm movement in the task for each group per condition. Both controls and SCA6 subjects focused significantly on the proximal arm muscles in the NoSleeve condition, although they focused on both distal and proximal part of the arm in the Sleeve condition, with an IR around the wrist. (C) Gaze position along the vertical axis throughout the task, showing tracking of upward going arm movements for both groups during both conditions. (D) Gaze position along the horizontal axis shows proximal arm focusing during arm movements in the NoSleeve condition. (E, F) Total gaze distance in the Sleeve condition along the V and H axis, respectively, shows no group differences. (G, H) Total gaze distance in the Nosleeve condition along the V and H axis, respectively, also shows no difference between groups.

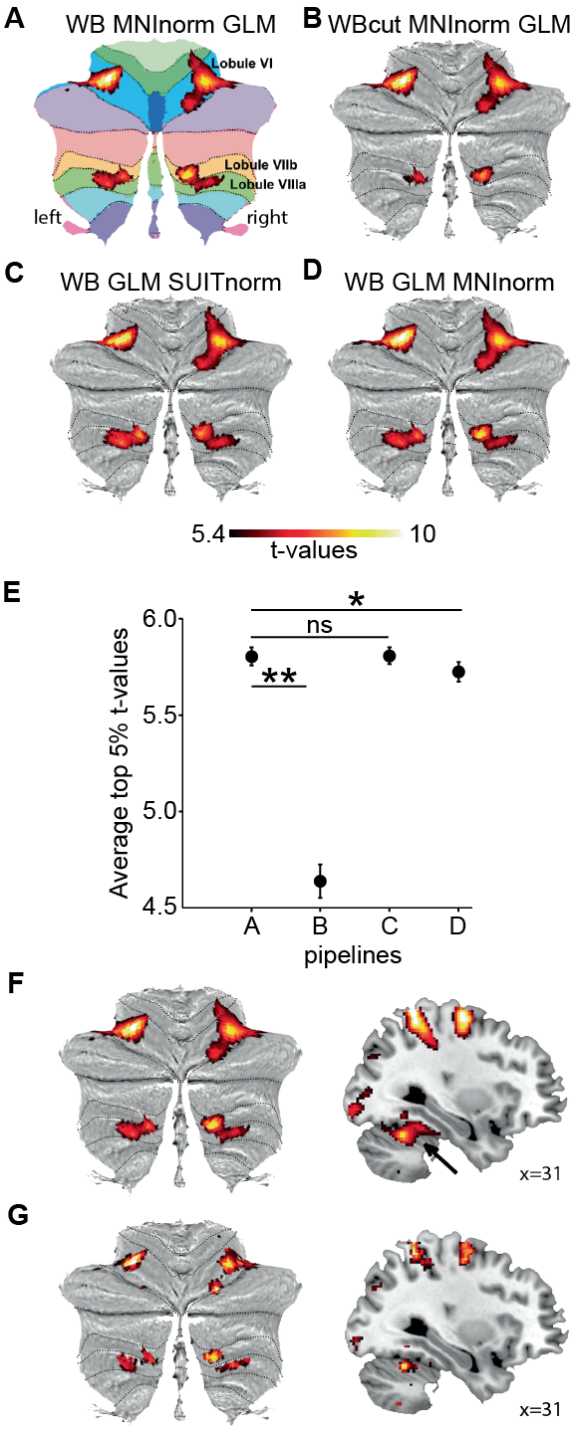
A
WB MNInorm GLM
Lobule VI
Lobule VIIb
Lobule VIIIa
left
right
B
WBcut MNInorm GLM
C
WB GLM SUITnorm
D
WB GLM MNInorm
5.4
t-values
10
E
*
ns
**
6.0
5.5
5.0
4.5
Average top 5% t-values
A
B
C
D
pipelines
F
x=31
G
x=31

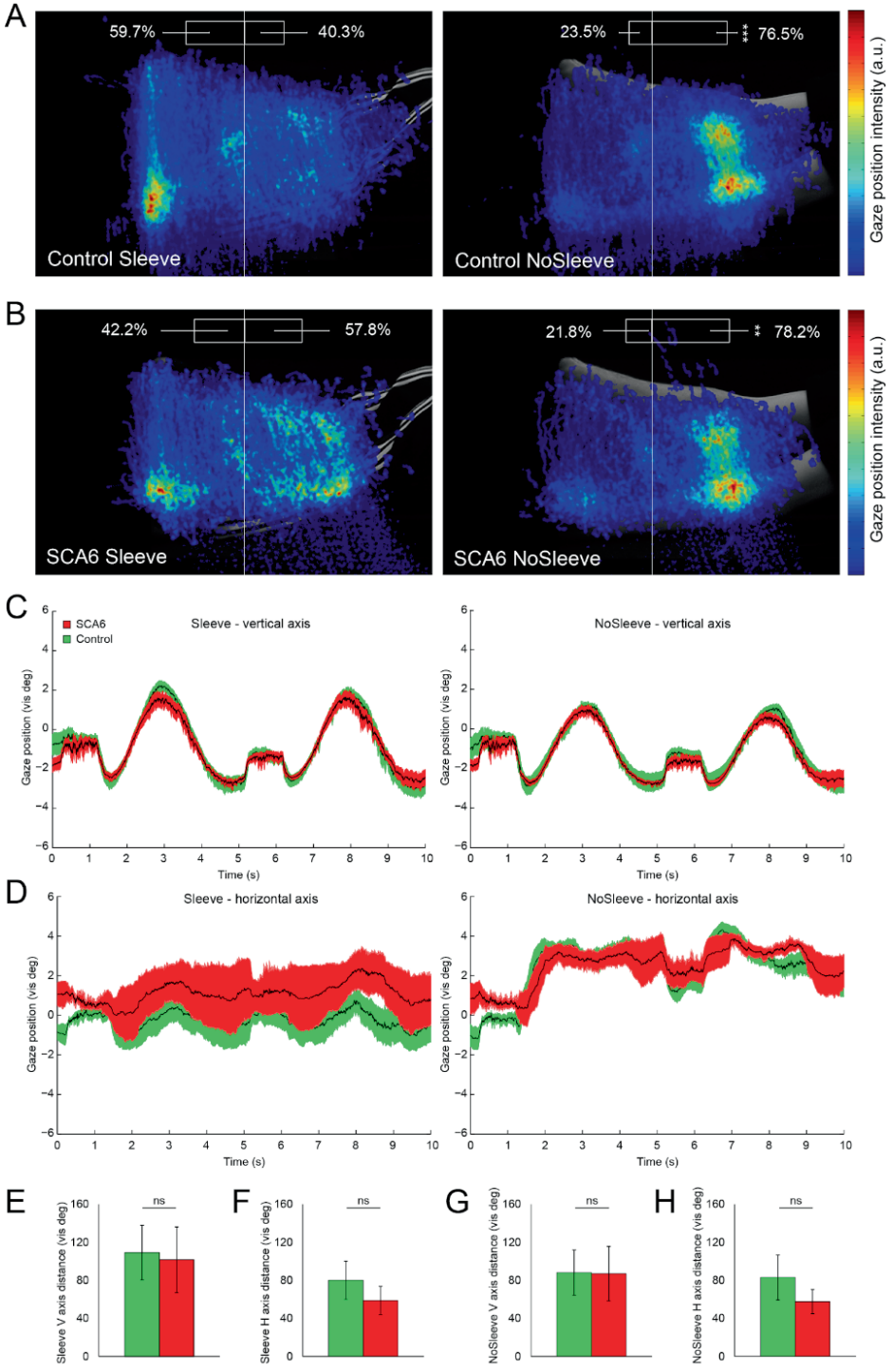
A
59.7%
40.3%
Control Sleeve
23.5%
***
76.5%
Control NoSleeve
Gaze position intensity (a.u.)
B
42.2%
57.8%
SCA6 Sleeve
21.8%
**
78.2%
SCA6 NoSleeve
Gaze position intensity (a.u.)
C
SCA6
Control
Sleeve - vertical axis
NoSleeve - vertical axis
Gaze position (vis deg)
Time (s)
D
Sleeve - horizontal axis
NoSleeve - horizontal axis
Gaze position (vis deg)
Time (s)
E
F
G
H
ns
Sleeve V axis distance (vis deg)
Sleeve H axis distance (vis deg)
NoSleeve V axis distance (vis deg)
NoSleeve H axis distance (vis deg)

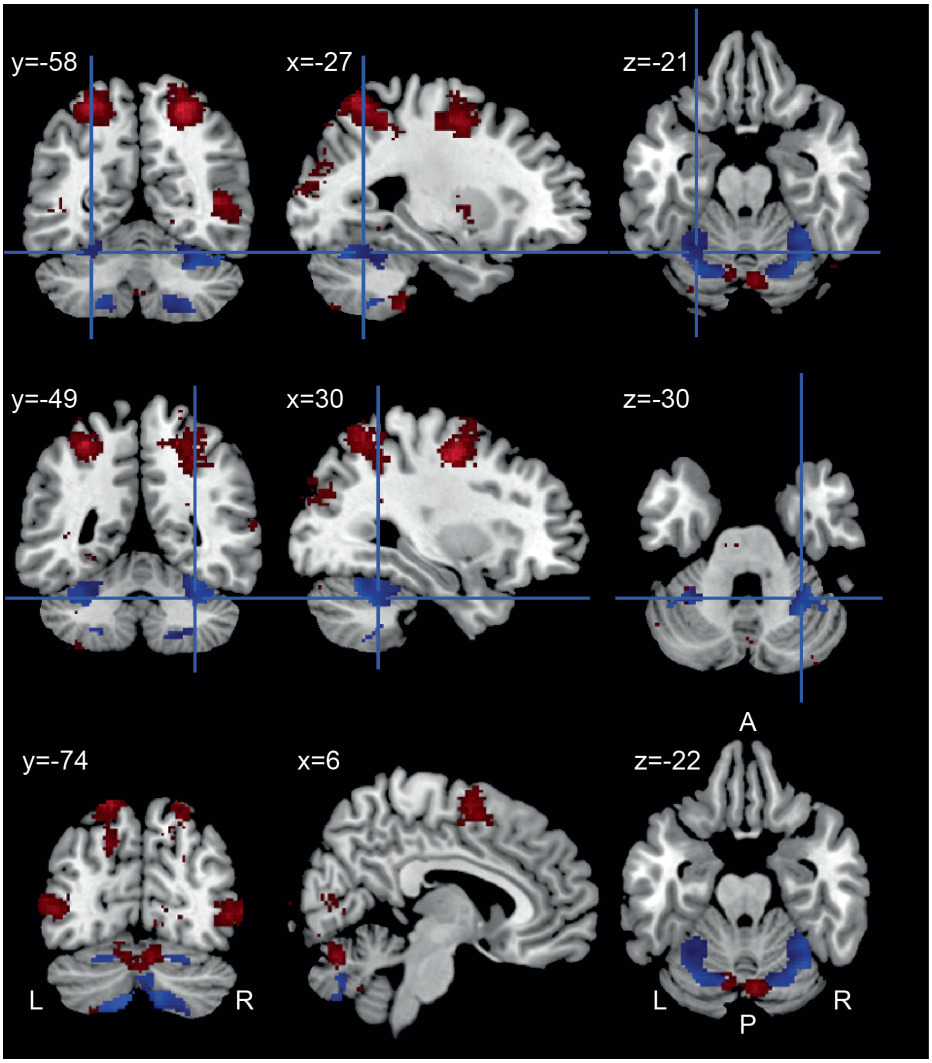

Fig S3. Comparison with locations of VBM changes and eye movement cerebellar activity. Red: location of cortical and cerebellar activity during eye movement tasks as identified by a Neurosynth (http://neurosynth.org/) meta-analysis with the term 'eye movements' (116 studies and 5486 activation clusters identified). Blue: cerebellar activation maps of the global null conjunction at pFWE < 0.05 of the Sleeve and NoSleeve conditions falling within the conjunction of the ActionOBS-ActionCtrl contrasts of Exp.#1,2 and 3. From top to bottom, the coordinates (and blue crosses when present) indicate the location of: the left (top row) and right (middle row) lobule VI peak of correlation between VBM and SCA6 patients' performance in the Grooved Pegboard (from Table 3 in (Rentiya et al. 2017)), and (bottom row) the lobule VI peak of activity to eye movements as identified by the met-analysis in Neurosynth. Note how the VBM results (crosses) associated with SCA6 overlap with the regions recruited by our task (blue) but fall lateral to the regions most involved in eye movements (red). L: left hemisphere. R: right hemisphere. A: anterior. P: posterior. The clusters of activity are shown on the ch2better template from MRIcron (https://www.nitrc.org/projects/mricron/).

5.10 Appendix - Layman information letter to participants

(In Dutch, sent on Tuesday December 24th 2018 to all participants in this study)

Action perception recruits the cerebellum and is impaired in spinocerebellar ataxia patients

'De perceptie van bewegingen activeert het cerebellum en is verminderd in patiënten met cerebellaire ataxie'

Auteurs: Abdel R. Abdelgabar*, Judith Suttrup*, Robin Broersen*, Ritu Bhandari*, Samuel Picard, Christian Keysers#, Chris I. De Zeeuw# en Valeria Gazzola#

* en # duiden een vergelijkbare bijdrage aan de studie aan

Deze studie is een samenwerking van: Erasmus Medisch Centrum, Rotterdam; Nederlands Herseninstituut, Amsterdam; Universitair Medisch Centrum, Groningen; Universiteit van Amsterdam, Amsterdam

Inleiding

Ons vermogen om een beweging, die uitgevoerd wordt door iemand anders, waar te nemen en te begrijpen is belangrijk als we zelf nieuwe bewegingen willen aanleren. Gespecialiseerde 'spiegelneuronen' in onze hersenen - dat zijn neuronen die communiceren met andere neuronen als iemand een beweging uitvoert én als bekeken wordt hoe iemand anders dezelfde beweging uitvoert - zijn cruciaal bij het kunnen begrijpen van bewegingen. Het cerebellum (of de 'kleine hersenen') is onder andere betrokken bij de coördinatie van onze eigen bewegingen en er wordt daarom gedacht dat het cerebellum ook betrokken is bij het begrijpen van bewegingen van anderen, maar overtuigend bewijs hiervoor is nog niet geleverd. Voor een deel is dit te wijten aan het feit dat veel fMRI studies, dat zijn studies die gebruik maken van een MRI scan om hersenactiviteit te meten tijdens een gedragstaak, wel hebben gekeken naar activiteit in andere hersengebieden, maar vaak lieten zij de hersenactiviteit van het cerebellum buiten beschouwing.

Om antwoord te krijgen op de vraag of het cerebellum betrokken is bij het begrijpen van bewegingen hebben wij in het eerste deel van dit artikel een fMRI studie uitgevoerd en daarbij gekeken naar de hersenactiviteit van het cerebellum tijdens (1) het bekijken van bewegingen en (2) het uitvoeren van een gedragstest. Tijdens het bekijken van bewegingen

(action observation task) (1) lagen proefpersonen in een MRI scanner en bekeken zij filmpjes waarop te zien was hoe een hand een betekenisvolle beweging uitvoerde met een object op tafel, zoals het inschenken van een glas wijn (**figuur 1;** ActionOBS). Tijdens de gedragstest (2) hebben we gemeten hoe goed iemand is in het begrijpen van bewegingen, door de 'weight-discrimination task' (vrije vertaling: gewichts-onderscheidings taak) uit te voeren. Tijdens deze test keek een proefpersoon naar twee filmpjes waarin een arm te zien was die een gewicht optilde, waarna de proefpersoon werd gevraagd in welk filmpje een zwaarder gewicht werd opgetild (**figuur 1**). Om deze taak goed te kunnen uitvoeren moest de proefpersoon gedetailleerde eigenschappen van een beweging gebruiken (zoals de snelheid van optillen en vervorming van de spieren in de arm). Om verder te onderzoeken of proefpersonen vooral de vorm van de spieren gebruiken of andere eigenschappen bij het maken van de beslissing, hebben we in een deel van de filmpjes de spieren bedekt met een mouw.

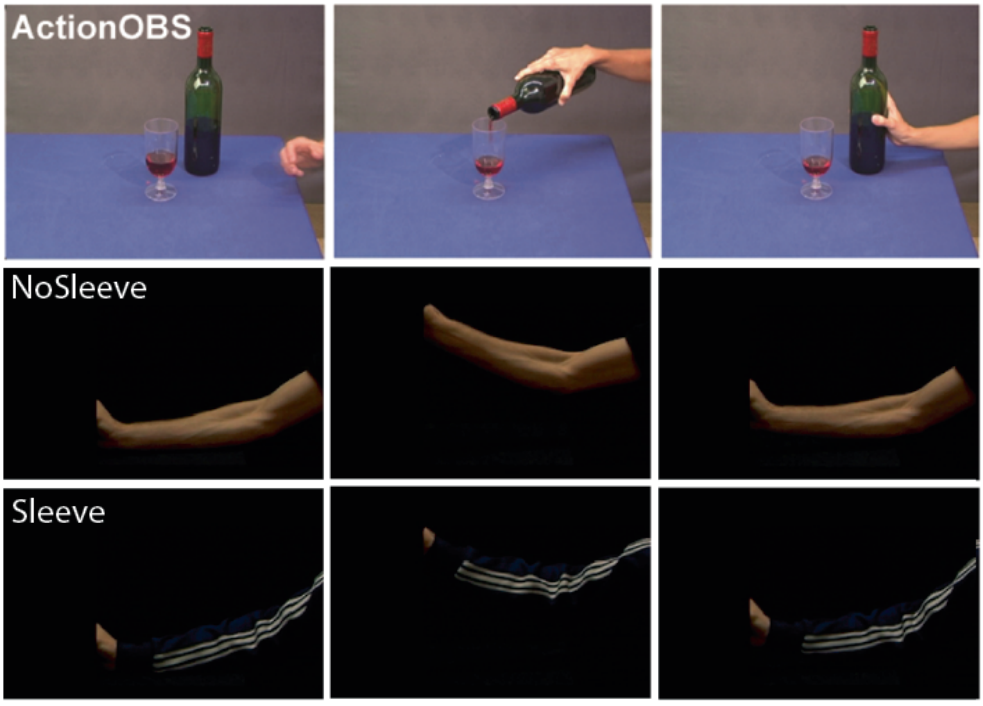

Figuur 1. Action observation task en weight-discrimination task. Tijdens de action observation task (ActionOBS; bovenste rij) bekeek een proefpersoon filmpjes van een hand die een betekenisvolle beweging uitvoerde met verschillende objecten op een tafel, zoals het inschenken van een glas wijn. Tijdens de weight-discrimination task (middelste en onderste rij) bekeek een proefpersoon twee filmpjes van een arm die een gewicht optilde, waarna hij/zij een keuze maakte in welk van de twee filmpjes een zwaarder gewicht werd opgetild. Er waren twee situaties: waarbij de arm volledig zichtbaar was ('NoSleeve') en waarbij de arm was bedekt door een mouw ('Sleeve').

In het tweede deel van het artikel hebben we onderzocht hoe goed mensen bewegingen begrijpen als het cerebellum niet goed werkt, zoals het geval is bij mensen met spinocerebellaire ataxie type 6 (SCA6). Wij hebben hierbij de weight-discrimination task uitgevoerd in SCA6 proefpersonen en controle proefpersonen zonder SCA6, waarbij we hun resultaten vergeleken. Wij verwachtten dat als het cerebellum inderdaad belangrijk zou zijn voor het begrijpen van bewegingen, SCA6 proefpersonen deze test dus minder goed zouden kunnen doen.

Resultaten

Uit het fMRI onderzoek (1) werd duidelijk dat er tijdens het bekijken van bewegingen in ~95% van de proefpersonen verschillende gebieden in het cerebellum actief werden. Grofweg dezelfde gebieden werden ook actief toen proefpersonen de weight-discrimination task uitvoerden in de MRI scanner (2). Door een vergelijking te maken tussen de hersenactiviteit met mouw ('Sleeve') en zonder mouw ('NoSleeve') werd duidelijk dat het cerebellum vooral de *bewegingsinformatie* van het optillen verwerkte en niet zozeer de vorm van de spieren. Met behulp van oogmetingsapparatuur konden we daarnaast vaststellen dat proefpersonen een verschillende strategie gebruikten in de situatie met of zonder mouw bij het uitvoeren van de test, waarbij er meer gefocust werd op de spieren aan de bovenkant van de onderarm bij de situatie zonder mouw, en meer op de gehele arm (en vooral de pols) bij de situatie met mouw (**figuur 2**).

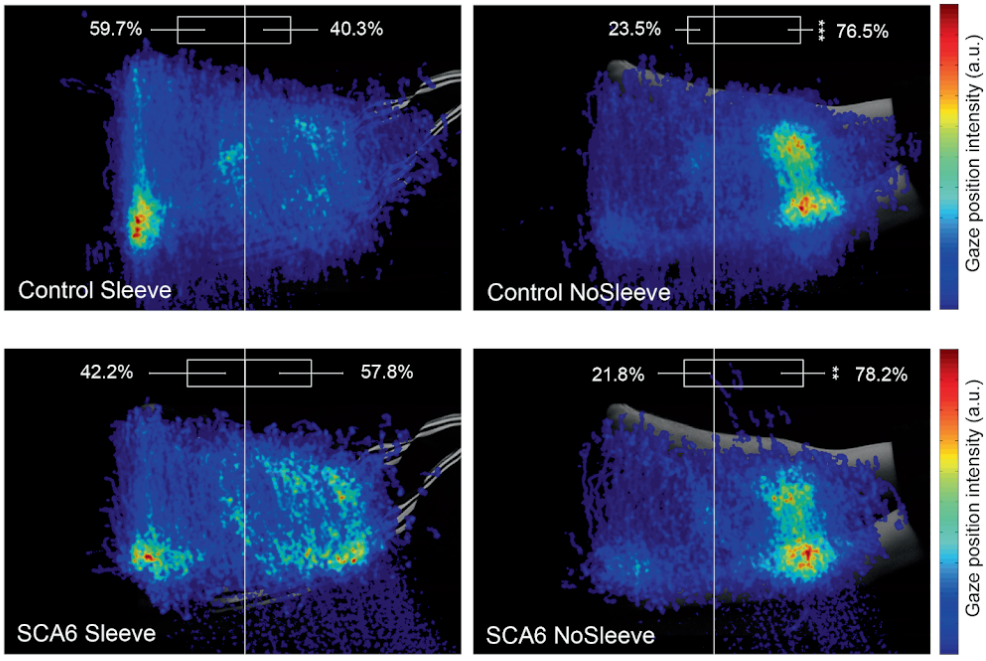

Figuur 2. Oogbewegingen tijdens de weight-discrimination task. Met gebruik van oogmetingsapparatuur werd gekeken waarnaar de proefpersonen keken tijdens het doen van de gedragstest. Als de proefpersonen meer focussen op een bepaald punt op de arm, is dit zichtbaar in dit figuur als een 'vlek' met een kleur die meer naar rood neigt. Het bleek dat zowel controle proefpersonen (bovenste twee plaatjes) als SCA6 proefpersonen (onderste twee plaatjes) meer naar het bovenste gedeelte van de onderarm keken als er geen mouw aanwezig was. Als er wel een mouw aanwezig was keken de proefpersonen gelijkmatiger naar de hele arm, hoewel de pols als voornaamste punt naar voren kwam.

Vervolgens werd er gekeken naar hoe goed SCA6 proefpersonen de gedragstest konden doen in vergelijking met controle proefpersonen. Uit de resultaten bleek dat SCA6 proefpersonen een lagere score behaalden tijdens de test, vooral in de situatie waarin de arm bedekt was met een mouw ('Sleeve') (**figuur 3A**). Ook vonden we een negatief verband tussen de score van elke SCA6 proefpersoon en de mate waarin de symptomen aanwezig waren. In andere woorden, hoe symptomatischer de proefpersonen waren (gemeten door een neuroloog als SARA score), hoe minder goed de score op de gedragstaak (**figuur 3B**).

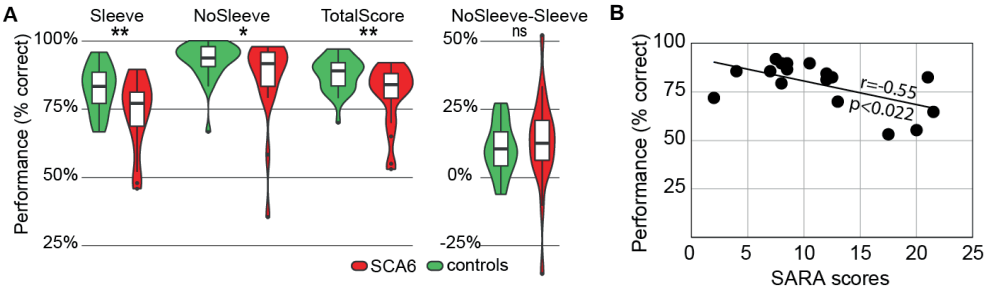

Figuur 3. Score op de weight-discrimination task. (A) Door een vergelijking te maken tussen de scores op de gedragstest tussen SCA6 proefpersonen en controle proefpersonen werd duidelijk dat SCA6 proefpersonen lager scoorden. Dat wil zeggen dat zij minder goed waren in het kunnen onderscheiden in welk van de filmpjes een zwaarder gewicht werd opgetild. (B) Ook bleek er een verband te zitten in hoe symptomatisch de SCA6 proefpersonen waren (gemeten als SARA score) en de scores op de weight-discrimination task.

Conlusie

Dit onderzoek levert het belangrijke bewijs dat het cerebellum is betrokken bij het begrijpen van bewegingen die gemaakt worden door anderen. We zagen met behulp van fMRI dat het cerebellum actief werd toen proefpersonen keken naar een hand die betekenisvolle bewegingen uitvoerde. Daarnaast zagen we dat het cerebellum actief werd tijdens het bekijken van een bewegende arm die een gewicht optilde (weight-discrimination task/gedragstaak). Ten slotte werd duidelijk dat mensen met SCA6 minder goed konden bepalen in welk van twee filmpjes een zwaarder gewicht wordt opgetild, op basis van het begrijpen van informatie uit de beweging van de arm. Dit lag waarschijnlijk niet aan verschillen in hun oogbewegingen, want zowel SCA6 proefpersonen als controle proefpersonen konden een vergelijkbare strategie gebruiken tijdens de gedragstest.

Dit onderzoek geeft meer inzicht in de manier waarop het cerebellum is betrokken bij de uitvoering, en nu dus ook het begrijpen van bewegingen. Het is belangrijk om te weten hoe schade of aandoeningen aan het cerebellum zoals SCA6 deze vaardigheden beïnvloeden, om zo meer kennis te vergaren over wat de consequenties zijn van cerebellaire aandoeningen in het dagelijks leven, maar ook als basis voor meer begrip voor mensen met cerebellaire aandoeningen. Dit soort kennis en onderzoek biedt een basis voor begrip van SCA6, maar ook voor de ontwikkeling van nieuwe diagnostische testen en therapieën.

5.11 References

Agnew ZK, Wise RJS, Leech R (2012) Dissociating object directed and non-object directed action in the human mirror system; implications for theories of motor simulation. PLoS ONE 7:. doi: 10.1371/journal.pone.0032517

Amunts K, Schleicher A, Bürgel U, et al (1999) Broca's region revisited: Cytoarchitecture and intersubject variability. J Comp Neurol 412:319–341. doi: 10.1002/(SICI)1096-9861(19990920)412:2<319::AID-CNE10>3.0.CO;2-7

Arnstein D, Cui F, Keysers C, et al (2011) μ-suppression during action observation and execution correlates with BOLD in dorsal premotor, inferior parietal, and SI cortices. J Neurosci Off J Soc Neurosci 31:14243–9. doi: 10.1523/JNEUROSCI.0963-11.2011

Aziz-Zadeh L (2006) Lateralization of the Human Mirror Neuron System. J Neurosci 26:2964–2970. doi: 10.1523/JNEUROSCI.2921-05.2006

Brunner IC, Skouen JS, Ersland L, Grüner R (2014) Plasticity and response to action observation: A longitudinal fMRI study of potential mirror neurons in patients with subacute stroke. Neurorehabil Neural Repair 28:874–884. doi: 10.1177/1545968314527350

Buccino G, Vogt S, Ritzl A, et al (2004) Neural circuits underlying imitation learning of hand actions: An event-related fMRI study. Neuron 42:323–334. doi: 10.1016/S0896-6273(04)00181-3

Buttner N, Geschwind D, Jen JC, et al (1998) Oculomotor phenotypes in autosomal dominant ataxias. Arch Neurol 55:1353–7

Caspers S, Geyer S, Schleicher A, et al (2006) The human inferior parietal cortex: Cytoarchitectonic parcellation and interindividual variability. NeuroImage 33:430–448. doi: 10.1016/j.neuroimage.2006.06.054

Caspers S, Zilles K, Laird AR, Eickhoff SB (2010) ALE meta-analysis of action observation and imitation in the human brain. NeuroImage 50:1148–67. doi: 10.1016/j.neuroimage.2009.12.112

Catmur C, Gillmeister H, Bird G, et al (2008) Through the looking glass: Counter-mirror activation following incompatible sensorimotor learning. Eur J Neurosci 28:1208–1215. doi: 10.1111/j.1460-9568.2008.06419.x

Cattaneo L, Fasanelli M, Andreatta O, et al (2012) Your actions in my cerebellum: Subclinical deficits in action observation in patients with unilateral chronic cerebellar stroke. Cerebellum 11:264–271. doi: 10.1007/s12311-011-0307-9

Choi HJ, Zilles K, Mohlberg H, et al (2006) Cytoarchitectonic identification and probabilistic mapping of two distinct areas within the anterior ventral bank of the human intraparietal sulcus. J Comp Neurol 495:53–69. doi: 10.1002/cne.20849

Christova P, Anderson JH, Gomez CM (2008) Impaired Eye Movements in Presymptomatic Spinocerebellar Ataxia Type 6. Arch Neurol 65:530. doi: 10.1001/archneur.65.4.530

Hamilton A, Joyce DW, Flanagan JR, et al (2007) Kinematic cues in perceptual weight judgement and their origins in box lifting. Psychol Res 71:13–21. doi: 10.1007/s00426-005-0032-4

Di Cesare G, Di Dio C, Marchi M, Rizzolatti G (2015) Expressing our internal states and understanding those of others. Proc Natl Acad Sci 112:10331–10335. doi: 10.1073/pnas.1512133112

di Pellegrino G, Fadiga L, Fogassi L, et al (1992) Understanding motor events: a neurophysiological study. Exp Brain Res 91:176–180. doi: 10.1007/BF00230027

Diedrichsen J (2006) A spatially unbiased atlas template of the human cerebellum. NeuroImage 33:127–138. doi: 10.1016/j.neuroimage.2006.05.056

Diedrichsen J, Balsters JH, Flavell J, et al (2009) A probabilistic MR atlas of the human cerebellum. NeuroImage 46:39–46. doi: 10.1016/j.neuroimage.2009.01.045

Diedrichsen J, Zotow E (2015) Surface-based display of volume-averaged cerebellar imaging data. PLoS ONE 10:. doi: 10.1371/journal.pone.0133402

Duque J, Thonnard J-L, Vandermeeren Y, et al (2003) Correlation between impaired dexterity and corticospinal tract dysgenesis in congenital hemiplegia. Brain J Neurol 126:732–47

Eickhoff SB, Heim S, Zilles K, Amunts K (2006) Testing anatomically specified hypotheses in functional imaging using cytoarchitectonic maps. NeuroImage 32:570–582. doi: 10.1016/j.neuroimage.2006.04.204

Eickhoff SB, Paus T, Caspers S, et al (2007) Assignment of functional activations to probabilistic cytoarchitectonic areas revisited. NeuroImage 36:511–521. doi: 10.1016/j.neuroimage.2007.03.060

Eickhoff SB, Stephan KE, Mohlberg H, et al (2005) A new SPM toolbox for combining probabilistic cytoarchitectonic maps and functional imaging data. NeuroImage 25:1325–1335. doi: 10.1016/j.neuroimage.2004.12.034

Eidelberg E, Yu J (1981) Effects of corticospinal lesions upon treadmill locomotion by cats. Exp Brain Res 43:101–3

Fogassi L, Ferrari PF, Geslerich B, et al (2005) Parietal lobe: From action organisation to intention understanding. Science 308:662–667. doi: 10.1126/science.1111199

Forssberg H, Eliasson AC, Redon-Zouitenn C, et al (1999) Impaired grip-lift synergy in children with unilateral brain lesions. Brain J Neurol 122 (Pt 6):1157–68

Fuentes CT, Bastian AJ (2007) "Motor cognition" - What is it and is the cerebellum involved? Cerebellum 6:232–236

Gallese V, Fadiga L, Fogassi L, Rizzolatti G (1996) Action recognition in the premotor cortex. Brain J Neurol 119 (Pt 2:593–609. doi: 10.1093/brain/119.2.593

Gao Z, Davis C, Thomas AM, et al (2018) A cortico-cerebellar loop for motor planning. Nature 563:113–116. doi: 10.1038/s41586-018-0633-x

Gazzola V, Keysers C (2009) The Observation and Execution of Actions Share Motor and Somatosensory Voxels in all Tested Subjects: Single-Subject Analyses of Unsmoothed fMRI Data. Cereb Cortex 19:1239–1255. doi: 10.1093/cercor/bhn181

Gazzola V, Rizzolatti G, Wicker B, Keysers C (2007a) The anthropomorphic brain: the mirror neuron system responds to human and robotic actions. NeuroImage 35:1674–84. doi: 10.1016/j.neuroimage.2007.02.003

Gazzola V, van der Worp H, Mulder T, et al (2007b) Aplasics born without hands mirror the goal of hand actions with their feet. Curr Biol CB 17:1235–40. doi: 10.1016/j.cub.2007.06.045

Geyer S (2004) The microstructural border between the motor and the cognitive domain in the human cerebral cortex. AdvAnatEmbryolCell Biol 174:I–89

Geyer S, Ledberg A, Schleicher A, et al (1996) Two different areas within the primary motor cortex of man. Nature 382:805–807. doi: 10.1038/382805a0

Geyer S, Schleicher a, Zilles K (1999) Areas 3a, 3b, and 1 of human primary somatosensory cortex. NeuroImage 10:63–83. doi: 10.1006/nimg.1999.0440

Geyer S, Schormann T, Mohlberg H, Zilles K (2000) Areas 3a, 3b, and 1 of human primary somatosensory cortex. 2. Spatial normalization to standard anatomical space. NeuroImage 11:684–696. doi: 10.1006/nimg.2000.0548

Gomez CM, Thompson RM, Gammack JT, et al (1997) Spinocerebellar ataxia type 6: gaze-evoked and vertical nystagmus, Purkinje cell degeneration, and variable age of onset. Ann Neurol 42:933–50. doi: 10.1002/ana.410420616

Grefkes C, Geyer S, Schormann T, et al (2001) Human somatosensory area 2: Observer-independent cytoarchitectonic mapping, interindividual variability, and population map. NeuroImage 14:617–631. doi: 10.1006/nimg.2001.0858

Grodd W, Hülsmann E, Lotze M, et al (2001) Sensorimotor mapping of the human cerebellum: fMRI evidence of somatotopic organization. Hum Brain Mapp 13:55–73. doi: 10.1002/hbm.1025

Hermsdörfer J, Hagl E, Nowak DA, Marquardt C (2003) Grip force control during object manipulation in cerebral stroke. Clin Neurophysiol Off J Int Fed Clin Neurophysiol 114:915–29

Hillis AE (2014) Inability to empathize: brain lesions that disrupt sharing and understanding another's emotions. Brain J Neurol 137:981–97. doi: 10.1093/brain/awt317

Horan WP, Iacoboni M, Cross KA, et al (2014) Self-reported empathy and neural activity during action imitation and observation in schizophrenia. NeuroImage Clin 5:100–108. doi: 10.1016/j.nicl.2014.06.006

Iacoboni M, Koski LM, Brass M, et al (2001) Reafferent copies of imitated actions in the right superior temporal cortex. Proc Natl Acad Sci U S A 98:13995–13999. doi: 10.1073/pnas.241474598

Iacoboni M, Woods RP, Brass M, et al (1999) Cortical mechanisms of human imitation. Science 286:2526–2528. doi: 10.1126/science.286.5449.2526

Jastorff J, Abdollahi RO, Orban GA (2012) Acting alters visual processing: Flexible recruitment of visual areas by one's own actions. Cereb Cortex 22:2930–2942. doi: 10.1093/cercor/bhr382

Jelsone-Swain L, Persad C, Burkard D, Welsh RC (2015) Action processing and mirror neuron function in patients with amyotrophic lateral sclerosis: An fMRI study. PLoS ONE 10:. doi: 10.1371/journal.pone.0119862

Kelly RM, Strick PL (2003) Cerebellar loops with motor cortex and prefrontal cortex of a nonhuman primate. J Neurosci Off J Soc Neurosci 23:8432–44

Keysers C, Gazzola V (2009) Expanding the mirror: vicarious activity for actions, emotions, and sensations. Curr Opin Neurobiol 19:666–671. doi: 10.1016/j.conb.2009.10.006

Keysers C, Kaas JH, Gazzola V (2010) Somatosensation in social perception. Nat Rev Neurosci 11:417–28. doi: 10.1038/nrn2833

Keysers C, Kohler E, Umiltà MA, et al (2003) Audiovisual mirror neurons and action recognition. Exp Brain Res 153:628–36. doi: 10.1007/s00221-003-1603-5

Keysers C, Paracampo R, Gazzola V (2018) What neuromodulation and lesion studies tell us about the function of the mirror neuron system and embodied cognition. Curr Opin Psychol 24:35–40. doi: 10.1016/j.copsyc.2018.04.001

Kohler E, Keysers C, Umiltà MA, et al (2002) Hearing Sounds, Understanding Actions: Action Representation in Mirror Neurons. Science 297:846–848. doi: 10.1126/science.1070311

Miall RC (2003) Connecting mirror neurons and forward models. Neuroreport 14:2135–2137. doi: 10.1097/01.wnr.0000098751.87269.77

Molenberghs P, Cunnington R, Mattingley JB (2012) Brain regions with mirror properties: A meta-analysis of 125 human fMRI studies. Neurosci. Biobehav. Rev. 36:341–349

Orr ELR, Lacourse MG, Cohen MJ, Cramer SC (2008) Cortical activation during executed, imagined, and observed foot movements. NeuroReport 19:625–630. doi: 10.1097/WNR.0b013e3282fbf9e0

Peirce JW (2009) Generating Stimuli for Neuroscience Using PsychoPy. Front Neuroinformatics 2:10. doi: 10.3389/neuro.11.010.2008

Plata Bello J, Modroño C, Marcano F, González-Mora JL (2014) The mirror neuron system and motor dexterity: What happens? Neuroscience 275:285–295. doi: 10.1016/j.neuroscience.2014.06.010

Pobric G, Hamilton A (2006) Action Understanding Requires the Left Inferior Frontal Cortex. Curr Biol 16:524–529. doi: 10.1016/j.cub.2006.01.033

Rentiya Z, Khan N-S, Ergun E, et al (2017) Distinct cerebellar regions related to motor and cognitive performance in SCA6 patients. Neuropsychologia 107:25–30. doi: 10.1016/J.NEUROPSYCHOLOGIA.2017.10.036

Rizzolatti G, Fadiga L, Gallese V, Fogassi L (1996) Premotor cortex and the recognition of motor actions. Cogn Brain Res 3:131–141. doi: 10.1016/0926-6410(95)00038-0

Rizzolatti G, Sinigaglia C (2010) The functional role of the parieto-frontal mirror circuit: interpretations and misinterpretations. Nat Rev Neurosci 11:264–74

Rocca MA, Filippi M (2010) FMRI correlates of execution and observation of foot movements in left-handers. J Neurol Sci 288:34–41. doi: 10.1016/j.jns.2009.10.013

Rozzi S, Ferrari PF, Bonini L, et al (2008) Functional organization of inferior parietal lobule convexity in the macaque monkey: Electrophysiological characterization of motor, sensory and mirror responses and their correlation with cytoarchitectonic areas. Eur J Neurosci 28:1569–1588. doi: 10.1111/j.1460-9568.2008.06395.x

Sasaki AT, Kochiyama T, Sugiura M, et al (2012) Neural networks for action representation underlying automatic mimicry: A functional magnetic-resonance imaging and dynamic causal modeling study. Front Hum Neurosci 6:. doi: 10.3389/fnhum.2012.00236

Saute JAM, Donis KC, Serrano-Munuera C, et al (2012) Ataxia Rating Scales—Psychometric Profiles, Natural History and Their Application in Clinical Trials. The Cerebellum 11:488–504. doi: 10.1007/s12311-011-0316-8

Schlerf JE, Galea JM, Spampinato D, Celnik PA (2015) Laterality Differences in Cerebellar-Motor Cortex Connectivity. Cereb Cortex N Y N 1991 25:1827–34. doi: 10.1093/cercor/bht422

Schmitz-Hubsch T, du Montcel ST, Baliko L, et al (2006) Scale for the assessment and rating of ataxia: Development of a new clinical scale. Neurology 66:1717–1720. doi: 10.1212/01.wnl.0000219042.60538.92

Sokolov AA, Gharabaghi A, Tatagiba MS, Pavlova M (2010) Cerebellar engagement in an action observation network. Cereb Cortex 20:486–491. doi: 10.1093/cercor/bhp117

Sokolov AA, Miall RC, Ivry RB (2017) The Cerebellum: Adaptive Prediction for Movement and Cognition. Trends Cogn. Sci. 21:313–332

Thomas RM, De Sanctis T, Gazzola V, Keysers C (2018) Where and how our brain represents the temporal structure of observed action. NeuroImage 183:677–697. doi: 10.1016/j.neuroimage.2018.08.056

Urgesi C, Candidi M, Avenanti A (2014) Neuroanatomical substrates of action perception and understanding: an anatomic likelihood estimation meta-analysis of lesion-symptom mapping studies in brain injured patients. Front Hum Neurosci 8:344. doi: 10.3389/fnhum.2014.00344

Valchev N, Gazzola V, Avenanti A, Keysers C (2016) Primary somatosensory contribution to action observation brain activity-combining fMRI and cTBS. Soc Cogn Affect Neurosci 11:1205–17. doi: 10.1093/scan/nsw029

Valchev N, Tidoni E, Hamilton A, et al (2017) Primary somatosensory cortex necessary for the perception of weight from other people's action: A continuous theta-burst TMS experiment. NeuroImage 152:195–206. doi: 10.1016/j.neuroimage.2017.02.075

Van Overwalle F, Baetens K, Mariën P, Vandekerckhove M (2014) Social cognition and the cerebellum: A meta-analysis of over 350 fMRI studies. NeuroImage 86:554–572

Weyer A, Abele M, Schmitz-Hübsch T, et al (2007) Reliability and validity of the scale for the assessment and rating of ataxia: A study in 64 ataxia patients. Mov Disord 22:1633–1637. doi: 10.1002/mds.21544

Wolpert DM, Doya K, Kawato M (2003) A unifying computational framework for motor control and social interaction. Philos Trans R Soc Lond B Biol Sci 358:593–602. doi: 10.1098/rstb.2002.1238

Chapter 6

Impaired spatio-temporal predictive motor timing associated with spinocerebellar ataxia type 6

Robin Broersen, Yoshiyuki Onuki, Abdel R. Abdelgabar, Cullen B. Owens, Samuel Picard, Jessica Willems, Henk-Jan Boele, Valeria Gazzola, Ysbrand D. Van der Werf, and Chris I. De Zeeuw (2016)

PLoS One, 11 (8): e0162042

6.1 Abstract

Many daily life activities demand precise integration of spatial and temporal information of sensory inputs followed by appropriate motor actions. This type of integration is carried out in part by the cerebellum, which has been postulated to play a central role in learning and timing of movements. Cerebellar damage due to atrophy or lesions may compromise forward-model processing, in which both spatial and temporal cues are used to achieve prediction for future motor states. In the present study we sought to further investigate the cerebellar contribution to predictive and reactive motor timing, as well as to learning of sequential order and temporal intervals in these tasks. We tested patients with spinocerebellar ataxia type 6 (SCA6) and healthy controls for two related motor tasks; one requiring spatio-temporal prediction of dynamic visual stimuli and another one requiring reactive timing only. We found that healthy controls established spatio-temporal prediction in their responses with high temporal precision, which was absent in the cerebellar patients. SCA6 patients showed lower predictive motor timing, coinciding with a reduced number of correct responses during the 'anticipatory' period on the task. Moreover, on the task utilizing reactive motor timing functions, control participants showed both sequence order and temporal interval learning, whereas patients only showed sequence order learning. These results suggest that SCA6 affects predictive motor timing and temporal interval learning. Our results support and highlight cerebellar contribution to timing and argue for cerebellar engagement during spatio-temporal prediction of upcoming events.

6.2 Introduction

Many daily life activities demanding immediate timed motor responses require integration of spatial and temporal information at the millisecond range (*e.g.* hitting a ball when playing tennis). Our ability to continuously create predictions based on spatial and temporal cues ('spatio-temporal prediction') aids us to make timed, coordinated movements and perceptual judgments in relation to changes in our environment. Using functional magnetic resonance imaging (fMRI), we have shown that co-activation of cerebellum and hippocampus occurred during spatio-temporal prediction when healthy participants were asked to make precisely timed finger movements based on moving visual cues, whereas no co-activation occurred during reactive timing or motor imagery tasks (Onuki et al. 2015). Interestingly, the participants tended to press buttons slightly prior to the optimal timing of visual cues as learning progressed, indicating anticipation in their responses. Those findings suggest that the cerebellum and hippocampus cooperate to plan ahead and execute precise spatial and temporal motor responses. The exact cerebellar contribution to temporal aspects in this task however, remains uncertain. A previous study has shown that patients with spinocerebellar ataxia (SCA) are impaired at intercepting a moving target by performing a timed button press to launch another moving object for collision, a task also requiring spatio-temporal prediction (Bareš et al. 2007). Only patients with disorders that affect the cerebellum such as SCA type 6 and 8 and head essential tremor (ET), scored significantly worse on this predictive timing task when compared to those with other neurological disorders, such as Parkinson's disease (Bareš et al. 2010). During the same task, higher blood oxygenation level-dependent (BOLD) signals in several cerebellar regions as well as thalamus and multiple cortical areas were associated with successful performance. In fact, the activity change during successful trials in several cerebellar regions was found to be higher in controls compared to SCA patients, indicating a role for the cerebellum in spatio-temporal prediction during target interception (Bareš et al. 2011). In a velocity judgement task that required purely perceptual spatio-temporal prediction, the posterior cerebellar lobule VII crus I was engaged when both temporal and spatial cues, but not when only spatial cues were used. Psychophysiological interactions (PPI) analysis further revealed that connectivity between the posterior cerebellum and several other upstream areas in the brain increased during spatio-temporal prediction in the perceptual domain (O'Reilly et al. 2008). This suggests that the cerebellum is important when integration of temporal information is required to complete the task goal.

Pioneering work to determine cerebellar contribution to timing processes has been done by Ivry and colleagues (Ivry and Keele 1989; Ivry 1996; Ivry et al. 2002; Spencer and Ivry 2013). Their work has received support from multiple studies in which timing elements of tasks were used explicitly or implicitly, depending on whether participants were required to use an overt estimation of time or to use time as a by-product to reach the task goal, respectively (Coull and Nobre 2008). Deficits at both explicit timing tasks (*e.g.* temporal discrimination, temporal reproduction and synchronized repetitive finger-tapping tasks)

and implicit timing tasks (*e.g.* spatio-temporal trajectory prediction and serial prediction tasks) have been found in patients with cerebellar disorders (Ivry et al. 1988; Ivry and Keele 1989; Casini and Ivry 1999; Jahanshahi et al. 2006; Bareš et al. 2007; Bueti et al. 2008; Bareš et al. 2010; Grube et al. 2010; Matsuda et al. 2015). These findings complement evidence from neuroimaging studies showing cerebellar activation associated with temporal processing (Rao et al. 1997; Jänke et al. 2000; Pollok et al. 2008; Bareš et al. 2011). Disrupted cerebellar activity may account for the observed deficits in these patients. Tasks employing repetitive transcranial magnetic stimulation (rTMS) furthermore show that temporal processing can be disrupted by interfering with cerebellar activity (Del Olmo et al. 2007; Koch et al. 2007). Together, these studies strongly implicate the cerebellum as part of a wider neuronal network involved in timing functions (Spencer and Ivry 2013).

In the present study, we investigated the role of the cerebellum in spatio-temporal prediction of moving visual stimuli. We tested patients with spinocerebellar ataxia type 6 (SCA6) and healthy age-matched controls on two related motor tasks: a predictive and a reactive motor timing task. This allowed us to study cerebellar contribution to predictive and reactive motor timing functions separately. We further employed an experimental design in which we randomized the sequence order of markers and temporal intervals between them so as to investigate cerebellar involvement in sequence order and temporal interval learning. We hypothesized that cerebellar patients would show a reduced temporal precision in responses, coinciding with reduced performance on the task requiring spatio-temporal prediction, but not on the reactive timing task. Furthermore, we expected that cerebellar patients would be impaired at both sequence order and temporal interval learning. SCA6 patients form an adequate subject group to test these hypotheses, since the atrophy specifically affects the cerebellum in adults (Zhuchenko et al. 1997; Mark et al. 2015). SCA6 is an autosomal dominant genetic disorder caused by a CAG repeat expansion in exon 47 of the CACNA1A gene, which encodes the α1A ($Ca_v2.1$) subunit of neuronal P/Q-type voltage-gated calcium channel. This causes essentially pure cerebellar atrophy with a profound loss of Purkinje cells (Koeppen 2005) and manifests with a range of symptoms including imbalance, dysarthria, gait ataxia, upper limb incoordination and tremor (Gomez et al. 1997; Solodkin and Gomez 2011).

Our main finding is that SCA6 patients failed to establish spatio-temporal prediction in timing of their responses, reflecting a deficit in motor anticipation to upcoming events. Whereas healthy participants timed their button presses on average before the optimal timing with better temporal precision, this anticipation was absent in SCA6 patients. Performance of patients was reduced during the predictive timing task, but this deficit was limited to early correct responses that were made during the anticipatory period of the task. On the reactive timing task, randomization of sequence order of stimuli and temporal intervals between them resulted in reduced performance of the healthy controls. In contrast, randomization of temporal intervals did not further reduce performance in SCA6 patients. In summary, our findings suggest that cerebellar dysfunction may impair spatio-

temporal prediction and prevent temporal interval learning to occur. These findings lend support to leading views on cerebellar involvement in timing functions.

6.3 Subjects and methods

6.3.1 Participants

We tested 19 patients with spinocerebellar ataxia type 6 (SCA6) (mean age 61.8 ± 7.2, standard deviation (SD), range 49-80) and 14 healthy control participants (mean age 64.5 ± 4.7, SD, range 58-74) for this experiment. We attempted to achieve homogeneity across participants by using several exclusion criteria, including suffering from fatigue, neuropsychological disorders or expertise with musical instruments, since our task requires skills often used in, for example, piano and guitar playing. We excluded 7 patients from our analysis based on the occurrence of severe tremors (unilateral or bilateral) and/or excessive fatigue and 2 control participants based on technical issues of the behavioral task during the experiment. We included the remaining participants: 12 SCA6 patients (3 males; 2 left-handed) and 12 healthy control participants (7 males; 2 left-handed) in our data analysis. The average age of these SCA6 patients was 60.3 ± 6.4, SD (range 49-67) and 64.8 ± 4.8, SD (range 58-74) of control participants (t_{22} = 1.985, P = 0.06, two-sample t-test). We did not detect significant correlations between age and performance on the predictive timing task (r = 0.139, P = 0.517, Pearson correlation) or performance on the reactive timing task (r = -0.213, P = 0.318, Pearson correlation). All participants met the criteria of normal or corrected-to-normal vision, no excessive computer gaming or playing musical instruments for more than five hours a week and no history of other neuropsychological or motor disorders at the time of measurements or in the past. Participants were instructed prior to measurements and a written informed consent was obtained from all participants. A neurological exam was performed by a certified neurologist prior to the experiment to obtain a measurement of severity of cerebellar ataxia, according to the guidelines of the Scale for the Assessment and Rating of Ataxia (SARA) (Schmitz-Hübsch et al. 2006). The average SARA scores in SCA6 patients was 9.5 ± 5.2, SD on a scale of 0-40. This score is the average of scores on eight different subtasks, comprising an assessment of gait, stance, sitting, speech, finger and hand movements, and leg coordination. A score of 0 indicates that no neurological manifestations could be observed, whereas a score of 40 reflects the occurrence of severe neurological manifestations (Schmitz-Hübsch et al. 2006). This study was approved by the medical ethical committee of Erasmus MC, Rotterdam (MEC-2013-095).

6.3.2 Behavioral task

All participants completed the entire experiment, which included two modified versions of the Serial Interception Sequence Learning task (Gobel et al. 2011; Onuki et al. 2015): a predictive timing task and a reactive timing task. In both tasks (Fig 1A and B), four empty white circles were placed on top of a gray rectangular background screen. Each of the white circles corresponded to four keys on a standard Qwerty-keyboard, which in turn were associated to a pre-determined finger: the 'e' key corresponded to the left middle finger, the 'f' key to the left index, the 'j' key to the right index and the 'o' key to the right middle. In the predictive timing task, participants were instructed to press the corresponding button on the keyboard at the moment upward moving black circles (moving markers) completely overlapped with the corresponding static white circles (target markers) at the top of the screen (Fig 1A). Only one moving marker could overlap with a target marker at a given moment. The diameter of the moving markers was 20 pixels smaller than that of the target marker to fit completely inside the target markers and not to interfere with the moment of the complete overlap between markers as observed by the participant.

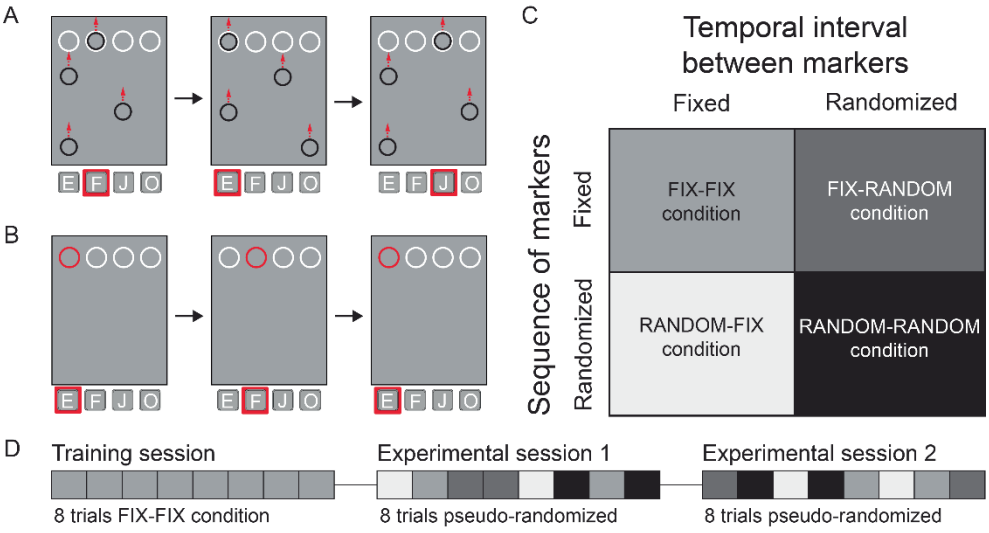

Fig 1. Behavioral task and experimental conditions. (A) During the predictive timing task black markers move from the bottom towards the four white target markers at the top of the screen. Participants are instructed to press the corresponding key at the moment that the black moving marker fully overlaps with the target marker (red square highlights the corresponding key). Target markers (from left to right) correspond to the 'e', 'f', 'j' and 'o' keys of a keyboard. (B) In the reactive timing task the white target markers change color to red for 200ms and participants are instructed to press the corresponding key as fast as possible. (C) Trials have one of four possible task conditions based on the sequence of and temporal interval between markers (fixed or randomized). (D) Both in the reactive timing task and predictive timing task, participants first complete a training session containing 8 trials of the FIX-FIX condition (i.e. fixed sequence and fixed interval), followed by two experimental sessions in which 2 trials of each condition are presented in a pseudo-randomized order.

Moving markers scrolled from the bottom of the screen to the top at a constant velocity (2.78 milliseconds per pixel). In the reactive timing task, participants were instructed to press the corresponding button on the keyboard as quickly as possible when the white target marker changed (flashed) to red for 200 milliseconds (Fig 1B). Only one target marker could flash at a given moment. Between each trial, a short task instruction appeared on the screen for 3 seconds: *'Press on the corresponding button with your finger as soon as the circles entirely overlap'* and *'Press on the corresponding button with your finger as soon as a circle flashes'* (translated from Dutch), during the predictive and reactive task, respectively. The duration of this task instruction formed the only intertrial interval time. Between each session, which lasted on average 7.9 ± 0.43 (SD) minutes participants took a short break (1-2 minutes) to reduce physical and mental fatigue. No feedback to indicate correct responses was given during the task. Both tasks were programmed in MATLAB R2010a (MathWorks, Massachusetts, USA) using Psychtoolbox-3 (Brainard 1997; Pelli 1997).

6.3.3 Task conditions

We studied the role of the cerebellum in sequence and temporal interval learning by employing in both tasks a 2-by-2 factorial task design with two factors: the sequential order of stimuli and temporal interval between them. The sequences of moving markers (or marker flashes) and the temporal intervals between stimuli were either according to a pre-defined order (FIX) or shuffled based on the pre-defined order (RANDOM) (Fig 1C). The combination of these resulted in four task conditions: FIX-FIX (*i.e.* fixed sequence and fixed intervals), FIX-RANDOM, RANDOM-FIX and RANDOM-RANDOM. For each condition, a sequence of 12 circles was presented 4 consecutive times, which resulted in 48 moving or flashing markers that were presented during each trial. In FIX-FIX condition of the predictive timing task, the sequence of moving markers followed the same order 4 consecutive times: F_{1386ms}-E_{718ms}-J_{852ms}-E_{852ms}-O_{852ms}-E_{702ms}-J_{969ms}-F_{952ms}-J_{1887ms}-O_{668ms}-F_{1420ms}-O_{668ms} (E: left-most trajectory, F: second trajectory, J: third trajectory, O: right-most trajectory, subscripted rates: temporal differences between moving markers in milliseconds). In FIX-FIX condition of the reactive timing task, the sequence of the marker flashes was E_{707ms}-F_{1345ms}-E_{1078ms}-O_{849ms}-J_{1200ms}-F_{703ms}-O_{1490ms}-E_{844ms}-J_{1824ms}-O_{1180ms}-F_{811ms}-J_{1075ms}. The average temporal interval between appearances was 1001 milliseconds (range 668-1887 milliseconds) in the predictive timing task and 1092 milliseconds (range 703-1824 milliseconds) in the reactive timing task.

6.3.4 Experimental protocol

All experiments were conducted in the participants' homes. A 13 or 15 inch computer screen was used to present the visual stimuli with a resolution of 1280 x 800 pixels (13 inch screen: all SCA6 patients and 4 out of 12 control participants). To rule out that screen size

had an effect on performance, we compared performance on both tasks of controls tested using a 13 inch screen (N = 4) versus controls tested using a 15 inch screen (N = 8). We did not find significant differences between these controls on both the predictive timing task (t_{10} = 0.981, P = 0.35, two-sample t-test) and on the reactive timing task (t_{10} = 0.869, P = 0.405). Participants were instructed prior to the experiment by an information letter mailed in advance. The tasks were also verbally explained to the participants right before starting the tasks. A summary of the instructions was finally displayed on the screen before the task began. When participants confirmed they fully understood the tasks, we started the experiment. Each task consisted of one training session and two experimental sessions. During the training session, eight trials with the FIX-FIX condition were presented. In each experimental session, each task condition was presented twice in a pseudo-randomized order using randomization algorithms in MATLAB (Fig 1D). All SCA6 patients and 5 out of 12 control participants started with the predictive timing task, followed by the reactive timing task as part of an experimental sequence. The remaining control participants (N = 7) first started with the reactive timing task, directly followed by the predictive timing task. To rule out that the order of tasks had an effect on performance, we compared performance on both tasks of controls tested first on the predictive task (N = 5) versus controls tested first on the reactive task (N = 7). We did not find significant differences between these controls on both the predictive timing task (t_{10} = 0.157, P = 0.878, two-sample t-test) and on the reactive timing task (t_{10} = 0.727, P = 0.484, two-sample t-test).

6.3.5 Analysis of behavioral data

Classification of correct responses depended on two factors, pressing the corresponding button and pressing the button within a given time window. To maximize the sensitivity of analyzing responses within a set time window, we calculated performance as the area under the curve of the correct ratio (AUCCR). The correct ratio was defined as the number of corresponding (correct) button presses within a time window, divided by the total number of markers within a trial. The minimum temporal interval between markers was 668 milliseconds in the predictive timing task and 703 milliseconds in the reactive timing task. Based on these minimum times, we used a time window between -334ms to +334ms relative to perfect marker overlap in the predictive timing task and 0 to 703ms after marker flash in the reactive timing task throughout our analysis. To assess spatio-temporal prediction in the predictive timing task, we calculated the AUCCR before marker overlap (-334ms to < 0ms) representing early correct responses and after marker overlap (> 0ms to +334ms), representing late correct responses. We ascertained normality of data distributions using the Shapiro-Wilk test. Unless indicated otherwise, we used one-way repeated measures analyses of variance (ANOVA) with trial number (for training sessions) or trial condition (for experimental sessions) as within-subject variable and group as between-subject variable to test AUCCR on both reactive and predictive tasks. We used the Mauchly's test to test the assumption of sphericity and in case this assumption was violated,

we applied the Greenhouse-Geisser correction. Levene's test of equality of error variances was used to test whether the assumption of equal error variances was met. To analyze pooled response and reaction times, we used the non-parametric Wilcoxon rank sum test and Wilcoxon signed rank test with Bonferroni correction for multiple comparisons, since these distributions violated the assumption of normality. We compared variances of these distributions using the Brown-Forsythe test. Comparison of the first principal component (PC1) of the AUCCR of both tasks was done using independent-samples t-tests and a correlation analysis was performed using the Pearson correlation. These performance measures were also used in the methods section to test for effects of age, screen size and task order. Statistics were conducted in SPSS version 22 (IBM, New York, USA) and MATLAB R2011b (MathWorks, Massachusetts, USA). Results are reported as mean ± standard error of the mean (SEM), unless indicated otherwise.

6.4 Results

6.4.1 SCA6 patients show lower predictive motor timing performance, localized to early correct responses

We used area under the curve of the correct ratio (AUCCR) to analyze performance of responses made within a temporal window around complete marker overlap (-334ms to +334ms; all correct responses). Over the course of the training session, both SCA6 patients and controls learned the sequence and timings of the markers (Fig 2A). Controls showed a significantly higher AUCCR compared to SCA6 patients during the training session, indicating that controls made more correct button presses within the assigned time window (main effect of trials: $F_{7,154} = 7.44$, $P < 0.001$; main effect of group: $F_{1,22} = 10.23$, $P < 0.01$; interaction trials x group: $F_{7,154} = 0.87$, $P = 0.53$). To assess the effect of spatio-temporal prediction in our task, we segregated the data based on the time of button press. Early and late correct responses correspond to button responses made before or after the moving marker completely overlapped with the target marker, respectively (Fig 2B and C). When analyzing early correct responses we found that controls showed a significantly higher AUCCR compared to SCA6 patients, although both groups showed a learning effect (main effect of trials: $F_{7,154} = 10.67$, $P < 0.001$; main effect of group: $F_{1,22} = 15.56$, $P = 0.001$; interaction trials x group: $F_{7,154} = 1.25$, $P = 0.28$). In contrast, for late correct responses we found no significant differences in AUCCR between groups and no learning effect (main effect of trials: $F_{3.313,\ 72.883} = 0.71$, $P = 0.56$; main effect of group: $F_{1,22} = 0.02$, $P = 0.89$; interaction trials x group: $F_{3.313,\ 72.883} = 2.4$, $P = 0.23$, with Greenhouse-Geisser correction). A third comparison including all factors revealed a significant interaction between groups and type of correct response (early versus late), confirming that the observed group difference was localized to early correct responses only ($F_{1,\ 22} = 10.09$, $P = 0.004$, with Greenhouse-Geisser correction; two-way repeated measures ANOVA). In short, our data

shows a performance difference between SCA6 patients and healthy controls during training on the predictive timing task, which is localized to (early) correct responses made during the anticipatory period of the paradigm.

6.4.2 SCA6 patients show impaired anticipation in motor timing

To gain insight in the characteristics of motor timing in the predictive task, we visualized response time distributions of correct button presses of both controls and SCA6 patients (Fig 2D and E). Negative and positive response times correspond to button presses before and after perfect marker overlap, respectively. We pooled response times of correct button presses from all participants per group, since some SCA6 patients had only few correct responses per trial. This resulted in analyses based on a fixed template design.

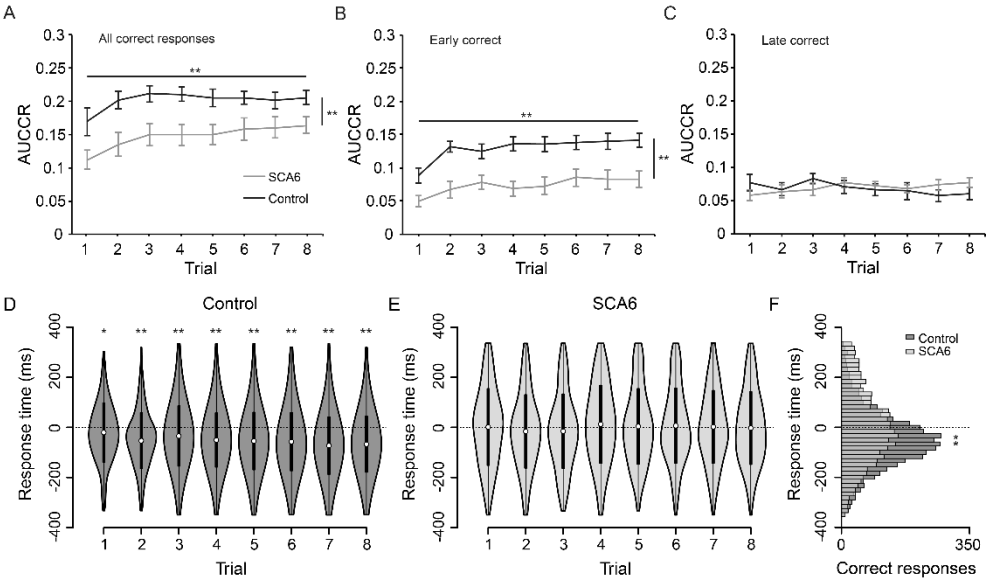

Fig 2. Results training session of predictive timing task. (A) Task performance showing all correct responses, expressed as area under the curve of the correct ratio (AUCCR) for both controls and SCA6 patients, showing a learning effect and a difference between groups. (B) AUCCR of early correct responses only, where the learning effect and group differences are present. (C) AUCCR of late correct responses only, where no learning effect or group differences are present. (D) Response times distributions of correct button presses of controls. Average response times are significantly lower than 0ms on all trials (asterisks). (E) Response times distributions of correct button presses of SCA6 patients. Average response times are not significantly different from 0ms on any of the trials. (F) Distribution of pooled response times for all training trials, showing that controls time their button press more precisely as observed by a smaller variance compared to SCA6 patients (asterisks). (A, B, C) Error bars represent SEM, ** indicates $P < 0.01$ for main effects of trials (asterisks horizontal line) and main effects of group (asterisks vertical line). (D, E) White dots represent the mean and black bars represent the SD. (F) Histogram shows 16.7ms bins. * indicates $P < 0.05$, ** indicates $P < 0.01$

We calculated average response times for each trial of the training session: trial 1 (SCA6: 2.7 ± 154.8ms, control: -20.2 ± 120.3ms; mean ± SD), trial 2 (SCA6: -15.9 ± 148.3ms, control -51.9 ± 113.3ms), trial 3 (SCA6: -14.8 ± 150.3ms, control: -33.9 ± 122.2ms), trial 4 (SCA6: 12.1 ± 157.4ms, control: -49.1 ± 110ms), trial 5 (SCA6: 4.5 ± 152.8ms, control: -53.2 ± 116.6ms), trial 6 (SCA6: 6.9 ± 151.2ms, control: -55.9 ± 117.8ms), trial 7 (SCA6: 1.7 ± 147ms, control: -71.1 ± 116.3ms) and trial 8 (SCA6: -1.4 ± 147ms, control: -65.8 ± 113.5ms). We found that response times of control participants were significantly lower than those of SCA6 participants on all trials, except on trial 1 and 3 (trial 1: mean difference (MD) = 22.9ms, $Z = 2.42$, $P = 0.12$; trial 2: MD = 36ms, $Z = 4.26$, $P < 0.001$; trial 3: MD = 19.1ms, $Z = 2.53$, $P = 0.09$; trial 4: MD = 61.2ms, $Z = 7.0$, $P < 0.001$; trial 5: MD = 57.7ms, $Z = 6.22$, $P < 0.001$; trial 6: MD = 62.8ms, $Z = 7.24$, $P < 0.001$; trial 7: MD = 72.8ms, $Z = 8.37$, $P < 0.001$; trial 8: MD = 64.4ms, $Z = 7.31$, $P < 0.001$; Wilcoxon rank sum test, with Bonferroni correction).

Previous findings have indicated that healthy participants establish spatio-temporal prediction during the training session of this predictive timing task (Onuki et al. 2015), as indicated by average response times lower than 0ms. Indeed, this effect was also present in our control group, since we found that response times were significantly lower than 0ms on all trials of the training session (trial 1: $Z = -2.84$, $P = 0.04$; trial 2: $Z = -9.51$, $P < 0.001$; trial 3: $Z = -6.5$, $P < 0.001$; trial 4: $Z = -9.46$, $P < 0.001$; trial 5: $Z = -9.85$, $P < 0.001$; trial 6: $Z = -10.16$, $P < 0.001$; trial 7: $Z = -12.13$, $P < 0.001$; trial 8: $Z = -11.65$, $P < 0.001$; Wilcoxon signed rank test, with Bonferroni correction) (Fig 2D). In contrast, we did not find this effect in our SCA6 patient group, given that average response times of SCA6 patients were not different from 0ms on any of the training trials (trial 1: $Z = -0.51$, $P = 1$; trial 2: $Z = -1.87$, $P = 1$; trial 3: $Z = -1.93$, $P = 1$; trial 4: $Z = -1.84$, $P = 1$; trial 5: $Z = -0.27$, $P = 1$; trial 6: $Z = -0.66$, $P = 1$; trial 7: $Z = -0.37$, $P = 1$; trial 8: $Z = -0.24$, $P = 1$; Wilcoxon signed rank test, with Bonferroni correction) (Fig 2E). These findings indicate that spatio-temporal prediction is established during the training session in control participants, but not in SCA6 patients.

6.4.3 SCA6 patients show reduced temporal precision in predictive motor timing

Since participants were instructed to time their button presses as closely as possible to perfect marker overlap, we investigated whether both groups were able to correctly time their button press. Therefore, we assessed whether there were differences in response time distributions between groups with variance as a measure of precision. A lower variance of response times would indicate a higher precision, whereas a higher variance would suggest a more temporally distributed response pattern, indicating a lower precision. To address this question, we compared the variance of pooled response time distributions of the training session between groups using the Brown-Forsythe test of variances, since this test is relatively robust and insensitive to deviations from normality (Brown and Forsythe 1974). We found that SCA6 patients showed a significantly higher variance of response times

compared to controls (SCA6: $2.284x10^4$ ms^2, control: $1.371x10^4$ ms^2, $F_{1,5808.03} = 239.98$, $P < 0.001$) (Fig 2F). To verify that this difference was also present during the experimental sessions, we compared the variance of pooled response times of correct responses during the experimental sessions and we found that also here controls had a significantly higher variance (SCA6: $2.195x10^4$ ms^2, control: $1.352x10^4$ ms^2, $F_{1, 14580.35} = 239.98$, $P < 0.001$). These results indicate that correct button presses were more temporally distributed in the SCA6 group, corresponding to a lower temporal precision of responses during both training and experimental sessions. Together, these findings suggest that healthy participants anticipate the upcoming event of a marker overlap with better temporal precision, whereas this anticipation of motor timing from the spatial and temporal cues is impaired in SCA6 patients.

6.4.4 Sequential or temporal order randomization of markers does not affect predictive motor timing performance

We investigated sequential order and temporal interval learning by randomizing the order and temporal intervals of markers, resulting in four conditions that were presented during experimental sessions (Fig 1C and D). We calculated the AUCCR for both groups during different trial conditions: FIX-FIX condition (SCA6: 0.18 ± 0.01, control: 0.21 ± 0.013), FIX-RANDOM condition (SCA6: 0.178 ± 0.011, control: 0.208 ± 0.012), RANDOM-FIX condition (SCA6: 0.183 ± 0.011, control: 0.208 ± 0.011) and RANDOM-RANDOM condition (SCA6: 0.177 ± 0.01, control: 0.204 ± 0.011). No significant differences in AUCCR between trial conditions or between groups were found, although the main effect of group approached the significance level and could be considered a trend (Fig 3A). Moreover, there was no interaction effect between conditions and groups (main effect of condition: $F_{3,66} = 0.82$, $P = 0.49$; main effect of group: $F_{1,22} = 3.46$, $P = 0.08$; interaction group x condition: $F_{3,66} = 0.31$, $P = 0.82$). Therefore, we could conclude from these data that randomizing sequences or temporal interval of markers did not lead to differences in performance or overall group differences when considering all correct responses.

Since we had found group differences in predictive motor timing for early correct responses during training (Fig 2B), we hypothesized that specifically these 'anticipatory' responses could be affected by randomization of sequence or temporal interval of markers. Therefore, we analyzed the data based on the timing of button presses and compared performance between conditions and groups (Fig 3B and C). We calculated the AUCCR of early correct responses on the FIX-FIX condition (SCA6: 0.091 ± 0.012, control: 0.139 ± 0.011), FIX-RANDOM condition (SCA6: 0.096 ± 0.012, control: 0.141 ± 0.009), RANDOM-FIX condition (SCA6: 0.099 ± 0.01, control: 0.144 ± 0.009), and RANDOM-RANDOM condition (SCA6: 0.091 ± 0.008, control: 0.137 ± 0.007) and we found that AUCCR differed significantly between groups. However, randomizing the sequence or temporal interval of markers did not lead to performance differences (main effect of condition: $F_{3,66} = 1.94$, $P = 0.132$; main

effect of group: $F_{1,22}$ = 11.95, P = 0.002; interaction group x condition: $F_{3,66}$ = 0.38, P = 0.99) (Fig 3B). In addition, we investigated whether randomization had an effect on performance for late correct responses (Fig 3C). We calculated the AUCCR during the FIX-FIX condition (SCA6: 0.084 ± 0.007, control: 0.069 ± 0.01), FIX-RANDOM condition (SCA6: 0.079 ± 0.009, control: 0.064 ± 0.009), RANDOM-FIX condition (SCA6: 0.08 ± 0.007, control: 0.061 ± 0.009), and RANDOM-RANDOM condition (SCA6: 0.082 ± 0.009, control: 0.065 ± 0.008) and performed the same analysis. We found that AUCCR of late correct responses did not differ between groups or between conditions. Also, the data did not reveal an interaction effect (main effect of condition: $F_{3,66}$ = 1.25, P = 0.30; main effect of group: $F_{1,22}$ = 2.09, P = 0.16; interaction group x condition: $F_{3,66}$ = 0.17, P = 0.92). A third analysis including all factors confirmed that the significant group difference was localized to early correct responses only (interaction group x type of correct response (early versus late): $F_{1, 22}$ = 10.01, P = 0.004; two-way repeated measures ANOVA). Thus, although there were group differences in early correct responses, randomizing the order and temporal intervals of markers did not influence predictive motor timing performance regardless of the timing of responses.

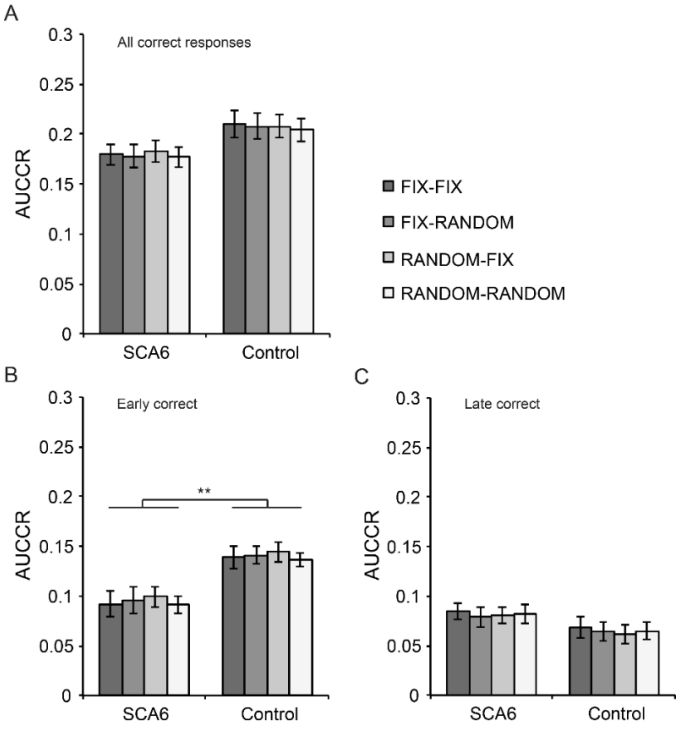

Fig 3. Results experimental sessions of predictive timing task. (A) Task performance on different trial conditions is visualized for both SCA6 patients and controls. No differences between groups or between conditions are observed in all correct responses. (B) AUCCR calculated for early correct responses shows a significant group difference between SCA6 patients and controls, but not between conditions. (C) AUCCR calculated for late correct responses does not show any differences between conditions or between groups. Error bars represent SEM, ** indicates P < 0.01

6.4.5 Lower predictive motor timing performance of SCA6 patients is limited to responses during the anticipatory period

To further compare performance of groups depending on the timing of response, but regardless of the trial condition, we conducted a principal component analysis (PCA) for dimension reduction. AUCCR scores for early correct responses between trial conditions were highly inter-correlated, at least $r = 0.91$ ($P < 0.001$, Pearson correlation). Kaiser-Meyer-Olkin measure of sampling adequacy was 0.87, Bartlett's test of sphericity was significant ($\chi^2(6) = 142.67$, $P < 0.001$) and all communalities were above 0.94, confirming that this data was suitable for PCA. We found that the first principal component (PC1) explained 95% of the variance and therefore we used this measure to represent performance of early correct responses. Next, we subjected AUCCR scores for late correct responses to PCA and consistently found a high inter-correlation between performance on different conditions (at least $r = 0.85$, $P < 0.001$, Pearson correlation). Kaiser-Meyer-Olkin measure of sampling adequacy was 0.87, Bartlett's test of sphericity was significant ($\chi^2(6) = 101.11$, $P < 0.001$) and all communalities were above 0.87. We found that the first principal component (PC1) explained 90.1% of the variance and therefore we used this measure to represent performance of late correct responses. We then used these measures to compare performance between groups, depending on the timing of response, regardless of the trial condition. We found a significant interaction effect between performance (PC1 of early vs late) and group ($F_{1, 22} = 9.76$, $P = 0.005$), although the main effect for group in this analysis did not reach the significance level ($F_{1,22} = 3.65$, $P = 0.069$). P*ost-hoc* tests confirmed that the group difference was localized to PC1 of early correct responses, but not to PC1 of late correct responses (early: $t_{22} = 3.34$, $P = 0.006$; late: $t_{22} = -1.44$, $P = 0.328$, two-sample t-test with Bonferroni correction). In summary, although task performance was not influenced by randomization of sequences or temporal intervals, we observed a higher performance of early correct responses in controls only, which is in line with our results from the training session.

6.4.6 SCA6 patients and controls perform comparably during reactive timing task training

To investigate whether SCA6, in addition to predictive motor timing, also affected reactive motor timing functions, we tested all participants on a related reactive motor timing task where no prediction could be made based on visual cues. We calculated AUCCR of corresponding button presses made after marker flash (0-703ms) as performance measure during the training session, in which eight trials of the FIX-FIX condition were presented (Fig 1D). Since this task was purely reactive, we did not make a distinction between early and late responses. Both groups showed learning of the task, evidenced by an increase in AUCCR over the course of the training (Fig 4A). We did not observe a group difference, although P-value approximation to significance threshold suggested a trend.

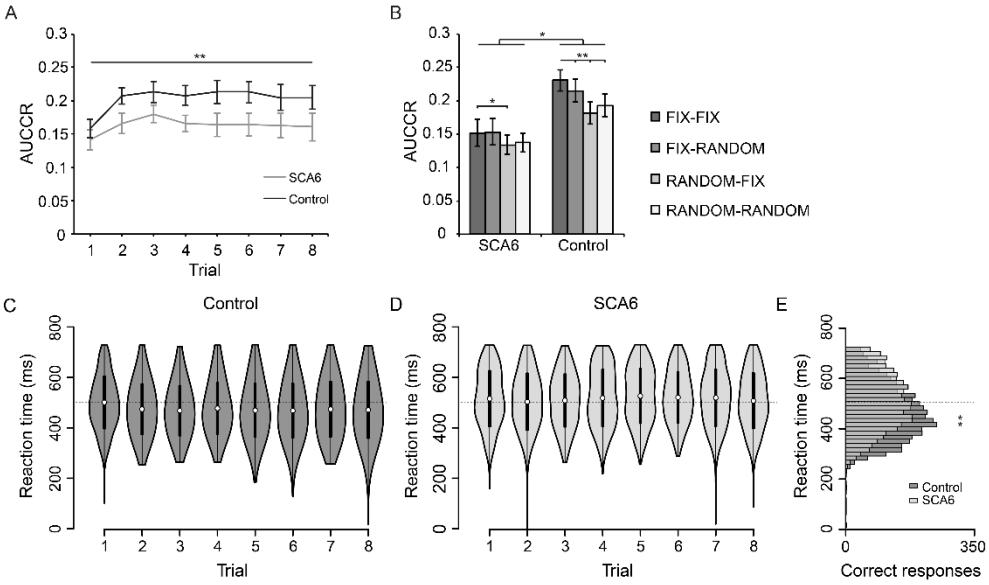

Fig 4. Results of reactive timing task. (A) Task performance expressed as AUCCR of correct responses after marker flash for both controls and SCA6 patients, showing that learning occurs over the course of the trials (asterisks horizontal line). (B) AUCCR calculated for different trial conditions during experimental sessions. The data shows group differences, as well as differences between all conditions with the FIX-FIX condition in the control group, but only between the RANDOM-FIX and the FIX-FIX condition in the SCA6 group. (C) Reaction time distributions of correct button presses during training for controls and (D) for SCA6 patients. (F) Distribution of pooled reaction times for all training trials. Variance of the reaction time distribution was smaller in controls (asterisks). (A, B) Error bars represent SEM, * indicates $P < 0.05$, ** indicates $P < 0.01$ for main effects of trials (asterisks horizontal line panel A) and main effects of condition and group (asterisks panel B). (D, E) Dotted line indicates 500ms for visual aid, white dots represent the mean and black bars represent the SD. (F) Histogram shows 16.7ms bins. ** indicates $P < 0.01$

We also did not observe an interaction effect between groups and trials (main effect of trials: $F_{7,154} = 9.88$, $P < 0.001$; main effect of group: $F_{1,22} = 3.47$, $P = 0.076$; interaction trials x group: $F_{7,154} = 1.41$, $P = 0.21$). In short, both groups increased their performance during the training, and overall there were no training differences between groups in this respect.

6.4.7 SCA6 patients and controls show differences in reaction times and precision during reactive timing task training

We visualized reaction time distributions of the reactive timing task, showing development of reaction times of both groups over the training session (Fig 4C and D). We then calculated average reaction times of pooled correct responses on all trials of the training session: trial 1 (SCA6: 518.9 ± 113.8ms, control: 499.8 ± 107ms; mean ± SD), trial 2 (SCA6:

506.8 ± 115.8ms, control 477.4 ± 103.4ms), trial 3 (SCA6: 510 ± 107.6ms, control: 471.5 ± 102ms), trial 4 (SCA6: 521.6 ± 115.9ms, control: 480.4 ± 105.3ms), trial 5 (SCA6: 529.4 ± 111ms, control: 473.1 ± 108.8ms), trial 6 (SCA6: 524.2 ± 104ms, control: 471.7 ± 110.1ms), trial 7 (SCA6: 522.4 ± 115.5ms, control: 475.2 ± 112.2ms) and trial 8 (SCA6: 510.4 ± 112.9ms, control: 474.3 ± 115ms). Significantly higher reaction times for SCA6 patients were observed for all trials, except for trial 1 (trial 1: mean difference (MD) = 19.1ms, Z = 2.49, P = 0.1; trial 2: MD = 29.4ms, Z = 4.34, P < 0.001; trial 3: MD = 38.5ms, Z = 5.64, P < 0.001; trial 4: MD = 41.1ms, Z = 5.56, P < 0.001; trial 5: MD = 56.3ms, Z = 7.62, P < 0.001; trial 6: MD = 52.5ms, Z = 7.3, P < 0.001; trial 7: MD = 47.2ms, Z = 6.2, P < 0.001; trial 8: MD = 36.1ms, Z = 4.78, P < 0.001; Wilcoxon rank sum test, with Bonferroni correction).

Next, we compared variances of pooled reaction times of correct button presses during training between groups and found a small but significant difference in variance, in which the SCA6 patient group showed a higher variance (SCA6: $1.258x10^4$ ms^2, control: $1.172x10^4$ ms^2, $F_{1,7107.19} = 249.6$, P < 0.001, Brown-Forsythe test of variances) (Fig 4E). We did the same analysis for pooled reaction times during the experimental sessions and found a consistent difference in variance between groups (SCA6: $1.342x10^4$ ms^2, control: $1.163x10^4$ ms2, $F_{1,13277.38} = 200.21$, P < 0.001). Together, these results indicate that average reaction times were significantly higher for SCA6 patients compared to controls. Furthermore, SCA6 patients also consistently showed a mildly reduced temporal precision, based on the observation that correct responses were more widely temporally distributed within this group.

6.4.8 SCA6 patients show impaired learning of temporal interval order

We hypothesized that SCA6 patients would be impaired at learning sequences and temporal intervals of stimuli on the reactive timing task. In addition, controls could potentially use this type of learning as strategy to gain increased performance on conditions using fixed sequence or temporal intervals. To test this hypothesis, we visualized the AUCCR during FIX-FIX condition (SCA6: 0.152 ± 0.02, control: 0.231 ± 0.016), FIX-RANDOM condition (SCA6: 0.153 ± 0.02, control: 0.215 ± 0.017), RANDOM-FIX condition (SCA6: 0.134 ± 0.015, control: 0.181 ± 0.014), and RANDOM-RANDOM condition (SCA6: 0.138 ± 0.014, control: 0.193 ± 0.017) (Fig 4B). Using a repeated measures ANOVA we found a main effect of group, as well as a main effect of condition and an interaction effect (main effect of condition: $F_{1.71, 37.56} = 22.82$, P < 0.001; main effect of group: $F_{1,22} = 7.1$, P = 0.014; interaction condition x group: $F_{1.71,37.56} = 4.12$, P = 0.03, with Greenhouse-Geisser correction). Closer inspection of only SCA6 performance furthermore showed a main effect of condition ($F_{1.56, 17.15} = 4.29$, P < 0.039, with Greenhouse-Geisser correction). Planned contrasts comparing FIX-FIX condition with the other conditions revealed that the difference was located between the FIX-FIX condition and the RANDOM-FIX condition ($F_{1,11} = 6.23$, P = 0.03). Performance of control participants also showed a significant main effect of condition ($F_{3,33} = 23.45$, P <

0.001) and contrasts indicated that AUCCR on the FIX-FIX condition was significantly higher compared to all other conditions (versus FIX-RANDOM: $F_{1,11}$ = 15.49, P = 0.002; versus RANDOM-FIX: $F_{1,11}$ = 72.05, P < 0.001; versus RANDOM-RANDOM: $F_{1,11}$ = 21.02, P = 0.001) (Fig 4B). Together, these results show that although overall performance was reduced in the SCA6 patient group, randomizing the sequential order of stimuli resulted in reduced performance in both groups, suggesting that sequential order learning occurred in both groups. In contrast, randomizing the temporal interval order resulted in reduced performance only in the control group, but not in the SCA6 patient group. This suggests that only controls learned the temporal order of stimuli sufficiently, whereas this type of learning was reduced in SCA6 patients.

Complementary to the predictive timing task, we performed a PCA on AUCCR scores of all trial conditions to compare performance on groups independent of trial condition. Scores on all conditions were highly inter-correlated, at least r = 0.92 (P < 0.001, Pearson correlation). Kaiser-Meyer-Olkin measure of sampling adequacy was 0.81, Bartlett's test of sphericity was significant ($\chi^2(6)$ = 173.12, P < 0.001) and all communalities were above 0.93, confirming that this data was suitable for PCA. We found that PC1 explained 96.2% of the variance and therefore we used this measure to represent performance on the experimental sessions of the reactive timing task. Confirming our earlier findings, PC1 differed significantly between groups (t_{22} = 2.69, P = 0.013, two-sample t-test).

6.4.9 Performance on predictive and reactive motor timing tasks does not correlate with SARA scores

We hypothesized that if predictive and reactive motor timing functions are linked to cerebellar function, we could possibly find a relation between SCA6 symptom severity and performance on the tasks. To test this hypothesis, we performed an exploratory correlation analysis between performance on the predictive task and reactive timing task with individual scores on the Scale for the Assessment and Rating of Ataxia (SARA), which we obtained from 11 of the 12 SCA6 participants. Performance of both tasks was represented as the PC1 of scores on each task, as explained earlier. We did not find significant correlations between SARA score and scores on the predictive timing task (PC1 all correct responses) (r = -0.07, P = 0.85, Pearson correlation), PC1 of early correct responses (r = -0.509, P = 0.11, Pearson correlation), PC1 of late correct responses (r = 0.36, P = 0.27, Pearson correlation) and PC1 of reactive timing task (r = -0.5, P = 0.12, Pearson correlation).

6.5 Discussion

In this study, we subjected cerebellar patients and control subjects to two finger-movement timing paradigms to find out to what extent the cerebellum contributes to spatio-temporal prediction and whether cerebellar dysfunction leads to changes in motor timing and coordination. We found that SCA6 patients were impaired at establishing spatio-temporal prediction of finger movements based on dynamic visual stimuli. Healthy control participants precisely timed their button-presses before a moving stimulus completely overlapped with a target stimulus, thereby anticipating or even 'over-predicting' their motor timing with approximately 66ms at the end of the training session, a behavioral effect that has also been observed previously (Onuki et al. 2015). Instead, cerebellar patients failed to establish spatio-temporal prediction and placed their button presses generally more temporally distributed, indicative of reduced temporal precision in responses. Concomitantly, SCA6 patients had significantly lower performance of early correct responses placed in the anticipatory period, but not of late correct responses placed in the period after the moving stimulus overlapped with the target stimulus.

Our results support previous work that has associated the cerebellum with spatio-temporal prediction processes and substantiate recent proposals arguing that the cerebellum is responsible for 'monitoring' ongoing timing and adjustment based on temporal predictions (Petter et al. 2016). Striking similarities can be found with a study in which cerebellar patients and healthy participants had to precisely time their button press to intercept a moving target with a moving ball (Bareš et al. 2007). Lower hit-rates were observed in cerebellar patients and errors were equally distributed between (too) early and late responses. Interestingly, both this study and our results show a higher variability in patient response times, although in this study the variability was found to be limited to the late error trials, whereas we did not make such a distinction in our study. Using the same paradigm, cerebellar activations were found to be related to performance and were reduced in SCA patients (Bareš et al. 2011). Both these and our data indicate a predictive sub-second motor timing deficit in cerebellar patients, which could lead to impaired motor anticipation in daily life situations. For instance, Lang and Bastian (1999) showed that cerebellar patients failed to show anticipatory muscle activity when catching a falling weight, which made them unable to control the impact of the falling weight (Lang and Bastian 1999). In a more general context, a considerable amount of literature has associated the cerebellum with temporal processing in the sub-second range, which are processes that are also engaged during predictive motor timing. A compelling example of this is that cerebellar patients show increased variation in timing, amplitude and velocity of finger opening in overarm throwing of a ball, which consequently results in reduced accuracy of throwing (Timmann et al. 1999). Moreover, cerebellar lesions in humans, as well as in rodents, affect the acquisition and particularly the timing of conditioned responses in Pavlovian eye blink conditioning (Topka et al. 1993), highlighting that the cerebellar cortex is specifically involved in the time course and amplitude of this learned motor behavior (McCormick and

Thompson 1984; Perrett et al. 1993). Other studies employing explicit timing tasks, such as rhythmic finger tapping and temporal interval discrimination and reproduction, have provided convincing evidence for cerebellar involvement in sub-second temporal processing. An increased temporal variability during rhythmic tapping with the finger or foot has been found in cerebellar patients (Ivry and Keele 1989; Matsuda et al. 2015), particularly associated with lesions in the lateral cerebellar regions (Ivry et al. 1988). Neuroimaging studies have found reliable activation of the cerebellum among several other areas in the cerebello-diencephalic-parietal network during finger-tapping in synchrony or continuation after tones at constant intervals (Rao et al. 1997; Jänke et al. 2000; Pollok et al. 2008). Consistent with this finding, inactivating the ipsilateral cerebellar regions using repetitive transcranial magnetic stimulation (rTMS) introduced variability in the inter-tap interval (Del Olmo et al. 2007). Moreover, impaired temporal discrimination in the sub-second range has been found in both cerebellar patients and animal studies (Ivry and Keele 1989; Breukelaar and Dalrymple-Alford 1999; Casini and Ivry 1999; Grube et al. 2010) (but see also: (Nichelli et al. 1996; Mangels et al. 1998). Gooch et al. (2010) however did not find impairments in temporal discrimination, although they did find impaired temporal estimation, production and reproduction in cerebellar lesion patients (Gooch et al. 2010). The reproduction of temporal intervals furthermore recruits cerebellar regions (Jahanshahi et al. 2006; Bueti et al. 2008). This cerebellar activation commonly coincides with activity in other cortical areas, *e.g.* basal ganglia, supplementary motor area (SMA), premotor area and inferior parietal cortex. Inactivating the left and right lateral cerebellum with rTMS impairs performance at a temporal reproduction task on short interval (millisecond range), but not at second range intervals (Koch et al. 2007). The present view posits that the cerebellum is particularly involved in temporal processing at the sub-second scale, whereas the basal ganglia as part of a wider cortical network processes information at longer timescales (Ivry 1996; Jahanshahi et al. 2006; Lee et al. 2007; Koch et al. 2007; Fierro et al. 2007; Bueti et al. 2008; Meck et al. 2008; Aso et al. 2010). This view is however still debated, as some researchers claim that the precise role of the cerebellum in timing processes has not been proven so far (Harrington 2004a, b; Ivry 2004).

To assess the relationship between the performance of both tasks and indicators of SCA6 disease progression, we conducted a correlation analysis including the first PC as a measure of task performance in both predictive and reactive timing tasks and scores on the SARA (Schmitz-Hübsch et al. 2006). Against expectations we failed to find a correlation between performance and SARA score. A possible explanation for this is that SARA score is based on multiple sub-scores assessing a wide range of functions, such as walking, stance, sitting and speech, whereas performance on our tasks depends specifically on the ability to precisely coordinate finger movements and to make precisely timed motor executions. A high SARA score does not necessarily translate into reduced fine motor skills, but could be the result of a broad spectrum of symptoms. Not finding a correlation could be explained by the fact that we had a rather small amount of participants for this exploratory correlation analysis, and that the SARA scores of our SCA6 participants were relatively low. Increasing

the amount of participants with higher SARA scores could still reveal such an underlying relationship between task performance and SCA6 symptom severity.

In our reactive motor timing paradigm, we found that cerebellar patients overall scored worse than controls, which could indicate a general motor coordination deficit. Nevertheless, randomizing the sequence of stimuli resulted in a lower performance in both groups, indicating that sequence learning did occur in both SCA6 and control participants. Randomizing the temporal interval between markers, however, did not affect the performance of SCA6 patients, suggesting that temporal interval learning is impaired or that a deficit exists in the integration of spatial and temporal information in cerebellar patients. Learning of the sequence and/or temporal interval of stimuli could potentially aid in creating an expectation of which button to press and when to make the motor execution, respectively. This spatial and temporal expectation could be used within a strategy used during both the predictive and the reactive timing task, although randomization only resulted in performance differences during the reactive timing task. Learning of new motor sequences has been associated with enhanced activity in several brain areas, including the prefrontal cortex (PFC), putamen, intraparietal sulcus region (IPS), precuneus, premotor cortex (PMC), supplementary motor area (SMA) and cerebellum (Jenkins et al. 1994; Grafton et al. 1995; Hazeltine et al. 1997; Jueptner et al. 1997; Honda et al. 1998; Sakai et al. 1998, 2002; Toni et al. 1998; Doyon et al. 2002) (but see: Seidler et al. (2002)). It has been shown in multiple studies that during the initial stages of motor sequence learning frontal areas in combination with bilateral cerebellar regions show enhanced activation, after which the representation shifts to activation within the cortical-striatal circuit when the sequence has been learned (Jueptner et al. 1997; Sakai et al. 1998; Toni et al. 1998; Doyon et al. 2002). Also, a shift in activity from the cerebellar cortex to deep cerebellar nuclei with sequence learning has been shown, suggesting segregation of neural networks involved at different stages of motor sequence learning (Doyon et al. 2002). Interestingly, the hippocampus has been shown to be active during learning of sequences (Schendan et al. 2003), but also during retrieval of learned sequences (Ross et al. 2009). A relationship between neural activity of hippocampal CA1 neurons and nonspatial sequence coding of odors has been found in rats, thus implying a role for the hippocampus in coding for sequential position of nonspatial objects (Allen et al. 2016). These hippocampal related findings are interesting in the light of our recent observations of cerebellar-hippocampal interaction during spatio-temporal prediction (Onuki et al. 2015), although the former sequences may not be related to timing at the millisecond level. Within the temporal domain, sustained activity in the lateral cerebellum and several structures within the neocortical-cerebellar network has been associated with temporal sequence learning in the form of intervals and rhythm (Ramnani and Passingham 2001; Schubotz and van Cramon 2001; Sakai et al. 2002). Based on the cerebellar involvement in these forms of sequence learning, it seems likely that the observed deficits in temporal order learning can be attributed to cerebellar Purkinje cell specific degeneration in SCA6. These findings are in agreement with a previous study showing that cerebellar patients are indeed impaired on

temporal, but also spatial sequence learning in a serial reaction time task (Shin and Ivry 2003). Still, it should be noted that we were unable to detect sequence learning in cerebellar patients and healthy controls in our paradigm where spatio-temporal cues were available for motor prediction.

There are several limitations to our experimental approach. First, SCA6 covers a wide spectrum of symptoms (Gomez et al. 1997; Solodkin and Gomez 2011), among others poor motor coordination of upper limbs, tremors, physical fatigue and oculomotor deficits. All of these may have affected participants' ability to execute the tasks, since performance on both tasks was not only dependent on motor timing (*i.e.* pressing the button on time or as fast as possible), but also depended on precise finger movement coordination for pressing the right button. The possible influence of reduced motor coordination on predictive timing performance in SCA6 patients, as shown by reactive timing group differences, cannot be fully discounted. We attempted to minimize this influence by designing the paradigm in a way that movement of only one finger at a time was required instead of multiple fingers at the same time, and that the movement-speed of markers was acceptable for both SCA6 and control participants. As such, SCA6 patients showed increasing performance during the training on both tasks, which could indicate that reduced motor coordination has played a relatively limited role in our predictive task. We furthermore excluded SCA6 patients exhibiting unilateral or bilateral tremors or pronounced physical fatigue, thereby attempting to reduce these additional influences. Consequently, this reduced the average SARA score in our patient group. Our findings suggest however that cerebellar patients with relatively mild symptoms (*i.e.* having a low SARA score) already exhibit pronounced deficits in predictive motor timing functions. Attentional deficits may also have played a role in our study. Cerebellar patients have been shown to exhibit deficits in shifting attention between visual stimuli (Akshoomoff and Courchesne 1994; Courchesne et al. 1994), although another study argues that response-related preparation processes rather than visuospatial attention shift are affected in cerebellar patients (Yamaguchi et al. 1998). Both of these are potentially of importance, particularly during motor sequence learning, since differences in brain activation have been found between implicitly and explicitly learned motor sequences, suggesting that a different set of brain structures is activated depending on the degree of attentional resources assigned to the learned motor sequence (Hazeltine et al. 1997). Furthermore, cerebellar activity has been shown during a verbal working memory task (Desmond et al. 1997) and a correlation between working memory and performance on temporal estimation, production and reproduction tasks has been found in subjects with cerebellar lesions (Gooch et al. 2010), although it remains unclear to what extent SCA6 affects working memory in our patients. The potential influence of oculomotor deficits can also not be fully discounted. Future research using eye-tracking hardware may clarify to what extent eye movement deficits in SCA6 patients affect predictive motor timing. Recently it has been shown in the mouse that inducing the expression of C terminus polypeptides in Purkinje cells, as seen in SCA6 patients, yields

both physiological and behavioral consequences, and may provide us with a new mouse model to study disease-related mechanisms of SCA6 in greater depth (Mark et al. 2015).

To conclude, we hereby provided evidence that SCA6 patients are impaired at establishing spatio-temporal prediction in timing of responses based on dynamic visual stimuli, reflecting a deficit in integration of spatial and temporal information and subsequently motor anticipation to upcoming events, using a task that demanded a prediction of when a stimulus would be at a certain target location. We propose that SCA6 patients are impaired in updating their forward internal model using spatial and temporal cues in the sub-second range, a process that has been postulated to require the cerebellum (Miall and Wolpert 1996; Wolpert et al. 1998).

6.6 Acknowledgements

We thank Dr. E. Brusse and Dr. R.S. van der Giessen for their clinical contribution to the study.

6.7 Appendix - Layman information letter to participants

(In Dutch, sent on Tuesday July 26th 2016 to all participants in this study)

Impaired spatio-temporal predictive motor timing associated with spinocerebellar ataxia type 6

'Aangetaste timing in het plannen van bewegingen bij mensen met spinocerebellaire ataxie type 6'

Auteurs: Robin Broersen, Yoshiyuki Onuki, Abdel R. Abdelgabar, Cullen B. Owens, Samuel Picard, Jessica Willems, Henk-Jan Boele, Valeria Gazzola, Ysbrand D. Van der Werf, en Chris I. De Zeeuw

Een samenwerking van: Erasmus Medisch Centrum, Rotterdam; Nederlands Herseninstituut, Amsterdam; Universiteit van Amsterdam en Vrije Universiteit, Amsterdam.

Inleiding

In het dagelijks leven maakt men veelal beslissingen op basis van ruimtelijke en tijdgerelateerde informatie uit de omgeving. Bijvoorbeeld, als u in een auto rijdt en er remt een auto voor u dan waarneemt u de ruimtelijke informatie ('waar') en tijdsgerelateerde informatie ('wanneer') van de auto. Een belangrijke functie van het brein is om deze informatie te integreren en op basis hiervan verschillende spiergroepen aan te sturen, zodat men goed en veilig kan functioneren. Een gepaste reactie in het voorbeeld van de auto zou zijn om uw been- en voetspieren aan te sturen om op de rem te trappen. Het cerebellum (of de 'kleine hersenen') is onder andere betrokken bij deze processen. Voorgaande onderzoeken hebben laten zien dat mensen met schade of een aandoening aan het cerebellum een scala aan symptomen vertonen. Onder andere spraakstoornissen, verstoringen van het evenwicht, oogbewegingen, lopen en incoördinatie van hand en arm komen voor. Daarnaast vinden er verstoringen plaats in de verwerking van tijdsgerelateerde informatie. Een van deze aandoeningen is spinocerebellaire ataxie type 6 (SCA6): een genetische aandoening waarbij sommige hersencellen in het cerebellum verloren gaan, waardoor het cerebellum niet goed meer werkt. Het is bekend dat SCA6 patiënten problemen kunnen hebben met het kunnen onderscheiden en reproduceren van de duur van geluidstonen of hebben moeite met het ritmisch tikken met de vinger. Bij het voorspellen van *waar* iets op *een bepaald moment in tijd* zal zijn speelt de tijdsgerelateerde

informatie dus een belangrijke rol en we kunnen veronderstellen dat dit proces verstoord zal zijn wanneer er schade is aan het cerebellum.

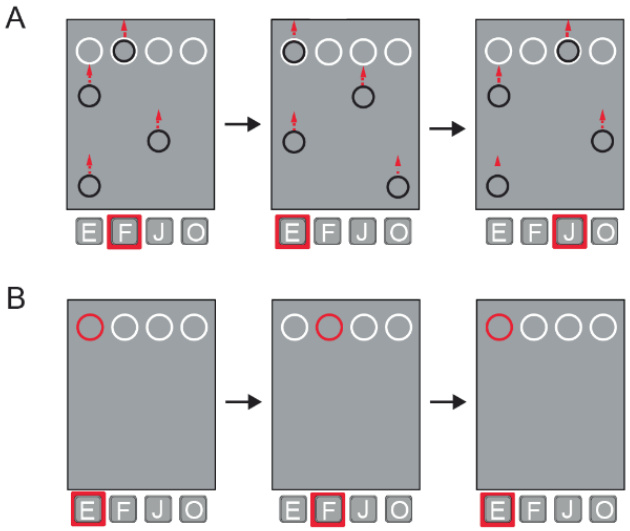

In ons onderzoek focussen we ons op de vraag of en op welke manier schade aan het cerebellum het voorspellen van bewegingen beïnvloedt. We testten 12 gezonde proefpersonen en 12 proefpersonen met SCA6 (leeftijd 49-74 jaar) op een computertaak waarbij een van vier corresponderende toetsen van een toetsenbord moest worden ingedrukt zodra een omhoogbewegende zwarte cirkel helemaal overlapte met een stilstaande witte cirkel **(figuur A)**. Binnen deze taak moest men dus voorspellen wanneer de cirkel op een bepaalde plaats zou zijn en op basis daarvan een vingerbeweging maken. Ter controle voerden proefpersonen ook een gerelateerde taak uit waarbij de witte cirkels een voor een in de kleur rood veranderde en zo snel mogelijk de corresponderende toets moest worden ingedrukt. Bij deze laatste taak was dus geen voorspelling in tijd nodig, alleen een reactie **(figuur B)**. Daarnaast onderzochten we of proefpersonen de volgorde waarin de cirkels verschenen en/of de tijdsintervallen tussen het verschijnen van de circkels konden leren.

Resultaten

Uit onze resultaten bleek dat SCA6 proefpersonen slechter scoorden op de 'bewegings-voorspel' taak **(figuur A)**. Echter was dit alleen het geval voor correcte bewegingen die gemaakt werden voordat de zwarte cirkel helemaal overlapte met de witte cirkel. In figuren C en D ziet u weergegeven wanneer correcte bewegingen werden gemaakt voor elk van de 8 training sessies, voor controle en SCA6 proefpersonen. Op de verticale as staat de tijd weergegeven rond cirkel overlap, waarin 0 milliseconden een perfecte overlap weergeeft.

Negatieve waarden (in milliseconden) geven een tijd weer vóórdat de overlap plaatsvindt en positieve waarden nadat de overlap heeft plaatsgevonden. De witte stippen geven het gemiddelde aan. Gezonde proefpersonen lieten tijdens de taak een verschuiving zien in correcte bewegingen naar de periode vóór cirkeloverlap en leerden dus een correcte beweging te maken voordat de cirkel helemaal overlapte **(figuur C)**.

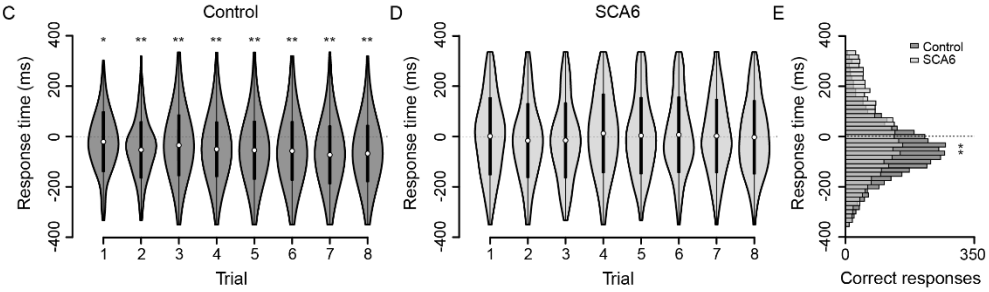

Echter, SCA6 proefpersonen lieten deze verschuiving niet zien: het moment waarop de correcte toets werd ingedrukt bleef onveranderd verdeeld rond cirkel-overlap **(figuur D)**. In figuur E ziet u de resultaten weergegeven voor alle trainingsessies per groep, waarin u kunt zien dat controle proefpersonen een hogere hoeveelheid correcte bewegingen (of: 'correct responses') laten zien met negatieve waarden, in vergelijking met SCA6 proefpersonen. We vonden echter geen verschillen in scores tussen beide groepen op het moment dat we de volgende van de cirkels en/of tijdsintervallen tussen de cirkels willekeurig veranderden (of 'randomiseerden').

Op de tweede 'reactie' taak **(figuur B)** scoorden beide groepen proefpersonen vergelijkbaar aan het begin van de taak, maar scoorden gezonde proefpersonen beter tijdens de rest van de taak. We zagen verder dat SCA6 proefpersonen iets langzamer waren in het maken van een correcte beweging dan gezonde proefpersonen. Toen we de volgorde van de cirkels en tijdsintervallen tussen de cirkels randomiseerden zagen we verschillen in scores binnen beide groepen **(figuur F)**. Het randomiseren van de volgorde van de cirkels leidde in beide groepen tot een lagere score, maar het randomiseren van de tijdsintervallen resulteerde in lagere scores alleen in gezonde proefpersonen.

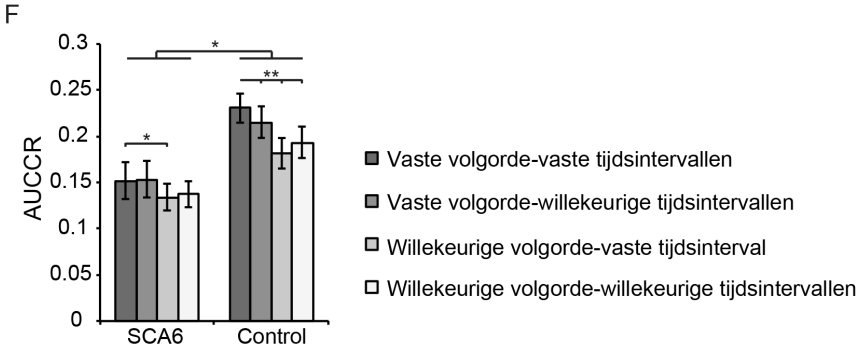

Conclusie

Dit onderzoek levert bewijs voor het bestaan van een vermindering van het vermogen een goed getimede beweging uit te voeren op basis van ruimtelijke en tijdsgerelateerde informatie in mensen met SCA6. De verschuiving van correcte bewegingen naar de tijd vóór overlap in gezonde proefpersonen kan mogelijk samenhangen met een verhoogde mate van voorspellen *waar* en *wanneer* de bewegende cirkel zal zijn. Dit kan leiden tot een hogere anticipatie van bewegingen in gezonde proefpersonen, waar mensen met een aandoening aan het cerebellum problemen kunnen ondervinden. Daarnaast blijkt uit onze resultaten dat er mogelijk een verminderd leervermogen van de volgorde van tijdsintervallen bestaat in SCA6 proefpersonen. Dit onderzoek geeft meer inzicht in de manier waarop het cerebellum betrokken is bij het integreren van ruimtelijke en tijdsgerelateerde informatie, en de daarop volgende planning en uitvoering van bewegingen. Het is belangrijk om te weten hoe schade of aandoeningen aan het cerebellum deze processen beïnvloeden, om zo meer kennis te vergaren over wat de consequenties zijn van cerebellaire aandoeningen in het dagelijks leven. Dit soort kennis biedt de basis voor begrip van ziekteprocessen, maar ook voor de ontwikkeling van nieuwe therapieën.

6.8 References

Akshoomoff NA, Courchesne E (1994) ERP evidence for a shifting attention deficit in patients with damage to the cerebellum. Cogn Neurosci J Of 6:388–399

Allen TA, Salz DM, McKenzie S, Fortin NJ (2016) Nonspatial Sequence Coding in CA1 Neurons. J Neurosci 36:1547–1563. doi: 10.1523/JNEUROSCI.2874-15.2016

Aso K, Hanakawa T, Aso T, Fukuyama H (2010) Cerebro-cerebellar interactions underlying temporal information processing. J Cogn Neurosci 22:2913–2925

Bareš M, Lungu O, Liu T, et al (2007) Impaired predictive motor timing in patients with cerebellar disorders. Exp Brain Res 180:355–365

Bareš M, Lungu OV, Husárová I, Gescheidt T (2010) Predictive Motor Timing Performance Dissociates Between Early Diseases of the Cerebellum and Parkinson's Disease. The Cerebellum 9:124–135. doi: 10.1007/s12311-009-0133-5

Bareš M, Lungu O V, Liu T, et al (2011) The neural substrate of predictive motor timing in spinocerebellar ataxia. The Cerebellum 10:233–244

Brainard DH (1997) The Psychophysics Toolbox. Spat Vis 10:433–436. doi: 10.1163/156856897X00357

Breukelaar JWC, Dalrymple-Alford JC (1999) Effects of lesions to the cerebellar vermis and hemispheres on timing and counting in rats. Behav Neurosci 113:78–90

Brown MB, Forsythe AB (1974) Robust Tests for the Equality of Variances. J Am Stat Assoc 69:364. doi: 10.2307/2285659

Bueti D, Walsh V, Frith C, Rees G (2008) Different brain circuits underlie motor and perceptual representations of temporal intervals. J Cogn Neurosci 20:204–214

Casini L, Ivry RB (1999) Effects of divided attention on temporal processing in patients with lesions of the cerebellum or frontal lobe. Neuropsychology 13:10

Coull JT, Nobre AC (2008) Dissociating explicit timing from temporal expectation with fMRI. Curr Opin Neurobiol 18:137–144. doi: 10.1016/j.conb.2008.07.011

Courchesne E, Townsend J, Akshoomoff NA, et al (1994) Impairment in shifting attention in autistic and cerebellar patients. Behav Neurosci 108:848–865

Del Olmo MF, Cheeran B, Koch G, Rothwell JC (2007) Role of the cerebellum in externally paced rhythmic finger movements. J Neurophysiol 98:145–152

Desmond JE, Gabrieli JD, Wagner AD, et al (1997) Lobular patterns of cerebellar activation in verbal working-memory and finger-tapping tasks as revealed by functional MRI. J Neurosci 17:9675–9685

Doyon J, Song AW, Karni A, et al (2002) Experience-dependent changes in cerebellar contributions to motor sequence learning. Proc Natl Acad Sci 99:1017–1022

Fierro B, Palermo A, Puma A, et al (2007) Role of the cerebellum in time perception: A TMS study in normal subjects. J Neurol Sci 263:107–112. doi: 10.1016/j.jns.2007.06.033

Gobel EW, Parrish TB, Reber PJ (2011) Neural correlates of skill acquisition: decreased cortical activity during a serial interception sequence learning task. NeuroImage 58:1150–1157

Gomez CM, Thompson RM, Gammack JT, et al (1997) Spinocerebellar ataxia type 6: gaze-evoked and vertical nystagmus, Purkinje cell degeneration, and variable age of onset. Ann Neurol 42:933–950

Gooch CM, Wiener M, Wencil EB, Coslett HB (2010) Interval timing disruptions in subjects with cerebellar lesions. Neuropsychologia 48:1022–1031. doi: 10.1016/j.neuropsychologia.2009.11.028

Grafton ST, Hazeltine E, Ivry R (1995) Functional mapping of sequence learning in normal humans. J Cogn Neurosci 7:497–510

Grube M, Cooper FE, Chinnery PF, Griffiths TD (2010) Dissociation of duration-based and beat-based auditory timing in cerebellar degeneration. Proc Natl Acad Sci 107:11597–11601. doi: 10.1073/pnas.0910473107

Harrington DL (2004a) Does the representation of time depend on the cerebellum?: Effect of cerebellar stroke. Brain 127:561–574. doi: 10.1093/brain/awh065

Harrington DL (2004b) Reply to: Evaluating the role of the cerebellum in temporal processing: beware of the null hypothesis. Brain 127:E14–E14. doi: 10.1093/brain/awh227

Hazeltine E, Grafton ST, Ivry R (1997) Attention and stimulus characteristics determine the locus of motor-sequence encoding. A PET study. Brain 120:123–140

Honda M, Deiber MP, Pascual-Leone A, et al (1998) Dynamic cortical involvement in implicit and explicit motor sequence learning. Brain 121:2159–2173

Ivry RB (1996) The representation of temporal information in perception and motor control. Curr Opin Neurobiol 6:851–857

Ivry RB (2004) Evaluating the role of the cerebellum in temporal processing: beware of the null hypothesis. Brain 127:E13–E13. doi: 10.1093/brain/awh226

Ivry RB, Keele SW (1989) Timing functions of the cerebellum. J Cogn Neurosci 1:136–152

Ivry RB, Keele SW, Diener HC (1988) Dissociation of the lateral and medial cerebellum in movement timing and movement execution. Exp Brain Res 73:167–180

Ivry RB, Spencer RMC, Zelaznik HN, Diedrichsen J (2002) The cerebellum and event timing. Ann N Y Acad Sci 978:302–317

Jahanshahi M, Jones CRG, Dirnberger G, Frith CD (2006) The Substantia Nigra Pars Compacta and Temporal Processing. J Neurosci 26:12266–12273. doi: 10.1523/JNEUROSCI.2540-06.2006

Jänke L, Loose R, Lutz K, et al (2000) Cortical activations during paced finger-tapping applying visual and auditory pacing stimuli. Cogn Brain Res 10:51–66

Jenkins IH, Brooks DJ, Nixon PD, et al (1994) Motor sequence learning: a study with positron emission tomography. J Neurosci 14:3775–3790

Jueptner M, Stephan KM, Frith CD, et al (1997) Anatomy of motor learning. I. Frontal cortex and attention to action. J Neurophysiol 77:1313–1324

Koch G, Oliveri M, Torriero S, et al (2007) Repetitive TMS of cerebellum interferes with millisecond time processing. Exp Brain Res 179:291–299. doi: 10.1007/s00221-006-0791-1

Koeppen A (2005) The pathogenesis of spinocerebellar ataxia. The Cerebellum 4:62–73. doi: 10.1080/14734220510007950

Lang CE, Bastian AJ (1999) Cerebellar subjects show impaired adaptation of anticipatory EMG during catching. J Neurophysiol 82:2108–2119

Lee K-H, Egleston PN, Brown WH, et al (2007) The role of the cerebellum in subsecond time perception: evidence from repetitive transcranial magnetic stimulation. J Cogn Neurosci 19:147–157

Mangels JA, Ivry RB, Shimizu N (1998) Dissociable contributions of the prefrontal and neocerebellar cortex to time perception. Cogn Brain Res 7:15–39

Mark MD, Krause M, Boele H-J, et al (2015) Spinocerebellar Ataxia Type 6 Protein Aggregates Cause Deficits in Motor Learning and Cerebellar Plasticity. J Neurosci 35:8882–8895. doi: 10.1523/JNEUROSCI.0891-15.2015

Matsuda S, Matsumoto H, Furubayashi T, et al (2015) The 3-Second Rule in Hereditary Pure Cerebellar Ataxia: A Synchronized Tapping Study. PLOS ONE 10:e0118592. doi: 10.1371/journal.pone.0118592

McCormick DA, Thompson RF (1984) Neuronal responses of the rabbit cerebellum during acquisition and performance of a classically conditioned nictitating membrane-eyelid response. J Neurosci 4:2811–2822

Meck WH, Penney TB, Pouthas V (2008) Cortico-striatal representation of time in animals and humans. Curr Opin Neurobiol 18:145–152. doi: 10.1016/j.conb.2008.08.002

Miall RC, Wolpert DM (1996) Forward models for physiological motor control. Neural Netw 9:1265–1279

Nichelli P, Alway D, Grafman J (1996) Perceptual timing in cerebellar degeneration. Neuropsychologia 34:863–871

Onuki Y, Van Someren EJW, De Zeeuw CI, Van Der Werf YD (2015) Hippocampal-cerebellar interaction during spatio-temporal prediction. Cereb Cortex 25:313–321

O'Reilly JX, Mesulam MM, Nobre AC (2008) The Cerebellum Predicts the Timing of Perceptual Events. J Neurosci 28:2252–2260. doi: 10.1523/JNEUROSCI.2742-07.2008

Pelli DG (1997) The VideoToolbox software for visual psychophysics: transforming numbers into movies. Spat Vis 10:437–442

Perrett SP, Ruiz BP, Mauk MD (1993) Cerebellar cortex lesions disrupt learning-dependent timing of conditioned eyelid responses. J Neurosci 13:1708–1718

Petter EA, Lusk NA, Hull C, et al (2016) Interactive roles of the cerebellum and striatum in sub-second and supra-second timing: Support for an initiation, continuation, adjustment, and termination (ICAT) model of temporal integration. Neurosci Biobehav Rev 71:739-755

Pollok B, Gross J, Kamp D, Schnitzler A (2008) Evidence for anticipatory motor control within a cerebello-diencephalic-parietal network. J Cogn Neurosci 20:828–840

Ramnani N, Passingham RE (2001) Changes in the human brain during rhythm learning. J Cogn Neurosci 13:952–966

Rao SM, Harrington DL, Haaland KY, et al (1997) Distributed neural systems underlying the timing of movements. J Neurosci 17:5528–5535

Ross RS, Brown TI, Stern CE (2009) The retrieval of learned sequences engages the hippocampus: Evidence from fMRI. Hippocampus 19:790–799. doi: 10.1002/hipo.20558

Sakai K, Hikosaka O, Miyauchi S, et al (1998) Transition of brain activation from frontal to parietal areas in visuomotor sequence learning. J Neurosci 18:1827–1840

Sakai K, Ramnani N, Passingham RE (2002) Learning of sequences of finger movements and timing: frontal lobe and action-oriented representation. J Neurophysiol 88:2035–2046

Schendan HE, Searl MM, Melrose RJ, Stern CE (2003) An FMRI study of the role of the medial temporal lobe in implicit and explicit sequence learning. Neuron 37:1013–1025

Schmitz-Hübsch T, Du Montcel ST, Baliko L, et al (2006) Scale for the assessment and rating of ataxia Development of a new clinical scale. Neurology 66:1717–1720

Schubotz RI, van Cramon Y (2001) Interval and ordinal properties of sequences are associated with distinct premotor areas. Cereb Cortex 11:210–222

Seidler RD, Purushotham A, Kim S-G, et al (2002) Cerebellum activation associated with performance change but not motor learning. Science 296:2043–2046

Shin J, Ivry RB (2003) Spatial and temporal sequence learning in patients with Parkinson's disease or cerebellar lesions. Cogn Neurosci J Of 15:1232–1243

Solodkin A, Gomez CM (2011) Spinocerebellar ataxia type 6. Ataxic Disord 103:461–473

Spencer RMC, Ivry RB (2013) Cerebellum and Timing. In: Manto M, Schmahmann JD, Rossi F, et al. (eds) Handbook of the Cerebellum and Cerebellar Disorders. Springer Netherlands, Dordrecht, pp 1201–1219

Timmann D, Watts S, Hore J (1999) Failure of cerebellar patients to time finger opening precisely causes ball high-low inaccuracy in overarm throws. J Neurophysiol 82:103–114

Toni I, Krams M, Turner R, Passingham RE (1998) The time course of changes during motor sequence learning: a whole-brain fMRI study. Neuroimage 8:50–61

Topka H, Valls-Solé J, Massaquoi SG, Hallett M (1993) Deficit in classical conditioning in patients with cerebellar degeneration. Brain 116:961–969. doi: 10.1093/brain/116.4.961

Wolpert DM, Miall RC, Kawato M (1998) Internal models in the cerebellum. Trends Cogn Sci 2:338–347

Yamaguchi S, Tsuchiya H, Kobayashi S (1998) Visuospatial attention shift and motor responses in cerebellar disorders. J Cogn Neurosci 10:95–107

Zhuchenko O, Bailey J, Bonnen P, et al (1997) Autosomal dominant cerebellar ataxia (SCA6) associated with small polyglutamine expansions in the alpha1A-voltage-dependent calcium channel. Nat Genet 15:62–69

Chapter 7

General discussion

Parts of this chapter have been adopted from:

Cathrin B. Canto, Robin Broersen and Chris I. De Zeeuw (2018). Intrinsic excitement in cerebellar nuclei neurons during learning

PNAS, 115 (40), p 9824-9826.

This thesis addresses the contribution of the cerebellum to time processing in relation to motor learning during simple and complex behaviors. A set of experiments is presented that explores this topic using invasive and non-invasive techniques in rodents and humans, respectively. The simplest form of behavior that has been examined in this thesis is delayed eyeblink conditioning (EBC), a type of associative learning that relies on precise integration of neuronal inputs in the cerebellum. This paradigm has served for many decades as a reliable measure of associative learning in cerebellar neuroscience, and its neuronal circuit is well understood. By employing this paradigm we focused our research in **Chapter 2 and 3** on the deep cerebellar nuclei (DCN), a region of the cerebellum that is essential for both the acquisition and expression of conditioned eyelid movements (Clark et al. 1984; Lavond et al. 1985; Yeo et al. 1985; Lavond and Steinmetz 1989; Sears and Steinmetz 1990; Bracha et al. 1994; Bao et al. 2000; Freeman and Rabinak 2004; Freeman et al. 2005; Ohyama et al. 2006; Mojtahedian et al. 2007). DCN neurons that provide the neuronal projections to the motor nuclei are interesting in this respect, because their positioning relative to their afferents is unique, they are one of the few cerebellar cell-types that are enveloped by perineuronal nets, and their activity represents the final output after the many computations that took place in the cerebellar cortex upstream. Therefore, studying how these neurons operate can be highly informative on cerebellar processing during various behaviors.

The second part of this thesis involves research in humans, where we could take advantage of the possibility to examine more complex behaviors. In **Chapter 4, 5 and 6** we studied different behaviors, but each in which the ability to utilize time-related information was essential. Timing was used implicitly in each paradigm, since we did not require our subjects to make an overt estimation of time (Coull and Nobre 2008). Rather, subjects used time and space information to estimate the trajectory of moving stimuli (spatio-temporal prediction) or to perceive the kinematic properties of ongoing hand/arm movements. Concurrent with the increased complexity of these non-standardized paradigms comes the increased difficulty to study temporal aspects of behavior in isolation. Often these behaviors rely on the concerted activity in cortico-cerebellar networks involving a range of brain areas, which complicates establishing the exact cerebellar contribution to timing aspects. Therefore, it serves the interpretation of the results to see the cerebellum as a 'node' within a brain-wide network rather than a segregated functional unit. Yet, we attempted to exactly pinpoint the loci of time-related activity in the cerebellum by separating timing processes from related motor components during the task. The use of adequate control task conditions was crucial to achieve this.

In this General discussion chapter we will provide a summary of our most important findings and we will describe our interpretations of these. Finally, we will discuss the findings in relation to the literature in order to arrive at a more elaborate understanding of timing in the cerebellum.

7.1 Plasticity during associative learning

In the first part of this thesis (**Chapter 2 and 3**) we sought to understand the anatomical and physiological changes that occur in the DCN during associative learning and the involvement of perineuronal nets (PNNs) thereof. These changes are important for animals to develop well-timed conditioned motor responses, such as during EBC (see General Introduction, **Chapter 1**). We found that during learning a multitude of plasticity mechanisms occur simultaneously and thus complement each other to accommodate memory storage. In order to identify causal relationships between DCN structure and function, we studied both synaptic markers and neuronal physiology. We found that PNNs in the DCN, known regulators of plasticity (van 't Spijker and Kwok 2017) are decreased after 5 days of EBC, coinciding with a reduction in the chemorepulsive protein Semaphorin-3A. To investigate whether there is a causal relationship between PNN decreases and learning, we enzymatically decreased PNNs in the same part of the DCN and found that learning is enhanced. Reductions in PNN and associated chemorepulsive molecules could allow structural plasticity changes to manifest during learning. Indeed, we found that after learning the density of mossy fiber (MF) terminals and Purkinje cell (PC) terminals is increased, particularly in the contralateral hemisphere (relative to the air puff). To further investigate whether PNNs are necessary for memory consolidation, we measured memory retention over a period of three weeks during which we presented periodic relearning sessions. The results suggest that despite the relearning sessions, mice without intact PNNs lose the memory trace. In addition, these mice are unable to quickly reacquire the previously-learned memory during a reacquisition session after the memory was extinct, suggesting that no previously stabilized synaptic contacts could facilitate memory recovery.

7.1.1 PNN-controlled adaptive changes in excitatory and inhibitory DCN afferents is a prominent mechanism during cerebellar learning

Our findings in **Chapter 2 and 3** emphasize that adaptive changes in afferent inputs to the DCN is a prominent mechanism in the cerebellum to facilitate learning. The observed increase in MFs is consistent with earlier reports (Kleim et al. 2002; Boele et al. 2013), whereas the increase in PC terminals has never been shown before. The findings further suggest that structural changes play a functional role during learning, since they are specifically localized to the eyeblink-encoding anterior interposed nucleus (IntA) and/or dorsolateral hump (DLH) (Heiney et al. 2014). MFs originating in the pontine nuclei (PN) are responsible for relaying the conditioned stimulus (CS) to the cerebellum (Solomon et al. 1986; Lewis et al. 1987; Bao et al. 2000; Freeman and Steinmetz 2011). An increase in MF terminals could therefore directly contribute to spike facilitation in the DCN during the CS to unconditioned stimulus (US) interval, which provides a mechanistic explanation for these observed increases. Interesting in this respect is that MFs are much more increased

in the DCN contralateral to the air puff (see also: Boele et al. 2013). Yet, these neurons innervate the eye contralateral to the air puff due to the double decussation in the descending motor pathway. EBC with a unilateral US however engages the bilateral DCN, since trigemino-olivary projections are bilateral (De Zeeuw et al. 1996), and the contralateral cerebellum also contributes to the conditioned response (CR) (Ivarsson and Hesslow 1993). To further investigate the role of this preferred laterality one could train mice in EBC with a bilateral US and study the associated MF changes, to establish whether this could cause a balanced MF increase.

A more remarkable finding from **Chapter 2** is the learning-related increase in PC terminals. From a physiological point of view this increase would not directly contribute to spike facilitation in the DCN, because an increased density of PC terminals leads to an increased inhibitory drive to DCN neurons (Telgkamp and Raman 2002; Pedroarena and Schwartz 2003; Hirono et al. 2018). During conditioning however, EBC-encoding PCs show a reduction in simple spike activity during the CS-US interval (Berthier and Moore 1986; Jirenhed et al. 2007; Ten Brinke et al. 2015). This synchronized disinhibition subsequently allows DCN neurons to increase spike activity (Gauck and Jaeger 2000; Person and Raman 2011) and as a result, evoke CRs (Berthier and Moore 1990; Ten Brinke et al. 2017). An important question that follows and still remains to be answered is how increased PC inhibition facilitates EBC learning. Our results from **Chapter 3** showing that enzymatically removing PNNs leads to increased PC inputs, lower basal spike frequencies and enhanced learning is consistent with the findings from **Chapter 2**, and with an earlier study (Hirono et al. 2018). However, it is unlikely that DCN neurons show sustained, lower spike activity after normal learning, which would imply that a decrease in PC-DCN synaptic strength would take place to counter this effect. This is conceivable since both long-term potentiation (LTP) and long-term depression (LTD) have been shown to occur at the PC-DCN synapse (Aizenman et al. 1998). If this indeed were the case, an advantage of receiving inputs from a more widespread population of PCs would be having a more robust representation of conditioned behavior, *i.e.* a higher amount of eyeblink-encoding PCs could relay task-related activity to the same DCN neuron. Further experiments that investigate the synaptic strength of PC-DCN synapses after learning may provide a more detailed perspective on this topic.

In addition to MFs and PCs, the third type of DCN afferents, climbing fibers collaterals (CFCs) that originate in the inferior olive (IO), remain enigmatic in the context of learning (Kitai et al. 1977; Andersson and Oscarsson 1978; Dietrichs and Walberg 1987; van der Want et al. 1989; De Zeeuw et al. 1997). This excitatory projection provides the DCN with a copy of the air puff-evoked 'teaching' signal (Ito 1984) that induces synaptic plasticity in the cerebellar cortex (Marr 1969; Albus 1971). Studies have shown that activity in CFCs leads to spike activity in a considerable proportion (~24%) of DCN neurons *in vivo* (Gould et al. 1993; Blenkinsop and Lang 2011). Our findings from **Chapter 2** further indicate that CFCs evoke short-latency spike activity after the US, since we could not block or diminish this activity by MF silencing. We found in ~18 percent of neurons an excitation, followed by a

clear inhibition presumably from PCs. However, to completely crystallize this finding one should inactivate CFCs specifically during and after the US. Nevertheless, the sequence of (CFC-mediated) excitation and (PC-mediated) inhibition could, in a similar way as in MFs, facilitate synaptic plasticity at the CFC-DCN synapse (Racine et al. 1986; Zhang and Linden 2006; Pugh and Raman 2006, 2008, 2009; Zheng and Raman 2010). On the other hand, more recent studies have argued that CFCs are far less effective at evoking excitatory currents in postsynaptic DCN neurons in adult animals compared to juveniles (Lu et al. 2016; Najac and Raman 2017), thereby calling their importance in adults into question.

Aside from their physiological relevance, is it possible that CFCs undergo structural changes during learning? In **Chapter 2** we studied the expression of vesicular glutamate transporter 2 (VGLUT2), which is expressed both in MFs and CFCs, whereas VGLUT1 is only expressed in MFs (Hioki et al. 2003). The absence of a learning-related increase in VGLUT2 suggests that they do not, however the accuracy of this approach is limited. In this way, we could potentially detect large structural changes in CFCs, but probably not detect smaller changes since it would be challenging to differentiate between MFs and CFCs. A better experimental approach that would generate a direct answer on this question would be to inject a viral vector in the IO, as done previously (Mathews et al. 2012), or to adopt a transgenic approach to achieve expression of a fluorescent protein in CFs. Studying the effect of EBC on reporter expression in the DCN would reveal structural changes in CFCs, if any would occur. For investigating the functional role of CFC activity during learning, one could specifically silence CFCs by locally injecting transgenic mice, after a cross between Ptf1a::creERT2 and vGLUT2$^{loxP/loxP}$ mice, with endoxifen, an active non-toxic derivative of tamoxifen that activates Cre-recombinase (Benedykcinska et al. 2016). This leads to local suppression of glutamate-based neurotransmission from CFCs (but inconveniently also passing fibers to the cortex), and represents to some extent a variation on the approach used previously (White and Sillitoe 2017). Altogether, due to the difficulty to genetically target CFCs and control their activity *in vivo*, so far studies have not been able to investigate their function and relevance yet (Pickford and Apps 2017).

7.1.2 MFs have only a minor contribution to neuronal activity in DCN during conditioned behavior

A compelling difference between the effects of EBC (**Chapter 2**) versus enzymatic PNN removal (**Chapter 3**) on DCN afferents is that during normal EBC learning VGLUT1+ MFs increase and after PNN removal they decrease, while learning is enhanced after PNN removal. This raises the question whether MF plasticity is at all required for learning. Previous studies have argued that MFs contribute to memory consolidation and may provide a structural basis for savings (Perrett et al. 1993; Medina et al. 2001; Ohyama et al. 2003, 2006), although our findings from optogenetic MF interference and whole-cell recordings during EBC imply that MFs do not substantially contribute to EBC-related spike

activity patterns in the DCN. We found that optogenetic MF activation and silencing induced spike activity changes and elicited eyelid movements after conditioning, yet such massive synchronized MF activity modulations are not likely to occur physiologically. Whereas direct electrical stimulation of MFs *in vitro* can clearly evoke DCN spike activity (Pugh and Raman 2008), dynamic clamp recordings have shown that asynchronous PC inputs can strongly diminish the effect of MF-driven excitation (Wu and Raman 2017). In line with this, electrical stimulation of the PN *in vivo*, presumably while DCN neurons receives asynchronous PC inputs, have been shown to evoke relatively small spike responses in the DCN (Gould et al. 1993). This would suggest that only when MF-driven excitation coincides with synchronous (or diminished) PC activity, can MFs effectively evoke excitatory responses in DCN neurons. Synchronous activity among PCs can occur for example during locomotion and depends on synchrony in the IO (De Gruijl et al. 2014; Hoogland et al. 2015).

Within EBC, a potential temporal window during which MFs could effectively evoke spike activity in DCN neurons is when PC activity is decreased during the CS-US interval in fully conditioned mice (Jirenhed et al. 2007). MFs are known to exhibit short spike-bursts with high frequencies *in vitro* (Rancz et al. 2007; Baade et al. 2016; Delvendahl and Hallermann 2016) and *in vivo* (Powell et al. 2015). Based on this pattern of activity, is likely that the highest MF activity can be observed shortly after CS onset, although no study has ever reported increased DCN spike activity during this period. Furthermore, in our *in vivo* awake whole-cell recordings in (**Chapter 2**)**,** we did not observe synaptic currents shortly after the CS or at another moment during the CS-US interval that could indicate MF activity. This all points to our hypothesis that MFs do not benefit from the window of reduced PC inhibition. Even when we activated or silenced MFs during this window we did not find alterations in parameters of conditioned behavior (**Chapter 2**). In support of this hypothesis, blocking glutamate neurotransmission in DCN has been shown to have only mild effects on CRs (Aksenov et al. 2005), whereas blocking GABA completely abolishes CRs (Aksenov et al. 2004). All evidence considered, we propose that PCs are the main driver, and other afferents have only a minor role, for EBC-related spike activity in the DCN. It is however important to know the exact subthreshold patterns of each input pathway to the DCN during the full 260 ms of the CS, which is information we were unable to provide here and as a consequence, is still lacking.

7.1.3 PNNs predominantly suppress upregulation of PC terminals in DCN

Removing PNNs leads to an increase in PC terminals and a decrease in VGLUT1+ MFs. In the cerebellar cortex, enzymatically removing PNNs also induces sprouting of PC axon collaterals (Corvetti and Rossi 2005). But why do we not observe a balanced increase in all afferents? We have to take into account that EBC-DCN neurons receive a relatively high percentage of PC inputs (interposed; 59.2%) (Palkovits et al. 1977) from Zebrin-II-negative cerebellar cortical areas with relatively high spontaneous spike frequencies (Sugihara and

Shinoda 2007; Mostofi et al. 2010; Zhou et al. 2014). These inputs are spatially organized in microzones that are synchronously active during similar physiological operations (Oscarsson 1979; De Zeeuw et al. 2011). Furthermore, synapses that are closely together on the dendrite are more coactive (Kleindienst et al. 2011) and it has been shown that synapses that are desynchronized relative to their neighbors, *e.g.* synchronous PC terminals versus asynchronous MF terminals, lead to reduced synaptic transmission efficiency (Winnubst et al. 2015). This in turn could lead to removal of these depressed synapses (Wiegert and Oertner 2013), and cause the effect predominantly on PCs as we have observed in **Chapter 3**. It should be realized however that these studies have been done in the developing visual cortex and hippocampus, although it is conceivable that the same mechanisms apply to the DCN as well. From this we conclude that PNNs predominantly suppress structural plasticity of PC terminals, since they appear to have a higher 'drive' for structural upregulation. At the same time, PNNs play a crucial role in maintaining the homeostatic balance between excitation (MFs and CFCs) and inhibition (PCs and local interneurons) in the DCN.

7.1.4 Future directions in cerebellar learning and plasticity research

The studies presented in **Chapter 2 and 3** aim to contribute to understanding the plasticity mechanisms that take place in the cerebellum during learning. Recently, interesting findings have emerged that call for further *in vivo* investigation. Using *in vitro* recordings Wang et al. (2018) reported an increased intrinsic excitability in DCN neurons of rats after they received several sessions of EBC training. The finding that neuronal excitability changes during learning in the cerebellum is not entirely new. PCs also display changes in membrane excitability 24 hours and 1 month after EBC learning, pointing toward both a short-term and long-term role of intrinsic plasticity in cerebellum-dependent learning (Schreurs et al. 1998). Different forms of plasticity may occur simultaneously during learning. In the cerebellum, synaptic plasticity may establish connectivity patterns via action potential firing, whereas intrinsic plasticity may facilitate a neuron to get integrated into an active engram (Belmeguenai et al. 2010; Ohtsuki and Hansel 2018). This is supported by various PC-specific mouse models that suffer from deficits in intrinsic excitability and/or plasticity as well as from abnormal cerebellar motor learning, including not only EBC but also adaptation of the vestibule-ocular reflex or locomotion learning (Schonewille et al. 2010; Peter et al. 2016; French et al. 2019). However, so far there is only indirect evidence that synaptic plasticity exists in the DCN after conditioning (Ten Brinke et al. 2017) — let alone that it has been studied whether synaptic plasticity and intrinsic excitability mechanisms complement each other during learning. If this is the case however, altering the excitability in DCN neurons (Wang et al. 2018) and PCs (Schreurs et al. 1998) simultaneously may increase the sensitivity to many sets of afferent inputs, thereby resulting in more changes of spiking events within the olivo-cerebellar system during conditioning. Determining whether intrinsic plasticity in DCN neurons is induced by an

intensified release of PC inhibition (Belmeguenai et al. 2010; Person and Raman 2011; Ten Brinke et al. 2017), by increased rebound activity subsequent to intensified PC inhibition (Hoebeek et al. 2010), by enhanced excitatory inputs from collaterals (Boele et al., 2013; **Chapter 2**), and/or by untightening of the perineuronal net (Hirono et al., 2018; **Chapter 3**) will need further study.

7.2 Time processing in the cerebellum

In the second part of this thesis (**Chapter 4, 5 and 6**) we examine the role of the cerebellum in the perception and processing of temporal information. Our findings underline the general consensus on cerebellar contribution to timing (Ivry and Keele 1989; Spencer and Ivry 2013; Bareš et al. 2018), while at the same time they emphasize that cerebellar dysfunction can severely compromise certain behaviors. On the other hand, repeated exposure to challenging situations where appropriate (spatio-)temporal processing is required may lead to changes in the way cognitive resources are allocated, and this form of training can improve performance in tasks that rely on these spatio-temporal processes.

7.2.1 Spatio-temporal prediction and experience-dependent improvements

In **Chapter 4** we present a study involving baseball athletes, who were previously trained by experiencing more than 5000 live pitches at the national level; *i.e.* situations comparable to the experimental task used in this study. Baseball players form an interesting model for study, since they may display expertise-level differences in structural connectivity, processing and modulatory attention (Muraskin et al. 2016). Participants were asked to touch a screen before a downward moving stimulus terminated *inside* a square at the bottom of the screen, or to refrain themselves from touching in case the stimulus terminated *outside* the square. This task particularly depends on the ability to make an accurate trajectory prediction, based on which a subsequent motor action is selected and executed (Go/No-Go task). There is evidence that action selection relies on activity in the basal ganglia (BG), in particular the subthalamic nucleus (Baunez et al. 2001; Eagle et al. 2008; Schmidt et al. 2013; Gaidica et al. 2018), in cooperation with other areas such as the prefrontal cortex (Rae et al. 2015). In line with this, optogenetic modulation of direct and indirect BG pathways can lead to movement initiation or evoke a parkinsonian state, respectively (Kravitz et al. 2010). Action preparation and execution is thought to rely on the cerebellum (Gaidica et al. 2018), where DCN activity precedes the execution of saccades or limb movements (Thach 1975; Ohmae et al. 2017), but also eyelid movements during EBC (Berthier and Moore, 1990; Ten Brinke et al., 2017; **Chapter 2**). It has been shown more recently that the DCN and frontal cortex cooperate during motor planning and preparation, even seconds before movements start (Gao et al. 2018). From this it becomes clear that the

cerebellum takes part in a brain-wide cortico-cerebellar network that is active during different parts of the task.

It is interesting in this respect that we did not observe activity in the BG during the task (**Chapter 4**), while medial and lateral regions in the cerebellum did become active. Neither was BG activity reported during the spatio-temporal prediction task used in **Chapter 6** (Onuki et al. 2015). A possible reason for this is that the relevant time intervals of stimuli in the former task varied between 385 and 585 ms. In the latter task it is more difficult to determine since multiple stimuli moved simultaneously, although it is likely that spatio-temporal prediction was performed within a one-second timeframe, starting as soon as the marker entered a certain distance from the target marker. This seems to be compatible with studies suggesting that the cerebellum is involved in sub-second timing, whereas the BG may be involved at longer time intervals (Ivry 1996; Jahanshahi et al. 2006; Lee et al. 2007; Koch et al. 2007; Fierro et al. 2007; Bueti et al. 2008; Meck et al. 2008; Aso et al. 2010; Petter et al. 2016; Ohmae et al. 2017). The tasks in these chapters also differ in the sense that the task in **Chapter 6** involves co-activation of hippocampal and cerebellar regions (Onuki et al. 2015), whereas the task in **Chapter 4** does not involve the hippocampus.

The processing of spatial information has been linked to activity in hippocampal 'place cells' (O'Keefe and Dostrovsky 1971; Best et al. 2001), but the cerebellum can significantly influence spatial representations in these cells. For example, disrupting protein kinase C (PKC)-dependent plasticity at the parallel fiber (PF)-PC synapse can disturb place cell properties and navigation capabilities when mice have to rely on self-motion cues (Rochefort et al. 2011). Furthermore, a functional link between cerebellar and hippocampal regions has been shown to be important during different forms of navigation (Iglói et al. 2015). With respect to our experiments, it could be that spatial information during the task in **Chapter 4** is used to a lesser extent, since the trajectory is predicted quickly during the initial part of the stimulus trajectory, *i.e.* when the stimulus has not moved very far yet. Gaze measurements support this view, since the athletes do not track the stimulus over the entire trajectory. During the upward moving stimuli in **Chapter 6** however, participants have to continuously compare the spatial locations of the moving and static stimuli, thereby depending more heavily on spatial information. It would be highly interesting to see future studies further differentiate the hippocampal and cerebellar contribution during these tasks, and clarify how the cerebellum contributes to spatial processing in hippocampal regions.

Chapter 4 demonstrates that previous experience in athletes leads to altered neural processes that give rise to increased performance (Yarrow et al. 2009), but only during the most challenging task conditions. It has been shown that different neuronal pathways may be activated for different stimulus parameters (Hazeltine et al. 1997). Parameters that determine the difficulty of the task are stimulus speed and preparation time, and it turns out that athletes excel during trials with a short preparation time (time while looking at a fixation cross) in combination with a medium or fast moving stimulus. It is likely that

spatio-temporal prediction and the subsequent decision-making are completed before full awareness of the stimulus information, especially during the fastest stimulus speeds. However, motor actions can be driven before full visual awareness, which can be facilitated by a shorter pathway involving subcortical circuits (Spering and Carrasco, 2015). An important experiment that is still lacking in this study is the comparison of cerebellar activity between athletes and control subjects during the task, where increased or an altered time course of activity could argue for optimized cerebellar function in athletes. This is necessary, because task performance relies on activity in a cortico-cerebellar network and not only on the cerebellum itself. Therefore, it could be that improved performance is the result of neural changes outside the cerebellum. In analogy with this it was shown previously that increased cerebellar activity during fMRI coincides with increased performance on a spatio-temporal prediction task (Bareš et al. 2011), suggesting that increased activity relates to better performance. It should be noted however that this experiment was performed in SCA6 patients, which can bias the relation between cerebellar activity and performance. Alternatively, by comparing volumetric measurements of the involved brain structures in athletes and controls could provide clues on changes in the task-related neuronal substrate. This has proven to be a useful measure of experience, as was famously demonstrated by the increased hippocampal volumes of taxi drivers with superior navigation skills (Maguire et al. 2000). However, if higher athletes performance is the result of improved connectivity within the network, diffuse tensor imaging (DTI) could be instrumental in detecting such changes (Hasan et al. 2011), as was done previously to investigate connectivity changes after reading practice in poor reading children (Keller and Just 2009).

7.2.2 Physiological task responses are changed in athletes *and* SCA6 patients

The study of eye movements in skilled sport athletes has been a highly popular topic for decades (Hüttermann et al. 2018), for a large part because the application of this knowledge in athletes is highly attractive for obvious reasons. However, for scientific research these measurements may provide a useful metric of underlying neural processes (Van der Stigchel et al. 2006). In **Chapter 4** we found that athletes employ more cost-efficient eye movements, *i.e.* closer gaze-to-stimulus distances and shorter stimulus tracking during trials. This suggests that the response decision is made at an earlier stage of the trial, making further close stimulus-tracking unnecessary. Another possibility is that athletes are better at perceiving stimuli in their peripheral vision (Zwierko 2008). During the task, athletes show earlier and faster pupillary responses on trials with short preparation time, indicating a faster recruitment of cognitive resources. On trials requiring action preparation and execution (hits and false alarms), athletes show larger peak pupil dilations. Since the amplitude of pupil changes has been linked to task complexity which requires more cognitive resources (van der Meer et al. 2010), one may argue that athletes were able to

engage a higher degree of cognitive resources. Taken together, these findings demonstrate that repeated training leads to psychological changes and improves performance.

In contrast to improved eye movements in athletes, SCA6 has been associated with a wide range of symptoms that includes eye movements alterations such as diplopia, dysmetric saccades, impaired smooth pursuit and downbeat nystagmus (Gomez et al. 1997; Geschwind et al. 1997; Schöls et al. 1998; Yabe et al. 2003; Solodkin and Gomez 2011; Bunn et al. 2015; Falcon et al. 2015). Some of these eye deficits can be detected already in the clinical 'presymptomatic' stage (Christova et al. 2008). In **Chapter 5** we aimed to characterize the extent to which eye movements could have influenced our findings by performing eye tracking during the task. Although we did not find major eye movement deficits, we cannot fully exclude that eye movement alterations could have introduced a limited bias in our results in **Chapter 5 and 6**, which is generally a consideration in studies involving SCA6 patients. Since we found that both controls and SCA6 participants were able to focus on regions of relevant information, in combination with their ability to adopt similar strategies for performing the task, we believe this bias was relatively limited. However, the ability to perceive visual information is dependent on the cerebellum as a critical structure for controlling eye movements (Katoh et al. 2015; Sun et al. 2017) in coordination with the superior colliculi (Lefèvre et al. 1998; Quaia et al. 1999) (see also the cover of this thesis).

From a personal perspective, while acting as experimenter more than once SCA6 patients reported that they felt unable to effectively translate their decision in an appropriate motor action during the task. This exemplifies that results from cerebellar patients should be interpreted with caution and that we should carefully consider whether motor deficits can bias measurements of a non-motor process. With the present neuroscientific toolbox available to us, we are still unable to fully separate non-motor from motor processing deficits. This is particularly important in cerebellar research, since the cerebellum is involved in both types of processing (Schmahmann 2004; Schmahmann et al. 2009; Baumann et al. 2015). For the studies described in this thesis, measuring a perceptual process like spatio-temporal prediction in SCA6 patients could be influenced by motor deficits. We attempted to rule out such a bias in **Chapter 6**, by employing a reactive (control) task. Here we observed only a small increase in patients' reaction time compared to controls (36.1 ms, last training), presumably too small to significantly influence our results on the predictive task. Also, these are much smaller than reported in a similar task in SCA6 patients (~90 ms; Bareš et al., 2007), possibly because the average Scale of the Assessment and Rating of Ataxia (SARA)-score of our SCA6 patients was relatively low (9.5 ± 5.2, on a scale of 0-40; Schmitz-Hübsch et al., 2006). Nonetheless, the evidence of spatio-temporal prediction as displayed by a 'predictive response' of ~60 ms before perfect marker overlap, temporal interval learning (Onuki et al., 2015; **Chapter 6**), and the absence of both in SCA6 patients (**Chapter 6**), still remains unambiguous.

7.2.3 Action observation recruits the cerebellum

Potential SCA6 motor deficits are likely not to have influenced performance on the task in **Chapter 5**, where participants had to judge the weight of an object being lifted based on kinematic and differential shape cues (Hamilton et al. 2007), since reaction time was not important for performance. There are two strong indications that this task critically relied on the cerebellum. Firstly, activation of cerebellar lateral hemispheres of lobule VI, and a cluster including lobules VIIb and VIIIa; the same areas that were activated when observing meaningful hand actions. Interestingly, activations became evident when contrasting with meaningless hand actions around the same object, suggesting that the cerebellum was particularly activated during goal-directed hand movements (Nathan et al. 2012). Secondly, SCA6 patients were significantly impaired at the weight judgement task, especially when only kinematic information was available, since in the other task condition they could benefit from muscle shape information. Action observation recruits a variety of brain areas among which frontal motor areas, the cerebellum and posterior parietal cortex have been reported repeatedly (Calvo-Merino et al. 2006; Gazzola and Keysers 2009). Weight judgement from action observation furthermore depends on activity in several areas including the premotor cortex and somatosensory cortex (Pobric et al. 2006; Valchev et al. 2017). The ability to 'mirror' the actions of others in order to understand their meaning has been hypothesized to be carried by neurons that show comparable activity during the *execution* as well as the *observation* of the same motor action - the so called 'mirror neurons' (Rizzolatti and Craighero 2004; Cattaneo and Rizzolatti 2009). In primates these mirror neurons have been found in the frontal, premotor and inferior parietal cortex (di Pellegrino et al. 1992; Gallese et al. 1996; Rizzolatti et al. 1996; Kohler et al. 2002; Keysers et al. 2003; Fogassi et al. 2005; Rozzi et al. 2008) and even extracellular recordings in humans have demonstrated their presence (Mukamel et al. 2010). From our studies it seems conceivable that these neurons, in cooperation with the cerebellum, facilitate a neural representation of the observed motor action. Exactly what aspect of this representation the cerebellum is responsible for remains unclear, but it could well be the encoding of temporal information, as suggested by our and previous results (Cattaneo et al. 2012). A potential promising approach for future studies to distinguish the cerebellar contribution to action observation would be to use non-invasive techniques such as transcranial direct current stimulation (tDCS) or repetitive transcranial magnetic stimulation (rTMS) of the cerebellum (van Dun et al. 2016). In the light of the present thesis, this has already been used effectively during EBC (Zuchowski et al. 2014; Beyer et al. 2017) as well as temporal motor skill learning (Wessel et al. 2016). Moreover, rTMS has been shown to introduce millisecond variability in the inter-tap interval during an explicit timing task, proving the applicability of this technique (Del Olmo et al. 2007; Koch et al. 2007).

7.2.4 Cerebellar loci for time processing

A good indicator for localized processing of temporal information in the cerebellum is finding consistent activity in the same cerebellar regions during different timing tasks. This may prove to be challenging because different forms of timing (explicit versus implicit) activate distinct neuronal systems (Coull and Nobre 2008). Nonetheless, our experiments in **Chapter 4 and 5** revealed activity in the bilateral cerebellar hemispheres, particularly in lobules VI, VII, VIII. Furthermore, our paradigm as used in **Chapter 6** was previously found to activate lobules VI and VIIIa, where motor imagery activated the bilateral lobule VI (Onuki et al. 2015). Both this paper and the task in **Chapter 4** showed activity in the cerebellar vermis, and there appeared to be a preference for activity in the right cerebellar hemisphere in general. Taken together, we conclude that temporal processing in the cerebellum is localized in (but not limited to) cerebellar lobules VI, VII and VIII. This fits well within the framework of the cerebellar timing literature, since there is overlap with previously identified cerebellar regions for time processing, *i.e.* cerebellar lobules V-VIII (Spencer and Ivry 2013). However, a multitude of perceptual (non-motor) processes have been associated with activity in and beyond these regions (Stoodley and Schmahmann 2009). In addition, the anterior part of lobule VI is associated with the primary sensorimotor map of finger motions in the cerebellum (Grodd et al. 2001; Schlerf et al. 2015). However, purely perceptual tasks that involve trajectory prediction (O'Reilly et al. 2008) or representation of temporal intervals (Bueti et al. 2008) also recruit similar cerebellar regions (lobule VII crus I, and left crus II/right lobule VI, respectively), further supporting perceptual processing in these regions.

7.3 Conclusion

As suggested early in the 1960s (Braitenberg 1961, 1967), the cerebellum shows several anatomical and physiological characteristics that make it a suitable structure for sub-second time processing. Its relatively uniform organization, presence of feedback and feedforward loops, high amount of both convergence and divergence ratios, and mechanisms that facilitate both fast (*e.g.* direct monosynaptic MF to DCN connections) and slow (*e.g.* glutamate spillover between CFs and molecular layer interneurons) neuronal transmission, may result in highly temporally precise spike coding patterns throughout the cerebellar circuit (De Zeeuw et al. 2011), that can facilitate a large range of behaviors. With the research presented in this thesis we aim to achieve a step forward towards understanding the (subthreshold and circuit) neuronal computations that take place in the cerebellum, and may underlie spatio-temporal processing. However, before arriving at this goal, many topics still require further investigation.

7.4 References

Aizenman CD, Manis PB, Linden DJ (1998) Polarity of Long-Term Synaptic Gain Change Is Related to Postsynaptic Spike Firing at a Cerebellar Inhibitory Synapse. Neuron 21:827–835. doi: 10.1016/S0896-6273(00)80598-X

Aksenov DP, Serdyunkova N, Irwin K, Bracha V (2004) GABA Neurotransmission in the Cerebellar Interposed Nuclei: Involvement in Classically Conditioned Eyeblinks and Neuronal Activity. J Neurophysiol 91:719–727. doi: 10.1152/jn.00859.2003

Aksenov DP, Serdyunkova N, Bloedel JR, Bracha V (2005) Glutamate Neurotransmission in the Cerebellar Interposed Nuclei: Involvement in Classically Conditioned Eyeblinks and Neuronal Activity. J Neurophysiol 93:44–52. doi: 10.1152/jn.00586.2004

Albus JS (1971) A theory of cerebellar function. Math Biosci 10:25–61

Andersson G, Oscarsson O (1978) Projections to lateral vestibular nucleus from cerebellar climbing fiber zones. Exp Brain Res 32:. doi: 10.1007/BF00239552

Aso K, Hanakawa T, Aso T, Fukuyama H (2010) Cerebro-cerebellar interactions underlying temporal information processing. J Cogn Neurosci 22:2913–2925

Baade C, Byczkowicz N, Hallermann S (2016) NMDA receptors amplify mossy fiber synaptic inputs at frequencies up to at least 750 Hz in cerebellar granule cells. Synapse n/a-n/a. doi: 10.1002/syn.21898

Bao S, Chen L, Thompson RF (2000) Learning- and cerebellum-dependent neuronal activity in the lateral pontine nucleus. Behav Neurosci 114:254–261. doi: 10.1037//0735-7044.114.2.254

Bareš M, Apps R, Avanzino L, et al (2018) Consensus paper: Decoding the Contributions of the Cerebellum as a Time Machine. From Neurons to Clinical Applications. The Cerebellum. doi: 10.1007/s12311-018-0979-5

Bareš M, Lungu O, Liu T, et al (2007) Impaired predictive motor timing in patients with cerebellar disorders. Exp Brain Res 180:355–365. doi: 10.1007/s00221-007-0857-8

Bareš M, Lungu OV, Liu T, et al (2011) The Neural Substrate of Predictive Motor Timing in Spinocerebellar Ataxia. The Cerebellum 10:233–244. doi: 10.1007/s12311-010-0237-y

Baumann O, Borra RJ, Bower JM, et al (2015) Consensus Paper: The Role of the Cerebellum in Perceptual Processes. The Cerebellum 14:197–220. doi: 10.1007/s12311-014-0627-7

Baunez C, Humby T, Eagle DM, et al (2001) Effects of STN lesions on simple vs choice reaction time tasks in the rat: preserved motor readiness, but impaired response selection: STN lesions in simple and choice reaction time. Eur J Neurosci 13:1609–1616. doi: 10.1046/j.0953-816x.2001.01521.x

Belmeguenai A, Hosy E, Bengtsson F, et al (2010) Intrinsic Plasticity Complements Long-Term Potentiation in Parallel Fiber Input Gain Control in Cerebellar Purkinje Cells. J Neurosci 30:13630–13643. doi: 10.1523/JNEUROSCI.3226-10.2010

Benedykcinska A, Ferreira A, Lau J, et al (2016) Generation of brain tumours in mice by Cre-mediated recombination of neural progenitors *in situ* with the tamoxifen metabolite endoxifen. Dis Model Mech 9:211–220. doi: 10.1242/dmm.022715

Berthier NE, Moore JW (1986) Cerebellar Purkinje cell activity related to the classically conditioned nictitating membrane response. Exp Brain Res 63:341–350

Berthier NE, Moore JW (1990) Activity of deep cerebellar nuclear cells during classical conditioning of nictitating membrane extension in rabbits. Exp Brain Res 83:44–54

Best PJ, White AM, Minai A (2001) Spatial processing in the brain: the activity of hippocampal place cells. Annu Rev Neurosci 24:459–486. doi: 10.1146/annurev.neuro.24.1.459

Beyer L, Batsikadze G, Timmann D, Gerwig M (2017) Cerebellar tDCS Effects on Conditioned Eyeblinks using Different Electrode Placements and Stimulation Protocols. Front Hum Neurosci 11:. doi: 10.3389/fnhum.2017.00023

Blenkinsop TA, Lang EJ (2011) Synaptic Action of the Olivocerebellar System on Cerebellar Nuclear Spike Activity. J Neurosci 31:14708–14720. doi: 10.1523/JNEUROSCI.3323-11.2011

Boele H-J, Koekkoek SKE, De Zeeuw CI, Ruigrok TJH (2013) Axonal Sprouting and Formation of Terminals in the Adult Cerebellum during Associative Motor Learning. J Neurosci 33:17897–17907. doi: 10.1523/JNEUROSCI.0511-13.2013

Bracha V, Webster ML, Winters NK, et al (1994) Effects of muscimol inactivation of the cerebellar interposed-dentate nuclear complex on the performance of the nictitating membrane response in the rabbit. Exp Brain Res 100:453–468

Braitenberg V (1961) Functional Interpretation of Cerebellar Histology. Nature 190:539–540

Braitenberg V (1967) Is the cerebellar cortex a biological clock in the millisecond range? Prog Brain Res 25:334–346

Bueti D, Walsh V, Frith C, Rees G (2008) Different brain circuits underlie motor and perceptual representations of temporal intervals. J Cogn Neurosci 20:204–214

Bunn LM, Marsden JF, Voyce DC, et al (2015) Sensorimotor processing for balance in spinocerebellar ataxia type 6: SENSORIMOTOR PROCESSING IN SCA6. Mov Disord 30:1259–1266. doi: 10.1002/mds.26227

Calvo-Merino B, Grèzes J, Glaser DE, et al (2006) Seeing or Doing? Influence of Visual and Motor Familiarity in Action Observation. Curr Biol 16:1905–1910. doi: 10.1016/j.cub.2006.07.065

Cattaneo L, Fasanelli M, Andreatta O, et al (2012) Your Actions in My Cerebellum: Subclinical Deficits in Action Observation in Patients with Unilateral Chronic Cerebellar Stroke. The Cerebellum 11:264–271. doi: 10.1007/s12311-011-0307-9

Cattaneo L, Rizzolatti G (2009) The mirror neuron system. Arch Neurol 66:557–560

Christova P, Anderson JH, Gomez CM (2008) Impaired eye movements in presymptomatic spinocerebellar ataxia type 6. Arch Neurol 65:530–536

Clark GA, McCormick DA, Lavond DG, Thompson RF (1984) Effects of lesions of cerebellar nuclei on conditioned behavior and hippocampal neuronal responses. Brain Res 291:125–136

Corvetti L, Rossi F (2005) Degradation of Chondroitin Sulfate Proteoglycans Induces Sprouting of Intact Purkinje Axons in the Cerebellum of the Adult Rat. J Neurosci 25:7150–7158. doi: 10.1523/JNEUROSCI.0683-05.2005

Coull JT, Nobre AC (2008) Dissociating explicit timing from temporal expectation with fMRI. Curr Opin Neurobiol 18:137–144. doi: 10.1016/j.conb.2008.07.011

Hamilton A, Joyce DW, Flanagan JR, et al (2007) Kinematic cues in perceptual weight judgement and their origins in box lifting. Psychol Res 71:13–21. doi: 10.1007/s00426-005-0032-4

De Gruijl JR, Hoogland TM, De Zeeuw CI (2014) Behavioral Correlates of Complex Spike Synchrony in Cerebellar Microzones. J Neurosci 34:8937–8947. doi: 10.1523/JNEUROSCI.5064-13.2014

De Zeeuw CI, Hoebeek FE, Bosman LWJ, et al (2011) Spatiotemporal firing patterns in the cerebellum. Nat Rev Neurosci 12:327–344. doi: 10.1038/nrn3011

De Zeeuw CI, Lang EJ, Sugihara I, et al (1996) Morphological Correlates of Bilateral Synchrony in the Rat Cerebellar Cortex. J Neurosci 16:3412–3426. doi: 10.1523/JNEUROSCI.16-10-03412.1996

De Zeeuw CI, Van Alphen AM, Hawkins RK, Ruigrok TJH (1997) Climbing fiber collaterals contact neurons in the cerebellar nuclei that provide a GABAergic feedback to the inferior olive. Neuroscience 80:981–986

Del Olmo MF, Cheeran B, Koch G, Rothwell JC (2007) Role of the cerebellum in externally paced rhythmic finger movements. J Neurophysiol 98:145–152

Delvendahl I, Hallermann S (2016) The Cerebellar Mossy Fiber Synapse as a Model for High-Frequency Transmission in the Mammalian CNS. Trends Neurosci. doi: 10.1016/j.tins.2016.09.006

di Pellegrino G, Fadiga L, Fogassi L, et al (1992) Understanding motor events: a neurophysiological study. Exp Brain Res 91:176–180. doi: 10.1007/BF00230027

Dietrichs E, Walberg F (1987) Cerebellar nuclear afferents—where do they originate? Anat Embryol (Berl) 177:165–172

Eagle DM, Baunez C, Hutcheson DM, et al (2008) Stop-Signal Reaction-Time Task Performance: Role of Prefrontal Cortex and Subthalamic Nucleus. Cereb Cortex 18:178–188. doi: 10.1093/cercor/bhm044

Falcon MI, Gomez CM, Chen EE, et al (2015) Early Cerebellar Network Shifting in Spinocerebellar Ataxia Type 6. Cereb Cortex bhv154. doi: 10.1093/cercor/bhv154

Fierro B, Palermo A, Puma A, et al (2007) Role of the cerebellum in time perception: A TMS study in normal subjects. J Neurol Sci 263:107–112. doi: 10.1016/j.jns.2007.06.033

Fogassi L, Ferrari PF, Gesierich B, et al (2005) Parietal lobe: From action organisation to intention understanding. Science 308:662–667. doi: 10.1126/science.1111199

Freeman JH, Halverson HE, Poremba A (2005) Differential Effects of Cerebellar Inactivation on Eyeblink Conditioned Excitation and Inhibition. J Neurosci 25:889–895. doi: 10.1523/JNEUROSCI.4534-04.2005

Freeman JH, Rabinak CA (2004) Eyeblink conditioning in rats using pontine stimulation as a conditioned stimulus. Integr Physiol Behav Sci 39:180–191

Freeman JH, Steinmetz AB (2011) Neural circuitry and plasticity mechanisms underlying delay eyeblink conditioning. Learn Mem 18:666–677. doi: 10.1101/lm.2023011

French CA, Veloz MFV, Zhou K, et al (2019) Differential effects of Foxp2 disruption in distinct motor circuits. Mol Psychiatry 24:447. doi: 10.1038/s41380-018-0199-x

Gaidica M, Hurst A, Cyr C, Leventhal DK (2018) Distinct Populations of Motor Thalamic Neurons Encode Action Initiation, Action Selection, and Movement Vigor. J Neurosci 38:6563–6573. doi: 10.1523/JNEUROSCI.0463-18.2018

Gallese V, Fadiga L, Fogassi L, Rizzolatti G (1996) Action recognition in the premotor cortex. Brain J Neurol 119 (Pt 2:593–609. doi: 10.1093/brain/119.2.593

Gao Z, Davis C, Thomas AM, et al (2018) A cortico-cerebellar loop for motor planning. Nature 563:113–116. doi: 10.1038/s41586-018-0633-x

Gauck V, Jaeger D (2000) The Control of Rate and Timing of Spikes in the Deep Cerebellar Nuclei by Inhibition. J Neurosci 20:3006–3016

Gazzola V, Keysers C (2009) The Observation and Execution of Actions Share Motor and Somatosensory Voxels in all Tested Subjects: Single-Subject Analyses of Unsmoothed fMRI Data. Cereb Cortex 19:1239–1255. doi: 10.1093/cercor/bhn181

Geschwind DH, Perlman S, Figueroa KP, et al (1997) Spinocerebellar ataxia type 6: Frequency of the mutation and genotype-phenotype correlations. Neurology 49:1247–1251. doi: 10.1212/WNL.49.5.1247

Gomez CM, Thompson RM, Gammack JT, et al (1997) Spinocerebellar ataxia type 6: gaze-evoked and vertical nystagmus, Purkinje cell degeneration, and variable age of onset. Ann Neurol 42:933–950

Gould TJ, Sears LL, Steinmetz JE (1993) Possible CS and US pathways for rabbit classical eyelid conditioning: electrophysiological evidence for projections from the pontine nuclei and inferior olive to cerebellar cortex and nuclei. Behav Neural Biol 60:172–185

Grodd W, Hülsmann E, Lotze M, et al (2001) Sensorimotor mapping of the human cerebellum: fMRI evidence of somatotopic organization. Hum Brain Mapp 13:55–73. doi: 10.1002/hbm.1025

Hasan KM, Walimuni IS, Abid H, Hahn KR (2011) A Review of Diffusion Tensor Magnetic Resonance Imaging Computational Methods and Software Tools. Comput Biol Med 41:1062–1072. doi: 10.1016/j.compbiomed.2010.10.008

Hazeltine E, Grafton ST, Ivry R (1997) Attention and stimulus characteristics determine the locus of motor-sequence encoding. A PET study. Brain 120:123–140

Heiney SA, Wohl MP, Chettih SN, et al (2014) Cerebellar-Dependent Expression of Motor Learning during Eyeblink Conditioning in Head-Fixed Mice. J Neurosci 34:14845–14853. doi: 10.1523/JNEUROSCI.2820-14.2014

Hioki H, Fujiyama F, Taki K, et al (2003) Differential distribution of vesicular glutamate transporters in the rat cerebellar cortex. Neuroscience 117:1–6. doi: 10.1016/S0306-4522(02)00943-0

Hirono M, Watanabe S, Karube F, et al (2018) Perineuronal Nets in the Deep Cerebellar Nuclei Regulate GABAergic Transmission and Delay Eyeblink Conditioning. J Neurosci 38:6130–6144. doi: 10.1523/JNEUROSCI.3238-17.2018

Hoebeek FE, Witter L, Ruigrok TJH, De Zeeuw CI (2010) Differential olivo-cerebellar cortical control of rebound activity in the cerebellar nuclei. Proc Natl Acad Sci 107:8410–8415. doi: 10.1073/pnas.0907118107

Hoogland TM, De Gruijl JR, Witter L, et al (2015) Role of Synchronous Activation of Cerebellar Purkinje Cell Ensembles in Multi-joint Movement Control. Curr Biol. doi: 10.1016/j.cub.2015.03.009

Hüttermann S, Noël B, Memmert D (2018) Eye tracking in high-performance sports: Evaluation of its application in expert athletes. Int J Comput Sci Sport 17:182–203. doi: 10.2478/ijcss-2018-0011

Iglói K, Doeller CF, Paradis A-L, et al (2015) Interaction Between Hippocampus and Cerebellum Crus I in Sequence-Based but not Place-Based Navigation. Cereb Cortex N Y N 1991 25:4146–4154. doi: 10.1093/cercor/bhu132

Ito M (1984) The Cerebellum and Neural Control. New York: Raven Press

Ivarsson M, Hesslow G (1993) Bilateral control of the orbicularis oculi muscle by one cerebellar hemisphere in the ferret. Neuroreport 4:1127–1130

Ivry RB (1996) The representation of temporal information in perception and motor control. Curr Opin Neurobiol 6:851–857

Ivry RB, Keele SW (1989) Timing functions of the cerebellum. J Cogn Neurosci 1:136–152

Jahanshahi M, Jones CRG, Dirnberger G, Frith CD (2006) The Substantia Nigra Pars Compacta and Temporal Processing. J Neurosci 26:12266–12273. doi: 10.1523/JNEUROSCI.2540-06.2006

Jirenhed D-A, Bengtsson F, Hesslow G (2007) Acquisition, Extinction, and Reacquisition of a Cerebellar Cortical Memory Trace. J Neurosci 27:2493–2502. doi: 10.1523/JNEUROSCI.4202-06.2007

Katoh A, Shin S-L, Kimpo RR, et al (2015) Purkinje cell responses during visually and vestibularly driven smooth eye movements in mice. Brain Behav. doi: 10.1002/brb3.310

Keller TA, Just MA (2009) Altering cortical connectivity: Remediation-induced changes in the white matter of poor readers. Neuron 64:624–631. doi: 10.1016/j.neuron.2009.10.018

Keysers C, Kohler E, Umiltà MA, et al (2003) Audiovisual mirror neurons and action recognition. Exp Brain Res 153:628–36. doi: 10.1007/s00221-003-1603-5

Kitai ST, McCrea RA, Preston RJ, Bishop GA (1977) Electrophysiological and horseradish peroxidase studies of precerebellar afferents to the nucleus interpositus anterior. I. climbing fiber system. Brain Res 122:197–214

Kleim JA, Freeman JH, Bruneau R, et al (2002) Synapse formation is associated with memory storage in the cerebellum. Proc Natl Acad Sci 99:13228–13231

Kleindienst T, Winnubst J, Roth-Alpermann C, et al (2011) Activity-Dependent Clustering of Functional Synaptic Inputs on Developing Hippocampal Dendrites. Neuron 72:1012–1024. doi: 10.1016/j.neuron.2011.10.015

Koch G, Oliveri M, Torriero S, et al (2007) Repetitive TMS of cerebellum interferes with millisecond time processing. Exp Brain Res 179:291–299. doi: 10.1007/s00221-006-0791-1

Kohler E, Keysers C, Umiltà MA, et al (2002) Hearing Sounds, Understanding Actions: Action Representation in Mirror Neurons. Science 297:846–848. doi: 10.1126/science.1070311

Kravitz AV, Freeze BS, Parker PRL, et al (2010) Regulation of parkinsonian motor behaviors by optogenetic control of basal ganglia circuitry. Nature 466:622–626. doi: 10.1038/nature09159

Lavond DG, Hembree TL, Thompson RF (1985) Effect of kainic acid lesions of the cerebellar interpositus nucleus on eyelid conditioning in the rabbit. Brain Res 326:179–182

Lavond DG, Steinmetz JE (1989) Acquisition of classical conditioning without cerebellar cortex. Behav Brain Res 33:113–164

Lee K-H, Egleston PN, Brown WH, et al (2007) The role of the cerebellum in subsecond time perception: evidence from repetitive transcranial magnetic stimulation. J Cogn Neurosci 19:147–157

Lefèvre P, Quaia C, Optican LM (1998) Distributed model of control of saccades by superior colliculus and cerebellum. Neural Netw 11:1175–1190. doi: 10.1016/S0893-6080(98)00071-9

Lewis JL, LoTurco JJ, Solomon PR (1987) Lesions of the Middle Cerebellar Peduncle Disrupt Acquisition and Retention of the Rabbit's Classically Conditioned Nictitating Membrane Response. Behav Neurosci 101:151–157

Lu H, Yang B, Jaeger D (2016) Cerebellar Nuclei Neurons Show Only Small Excitatory Responses to Optogenetic Olivary Stimulation in Transgenic Mice: In Vivo and In Vitro Studies. Front Neural Circuits 10:. doi: 10.3389/fncir.2016.00021

Maguire EA, Gadian DG, Johnsrude IS, et al (2000) Navigation-related structural change in the hippocampi of taxi drivers. Proc Natl Acad Sci U S A 97:4398–4403

Marr D (1969) A theory of cerebellar cortex. J Physiol 202:437–470

Mathews PJ, Lee KH, Peng Z, et al (2012) Effects of Climbing Fiber Driven Inhibition on Purkinje Neuron Spiking. J Neurosci 32:17988–17997. doi: 10.1523/JNEUROSCI.3916-12.2012

Meck WH, Penney TB, Pouthas V (2008) Cortico-striatal representation of time in animals and humans. Curr Opin Neurobiol 18:145–152. doi: 10.1016/j.conb.2008.08.002

Medina JF, Garcia KS, Mauk MD (2001) A Mechanism for Savings in the Cerebellum. J Neurosci 21:4081–4089. doi: 10.1523/JNEUROSCI.21-11-04081.2001

Mojtahedian S, Kogan DR, Kanzawa SA, et al (2007) Dissociaton of conditioned eye and limb responses in the cerebellar interpositus. Physiol Behav 91:9–14. doi: 10.1016/j.physbeh.2007.01.006

Mostofi A, Holtzman T, Grout AS, et al (2010) Electrophysiological Localization of Eyeblink-Related Microzones in Rabbit Cerebellar Cortex. J Neurosci 30:8920–8934. doi: 10.1523/JNEUROSCI.6117-09.2010

Mukamel R, Ekstrom AD, Kaplan J, et al (2010) Single-Neuron Responses in Humans during Execution and Observation of Actions. Curr Biol 20:750–756. doi: 10.1016/j.cub.2010.02.045

Najac M, Raman IM (2017) Synaptic excitation by climbing fibre collaterals in the cerebellar nuclei of juvenile and adult mice. J Physiol. doi: 10.1113/JP274598

Nathan DE, Prost RW, Guastello SJ, et al (2012) Investigating the neural correlates of goal-oriented upper extremity movements. NeuroRehabilitation 31:421–428. doi: 10.3233/NRE-2012-00812

Ohmae S, Kunimatsu J, Tanaka M (2017) Cerebellar roles in self-timing for sub- and supra-second intervals. J Neurosci 2221–16. doi: 10.1523/JNEUROSCI.2221-16.2017

Ohtsuki G, Hansel C (2018) Synaptic Potential and Plasticity of an SK2 Channel Gate Regulate Spike Burst Activity in Cerebellar Purkinje Cells. iScience 1:49–54. doi: 10.1016/j.isci.2018.02.001

Ohyama T, Nores WL, Mauk MD (2003) Stimulus generalization of conditioned eyelid responses produced without cerebellar cortex: implications for plasticity in the cerebellar nuclei. Learn Mem 10:346–354

Ohyama T, Nores WL, Medina JF, et al (2006) Learning-Induced Plasticity in Deep Cerebellar Nucleus. J Neurosci 26:12656–12663. doi: 10.1523/JNEUROSCI.4023-06.2006

O'Keefe J, Dostrovsky J (1971) The hippocampus as a spatial map. Preliminary evidence from unit activity in the freely-moving rat. Brain Res 34:171–175. doi: 10.1016/0006-8993(71)90358-1

Onuki Y, Van Someren EJW, De Zeeuw CI, Van der Werf YD (2015) Hippocampal-Cerebellar Interaction During Spatio-Temporal Prediction. Cereb Cortex 25:313–321. doi: 10.1093/cercor/bht221

O'Reilly JX, Mesulam MM, Nobre AC (2008) The Cerebellum Predicts the Timing of Perceptual Events. J Neurosci 28:2252–2260. doi: 10.1523/JNEUROSCI.2742-07.2008

Oscarsson O (1979) Functional units of the cerebellum - sagittal zones and microzones. Trends Neurosci 2:143–145. doi: 10.1016/0166-2236(79)90057-2

Palkovits M, Mezey É, Hámori J, Szentágothai J (1977) Quantitative histological analysis of the cerebellar nuclei in the cat. I. Numerical data on cells and on synapses. Exp Brain Res 28–28:. doi: 10.1007/BF00237096

Pedroarena CM, Schwartz C (2003) Efficacy and Short-Term Plasticity at GABAergic Synapses Between Purkinje and Cerebellar Nuclei Neurons. J Neurophysiol 89:704–715. doi: 10.1152/jn.00558.2002

Perrett SP, Ruiz BP, Mauk MD (1993) Cerebellar cortex lesions disrupt learning-dependent timing of conditioned eyelid responses. J Neurosci 13:1708–1718

Person AL, Raman IM (2011) Purkinje neuron synchrony elicits time-locked spiking in the cerebellar nuclei. Nature 481:502–505. doi: 10.1038/nature10732

Peter S, ten Brinke MM, Stedehouder J, et al (2016) Dysfunctional cerebellar Purkinje cells contribute to autism-like behaviour in Shank2-deficient mice. Nat Commun 7:12627. doi: 10.1038/ncomms12627

Petter EA, Lusk NA, Hesslow G, Meck WH (2016) Interactive Roles of the Cerebellum and Striatum in Sub-Second and Supra-Second Timing: Support for an Initiation, Continuation, Adjustment, and Termination (ICAT) Model of Temporal Processing. Neurosci Biobehav Rev. doi: 10.1016/j.neubiorev.2016.10.015

Pickford J, Apps R (2017) Collateral impact: a dual role for climbing fibre collaterals to the cerebellar nuclei? J Physiol. doi: 10.1113/JP275091

Pobric G, De AF, Hamilton C (2006) Action Understanding Requires the Left Inferior Frontal Cortex. Curr Biol 16:524–529. doi: 10.1016/j.cub.2006.01.033

Powell K, Mathy A, Duguid I, Häusser M (2015) Synaptic representation of locomotion in single cerebellar granule cells. eLife 4:. doi: 10.7554/eLife.07290

Pugh JR, Raman IM (2008) Mechanisms of Potentiation of Mossy Fiber EPSCs in the Cerebellar Nuclei by Coincident Synaptic Excitation and Inhibition. J Neurosci 28:10549–10560. doi: 10.1523/JNEUROSCI.2061-08.2008

Pugh JR, Raman IM (2006) Potentiation of Mossy Fiber EPSCs in the Cerebellar Nuclei by NMDA Receptor Activation followed by Postinhibitory Rebound Current. Neuron 51:113–123. doi: 10.1016/j.neuron.2006.05.021

Pugh JR, Raman IM (2009) Nothing can be coincidence: synaptic inhibition and plasticity in the cerebellar nuclei. Trends Neurosci 32:170–177. doi: 10.1016/j.tins.2008.12.001

Quaia C, Lefèvre P, Optican LM (1999) Model of the Control of Saccades by Superior Colliculus and Cerebellum. J Neurophysiol 82:999–1018. doi: 10.1152/jn.1999.82.2.999

Racine RJ, Wilson DA, Gingell R, Sunderland D (1986) Long-term potentiation in the interpositus and vestibular nuclei in the rat. Exp Brain Res 63:. doi: 10.1007/BF00235658

Rae CL, Hughes LE, Anderson MC, Rowe JB (2015) The Prefrontal Cortex Achieves Inhibitory Control by Facilitating Subcortical Motor Pathway Connectivity. J Neurosci 35:786–794. doi: 10.1523/JNEUROSCI.3093-13.2015

Rancz EA, Ishikawa T, Duguid I, et al (2007) High-fidelity transmission of sensory information by single cerebellar mossy fibre boutons. Nature 450:1245–1248. doi: 10.1038/nature05995

Rizzolatti G, Craighero L (2004) The mirror-neuron system. Annu Rev Neurosci 27:169–192. doi: 10.1146/annurev.neuro.27.070203.144230

Rizzolatti G, Fadiga L, Gallese V, Fogassi L (1996) Premotor cortex and the recognition of motor actions. Cogn Brain Res 3:131–141. doi: 10.1016/0926-6410(95)00038-0

Rochefort C, Arabo A, André M, et al (2011) Cerebellum Shapes Hippocampal Spatial Code. Science 334:385–389. doi: 10.1126/science.1207403

Rozzi S, Ferrari PF, Bonini L, et al (2008) Functional organization of inferior parietal lobule convexity in the macaque monkey: Electrophysiological characterization of motor, sensory and mirror responses and their correlation with cytoarchitectonic areas. Eur J Neurosci 28:1569–1588. doi: 10.1111/j.1460-9568.2008.06395.x

Schlerf JE, Galea JM, Spampinato D, Celnik PA (2015) Laterality Differences in Cerebellar-Motor Cortex Connectivity. Cereb Cortex N Y N 1991 25:1827–34. doi: 10.1093/cercor/bht422

Schmahmann JD (2004) Disorders of the cerebellum: ataxia, dysmetria of thought, and the cerebellar cognitive affective syndrome. J Neuropsychiatry Clin Neurosci 16:367–378

Schmahmann JD, MacMore J, Vangel M (2009) Cerebellar stroke without motor deficit: clinical evidence for motor and non-motor domains within the human cerebellum. Neuroscience 162:852–861. doi: 10.1016/j.neuroscience.2009.06.023

Schmidt R, Leventhal DK, Mallet N, et al (2013) Canceling actions involves a race between basal ganglia pathways. Nat Neurosci 16:1118–1124. doi: 10.1038/nn.3456

Schmitz-Hübsch T, Du Montcel ST, Baliko L, et al (2006) Scale for the assessment and rating of ataxia Development of a new clinical scale. Neurology 66:1717–1720

Schöls L, Krüger R, Amoiridis G, et al (1998) Spinocerebellar ataxia type 6: genotype and phenotype in German kindreds. J Neurol Neurosurg Psychiatry 64:67–73

Schonewille M, Belmeguenai A, Koekkoek SK, et al (2010) Purkinje Cell-Specific Knockout of the Protein Phosphatase PP2B Impairs Potentiation and Cerebellar Motor Learning. Neuron 67:618–628. doi: 10.1016/j.neuron.2010.07.009

Schreurs BG, Gusev PA, Tomsic D, et al (1998) Intracellular correlates of acquisition and long-term memory of classical conditioning in Purkinje cell dendrites in slices of rabbit cerebellar lobule HVI. J Neurosci 18:5498–5507

Sears LL, Steinmetz JE (1990) Acquisition of classically conditioned-related activity in the hippocampus is affected by lesions of the cerebellar interpositus nucleus. Behav Neurosci 104:681

Solodkin A, Gomez CM (2011) Spinocerebellar ataxia type 6. Ataxic Disord 103:461–473

Solomon PR, Lewis JL, LoTurco JJ (1986) The role of the middle cerebellar peduncle acquisition and retention of the rabbit's classically conditioned nictitating membrane response. Bull Psychon Soc 24:75–78

Spencer RMC, Ivry RB (2013) Cerebellum and Timing. In: Manto M, Schmahmann JD, Rossi F, et al. (eds) Handbook of the Cerebellum and Cerebellar Disorders. Springer Netherlands, Dordrecht, pp 1201–1219

Stoodley C, Schmahmann J (2009) Functional topography in the human cerebellum: A meta-analysis of neuroimaging studies. NeuroImage 44:489–501. doi: 10.1016/j.neuroimage.2008.08.039

Sugihara I, Shinoda Y (2007) Molecular, Topographic, and Functional Organization of the Cerebellar Nuclei: Analysis by Three-Dimensional Mapping of the Olivonuclear Projection and Aldolase C Labeling. J Neurosci 27:9696–9710. doi: 10.1523/JNEUROSCI.1579-07.2007

Sun Z, Smilgin A, Junker M, et al (2017) The same oculomotor vermal Purkinje cells encode the different kinematics of saccades and of smooth pursuit eye movements. Sci Rep 7:40613. doi: 10.1038/srep40613

Telgkamp P, Raman IM (2002) Depression of inhibitory synaptic transmission between Purkinje cells and neurons of the cerebellar nuclei. J Neurosci 22:8447–8457

Ten Brinke MM, Heiney SA, Wang X, et al (2017) Dynamic modulation of activity in cerebellar nuclei neurons during pavlovian eyeblink conditioning in mice. eLife 6:

Ten Brinke MM, Boele H-J, Spanke JK, et al (2015) Evolving Models of Pavlovian Conditioning: Cerebellar Cortical Dynamics in Awake Behaving Mice. Cell Rep 13:1977–1988. doi: 10.1016/j.celrep.2015.10.057

Thach WT (1975) Timing of activity in cerebellar dentate nucleus and cerebral motor cortex during prompt volitional movement. Brain Res 88:233–241. doi: 10.1016/0006-8993(75)90387-X

Valchev N, Tidoni E, Hamilton AF de C, et al (2017) Primary somatosensory cortex necessary for the perception of weight from other people's action: A continuous theta-burst TMS experiment. NeuroImage 152:195–206. doi: 10.1016/j.neuroimage.2017.02.075

van der Meer E, Beyer R, Horn J, et al (2010) Resource allocation and fluid intelligence: Insights from pupillometry. Psychophysiology 47:158–169. doi: 10.1111/j.1469-8986.2009.00884.x

Van der Stigchel S, Meeter M, Theeuwes J (2006) Eye movement trajectories and what they tell us. Neurosci Biobehav Rev 30:666–679. doi: 10.1016/j.neubiorev.2005.12.001

van der Want JJL, Wiklund L, Guegan M, et al (1989) Anterograde tracing of the rat olivocerebellar system with phaseolus vulgaris leucoagglutinin (PHA-L). Demonstration of climbing fiber collateral innervation of the cerebellar nuclei. J Comp Neurol 288:1–18. doi: 10.1002/cne.902880102

van Dun K, Bodranghien FCAA, Mariën P, Manto MU (2016) tDCS of the Cerebellum: Where Do We Stand in 2016? Technical Issues and Critical Review of the Literature. Front Hum Neurosci 10:. doi: 10.3389/fnhum.2016.00199

van 't Spijker HM, Kwok JCF (2017) A Sweet Talk: The Molecular Systems of Perineuronal Nets in Controlling Neuronal Communication. Front Integr Neurosci 11:. doi: 10.3389/fnint.2017.00033

Wang D, Smith-Bell CA, Burhans LB, et al (2018) Changes in membrane properties of rat deep cerebellar nuclear projection neurons during acquisition of eyeblink conditioning. Proc Natl Acad Sci 115:E9419–E9428. doi: 10.1073/pnas.1808539115

Wessel MJ, Zimerman M, Timmermann JE, et al (2016) Enhancing Consolidation of a New Temporal Motor Skill by Cerebellar Noninvasive Stimulation. Cereb Cortex 26:1660–1667. doi: 10.1093/cercor/bhu335

White JJ, Sillitoe RV (2017) Genetic silencing of olivocerebellar synapses causes dystonia-like behaviour in mice. Nat Commun 8:14912. doi: 10.1038/ncomms14912

Wiegert JS, Oertner TG (2013) Long-term depression triggers the selective elimination of weakly integrated synapses. Proc Natl Acad Sci 110:E4510–E4519. doi: 10.1073/pnas.1315926110

Winnubst J, Cheyne JE, Niculescu D, Lohmann C (2015) Spontaneous Activity Drives Local Synaptic Plasticity In Vivo. Neuron 87:399–410. doi: 10.1016/j.neuron.2015.06.029

Wu Y, Raman IM (2017) Facilitation of mossy fibre driven spiking in the cerebellar nuclei by the synchrony of inhibition. J Physiol. doi: 10.1113/JP274321

Yabe I, Sasaki H, Takeichi N, et al (2003) Positional vertigo and macroscopic downbeat positioning nystagmus in spinocerebellar ataxia type 6 (SCA6). J Neurol 250:440–443. doi: 10.1007/s00415-003-1020-5

Yarrow K, Brown P, Krakauer JW (2009) Inside the brain of an elite athlete: the neural processes that support high achievement in sports. Nat Rev Neurosci 10:585–596. doi: 10.1038/nrn2672

Yeo CH, Hardiman MJ, Glickstein M (1985) Classical conditioning of the nictating membrane of the rabbit. I. Lesions of the cerebellar nuclei. Exp Brain Res 60:87–98

Zhang W, Linden DJ (2006) Long-Term Depression at the Mossy Fiber-Deep Cerebellar Nucleus Synapse. J Neurosci 26:6935–6944. doi: 10.1523/JNEUROSCI.0784-06.2006

Zheng N, Raman IM (2010) Synaptic Inhibition, Excitation, and Plasticity in Neurons of the Cerebellar Nuclei. The Cerebellum 9:56–66. doi: 10.1007/s12311-009-0140-6

Zhou H, Lin Z, Voges K, et al (2014) Cerebellar modules operate at different frequencies. eLife 3:. doi: 10.7554/eLife.02536

Zuchowski ML, Timmann D, Gerwig M (2014) Acquisition of Conditioned Eyeblink Responses is Modulated by Cerebellar tDCS. Brain Stimulat 7:525–531. doi: 10.1016/j.brs.2014.03.010

Zwierko T (2008) Differences in Peripheral Perception between Athletes and Nonathletes. J Hum Kinet 19:. doi: 10.2478/v10078-008-0004-z

Summary

Our ability to perceive and process temporal and spatial information from our environment is crucial for our survival and we perform this process constantly in our daily life. There is ample evidence that the cerebellum, a brain area located at the back within the skull, is participating in the encoding and integration of temporal and spatial information. Not surprisingly, behaviors that directly rely on the correct execution of this process are promptly affected in the case of cerebellar damage or disorders. However, the neuronal mechanisms the cerebellum utilizes to carry out this type of spatio-temporal processing, as well as the precise cerebellar contribution to temporal aspects of various behaviors, still remain to be clarified. The experimental work described in this thesis aims to contribute to our understanding of these cerebellar functions, with the goal of bridging the gap between neuronal encoding mechanisms in mice and cerebellar-dependent behaviors in humans.

Special attention is given to the cerebellar nuclei, an important 'hub' in the olivo-cerebellar circuitry that provides the sole cerebellar output to other brain areas. At the level of the individual nuclei neuron, integration of many converging neuronal inputs with high temporal precision occurs continuously. A powerful approach to investigate how the cerebellum contributes to behavior is therefore, to study the plasticity mechanisms that take place during learning in the nuclei, an approach that was adopted in several chapters of this thesis. The paradigm that we used to investigate cerebellar learning in rodents is delayed eyeblink conditioning, a type of associative behavior where the underlying neuronal circuitry is well understood, thus allowing for more in-depth experimental approaches. In humans, more complex yet essential behaviors were studied, with the understanding and applying time-related information during the task as common denominator.

Chapter 2 provides a detailed study on the intra- and extracellular electrophysiological characteristics of nuclei neurons during delayed eyeblink conditioning, a paradigm where precise timing is imperative for making appropriate eyelid movements. Using a combination of whole-cell recordings in awake behaving animals, input-specific optogenetic modulation of neuronal activity and examination of synaptic markers, we characterize the contribution of afferent inputs to task-related activity and eyelid movements. We show that both excitatory mossy fiber inputs and inhibitory Purkinje cell afferents undergo structural increases during conditioning. Although optogenetic activation and silencing of mossy fibers can elicit eyelid movements after conditioning, their contribution to conditioned responses and eyeblink-related nuclei activity appears to be limited. We found furthermore that learning-related changes in subthreshold synaptic encoding after the conditioned stimulus are likely to be carried mainly by changes in Purkinje cell firing. Both conditioned responses and voluntary eyelid movements are encoded in the nuclei, where synaptic activity may correlate with the behavior, although the contribution of the nuclei to initiation of movements is likely to be different.

Interestingly, we also found that synaptic encoding of the unconditioned stimulus is increased after conditioning. This study provides for the first time insight into the membrane potential dynamics and learning-associated changes in nuclei neurons during delayed eyeblink conditioning.

Cerebellar nuclei neurons are surrounded by an extracellular matrix structure called the perineuronal net, which is known to modulate plasticity mechanisms. As a logical follow-up on previous **Chapter 2**, in **Chapter 3** we investigate how perineuronal nets in the cerebellar nuclei are involved in associative learning during delayed eyeblink conditioning. We found that 5 days of conditioning induces pronounced decreases in perineuronal nets, together with decreases in the chemorepulsive protein Semaphorin-3A, a mechanism that could potentially facilitate the formation of new synaptic contacts. In addition, enzymatically decreasing perineuronal nets in the nuclei results in improved learning. Preliminary data on memory retention furthermore indicate that a sustained decrease in perineuronal nets impairs the ability to consolidate and form long-term memory, which depends on stabilization of synapses. We further show that decreasing perineuronal nets leads to an imbalance between inhibitory and excitatory inputs. More specifically, we observed an increase in inhibitory GABAergic terminals and a decrease in excitatory VGLUT1-positive terminals. This in turn results in altered spontaneous spike activity in the awake behaving mouse. From this study we conclude that perineuronal nets in the cerebellar nuclei play an important role as a gating mechanism for plasticity during cerebellar associative behavior. On the one hand they restrict plasticity, possibly through Semaphorin-3A-mediated mechanisms, whereas on the other hand they facilitate the stabilization and consolidation of the memory trace.

Sustained learning, both during an experimental task and during activities like sports, results in optimized neuronal circuits and allows for excellent performance. Elite human athletes at the national level utilize their trained neuronal system to achieve maximum performance during demanding sport situations. To investigate how a well-trained cerebellar system influences temporal and spatial processing, in **Chapter 4** we switched to human psychophysiology. We asked whether optimized feedback control relying on the cerebellar network could enhance spatio-temporal trajectory prediction during a Go/No-Go timed decision-making task. Using fMRI we found that this task, essentially simulating a real-live baseball pitch, activates medial and lateral cerebellar areas which coincides with activations in the cerebral cortex. This interplay between cerebellar and cerebral areas indicates that the cerebellum, as part of a larger neuronal network, becomes active in tasks that require optimal spatio-temporal processing. Elite athletes furthermore show increased performance only for the most demanding conditions of the task, at which times they employ more cost-efficient gaze-tracking of the stimulus. Using pupillary response dynamics as a metric for cognitive load we show that athletes mobilize their cognitive resources more rapidly during stringent task conditions when the preparation time is short. However, when preparation time is long, this effect is reversed, suggesting that cognitive resources are efficiently applied depending on task conditions in athletes.

Interpreting temporal information is not only required for demanding activities such as described in **Chapter 4**, but also during more basic functions such as understanding motor actions that are made by others. **Chapter 5** describes a study where we aimed to elucidate the involvement of the cerebellum in perceiving meaningful hand actions made by others, as well as the cerebellar involvement in extracting shape and kinematic characteristics from arm movements. We found that observing goal directed hand actions such as pouring wine in a glass, and observing an arm lifting a weight, consistently recruits bilateral cerebellar Lobules VI, VIIb and VIIIa. With this evidence in hand we proceeded to investigate cerebellar activations while differentiating between shape and kinematic information of the arm lifting a weight. Hiding the musculature of the arm with a sleeve, thereby occluding shape information, does not result in altered patterns of cerebellar recruitment. This indicates that the cerebellum is specifically involved in processing kinematic information, which can be perceived from observing both a sleeved and non-sleeved arm. Consistent with these findings, patients with spinocerebellar ataxia type 6 (SCA6), a genetic disorder that manifests as cerebellum-specific progressive dystrophy, are significantly impaired at judging the weight being lifted during observation of both a sleeved and non-sleeved arm. Further localization of the deficit in processing kinematic rather than shape information can only be claimed to a moderate extent. A significant negative correlation between task performance and a neurological metric for SCA6 based on severity of symptoms further indicates that the impairment is a direct result of cerebellar dysfunction.

After having established that the cerebellum is recruited during interpretation of kinematic information, in **Chapter 6** we continue to investigate cerebellar temporal processing from a different angle. Here, we used a spatio-temporal trajectory prediction paradigm that has been previously shown to induce co-activation of cerebellar and hippocampal areas (Onuki et al. 2015). SCA6 patients and healthy controls were asked to make precisely-timed finger movements when upward-moving markers completely overlapped with target markers, a task that depends heavily on their ability to generate a prediction based on spatial and temporal information. Our results show that whereas healthy control subjects learn to make timed movements, apparent as a shift in response times towards the 'anticipatory' period before perfect overlap, this learning process is impaired in SCA6 subjects. In addition, the SCA6 group has a lower temporal precision in response times, indicating that the cerebellar component for executing the task mainly concerns information in the time domain. Performance on a simple reaction time task is reduced in SCA6 patients, possibly due to a motor component of the disorder. However, healthy subjects benefit from both a fixed order and temporal interval order of stimuli, whereas SCA6 subjects only benefit from a fixed order of stimuli. Taken together, this study further substantiates leading hypotheses regarding temporal processing in the cerebellum.

Samenvatting

Ons vermogen om tijd- en plaatsgerelateerde informatie uit onze omgeving te kunnen waarnemen en te verwerken is van cruciaal belang om te overleven. We voeren dit proces dan ook voortdurend uit in ons dagelijks leven. Er is bewijs dat de kleine hersenen ('cerebellum'), een hersengebied dat zich aan de achterkant van ons brein bevindt, deelneemt aan de codering en integratie van tijd- en plaatsgerelateerde informatie. Verschillende vormen van gedrag die afhankelijk zijn van de integratie van tijd- en plaatsgerelateerde informatie kunnen daardoor gemakkelijk zijn aangetast in het geval van schade of een aandoening aan het cerebellum. Het is echter nog niet voldoende bekend van welke neuronale mechanismen het cerebellum gebruik maakt tijdens de integratie van tijd- en plaatsgerelateerde informatie en wat de precieze bijdrage van het cerebellum is voor de verwerking van tijdsgerelateerde aspecten van verschillende soorten gedrag. De experimenten die beschreven zijn in dit proefschrift hebben tot doel bij te dragen aan ons begrip van de functies van het cerebellum, waarbij een verbinding wordt gelegd tussen de neuronale coderingsmechanismen en cerebellum-afhankelijk gedrag dat daarmee samenhangt.

In dit proefschrift wordt in het bijzonder aandacht besteed aan de cerebellaire kernen, een belangrijk 'centrum' binnen het olivo-cerebellaire circuit. De kernen is het enige gebied die de verbindingen vanuit het cerebellum naar andere hersengebieden verzorgt. In individuele kerncellen vindt er een constante integratie van grote getalen neuronale verbindingen plaats - een proces dat zich voltrekt met een grote mate van precisie in het tijdsdomein. Een effectieve manier om te onderzoeken hoe het cerebellum bijdraagt aan gedrag is door te kijken naar de mechanismen in de kernen waarmee neuronale verbindingen zich aanpassen tijdens leren (neuronale plasticiteit). Deze aanpak hebben we gebruikt in verschillende hoofdstukken van dit proefschrift. Het gedragsparadigma dat we hebben gebruikt om cerebellair-afhankelijk leren te onderzoeken in knaagdieren is vertraagd ooglid conditionering. Dit is een vorm van associatief leergedrag waarvan we het onderliggende neuronale circuit al goed begrijpen. Dit maakt het mogelijk om diepgaande vragen te onderzoeken. In mensen werden complexere maar tegelijkertijd noodzakelijkere vormen van gedrag onderzocht. Zowel in deze vormen van gedrag, alsook het gedrag onderzocht in knaagdieren, was het kunnen begrijpen en toepassen van tijdsgerelateerde informatie van belang.

Hoofdstuk 2 beschrijft een gedetailleerde studie naar de intra- en extracellulaire electrofysiologische eigenschappen van kerncellen tijdens vertraagd ooglid conditionering, een vorm van gedrag waarbij een precieze timing van ooglid bewegingen noodzakelijk is. Door gebruik te maken van een combinatie van 'whole-cell' afleidingen in wakkere dieren tijdens gedrag, verbinding-specifieke optogenetische beïnvloeding van neuronale activiteit en de bestudering van synaps-specifieke eiwitten, kunnen we karakteriseren hoe individuele verbindingen bijdragen aan taak-gerelateerde neuronale activiteit in de kernen

en ooglid bewegingen. We laten zien dat excitatoire mosvezelverbindingen en inhibitoire Purkinje celverbindingen structurele veranderingen ondergaan tijdens conditionering. Hoewel optogenetische activatie en remming van mosvezels ooglid bewegingen kunnen veroorzaken in knaagdieren na conditionering, de bijdrage die ze leveren aan de uitvoering van geconditioneerde bewegingen en gerelateerde neuronale activiteit in de kernen blijkt relatief klein te zijn. We ontdekten verder dat leergerelateerde veranderingen in synaptische codering onder de drempel voor actiepotentialen volgend op de geconditioneerde stimulus hoofdzakelijk veroorzaakt worden door veranderingen in de activiteit van Purkinje cellen. Zowel geconditioneerde alsook vrijwillige ooglid bewegingen worden gecodeerd in de kernen, waarbij de eigenschappen van de synaptische activiteit samenhangt met het gedrag. Echter, de bijdrage van neuronale activiteit in de kernen aan het ontstaan van deze vormen van ooglid bewegingen lijkt verschillend te zijn. We hebben ook vastgesteld dat de synaptische codering van ongeconditioneerde ooglid bewegingen in de kernen is toegenomen na conditionering. Deze studie geeft voor het eerst inzicht in de dynamische veranderingen van de membraan potentiaal en de leergerelateerde veranderingen in kerncellen tijdens vertraagd ooglid conditionering.

Neuronen in de cerebellaire kernen zijn omgeven door een extracellulaire matrix-structuur genaamd het perineuronaal net, waarvan we weten dat het plasticiteitsmechanismen beïnvloedt. Als een logisch vervolg op hoofdstuk 2 onderzoeken we in **hoofdstuk 3** hoe perineuronale netten in de kernen betrokken zijn bij associatief leren tijdens vertraagd ooglid conditioneering. We hebben ontdekt dat 5 dagen van conditioneering een sterke afname van het perineuronaal net veroorzaakt, tegelijkertijd met een afname van het chemorepulsieve eiwit Semaphorin-3A. Dit zou een mechanisme kunnen zijn om de vorming van nieuwe synaptische verbindingen te ondersteunen. Maar ook omgekeerd, het enzymatisch verminderen van de perineuronale netten in de kernen leidt tot een beter leervermogen. Nieuwe data laten verder zien dat een voortdurende enzymatische afname van perineuronale netten leidt tot verminderd vermogen om geheugen op te slaan als langetermijnsgeheugen, een proces dat afhangt van het vermogen nieuwe synaptische verbindingen te vormen. De afname in perineuronale netten leidt verder tot een verstoring in de balans tussen inhibitoire en excitatoire verbindingen. In het bijzonder vonden we een toename van inhibitoire GABAerge verbindingen en een afname van excitatoire VGLUT1-positieve verbindingen. Dit leidt vervolgens tot veranderingen in de eigenschappen van spontane neuronale activiteit in wakkere muizen. Uit deze studie concluderen we dat perineuronale netten in de cerebellaire kernen een belangrijke rol spelen voor de beïnvloeding van plasticiteitsmechanismen tijdens cerebellair associatief gedrag. Aan de ene kant verminderen ze plasticiteit, mogelijk via Semaphorin-3A-gerelateerde mechanismen. Aan de andere kant ondersteunen ze de stabilisatie en consolidatie van het geheugen.

Aanhoudend leren, zowel tijdens een experimentele taak alsook tijdens activiteiten zoals sport, resulteert in de optimalisatie van neuronale circuits wat het mogelijk maakt buitengewoon te presteren. Menselijke sportatleten op nationaal niveau gebruiken hun

getrainde neuronale circuits om maximaal te presteren tijdens veeleisende sportsituaties. Om te onderzoeken hoe een goed getraind cerebellair systeem bijdraagt aan de verwerking van tijd- en plaatsgerelateerde informatie wordt in **hoofdstuk 4** een overstap gemaakt naar humane psychofysiologie. We onderzochten hier of een geoptimaliseerd terugkoppelingssysteem, afhankelijk van het cerebellaire netwerk, leidt tot een verhoogd vermogen een traject te voorspellen op basis van plaats- en tijdgerelateerde informatie tijdens een Go/No-Go getimede beslistaak. Door gebruik te maken van fMRI ontdekten we dat deze taak, die in principe een honkbal worp-en-slag-situatie simuleert, leidt tot activatie in de mediale en laterale delen van het cerebellum. Deze activaties vallen samen met activaties in de grote hersenen ('cerebrum'). Deze samenwerking tussen cerebellaire en cerebrale gebieden geeft aan dat het cerebellum deel uitmaakt van een groter neuronaal netwerk dat actief wordt tijdens de verwerking van plaats- en tijdgerelateerde informatie. We ontdekten verder dat atleten verhoogde prestaties laten zien in de moeilijkste varianten van de taak. Tijdens deze moeilijkste omstandigheden laten ze efficiëntere oogbewegingen zien tijdens het volgen van de visuele stimuli. Door gebruik te maken van veranderingen in pupilgrootte als een maat voor cognitieve belasting tijdens de taak, lieten we verder zien dat atleten een versnelde mate van cognitieve activatie laten zien als ze een korte voorbereidingstijd hebben. In het geval ze een lange voorbereidingstijd hebben, dan is dit effect omgedraaid. De bevindingen uit deze studie wekken de suggestie dat atleten hun cognitieve belasting op een efficiente manier aanspreken, afhankelijk van de omstandigheden van de gedragstaak.

Het interpreteren en verwerken van tijdgerelateerde informatie is niet alleen belangrijk voor veeleisende activiteiten zoals beschreven in hoofdstuk 4, maar het is ook nodig voor het uitvoeren van meer basale functies, zoals het begrijpen van bewegingen die gemaakt worden door anderen. **Hoofdstuk 5** beschrijft een studie waarbij we onderzochten wat de bijdrage is van het cerebellum bij het waarnemen van betekenisvolle handbewegingen die gemaakt worden door anderen. Ook onderzochten we de rol van het cerebellum bij het interpreteren van vorm- en bewegingsgerelateerde informatie van armbewegingen. We ontdekten dat het observeren van doelgerichte handbewegingen, zoals het inschenken van een glas wijn, stelselmatig leidt tot hersenactiviteit in cerebellaire Lobules VI, VIIb and VIIIa in beide hersenhelfden. Op basis van dit bewijs vervolgden we ons onderzoek, waarbij we onderscheid maakten tussen vorm- en bewegingsgerelateerde informatie tijdens het observeren van een arm die een gewicht optilt. Het verbergen van de arm musculatuur (vormgerelateerde informatie) met een mouw leidt niet tot veranderde cerebellaire activaties. We kunnen hieruit concluderen dat het cerebellum specifiek betrokken is bij het verwerken van bewegingsgerelateerde informatie, wat waargenomen kan worden tijdens de observatie van een arm met én zonder mouw. Coherent met dit gegeven is onze bevinding dat patiënten met cerebellaire ataxie type 6 (SCA6), een genetische aandoening die tot uiting komt als een progressieve dystrofie van het cerebellum, een significant verminderd vermogen hebben om op basis van de observatie van een arm (met of zonder mouw) die een object optilt, een schatting te kunnen maken van het gewicht van het

opgetilde object. Met matige zekerheid kan worden vastgesteld dat dit komt door een verminderd vermogen om bewegingsgerelateerde informatie te kunnen waarnemen. Echter, onze bevinding dat er een negatieve relatie bestaat tussen hoe goed de patiënt presteert tijdens de taak en hoever SCA6 is gevorderd op basis van symptomatologie, levert sterk bewijs voor onze hypothese dat de verminderde prestatie op de taak een directe consequentie is van een verminderde werking van het cerebellum door SCA6.

Na vastgesteld te hebben dat het cerebellum is betrokken is bij de interpretatie van bewegingsgerelateerde informatie, vervolgden we ons onderzoek naar verwerking van tijdgerelateerde informatie in het cerebellum in **hoofdstuk 6** vanuit een andere invalshoek. In dit hoofdstuk presenteren we een studie waarbij we gebruik maakten van een gedragstaak waarbij het voorspellen van een traject op basis van plaats- en tijdgerelateerde informatie belangrijk is. Van deze gedragstaak is het bekend dat het een co-activatie van cerebellaire en hippocampale gebieden teweegbrengt (Onuki et al. 2015). Tijdens deze taak werden SCA6 patiënten en gezonde controle proefpersonen gevraagd precies getimede vingerbewegingen te maken op het moment dat omhoog-bewegende cirkels precies overlapten met statische cirkels bovenaan een computerscherm. Een belangrijke voorwaarde voor het succesvol doen van deze taak is het vermogen om een voorspelling te maken waar (plaatsgerelateerd) een cirkel op een bepaald moment (tijdgerelateerd) gaat zijn. Onze resultaten laten zien dat tijdens het verloop van de taak gezonde proefpersonen leren om getimede vingerbewegingen te maken, waar een verschuiving zichtbaar is naar het moment vóór volledige overlap, ook wel de 'anticipatie periode' genoemd. SCA6 patiënten laten dit leereffect echter niet zien. Daarnaast is er een grotere variatie zichtbaar met betrekking tot het moment dat de vingerbewegingen worden gemaakt. Dit geeft aan dat de bijdrage van het cerebellum voor de uitvoer van de gedragstaak vooral gericht is op informatie in het tijdsdomein. Prestaties op een simpele reactie-taak waren verminderd in SCA6 patiënten, mogelijk veroorzaakt door het effect van de aandoening op motorische functies. Echter, gezonde proefpersonen konden profiteren van hun vermogen om de volgorde van de stimuli, alsook de volgorde van temporele intervallen (ook wel: ritme) te leren. SCA6 proefpersonen profiteren alleen van het leren van de volgorde van stimuli, maar laten geen hogere prestaties zien door het leren van ritme. Deze resultaten samengenomen onderbouwen vooraanstaande theorieën over de verwerking van tijdsgerelateerde informatie in het cerebellum.

Curriculum vitae

Robin Broersen was born in Ridderkerk, the Netherlands on September 8, 1989. After having completed three years of pre-conservatory education with jazz piano as main instrument, he switched to pre-university education (Athenaeum) with a curricular specialization in the natural and health sciences. He finished his pre-university studies in June 2008 at the Dalton Lyceum in Barendrecht.

In September 2009 he started his Bachelor of Science (BSc) program Psychobiology (specialization Molecular and Cell Biology) at the University of Amsterdam. He concluded his curriculum with an internship under the supervision of dr. A. Korosi on the changes in neurogenesis after early-life stress.

After graduating in July 2011, he started the Master of Science (MSc) program Biomedical Sciences (specialization Basic and Applied Neuroscience) at the University of Amsterdam. His first research internship took place in 2012 at the Netherlands Institute for Neuroscience (NIN) in Amsterdam. Under the supervision of Prof.dr. C. Lohmann he studied the spontaneous activity patterns of hippocampal neurons during development.

His basis for *in vivo* electrophysiology was laid in 2013 in the lab of dr. C.P.J. De Kock at the VU University Amsterdam, where he studied the integration of tactile information in the posterior parietal cortex in rats. During this research internship he performed *in vivo* extracellular recordings after which he labeled the neurons with the help of the juxtasomal fillings technique. He wrote his MSc thesis on the relation between microtubule-mediated intracellular transport mechanisms and synaptic plasticity, under the supervison of dr. K. Boekhoorn of the Utrecht University. In August 2013 he graduated with distinction (*cum laude*) for his MSc degree.

He commenced his academic career in November 2013 as research technician with Prof.dr. C.I. De Zeeuw at the Erasmus MC in Rotterdam and the NIN in Amsterdam. Ten months later, he started his doctoral studies within the same departments, studying temporal processing in the cerebellum. During his work as Ph.D. candidate he used different techniques, ranging from *in vivo* electrophysiology to patient research at both locations. In 2016 he was awarded the NIN Brain Award for Collaborative Excellence as first-author on a patient-oriented research project involving collaboration between three research groups.

In 2019 he was recruited as postdoctoral fellow by Prof.dr. G.J. Stuart at the Australian National University in Canberra, Australia.

Education and scientific employment

Postdoctoral fellow — **Canberra, AU**
With dr. G.J. Stuart — Mar. 2019 - present

Eccles Institute of Neuroscience, JCSMR
Australian National University, AU

Ph.D. candidate — **Rotterdam / Amsterdam**
Promotor: dr. C.I. De Zeeuw / Co-promotor: dr. C.B. Canto — Sep. 2014 - 2019

Dept. of Neuroscience / Dept. of Cerebellar Coordination and Cognition
Erasmus Medical Center / Netherlands Institute for Neuroscience, NL

Research technician — **Rotterdam / Amsterdam**
With dr. C.I. De Zeeuw — Nov. 2013 - Aug. 2014

Dept. of Neuroscience / Dept. of Cerebellar Coordination and Cognition
Erasmus Medical Center / Netherlands Institute for Neuroscience, NL

Student MSc Biomedical Sciences — **Amsterdam**
Specialization: Basic and Applied Neuroscience — Sep. 2011 - Aug. 2013

Faculty of Science, Mathematics and Computer Science
University of Amsterdam, NL

Student BSc Psychobiology — **Amsterdam, NL**
Specialization: Molecular and Cell Biology — Sep. 2008 - Aug. 2011

Faculty of Science, Mathematics and Computer Science
University of Amsterdam, NL

Publications

Learning-related changes in synaptic inputs and encoding in cerebellar nuclei neurons during eyeblink conditioning
Broersen, R., Carulli, D., Verhaagen, J., Canto*, C.B. and De Zeeuw*, C.I.
In preparation

Interplay between perineuronal nets in the cerebellar nuclei and Pavlovian eyeblink conditioning
Carulli*, D., Broersen*, R., Canto, C.B., De Winter, F., Boele, H-J., Hobo, B., De Zeeuw, C.I. and Verhaagen, J.
In preparation

Action perception recruits the cerebellum and is impaired in spinocerebellar ataxia patients
Abdelgabar*, A-R., Suttrup*, J., Broersen*, R., Bhandari*, R., Picard, S., Thioux, M., Keysers^, C., De Zeeuw^, C.I. and Gazzola^, V.
Submitted

Functional architecture and encoding of tactile sensorimotor behavior in rat posterior parietal cortex
Mohan, H., De Haan, R., Broersen, R., Pieneman, A., Helmchen, F., Staiger, J.F., Mansvelder, H.D. and De Kock, C.P.J.
Journal of Neuroscience (accepted), doi: 10.1523/JNEUROSCI.0693-19.2019

Intrinsic excitement in cerebellar nuclei neurons during learning
Canto, C.B., Broersen, R. and De Zeeuw, C.I.
PNAS, 2018, doi: 10.1073/pnas.1813866115

Early trajectory prediction in elite athletes
Owens, C.B., De Boer, C., Gennari, G., Broersen, R., Pel, J.J., Miller, B., Clapp, W., Van der Werf, Y.D. and De Zeeuw, C.I.
The Cerebellum, 2018, doi: 10.1007/s12311-018-0975-9

An expandable embryonic stem cell-derived Purkinje neuron progenitor population that exhibits in vivo maturation in the adult mouse cerebellum
Higuera, G.A., Iaffaldano, G., Bedar, M., Shpak, G., Broersen, R., Munshi, S.T., Dupont, C., Gribnau, J., De Vrij, F.M.S., Kushner, S.A. and De Zeeuw, C.I.
Scientific Reports, 2017, doi: 10.1038/s41598-017-09348-1

Impaired spatio-temporal predictive motor timing associated with spinocerebellar ataxia type 6
Broersen, R., Onuki, Y., Abdelgabar, A-R., Owens, C.B., Picard, S., Willems, J., Boele, H-J., Gazzola, V., Van der Werf, Y.D. and De Zeeuw, C.I.
PLoS ONE, 2016, doi: 10.1371/journal.pone.0162042

Juxtasomal biocytin labeling to study the structure-function relationship of individual cortical neurons
Narayanan*, R., Mohan*, H., Broersen*, R., De Haan, R., Pieneman, A.W. and De Kock, C.P.J.
Journal of Visualized Experiments, 2014, doi: 10.3791/51359

Book chapters

Physiology of olivo-cerebellar loops
Broersen, R., Winkelman, B.H.J., Özyıldırım, Ö. and De Zeeuw, C.I.
In: "Essentials of Cerebellum and Cerebellar Disorders", 2016, published by Springer
Editors: Gruol, D.L., Koibuchi, N., Manto, M., Molinari, M., Schmahmann, J.D. and Shen, Y.
doi: 10.1007/978-3-319-24551-5_44

Refereed abstracts

Interfering with Semaphorin 3A in perineuronal nets to enhance plasticity
Carulli, D., Broersen, R., De Winter, F., Boele, H-J., Canto, C.B., Hobo, B., De Zeeuw, C.I. and Verhaagen, J.
SfN, 2018, November 3-7, San Diego, CA, USA

In vivo whole-cell recordings of cerebellar nuclei neurons in awake head-fixed mice during Pavlovian eyeblink conditioning
Broersen, R., Canto, C.B. and De Zeeuw, C.I.
Procedural Learning Summer School, 2017, June 26-28, Amsterdam, NL

Shared circuits in the cerebellum
Abelgabar*, A-R., Broersen*, R., Picard*, S., De Zeeuw^, C.I., Keysers^, C. and Gazzola^, V.
ICPS, 2015, March 12-14, Amsterdam, NL

Measuring mechanical changes of ex vivo brain tissue in an Alzheimer's mouse model
Beekmans, S.V., Antonovaite, N., Broersen, R., Hoogland, T.M., De Zeeuw, C.I., Hol, E.M. and Iannuzzi, D.
Physics@FOM, 2015, January 20-21, Veldhoven, NL

Mirror neuron system and the cerebellum
Broersen, R., Picard, S., Abdelgabar, A-R., Ten Brinke M.M., Keysers, C., Gazzola, V. and De Zeeuw, C.I.
FENS, 2014, July 5-9, Milan, IT

* / ^ indicates equal contribution

PhD Portfolio

Summary of PhD training and teaching

Name PhD student: **R. Broersen**	PhD period: **2014 - 2019**
Erasmus MC Department: **Neurosciences**	Promotor(s): **Prof.dr. C.I. De Zeeuw**
Research School: **None**	Supervisor: **Dr. C.B. Canto**

1. PhD training

	Year	Workload (Hours/ECTS)
General courses		
- Laboratory animal science (LAS; article 9 course)	2014	3.9 ECTS
Specific courses		
- '*In vivo* Intracellular Recordings' course, Eilat, Israel	2015	5 ECTS
Seminars and workshops		
- Department journal club (including oral presentations)	2014-2019	2 ECTS
- Neuroscience Symposiums, Amsterdam, Netherlands	2014-2019	2 ECTS
Presentations		
- Department data presentations (NIN-KNAW)	2014-2019	2.5 ECTS
- Department research presentations (Erasmus MC)	2014-2019	2.5 ECTS
- Neuroscience Symposium - PhD Brain award seminar	2016	1 ECTS
(Inter)national conferences		
- FENS Milan, Italy (including poster presentation)	2014	2 ECTS
- SRC conference Brussels, Belgium	2015	1 ECTS
- Procedural learning summer school, Amsterdam, Netherlands (including poster presentation)	2017	2 ECTS

2. Teaching

	Year	Workload (Hours/ECTS)
Supervising practicals and excursions, Tutoring		
- Supervision and teaching of 4 internship students	2015-2018	10 ECTS

Acknowledgements

It has been about *four-and-a-half* years since I started my PhD journey and, while writing these last few pages of my thesis, the finish line feels very much within reach. However, I don't feel entirely done yet – and wow, the time has gone by so incredibly fast! However, all good things must come to an end, and I'm grateful for the chance I've been given to walk down this path. Now it's time to take the next step in my career as a postdoc elsewhere.

Throughout the years of my PhD, I've met a large number of passionate and great people. Many of these people have become good friends. Without their work, my PhD research would have been impossible. Hereby I would like to thank all people that have contributed to my PhD research and my thesis, as it lies before you today. The list of people to thank is long, but there are a number of people that I would like to mention in particular.

First and foremost, I am profoundly grateful to my promotor **Chris de Zeeuw.** Chris, you gave me the chance to start my career in science. I first started as a research technician and later as a PhD student in your lab, where I also met my wife. I highly value the guidance, ideas, freedom and trust you gave me during my work, as well as the many exciting studies you let me be involved in. Your endless passion and enthusiasm for science are inspiring.

My research would not have been possible without the aid and support of my co-promotor **Cathrin Canto.** Cathrin, not only did you teach me the essential *in vivo* skills and techniques, but also you guided me through the difficult days of my PhD and pulled me back on track as soon as I'd drift off course. I'm grateful for your advice on many science and non-science issues, and I'm going to miss our sessions of studying data traces, scientific discussions, as well as the small talk. Thank you very much for all your help.

I want to thank all **members of my assessment and defense committee** for their time and energy in reading my thesis. I'm truly honored to have you present at my defense.

For several years I've had the pleasure of working closely with two great scientists, **Joost Verhaagen** and **Daniela Carulli**. It has been a great experience to do science with you, I've learned so much along the way. Thank you for our fruitful collaboration.

Many thanks to all current and previous colleagues of De Zeeuw lab in Amsterdam, in particular, **Sebastian Loyola, Sehrazat Kavraal, Rachel Koops, Emilie van der Sande, Tycho Hoogland, Devika Narain, Aleksandra Badura, Cynthia Geelen, Anna Court, Hugo Hoedemaker, Roxanne ter Haar** and **Gerco Beekhof.** Your hard work and passion for science are remarkable. Thank you for your help, as well as for creating a highly motivating and supportive environment in the lab. I wish you all the best, and I hope we meet again in the future.

Beerend Winkelman, I would like to thank you in particular for your time and energy in helping me out with MATLAB coding, discussing filter/Fourier analysis/spike sorting/spike

density estimation stuff, your Game of Thrones predictions and for sharing your (sometimes pretty random) knowledge. Your input has helped me further many times.

Nico Flierman, thank you for enduring the PhD hardship together, it was a hell of a ride. I hope by now you've found another gym buddy, because you've got to keep lifting, man. I do miss your daily clichés around here ;-)

Mohit Dubey, I admire your passion and enthusiasm for science. It was a pleasure sharing the office with you during the last couple of stressful months of my PhD time.

Over the years, I have enjoyed (co-)supervising several BAS students in the lab, who gave me invaluable help with my experiments. Many thanks go to **Melanie Bouw, Maja Mešković, Sanne Stokman** and **Gizem Özel** for all their efforts and countless hours in the lab habituating and training mice. You were truly great to work with.

For my experimental work with human subjects, I've collaborated with several great people that I would like to mention here. **Yoshiyuki Onuki,** working together on the finger-dancing paper has been a true pleasure, and your coding and fMRI research skills are outstanding. It was also good fun to be your paranymph and to plan your defense together. I'm happy we stay in touch. **Cullen Owens,** I've had a great time working together and going around with the Neurasbus to measure baseball players, it was cool. Wishing you all the best in Singapore and beyond. Thanks also to **Casper de Boer, Samuel Picard** and **Ysbrand van der Werf** for collaborating on multiple projects.

From the Social Brain Lab at the NIN, I'm grateful to **Abdel Abdelgabar, Valeria Gazzola** and **Christian Keysers**. I very much enjoyed our constructive conversations and discussions. Seeing multiple papers come to fruition through our collaboration has been an exciting experience for me.

Importantly, I would like to express my gratitude to all **SCA6 patients** and other participants involved in human studies. It was very motivating to experience first-hand your optimism, friendliness and dedication to participate in scientific research, sometimes despite the symptoms of SCA6. Special thanks to the **ADCA Vereniging Nederland** for their financial support for this thesis, as well as their contribution to the research.

Many thanks go to current and previous members of the Erasmus MC eyeblink lab, **Jochen Spanke, Henk-Jan Boele, Bas Koekkoek, Ilja IJpelaar** and **Michiel ten Brinke.** Your time and energy setting up eyeblink conditioning at the NIN and teaching me to do the technique have been critically important for my PhD research. It's impressive to see your lab run so efficiently and produce so many great papers.

Thanks also to other colleagues from the Erasmus MC, particularly to **Zhenyu Gao, Jan-Willem Potters, Jessica Willems, Gustavo Higuera, Laurens Bosman, Mario Negrello** and **Elise Buitenhuis-Linssen.**

My sincere gratitude to all research technicians and support staff I have worked with, particularly the **NIN animal caretakers** and other research support staff. Thanks also to

all current and previous members of the **Borrelsquad** for keeping me busy with fun stuff (except cleaning up early in the morning after the Christmas party).

Several people have been immensely influential in my choice to pursue a PhD in neuroscience by providing excellent supervision and support during my internship in their lab. I'm grateful to **Christiaan de Kock, Hemanth Mohan, Anton Pieneman, Christian Lohmann, Johan Winnubst, Aniko Korosi** and **Eva Naninck** for this.

I thank my **family and friends** for their great support and interest in my work. Thanks especially to those that have participated in the experiments described in Chapters 5 and 6.

To my **friends**, I particularly appreciate your (sometimes successful) attempts to stop me from focusing on my PhD work. In particular, organizing my bachelor party a few weeks before the submission of my thesis has been extremely helpful :-) I miss all of you guys.

A special shout-out to **Youri Havenaar** for his friendship and his unavailing efforts to muscle-up my body in the gym: I thank you, as well as your roommates, for providing me with a welcoming home in Rotterdam, it has saved me a lot of time in public transport.

I'm particularly indebted to **Niels Stadthouders** and **Astrid Vincendon**, who are both my family as well as my good friends. You have done so much for Özgecan and me, but let me start by thanking you for all your time and efforts as masters of ceremonies for our wedding and as paranymph for my defense. I'm lucky to have you in my life.

I'm deeply grateful to my parents and brothers, **Ton, Brigitta, Nick** and **Tigo Broersen,** for their unconditional love and support, making me to the person I am now. I would not be where I am now without you. Throughout my life, you have encouraged me to follow my curiosity and my dreams. Thank you for this great freedom. Ik hou van jullie. Ik draag mijn proefschrift op aan jullie.

My dear wife **Özgecan**, if anyone deserves recognition for their contribution to this thesis, it is you. You know this all too well, as you often tell me you'll claim the 'r' and '.' from my Dr. title after my defense, leaving me with only the 'D'. Thank you for your endless support, your belief in me, and the time and space you've given me to let me study, write, think and… just *be* myself. I know that it has been difficult at times, but we've endured as a team. I love you. This thesis is also dedicated to you.